

# FATIGUE BEHAVIOR OF WELD ROOT CRACK AND STRUCTURAL RESPONSE IN ORTHOTROPIC STEEL DECKS

杨, 沐野

<https://doi.org/10.15017/1866286>

---

出版情報：九州大学, 2017, 博士（工学）, 課程博士  
バージョン：  
権利関係：

**FATIGUE BEHAVIOR OF WELD ROOT CRACK  
AND STRUCTURAL RESPONSE IN ORTHOTROPIC  
STEEL DECKS**

**Yang Muye**

# **FATIGUE BEHAVIOR OF WELD ROOT CRACK AND STRUCTURAL RESPONSE IN ORTHOTROPIC STEEL DECKS**

A Thesis Submitted  
In Partial Fulfillment of the Requirements  
For the Degree of  
**Doctor of Engineering**

By  
**Muye Yang**



to the  
DEPARTMENT OF URBAN AND ENVIRONMENTAL ENGINEERING  
GRADUATE SCHOOL OF ENGINEERING  
**KYUSHU UNIVERSITY**

Fukuoka, Japan  
September, 2017

DEPARTMENT OF URBAN AND ENVIRONMENTAL ENGINEERING  
GRADUATE SCHOOL OF ENGINEERING  
**KYUSHU UNIVERSITY**  
Fukuoka, Japan

CERTIFICATE

The undersigned hereby certify that they have read and recommended to the Graduate School of Engineering for the acceptance of this thesis entitled, “*Fatigue Behavior of Weld Root Crack and Structural Response in Orthotropic Steel Decks*” by **Muye Yang** in partial fulfillment of the requirements for the degree of **Doctor of Engineering**.

Dated: September, 2017

Thesis Supervisor:

\_\_\_\_\_  
Prof. Shigenobu KAINUMA, Dr. Eng.

Examining Committee:

\_\_\_\_\_  
Prof. Yoshimi SONODA, Dr. Eng.

\_\_\_\_\_  
Prof. Hidenori HAMADA, Dr. Eng.

## ABSTRACT

The orthotropic steel decks have been commonly applied to long-span bridges and expressways because of the structural properties such as low self-weight, high load-carrying capacity and high stiffness. The main components of an orthotropic steel deck including the deck plate, longitudinal stiffeners and transverse crossbeams, these members are connected by welding. In the past decades, severe fatigue cracks have been reported at several welded joints in orthotropic steel bridge decks in Europe and other countries. In Japan, many orthotropic steel bridges were extensively constructed in the 1960s-80s during the period of rapid economic growth. Until now, various types of fatigue damages to the steel decks were reported owing to long-term operation and the changed operating environment including the emergence of heavy-duty vehicles and increasing traffic volume beyond design expectations.

A fatigue crack initiation from the weld root tip is one kind of most common and adverse damage, which usually occurred from the rib-to-deck connection and rib-to-rib butt weld, etc. The rib-to-deck structure includes a large number of single-fillet weld joint, root crack is easy to occur due to the inadequate welding details in conjunction with the residual stress induced by the welding process and unfavorable weld shape. Besides, root crack cannot be observed by visual inspection, which might have severe impacts to bridge safety.

Depending on the randomness of vehicle loading in actual bridge, dispersion of fatigue life, and the indeterminacy of crack propagation. The objective of this research is to direct towards cracks at the welded joints of steel bridge with U-shape ribs. The principal aim is to investigate the fatigue behaviors and crack characteristics of welded joints. The methods used in this research is based on the dynamic experimental simulation and parametric numerical analysis. The dissertation is divided into two main parts: (I) Fatigue crack behavior analysis; (II) Structure response of artificial crack simulation.

In **Chapter 1**, the background and topic review was described, and structure of dissertation was presented.

In **Chapter 2**, the fatigue damage cases and related theoretical foundation was clarified.

The part I focused at certain location of orthotropic steel deck and conducted with crack behavior analysis which taking into account structural parameters and fabrication process. This part including three sub-objectives in Chapter 3, 4, 5.

In **Chapter 3**, the fatigue behaviors of rib-to-deck welded joints were experimentally evaluated according to the most adverse loading position. Typical crack patterns were obtained from fatigue tests by cutting and MPT inspection. The relationship between reference stress condition and crack depth of specimens could be understand, according to six types of structural parameters.

In **Chapter 4**, the cause identification of the crack initiation of this structural detail were clarified by

analyze on the fatigue test results. The effect of weld residual stress on root crack initiation were clarified by using a cutting method and thermo-elastic-plastic FE analysis. The fatigue cracking patterns and their influence factors were discussed by comparing the crack sizes and crack angles in the cross section.

In **Chapter 5**, the cracking mechanism and stress responses around root tip were analyzed by establishing the matching FE models, to verify with fatigue tests results. The effect of root gap shapes, weld penetrations, and plate thicknesses on crack initiation were discussed. Besides, various root crack depths were simulated in models to clarify the stress variations occurring during the propagation stage under cyclic loading.

The part II focused on the stress responses in different locations of orthotropic steel deck which including various crack combination, and investigated the structural characteristics and mechanical properties of structure. This part was investigated in chapter 6 and chapter 7.

In **Chapter 6**, to investigate the effect of rib fractures, and the combination of rib crack and rib-to-deck cracks, the field tests results were compared with FEA by simulating the long artificial cracks. The structure responses and stress behaviors were analyzed, the effects of asphalt stiffness and various loading positions were also discussed.

In **Chapter 7**, the FEA on three-span steel deck was conducted to investigate the stress characteristics of structure with artificial crack combinations. By establishing the solid-shell hybrid models, the interaction between rib cracks and other weld details were clarified. Thus not only the local stress around crack position, but also the crossbeam response was evaluated by hot spot stress method.

In **Chapter 8**, it summarized the conclusions of the obtained results for the experimental and numerical studies.

## ACKNOWLEDGEMENTS

After an intensive period of three years, today is the day: writing this note of thanks is the finishing touch on my dissertation. It has been an indelible period for me, I got so much help from many people and grown up under their care.

I would like to express my special appreciation and sincere gratitude to my supervisor Assoc. Prof. Shigenobu KAINUMA. For his patience, motivation, enthusiasm, endless encouragement, immense knowledge and guide throughout my three years of research. He always been available to advise me even he is busy with his daily routine work, make him a great mentor. He inspired me about the research in any way deeply. Thank you for your kindness and for accepting me three years ago to experience your extensive knowledge in steel bridge. Likewise, my thousands of appreciation also goes to Advisory Committee, Prof. Yoshimi SONODA, Prof. Hidenori HAMADA. For their precious suggestions and insightful comments with regard to improve this research work. Thank you also for letting my defense be a memorable moment.

Additionally, thanks to our Prof. Shinichi HINO, the vice-president of Kyushu University. Thank you for giving me the chance to participate the site visit. I really learnt a lot from you even only have a talk for few times. You are our spiritual leader, I feel very grateful to be a member of your lab. I would also like to address my thanks to the tender secretary of my laboratory Ms. KATO, gentle teaching assistant Mr. HATAKEYAMA, and also goes to Mr. SHIBATA for his tremendous help, for his non-stop help throughout my experimental work. Moreover, I would like to thank Prof. Hanbin GE and Prof. Hohai JI for giving me the opportunity to perform my study in the Kyushu University, you are not only my best teachers but also helpful friends.

My special gratitude also is dedicated to the Ministry of Education, Culture, Sports, Science and Technology (MEXT) of Japan for providing financial study assistance during my doctoral program in Japan. My grateful acknowledgement. I'd like to show my grateful to Miss. OOIWA, she gave me help and care about all issues in my studying life.

Also, I wish to express my gratitude to my colleagues, seniors and juniors, who supported me during the research. They provided me not only with their academic knowledge but also with their enthusiasm. I really enjoyed the study life here. A special thanks to Young-Soo JEONG San for supporting me during these years, he led me do a vast of experiment and taught me a lot. Without his help in patience, I will not achieve so good performance as now. I'd like to say thank you to my office neighbor Doctor Rui GUO. As a Chinese upperclassman, he gave me many useful advices. Last not least, there are my friends. Thanks to Minami HIRAO, Hiroshi FUJIMOTO, Ryouta WATANABE, Jingxuan DU, Gaku MASHIMOTO, Kousuke YAGI, Hiroyuki MOMOTA, Fumi YAMAGATA, Keita TANIGAWA, Shaofu LIU, Katsuya YAMASHITA, we always get together, laughing and discussing something funny, it

makes me feel warm and confident to study abroad happily. Particularly to Miss. HIRAO and Miss. YAMAGATA, you are great companions, we progress together and I will never forget your kind helps.

Finally, I would also like to take this opportunity to express the profound gratitude from my deep heart to my dear Mr. Right, and my beloved mother and sister. It is because of you, I didn't feel lonely, got confidence and power to continue. All of you always there for me.

Thank you very much, everyone!

*Muye Yang*

Fukuoka, July, 2017.



---

**TABLE OF CONTENTS**

<b>ABSTRACT .....</b>	<b>I</b>
<b>ACKNOWLEDGEMENTS .....</b>	<b>III</b>
<b>TABLE OF CONTENTS .....</b>	<b>V</b>
<b>LIST OF FIGURES .....</b>	<b>IX</b>
<b>LIST OF TABLES .....</b>	<b>XIII</b>
<b>CHAPTER 1 INTRODUCTION .....</b>	<b>1</b>
1.1 BACKGROUND .....	1
1.2 OBJECTIVES .....	4
1.3 LITERATURE REVIEW .....	6
1.3.1 Specifications of orthotropic steel deck structure .....	6
1.3.2 Structural parametric analysis .....	8
1.3.3 Fatigue experimental studies .....	9
1.3.4 Fatigue crack behavior and detections .....	11
1.3.5 Finite element method .....	12
1.4 OUTLINE OF DISSERTATION .....	13
<b>CHAPTER 2 FATIGUE DAMAGES AND MECHANISMS .....</b>	<b>16</b>
2.1 INTRODUCTION .....	16
2.2 FATIGUE CASES IN ORTHOTROPIC STEEL BRIDGE DECKS .....	17
2.3 FATIGUE MECHANISMS OF WELDED JOINT .....	21
2.3.1 Fatigue life evaluation .....	21
2.3.2 Fatigue cracking process .....	23
2.3.3 Design philosophy and assessment .....	24
2.3.4 Other influence factors .....	26
2.4 MECHANICAL BEHAVIOR OF ORTHOTROPIC STEEL DECK .....	27
2.4.1 Deformation of rib and deck plate connection .....	27
2.4.2 Mechanical behavior of the rib splice joint .....	28
2.4.3 Mechanical behavior of other sub-systems .....	29

<b>CHAPTER 3 EXPERIMENTAL ANALYSIS ON FATIGUE BEHAVIOR OF RIB-TO-DECK WELD JOINT .....</b>	<b>30</b>
3.1 INTRODUCTION.....	30
3.2 FIELD LOADING TEST OF ORTHOTROPIC STEEL BRIDGE.....	30
3.3 FATIGUE TEST.....	32
3.3.1 Test specimen .....	32
3.3.2 Test set-up .....	34
3.3.3 Loading condition.....	37
3.4 TEST PROCESS AND RESULTS.....	40
3.4.1 Test process.....	40
3.4.2 Crack category.....	41
3.5 SUMMARY .....	46
<b>CHAPTER 4 RESIDUAL STRESS TEST AND CRACK BEHAVIOR ANALYSIS .....</b>	<b>48</b>
4.1 INTRODUCTION.....	48
4.2 EXPERIMENTAL MEASUREMENT OF WELDING RESIDUAL STRESS .....	48
4.2.1 Three-scale specimens and cutting method .....	48
4.2.2 Test and FE results comparison on residual stress.....	50
4.2.3 Welding residual stress of FE partial models .....	52
4.2.4 Effect of residual stress on full-scale specimen .....	55
4.3 PARAMETRIC ANALYSIS OF FATIGUE CRACK SIZES.....	57
4.3.1 Crack sizes comparison .....	57
4.3.2 Effect of stress range on crack propagation.....	60
4.4 CRACK PROPAGATION ANALYSIS .....	63
4.4.1 Crack propagation directions.....	63
4.4.2 Effect of penetration rate on crack angles .....	64
4.4.3 Effect of weld toe on root crack .....	65
4.5 SUMMARY .....	66
<b>CHAPTER 5 NUMERICAL ANALYSIS OF RIB-TO-DECK WELD JOINT WITH ARTIFICIAL ROOT CRACKS .....</b>	<b>68</b>
5.1 INTRODUCTION.....	68
5.2 FE MODELS.....	68
5.2.1 FE models with non-crack.....	68

5.2.2	FE models with artificial root cracks.....	71
5.3	PARAMETRIC ANALYSIS ON NON-CRACK MODEL .....	73
5.3.1	Effect of root gap shapes.....	73
5.3.2	Effect of weld penetration.....	75
5.3.3	Effect of plate thickness.....	77
5.4	STRESS ANALYSIS OF MODELS WITH ARTIFICIAL ROOT CRACKS .....	81
5.4.1	Effect of crack depth on stress response.....	81
5.4.2	Other influence factors .....	83
5.5	SUMMARY .....	85
<b>CHAPTER 6 STRUCTURAL BEHAVIOR OF ORTHOTROPIC STEEL DECKS WITH ARTIFICIAL CRACKS IN LONGITUDINAL RIBS.....</b>		<b>87</b>
6.1	INTRODUCTION.....	87
6.2	FIELD MEASUREMENTS .....	88
6.3	COMPARISON OF FIELD RESULTS AND FEA.....	90
6.3.1	FE models .....	90
6.3.2	FEA and field measurement comparison of double tire load tests.....	91
6.3.3	FEA and field measurement comparison of single tire load tests .....	93
6.4	COMPARISON OF RIB FRACTURE LOCATIONS .....	95
6.4.1	Effect of the mid-span and quarter span cracks on stress responses .....	95
6.4.2	Torsional rigidity of rib with butt weld crack at quarter span .....	97
6.5	STRUCTURAL RESPONSES WHEN MULTIPLE RIBS FRACTURED.....	98
6.5.1	FEA analysis under double tire loading.....	98
6.5.2	Structural responses under various transverse load cases.....	99
6.5.3	Effect of rib cracks on stress ranges at adjacent rib.....	101
6.5.4	Stress variations depending on pavement stiffness .....	103
6.6	SUMMARY .....	105
<b>CHAPTER 7 STRESS CHARACTERISTICS OF DECK PLATE AND CROSSBEAM WITH BUTT WELD CRACK COMBINATIONS.....</b>		<b>106</b>
7.1	INTRODUCTION.....	106
7.2	FE ANALYSIS OF RIB CRACK COMBINATIONS .....	107
7.2.1	FE models .....	107
7.2.2	Local deformations at crack cross section .....	110
7.2.3	Local stress variations at crack cross section .....	112

7.2.4	Stress response of other structural details .....	113
7.3	STRESS CHARACTERISTIC OF RIB-TO-CROSSBEAM CONNECTIONS .....	115
7.3.1	Effect of transverse loading on cut-out stress.....	115
7.3.2	Effect of longitudinal loading on cut-out stress .....	116
7.3.3	Evaluation on cope hole stresses by hot spot method .....	118
7.4	STRESS CHARACTERISTICS OF STRUCTURE WITH 16MM-DECK PLATE .....	121
7.4.1	Effect of rib cracks on stress ranges at adjacent rib .....	121
7.4.2	Effect of pavement stiffness on structural response .....	122
7.4.3	Effect of rib cracks on cut-out stresses .....	122
7.5	CONCLUSIONS .....	124
<b>CHAPTER 8 SUMMARY AND CONCLUSIONS .....</b>		<b>126</b>
8.1	SUMMARY OF WORKS .....	126
8.2	CONCLUSIONS .....	127
8.3	RECOMMENDATIONS FOR FUTURE WORKS .....	129
<b>BIBLIOGRAPHY.....</b>		<b>131</b>

## LIST OF FIGURES

Figure 1.1 Perspective drawing of a typical orthotropic steel deck structure.....	1
Figure 1.2 Typical fatigue cracks in orthotropic steel bridges .....	3
Figure 1.3 Occurrence proportion of typical fatigue cracks in Japan.....	3
Figure 1.4 Root-deck cracks at rib-to-deck welded joints.....	5
Figure 1.5 Rib-to-rib cracks at field weld [10].....	5
Figure 1.6 Typical shape of U-rib in orthotropic steel decks .....	7
Figure 1.7 The cut-outs of crossbeam at rib-to-crossbeam connections .....	9
Figure 1.8 Cracks of butt weld and fillet welded joint.....	11
Figure 1.9 Scheme of this study .....	15
Figure 2.1 Fatigue cracks of steel bridge in Japan [18].....	18
Figure 2.2 Crack visible at downside and upside of deck plate .....	19
Figure 2.3 Root crack visible under wearing course [24] .....	19
Figure 2.4 Root cracks in other countries [79].....	21
Figure 2.5 Crack occurred at the rib splice joint .....	21
Figure 2.6 Fatigue strength and S-N curve of JSSC specification .....	22
Figure 2.7 A schematic of the typical fatigue growth behavior of cracks .....	23
Figure 2.8 Effective stress at the weld joint [10] .....	27
Figure 2.9 Local effects on rib-to-deck connection from wheel loading .....	28
Figure 2.10 Mechanical behavior of the rib splice joint.....	29
Figure 3.1 Field measurements in loading test of orthotropic deck bridge .....	31
Figure 3.2 Field stress histogram measurement for three-days.....	32
Figure 3.3 Three views of specimens.....	32
Figure 3.4 Weld joint photos of specimens in etching test.....	33
Figure 3.5 Test setup and loading cases .....	35
Figure 3.6 Loading jig and wheel load dispersion .....	35
Figure 3.7 Loading dispersion static tests .....	37
Figure 3.8 Reference strain distributions of static loading tests.....	37
Figure 3.9 Measured reference stress range of specimens .....	40
Figure 3.10 Reference stress ranges and cycles during fatigue loading tests.....	40
Figure 3.11 Typical crack patterns of test results .....	41
Figure 3.12 Crack depth distribution of deck/root cracks .....	43
Figure 3.13 MT inspections of typical cracking specimens [100] .....	46
Figure 4.1 Dimensions and cutting positions of specimen.....	49

---

Figure 4.2 Dimension of specimens and welding joints.....	49
Figure 4.3 Location of strain gages in the cutting method (unit: mm) .....	50
Figure 4.4 Residual stress distribution comparison.....	50
Figure 4.5 FE analysis model and root gaps.....	51
Figure 4.6 Temperature dependencies of the thermal and mechanical properties .....	51
Figure 4.7 Residual stress distribution in deck plate to U-rib .....	52
Figure 4.8 FE analysis results.....	54
Figure 4.9 FE analysis on principal stress of D12U6SP75G0.....	54
Figure 4.10 The location of cut out pieces of specimen .....	55
Figure 4.11 Residual stress distribution comparison .....	56
Figure 4.12 Measured reference stress of D12U6SP75.....	57
Figure 4.13 Definition of root crack parameters .....	58
Figure 4.14 Measures data of root cracks of all specimens .....	58
Figure 4.15 Effect of structural parameters on root crack propagation .....	59
Figure 4.16 Effect of weld penetration rate on crack propagation .....	60
Figure 4.17 Relationship between crack depth and length (Effect of penetration rate).....	61
Figure 4.18 Effect of weld penetration rate on crack propagation .....	62
Figure 4.19 Relationship between crack depth and length (Effect of plate thickness).....	62
Figure 4.20 Dynamic reference stress range at mid-span.....	62
Figure 4.21 Root crack propagation angles of cross-sections .....	63
Figure 4.22 Crack depth comparison of D12U6SP0-1 cross sections.....	64
Figure 4.23 Average crack tip angles of specimens under -140 to 40 MPa.....	64
Figure 4.24 Comparison of root and toe crack tips of D12U8SP50-1.....	65
Figure 4.25 Comparison of toe and root cracks (40 to -140MPa).....	66
Figure 5.1 FE models and the loading conditions .....	69
Figure 5.2 Basic FE model and the dimensions of root gaps (D12U6SP75).....	69
Figure 5.3 Stress distributions of specimens in longitudinal direction.....	71
Figure 5.4 Relationship between reference stress and root stress .....	71
Figure 5.5 Stress distribution at welded joint of model D12U8SP50.....	71
Figure 5.6 Definitions of FE Analytical model .....	72
Figure 5.7 Transverse stress of models in cracking direction with artificial root cracks.....	73
Figure 5.8 Details of tria-gap of model D12U6SP75 .....	73
Figure 5.9 Comparison of models with different root gap geometry (D12U6SP75).....	74
Figure 5.10 Major principal stress contours .....	75
Figure 5.11 Effect of weld penetration rate on root tip stress of D12U6.....	76
Figure 5.12 Stress comparison of (D12) U8SP75/U8SP50/U6SP75.....	76

---

Figure 5.13 Stress distribution in y direction at mid-span .....	77
Figure 5.14 Stress response of models in longitudinal direction.....	77
Figure 5.15 Effect of deck plate thickness on stress .....	78
Figure 5.16 Unit stress comparison of D12/D14/D16 deck plate under $P_{max}$ .....	78
Figure 5.17 Displacements of root tips in y and z directions .....	78
Figure 5.18 Structural deformation and principal stress of root tip at mid-span.....	79
Figure 5.19 Structural deformation and principal stress of root tip at mid-span.....	80
Figure 5.20 Stress variations in deck plate thickness.....	81
Figure 5.21 Stress variations at crack tip surrounding under half loading cycle .....	82
Figure 5.22 8mm-crack models during half cycle.....	82
Figure 5.23 Major principal stress contours of 8 mm-crack model .....	83
Figure 5.24 Stress range comparison of reference point and crack tip surrounding .....	84
Figure 5.25 Effect of penetration rate on stress during crack propagation.....	85
Figure 5.26 Effect of structural dimensions on fatigue strength. ....	85
Figure 6.1 Field welding of trough splice joints [10].....	87
Figure 6.2 Loading cases of field measurement (Unit: mm).....	89
Figure 6.3 Artificial cracks by gas-cut in actual bridge .....	89
Figure 6.4 FE model of solid elements .....	90
Figure 6.5 FE models with artificial cracks .....	91
Figure 6.6 Test results and FEA comparisons .....	92
Figure 6.7 Displacement of deck plate bottom.....	93
Figure 6.8 Transverse stress of deck plate bottom .....	94
Figure 6.9 Longitudinal stress of rib bottom.....	94
Figure 6.10 Images of artificial cracks in FE models (Unit: mm).....	95
Figure 6.11 Comparison of the mid-span and quarter span cracks .....	96
Figure 6.12 Deformation of D3-Qua model.....	96
Figure 6.13 Crossbeam deformation of the models with quarter crack under loadcase2.....	98
Figure 6.14 Stress responses with rib-to-rib cracks at quarter span .....	98
Figure 6.15 Details of various models with artificial crack combinations at mid-span .....	99
Figure 6.16 Deformations at mid-span of models.....	100
Figure 6.17 Stress distribution at mid-span under three loading positions of model N .....	101
Figure 6.18 Longitudinal stress of rib bottom under the load position t3 .....	102
Figure 6.19 Effect of pavement stiffness on structural response at certain location .....	103
Figure 6.20 Stress and stress ratio variations depending on the pavement stiffness .....	104
Figure 7.1 The cut-outs and typical cracks at crossbeams .....	106
Figure 7.2 Solid-shell hybrid element models.....	108

---

Figure 7.3 Loading conditions of FE models .....	109
Figure 7.4 Major principal stress contours of models under t1 (Deformation: 100) .....	110
Figure 7.5 Deformation of the deck plate.....	111
Figure 7.6 Transverse stress distribution at the bottom of the deck plate.....	112
Figure 7.7 Longitudinal stress distribution at the bottom of ribs .....	113
Figure 7.8 Stress distributions at rib-to-deck connections in longitudinal direction .....	114
Figure 7.9 Toe stresses at rib-to-deck connections in longitudinal direction.....	114
Figure 7.10 The crossbeam stress of rib2 under transverse loading t1 .....	115
Figure 7.11 Stress distributions at middle axial plane of cut-outs in model-e.....	116
Figure 7.12 Crossbeam details of FE models .....	117
Figure 7.13 Target crossbeam and five longitudinal loading positions .....	117
Figure 7.14 Maximum principal stresses of model-f crossbeam.....	118
Figure 7.15 Maximum principal stresses at Toe7 of cope holes.....	118
Figure 7.16 Comparison of inside and outside stresses at rib2 by hot spot method .....	119
Figure 7.17 Node stress and hot spot stress hs1/2(outside) of crossbeam.....	120
Figure 7.18 Comparison of node stress / hot spot stress at cope hole path .....	120
Figure 7.19 Longitudinal stress distribution of rib1 .....	121
Figure 7.20 The structural response of deck plate bottom at mid-span of 16mm-models.....	122
Figure 7.21 The stress distributions at scallops in middle-axial plane of crossbeam .....	123
Figure 7.22 The stresses at welded joint of cope holes .....	123



---

## LIST OF TABLES

Table 1.1 Dimensions of U-rib in orthotropic steel decks.....	7
Table 2.1 Typical cases of bridge damages in Japan [73] .....	18
Table 2.2 The cases of through-deck crack of steel bridges in Holland [77] .....	20
Table 2.3 Review of range of detail categories in different codes .....	22
Table 2.4 Type of stress for fatigue assessment .....	26
Table 2.5 Assembly and description of orthotropic deck systems and their behavior [4] .....	29
Table 3.1 Dimensions of the orthotropic steel decks of A1 Bridge.....	31
Table 3.2 Chemical composition and mechanical properties .....	33
Table 3.3 Welding conditions of specimens .....	33
Table 3.4 Dimensions of specimens .....	34
Table 3.5 Stress conditions of all specimens.....	39
Table 3.6 Relationship between stress condition and crack depth .....	43
Table 3.7 Test stresses and the measured crack depth.....	44
Table 4.1 Welding conditions of three-scale specimens.....	49
Table 4.2 Parameters of FE analysis models.....	53
Table 4.3 Geometry of weld toe .....	65
Table 5.1 Loading cases of FE models.....	70
Table 5.2 The correlation coefficient between root tip and reference stress .....	70
Table 6.1 Effect of the rib-to-rib crack locations on structural responses.....	96
Table 6.2 Maximum stress range at the bottom of rib1 and equivalent conversion .....	102
Table 7.1 The models with artificial cracks at ribs.....	109
Table 7.2 Criteria for deflection of orthotropic plate decks .....	111
Table 7.3 The relative displacement and allowable deflection of deck plate .....	111
Table 7.4 The maximum stress range and the amplification of rib1 .....	121



## Chapter 1 Introduction

### 1.1 Background

The orthotropic steel decks (OSDs) have been commonly applied to long-span bridges and expressways because of the structural properties such as low self-weight, high load-carrying capacity and high stiffness [1]. There are some other good characteristics like slenderness, durability, shop welding and rapid construction [2] also given the orthotropic steel decks high popularity all over the world. An orthotropic steel deck (OSD) consists of a deck plate supported in two perpendicular directions by a system of longitudinal stiffeners and transverse crossbeams, which are spanned by main girders in turn [3]. Orthotropic bridges have been built in several ways, and there are many different details and typical connections. Most elements are connected by welding. A part view of a typical orthotropic steel deck structure as shown in Figure 1.1.

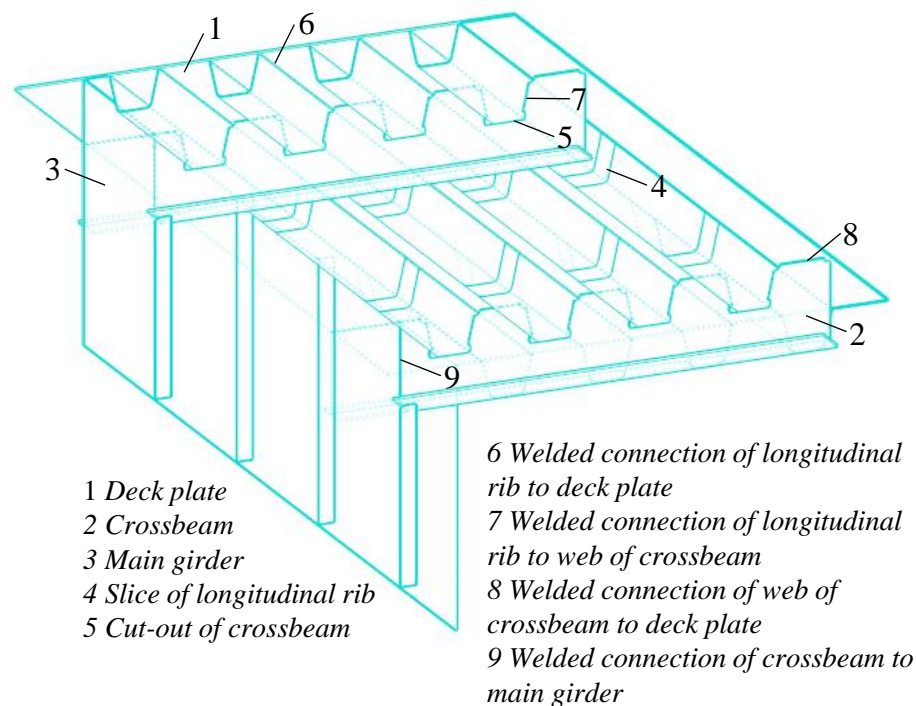


Figure 1.1 Perspective drawing of a typical orthotropic steel deck structure

The development of the OSD began in the 1930's in Germany, and continued throughout the last century [4]. In the post-war the orthotropic systems were favored and further improved [5]. Many orthotropic steel decks were constructed in Europe and other countries since the 1960's. Nowadays there are more than 1000 orthotropic steel bridges in Europe, out of which 86 are in the Netherlands. In Asia, there are several bridges that are built or being built, especially in Japan and China [6]. In the USA, their number of is remarkably small as only 51 out of its 650,000 bridges are orthotropic steel bridges [7].

The orthotropic steel deck structures are widely used in longest-span bridges, for example, the Akashi-Kaikyo Bridge situated in Japan is a representative bridge.

Despite inherently possessing excellent structural properties of the OSD system, the fatigue damages have been observed earlier than expected in several bridges built with orthotropic decks [4]. Orthotropic steel decks have a relatively long service life, but the OSDs have shown prone to fatigue and are expensive to repair if critical cracks appear and this must be taken into consideration during design and construction [1]. Therefore, take full account of the economy and durability, the OSD would become an economical alternative when the following issues are important: lower mass, thinner sections, rapid installation, and cold-weather construction [8].

The lower superstructure mass is the primary reason for the use of orthotropic decks in long-span bridges. Generally, the OSD allow a decrease in the deadweight to about 1/3 to 1/2 compared with that of concrete bridges [9]. The amount of material to be saved increases with the length of the spans (AISC, 1962). For most of the long-span cable supported bridges, it is a significant improvement when the dead load reduction achieved by abandoning the reinforced concrete deck and switching to an OSD system. Because the structure dead load causes 60 to 70% of the stresses in the cables and towers of long span bridges [10,11]. Besides, the improved performance of the bridge during an earthquake also related with its lower self-weight (Magnus and Sun, 2000).

According to statistics in Japan, the steel bridges accounted for about 40% of the total number of bridges on the major expressways in 2003 [12]. The vast majority of orthotropic steel bridges were extensively constructed in the 1960s to 1980s. The fatigue cracks have been reported in the welded joints of OSDs after several years in service [13–15]. This is partly a consequence of the significant increase of both traffic load and the fact that orthotropic decks chiefly were designed with regard to static load behavior [16].

In the last decades, due to the changed operating environment including the emergence of heavy-duty vehicles and increasing traffic volume, several fatigue cracks were detected in the deck structures of these bridges under the heavy vehicle lanes. Especially for the bridges in some important transportation routes which over 20years of service with the frequent passage of overloaded transport vehicles [17]. In addition, an OSD is involved the numerous plates and welded joints, as a consequence of high cyclic stresses by wheel loads, in conjunction with inevitable fabrication defects have seen an increase in fatigue cracks. Fatigue cracks have been recognized as a major concern in OSDs.

The ribs in the OSD can either be open or closed. The most common type is closed trapezoidal ribs [10]. Advantages of an open rib system are ease of production, inspections and maintenance as well as flexibility in dimensions and easy assembling with rest of the deck [4]. However, about twice as much welding is required in a deck with open stiffeners compared to an equivalent deck with closed ribs. An orthotropic deck with closed stiffeners has a significantly better capacity to distribute the traffic loads compared to a system with open ribs (AISC, 1962). The high flexural and torsional rigidity of the closed rib system makes it superior regarding erection and construction of the bridge. However, the field splices

for closed ribs are more difficult to perform than the ones for open ribs. Also the fatigue sensitive welds between the deck plate and stiffener requires high quality and care in fabrication [4].

After 1975, the U-shape longitudinal rib was mainly used in OSD construction in Japan. For the bridge structure with U-ribs, the following typical fatigue cracks have been reported in recent years [15], as shown in Figure 1.2. These fatigue cracks mostly occurred at the welding connections between the ribs and crossbeams; the rib-to-deck welded joints; and the butt welds of trough ribs, etc. The proportion of typical crack types at the Metropolitan Expressway, Hanshin Expressway[18] and the statistical analysis on urban highway by Mori et al [14], as shown in Figure 1.3.

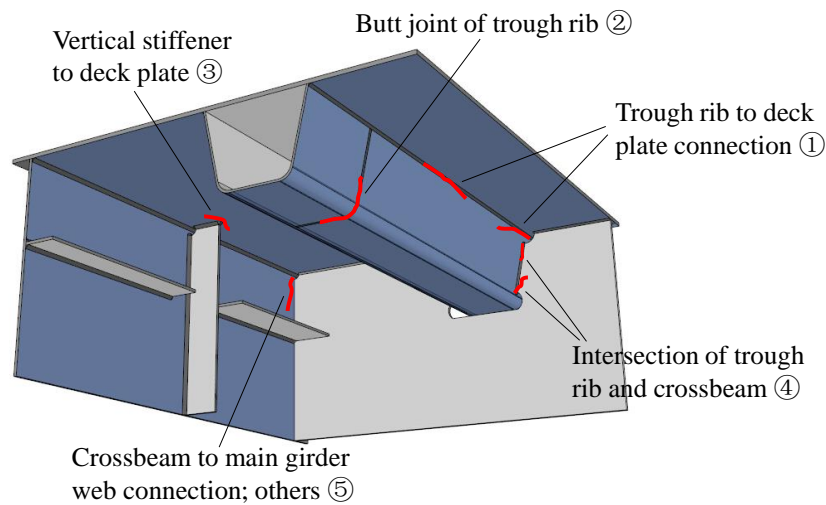


Figure 1.2 Typical fatigue cracks in orthotropic steel bridges

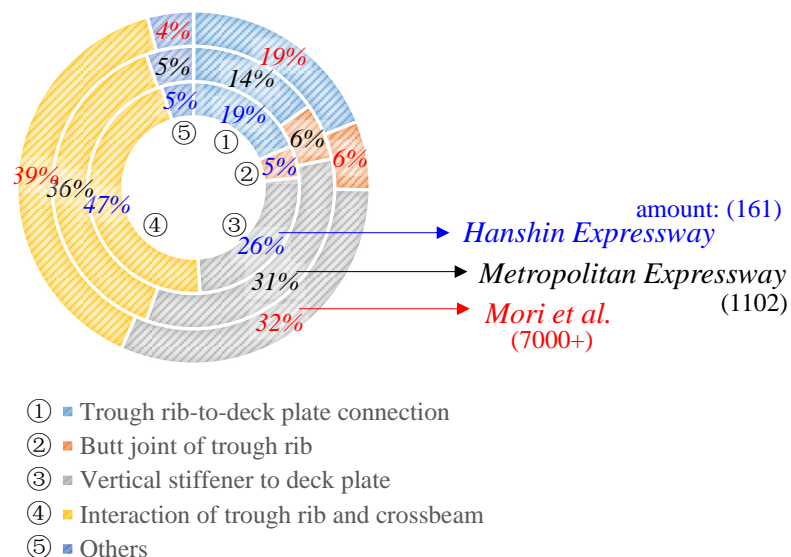


Figure 1.3 Occurrence proportion of typical fatigue cracks in Japan

Among the various fatigue cracks reported in OSDs in Japan, the weld toe crack which located at the rib-to-cross beam connection(type ④) with a partially welded joint, and the crack occurring at the

connection of vertical stiffener to deck plate (type ③), are most common types. Because for either open or closed ribs in the OSD, crack types ③ and ④ might occurred. However, a crack occurred at root tip of rib-to-deck connection (type ①) or at butt joint of trough ribs (type ②) are the two types of principal crack modes associated with the OSD with U-shape ribs. It has been reported that fatigue cracks occurred at the field welds of U-ribs account for about 5~6% of the total damage types in orthotropic steel decks [14]; the fatigue cracks initiated at the weld roots of the fillet welds accounts for about 14~19% of the total damage types in OSDs [19].

Fatigue cracks in orthotropic steel bridges significantly occurred at partial-penetration fillet-welded connections owing to the cyclic load stress. Rib-to-deck welded connections are directly supported the traffic, and submitted to local transverse bending moments. Besides, high residual stress and inherent defects existed at welded joint. Moreover, the variable combination of local load effects made it susceptible to fatigue cracking. A rib-to-deck crack (type ①) usually initiated at the weld root, and propagated into the deck plate or through the weld bead. These fatigue cracks initiated from the hidden location might causing other secondary damages. For instance, the root-deck cracks have potential directly lead to pavement damages such as asphalt cave in, and then affect traffic safety. In particular, the root-deck crack is very hard to be detected and repaired even after it grown through the deck plate due to the covered wearing surface, which might have serious implications to bridge safety. Thus, the fatigue cracks of the weld root between the deck plate and U-rib are one of the most serious cracks, and have received much attention [20]. Recently, even the long through thickness root cracks have been reported and are gradually increasing in occurrence [13,14,21,22].

The rib-to-rib cracks (type ②) might be propagate to be a large crack rapidly once this type of crack occurred, because the bottom of U-ribs mainly subjected to the tensile stress in service. Moreover, the longitudinal ribs were usually connected by field welding, most of the rib cracks were found in the welding material, along the lines of the butt welds [23]. Thus the quality of butt welded joint which depend on the site fabrication might be not so stable relative to the shop welding. The occurrence of fatigue cracks at multiple U-rib were often been detected in actual bridges.

At present, U-ribs account for about 60% stiffeners in the OSD construction of national road in Japan. Therefore, a large number of single-fillet weld joints and butt joints are existing in steel bridges, because of the wide use of closed ribs [24]. Above all, study on the fatigue behavior of these welded joints and root cracks in OSDs with U-ribs would always be an important issue that we face.

## 1.2 Objectives

The research presented in this thesis is directed towards cracks at the welded joints of steel bridges with closed stiffeners. The principal aim is to investigate the fatigue behaviors and cracking characteristics of welded joints in OSD. For an OSD structure, the crack types which associated with U-rib component could be mainly divided into three categories as mentioned previously:

*Category-1. Cracks in the longitudinal weld between deck plate and rib.*

*Category-2. Cracks in the butt joint of rib splice.*

*Category-3. Cracks in the connection between longitudinal rib and crossbeam.*

This thesis mainly deal with the case that cracks occurred at root tip of U-rib, and the rib cracks located at mid-span between two crossbeams, which are defined in category 1 and 2 above. Besides, the stress characteristics of the welded joint between rib and crossbeam would be effected by category 1 and 2, and then Category 3 crack might be easier to occur.

Firstly, the category-1 is the crack in the longitudinal weld between deck plate and rib. There are four crack initiation positions in the rib-to-deck connection, as shown in Figure 1.4. Among them, only root cracks were observed in actual bridge in Japan, and the root-deck crack was detected more frequently than the root-bead crack based on the field investigation. The root-deck is recognized as one of the most dangerous cracks in OSD. Moreover, there are numerous factors influencing the structural performance and its cracking mechanism still insufficient. Therefore, the local stress of rib-to-deck fillet weld and the crack patterns of root-deck welded joints were investigated in this study by test and numerical parametric analysis.

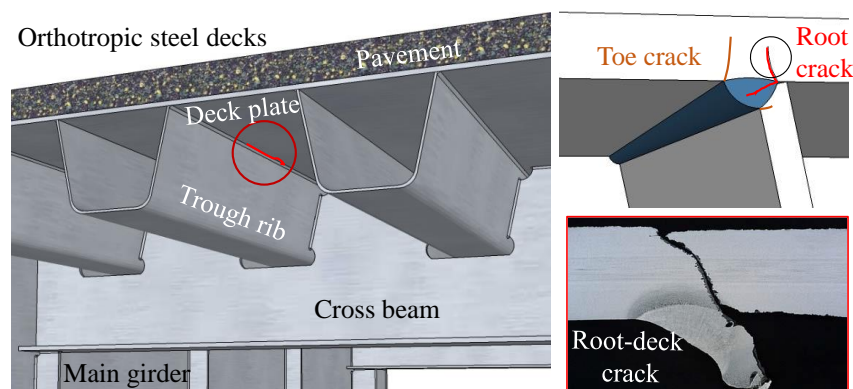


Figure 1.4 Root-deck cracks at rib-to-deck welded joints

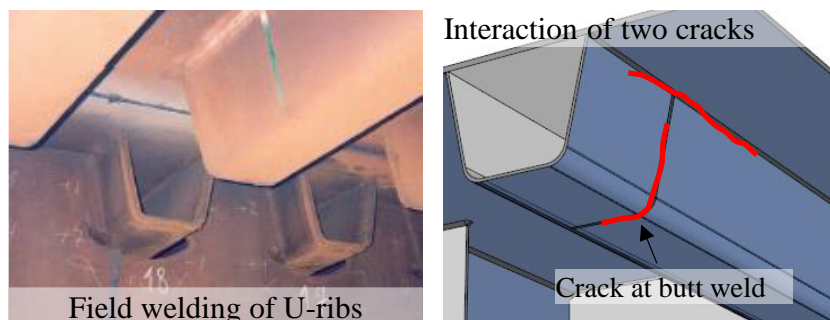


Figure 1.5 Rib-to-rib cracks at field weld [10]

Secondly, the crack in the butt joint of rib splices (Category-2) as shown in Figure 1.5, would lead to the changing of global stress response. The local stress would also be enlarged which is important for the security prediction and bridge maintenance. It is significant to consider the combination of rib

fractures and rib-to-deck cracks, the mutual effect of large cracks at adjacent U-ribs. In this study, the global structural response of different cracked combinations were clarified by consider the different loading cases and pavement stiffness according to seasonal temperatures. Furthermore, the stress characteristics at the connection between rib and crossbeam (Category-3) were evaluated under various loading positions.

### **1.3 Literature review**

There were many provisions regarding the structural dimensions of OSD bridges, and the criteria for deflection, displacement and penetration rates were suggested in different specifications. Besides, the cracking mechanisms of fatigue cracks in OSD were studied by several researchers. In particular, the local stress around rib-to-deck welded joints had been investigated based on experimental and numerical analysis results. In recent years, various field measurements, fatigue tests, and stress analyses have been conducted [9-11]. Fatigue tests of full-scale orthotropic steel decks have also been carried out, focusing on determining fatigue resistance and demonstrating the applicability of the fatigue assessment approaches for various structural details [12]. Most of these studies investigated the fatigue behaviors of rib-to-deck welded joints [13], rib-to-crossbeam welded joints [14], and the variation of these flexural stresses at the deck plate and U-ribs under the action of wheel loads [15]. An overview of previous research is presented in the following:

#### **1.3.1 Specifications of orthotropic steel deck structure**

The stiffeners of OSD were developed with various cross sections, including open stiffeners and closed stiffeners. To increasing the stiffener span length and reduce the number of crossbeams needed and thus reduce the number of structural elements and connections, it was found that the closed stiffener with one-side fillet weld is a good solution. Large cost savings resulted from the reduced amount of welded connections. For instance, a weld length of the rib-to-deck welded joint could reduce to 50% achieved by the one-sided longitudinal welds compared with the both sided welds of the open stiffeners.

Usually, the V, U and Trapezoidal shapes were used as closed rib. They were made from cold pressed plates and were known as “Trough” stiffeners. Initially the V-shape was used in OSDs, with a depth of 200 mm and a plate thickness of 6 mm, but due to its small cross sectional area, the increase in bending capacity was limited compared to that of the open stiffeners. Then, an improvement was the U-shaped stiffener. Tromp reported tests on U-shaped stiffeners for crossbeams in Floating Decks and Ypeij [25] showed the application of these decks. The bottom of these stiffeners acts like a true bottom flange and the maximum spans are approximately 3.5 m.

In Japan, the U-shape longitudinal rib were widely used in steel bridge constructions with the increase in numbers of medium-sized span. At present, the application of U-shape rib has become mainstream for the rationality of structure. Except some special case, the U-ribs are hardly used in curved bridges, because it is difficult to fabricate curved U-ribs. In general, the dimensions of U-rib were based on the



recommendation by Japan Society of Steel Construction (JSS II 08-2006)[26], as shown in Figure 1.6.

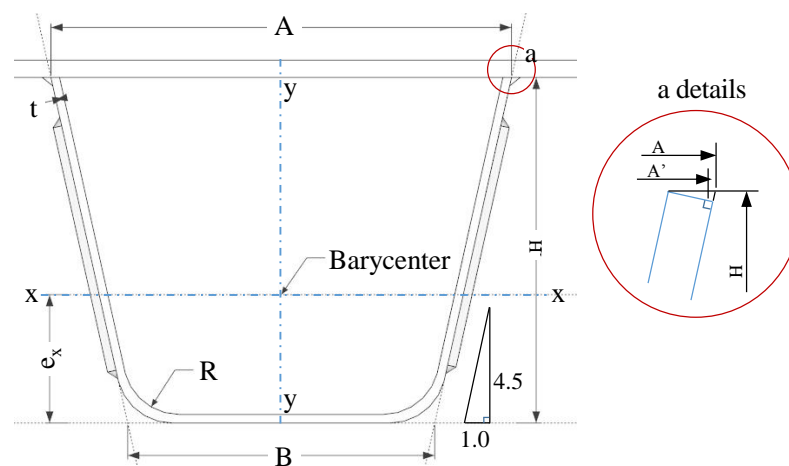


Figure 1.6 Typical shape of U-rib in orthotropic steel decks

Moreover, the requirements for fatigue design should be significant. The revision of “Specifications for Highway Bridges” in 2002 enhanced the provisions of the fabrication and construction of OSD according to fatigue design [27]. Based on “Fatigue design guidelines for steel highway bridges” [21], the applicability of an OSD should follow as:

- 1) The spacing between crossbeams,  $L \leq 2.5\text{m}$

The structural details were designed different before and after 2002 in Japan, because of the revision of specification. Therefore, the crossbeam spacing is limited to 2.5m in the conventional structure currently, but the case of 3~4m spacing were also existed.

- 2) The dimensions of typical U-rib

At first, three types of U-rib was adopted:  $300 \times 220 \times 6-30$ ,  $320 \times 240 \times 6-30$ ,  $320 \times 260 \times 6-30$ , the radius of cut-outs are set to  $R=5 \cdot t=30\text{mm}$ . After 1983, the type of  $300 \times 220 \times 6-30$  was canceled, and 8mm-thick rib was added. The radius of cut-outs were all changed into  $R=40\text{mm}$ . The parameters of these four types of U-rib as shown in Table 1.1.

Table 1.1 Dimensions of U-rib in orthotropic steel decks

Specimens (mm)	A	A'	B	H (mm)	t	R	$e_x$	$I_x \times 10^4$ ( $\text{mm}^4$ )
① $320 \times 240 \times 6-40$	320	319.4	213.3	240	6	40	88.6	2460
② $320 \times 260 \times 6-40$	320	319.4	204.4	260	6	40	99.1	3011
③ $320 \times 240 \times 8-40$	324.1	323.3	216.5	242	8	40	89.9	3315
④ $320 \times 260 \times 8-40$	324.1	323.3	207.7	262	8	45	100.3	4055

- 3) Thickness of deck plate  $t_d$ ,  $12\text{mm} \leq t_d \leq 16\text{mm}$

In addition, to ensure the fatigue durability of OSD, the provisions of the steel deck provided in fatigue guidelines. The revision of “Specifications for Highway Bridges” in 2012 shows the deck plate thickness should increase from 12mm to 16mm to prevent the fatigue cracks propagating through the deck plate.

In particular, when U-shape closed rib was used, the thickness of the deck plate should equal to or larger than 16mm where the position directly under the wheel load of large automobiles.

4) Penetration rate of rib-to-deck welded joint  $\geq 75\%$  of rib thickness

The throat thickness of rib-to-deck welded joint was controlled for ensuring the fatigue durability against the bead crack. The penetration rate of rib-to-deck welded joints in longitudinal was suggested that more than 75% of the rib plate thickness (JSS II 08-2006-5.3.1) [26].

5) Longitudinal rib welded joints of closed section

In general, the friction joint of high-strength bolts was recommended in “Specifications for Highway Bridges II 9.4.7” [27]. In the case of a welded joint of closed rib, the full penetration butt welded joints using a backing strip was also suggested in provisions.

6) The distributed loads according to thickness of pavement

From 1964 to present, the effect of pavement distributed load has never taken into account by “Specifications for Highway Bridges” in Japan.

The steel properties of material, welding technique, and the dimensions of structure detail, were varies in different countries, thus the specifications were different from one to another. But the durability design and fatigue design principles of OSD were similar. Some comparison would be listed in Chapter 2.

### 1.3.2 Structural parametric analysis

The local stress at structural details are sensitive to factors like weld penetration rate, fabricate process, fatigue load cases and even pavement properties. In general, the structural optimization by parametric analysis were steadily conducted during fatigue design of OSD. Deck plate thickness and weld penetration rate were two kinds of parameters that are discussed mostly.

A new rib-to-deck detail was proposed for orthotropic steel deck, in which the deck plate is 1.5times thicker and the closed ribs are approximately 1.5times larger than those of the standard deck [28]. In addition, the use of a thicker deck plate (14 or 16mm) was recommended (instead of 12mm), because this significantly increases the fatigue life of a rib to deck welded connection [17]. Until now, fatigue cracking from the weld root has not been reported in thicker deck plates. There has been a tendency to use thicker plates as preventive measures to avoid fatigue cracking in new orthotropic steel bridges. However, even though it was summarized that the use of thick deck plate (~16 mm) might improve the fatigue durability of the rib-to-deck joints, whereas the fatigue strength gradually decrease as the deck plate thickness increases which might due to thickness effect [17,22].

As mentioned before, high penetration rate of rib-to-deck welds could prevent from bead cracks. Currently the requirement by LRFD Bridge Design Specifications [29](AASHTO 2010) is that the rib-to-deck welds need to be fabricated with minimum penetration of 80% of the rib thickness, while it is required as 75% in Japan Road Association Specifications [27](JRA 2002). Most researchers considered that a higher penetration rate could lead to a higher strength in the weld joint. Recently, full-scale fatigue

tests of orthotropic steel decks conducted by some researchers have proved that a shallower weld penetration at the partial joint penetration (PJP) joint appeared to have a positive effect on enhancing the fatigue resistance. Rib-to-deck fatigue tests of small specimens also showed that the specimens with weld melt-through seemed to have slightly lower fatigue strengths than those with 80% PJP [17,30]. The finite element analyses [30] indicated that a shallower weld penetration (among 40%, 60%, and 80% penetration rates) at a PJP joint had a positive effect in enhancing the fatigue resistance.

Although most researchers agree that a penetration rate below 75~80% is beneficial to fatigue durability, it is still inconclusive whether full penetration could enhance the fatigue strength of a rib-to-deck weld joint. Furthermore, In practice, the amount of penetration into the rib is difficult to control, and the actual weld size achieved varies due to many parameters, including rib plate thickness, welding process, fit-up tolerances, etc. [31]. The welding process of full penetration weld is more complex. Its reheat cycle would reduce the performance of the welded joint and easily cause weld defects.

Optimization of the shape and geometry of the cut-outs is also an important issue to enhance the performance of OSD. As a rule of thumb by Kolstein: “the sharper the notch the shorter the fatigue life” [10]. Thus the rib-deck-crossbeam welded connection is a high risk locations for the initiation of a fatigue crack. To avoid stress concentration points at the intersections between the crossbeams and ribs, cut-outs can be provided, as they have smooth edges to avoid potential defects and thus fatigue cracking. The cut-outs of crossbeam at rib-to-crossbeam connections as shown in Figure 1.7. It was suggested a well-designed cut-out results in a decrease of the out-of-plane stresses which can be kept below 25% of the in-plane stresses if the geometry is beneficial [4].

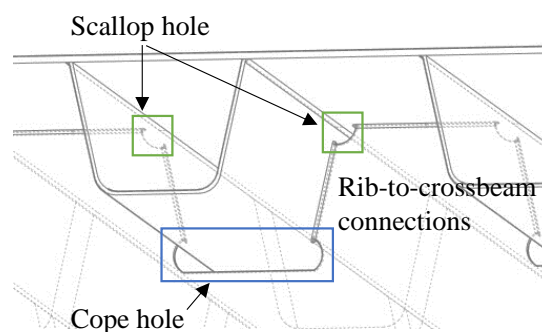


Figure 1.7 The cut-outs of crossbeam at rib-to-crossbeam connections

### 1.3.3 Fatigue experimental studies

Currently, related researches were usually focused on the fatigue strength and crack mechanism of the weld connections in OSD, which mainly based on fatigue test results. Quite a few experimental studies about the fatigue strength and influence factors of root crack were investigated by scholars. Over the period between 1974~2000, 181 fatigue tests were performed in 7 research projects with a similar setup and specimen geometry. A thorough description of them can be found in Thesis of Kolstein, 2007 [10]. In recent years, both field measurement of actual bridge and small-scale specimens were continued

conducted [13,17]. Full-scale fatigue tests of orthotropic steel decks are usually conducted to evaluate the fatigue performance, the full-scale specimens consisted of one or two panel decks were also tested under fixed fatigue loading or moving wheel loading [32–34].

Some investigators have recognized the fatigue behavior of welded joint were usually subjected to bending load a few years ago. Maddox provided the test results of as-welded joints with 11 mm thick plate loaded in bending. He presented the fatigue strength of welded joints, which had failed at weld toe or weld root, and summarized that bending tests could assure longer fatigue life than tension tests [35]. Four-point bending and tensile tests of rib-to-deck welded joints had been employed by Yamada et al. to observe the initiation point and fatigue strength, and it was found that a larger fillet weld size tended to have a higher fatigue strength[36]. Fatigue tests were also carried out by Baik et al. on non-load carrying fillet welded joint subjected plate bending. In particular, a correction factor equation has been developed for covering linearly varying stress distribution along crack propagation path under bending load [37].

These bending fatigue tests of small specimens can be conducted to evaluate the fatigue life of crack initiation and propagation within a certain length of the specimens, and it is possible to assess the fatigue crack growth and the fatigue strength. However, the boundary condition is different between the actual orthotropic steel decks and small specimens. It is difficult to compare the fatigue behavior of small specimens with that of actual orthotropic steel decks. This is because the tests are performed under constant strain range and without restraint on the rib. Moreover, the secondary stress caused by deformation and the effect of release of the welding residual stress after crack initiation could not be properly simulated in these tests.

It is still the mainstream of fatigue test by using full-scale specimen which including the deck plate, ribs and crossbeam, because of their rational boundary conditions. Many full-scale fatigue tests have been carried so far [9,33,38,39]. For instance, the wheel running tests of full-scale OSD test specimen were also been conducted. For example, Murakoshi et al. observe crack propagation behavior and evaluate fatigue durability improvement by the wheel running tests with various dimensions of full-scale OSD[40]. Sim et al. focused on the effects of fabrication procedures on fatigue resistance, full-scale two-span orthotropic deck specimens were subjected to laboratory testing, to study the effects of both weld melt-through and distortion control measures on the fatigue resistance of the rib-to-deck plate welded joint [33].

A new type of the experimental system with fixed fatigue loading were designed by Kainuma et al. to simulate the tensile stress in full-scale test, which focusing on root cracks at rib-to-deck welded joint at mid-span. Finally, the test data of field measurement were usually used to verify the accuracy of laboratory full-scale test results, based on the dynamic loading test and the stress histogram measurement [41].

Orthotropic steel decks are reviewed by Fisher et al. based on the results of full-scale prototype laboratory fatigue tests which identified the complex behavior that occurs at fatigue sensitive details and were verified by field measurements on field installations. As a result of extensive large-scale fatigue

testing, it is now possible to clearly identify and avoid details which are expected to have low fatigue strength [42].

Some researchers were also focused on effect of pavement damages on structure. The field surveys of fifty orthotropic steel decks were carried out by Inokuchi et al. to grasp their fatigue damages, asphalt pavement failures and so on. One of the major types of pavement failures was the crack that occurred just over the weld between deck plate and U-shaped rib. Then field measurements was conducted at the orthotropic steel decks which had such pavement failures. It became clear that some pavement failures might make higher stress around the weld between U-shaped rib and deck plate[43]. Four-point shear tests have been also used to study shear failure and the behavior of a bituminous-based membrane material in an OSD bridge. Shear fatigue test were conducted to investigate the pavement effect. Experience in the United States (Dublin Bridge in California), Switzerland (St. Albans Bridge in Basel), Germany (the Köln-Mulheim Bridge) indicates that once the bond between the steel deck and the surfacing is destroyed, failure of the pavement follows after a short time [44].

#### 1.3.4 Fatigue crack behavior and detections

For a fatigue crack that initiates at the welded joint of OSD, such as weld root and propagates into the deck plate, it is nearly impossible to detect it in the early stage of propagation by visual inspection. The crack at root tip of butt weld and fillet welded joint as shown in Figure 1.8.

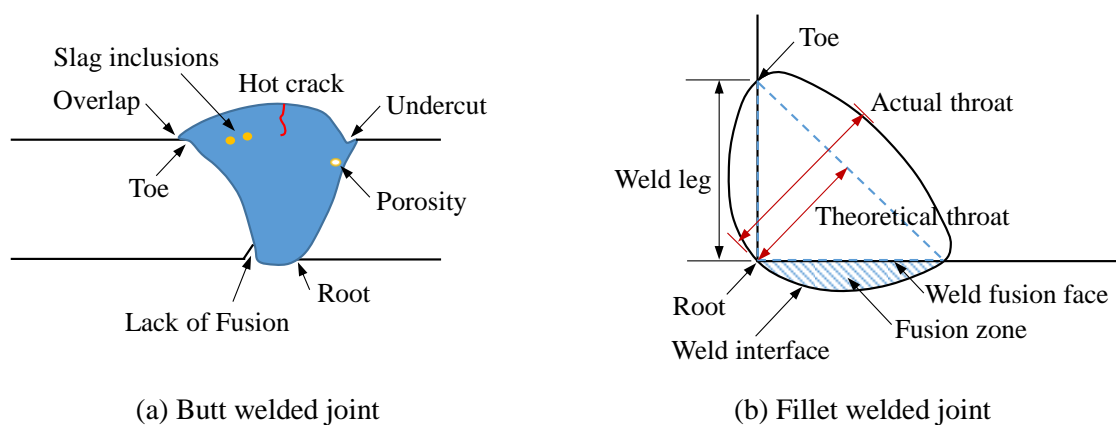


Figure 1.8 Cracks of butt weld and fillet welded joint

In Japan, as previously suggested, these studies mostly focused on an overview of macroscopic cracking and the fatigue strength assessment of the welded joints of orthotropic steel decks. For a root crack at rib-to-deck welded joint, tested specimens have been conducted to describe the typical fracture surface and macro-sections of root cracks in general using beach marks and dye marks [45]. For instance, the test results of Baik et al. showed that fatigue crack forms flat semi-ellipse during crack propagation and propagates to about 80% of plate thickness before failure [46]. The weld configuration and crack path could also be shown in cross-sections using etching tests [32]. Most other scholars have estimated the initiation and propagation process of toe cracks, typical fracture surfaces and crack shape variations of other types of weld cracks have been discussed [37,47]. The relative research about root crack

behavior still insufficient and ambiguous.

Some inspection and retrofit methods of fatigue cracks and their applicability in the field have been conducted [19,48]. The non-destructive testing (NDT) technology, e.g. dye penetration, ultrasonic, eddy current and radiology methods is also used to inspect fatigue cracks [49]. Some NDT technologies had been applied to actual bridges. For example, the non-destructive SAUT inspection were used to detect the root-deck crack which were over 6mm-depth; the infrared inspection and eddy-current inspection methods were adopted for the Hanshin Expressway[50] to detect deck plate cracks from the upper side of the pavement, and phased array ultrasonic inspection had been used to detect the through-wall flaws formed at the bottom surface of a deck plate. However, it takes a lot extra time to prepare the NDT test. It would be impossible to inspect the complete structure or to inspect all potential crack areas within a limited time. And until now, these methods were still indeterminate, and effective repair techniques had not yet been formed.

In addition, the fatigue strength can be improved by post weld treatments, and different post treatment methods were advanced. Generally, the methods can be divided into two groups [51,52]. Firstly, the changing of shape or improvement of the surface geometry at welded joint, where the stress concentration factor can be reduced. The burr grinding and TIG dressing are the main approaches to improve the shape and surface geometry of welded joints [53]. Secondly, the correction of initial residual stress is also important for fatigue strength.

Thereby, the press reforming in fabrication process; hammer and needle peening; as well as Ultrasonic Impact Treatment (UIT), are the primary approaches used to improve the residual stress conditions by inducing residual compressive stress at the weld toe, thus the fatigue life can be extended [54–57]. However, those methods could only be used before crack occur, which narrows down their applicability. During the design and maintenance phases, the re-decking with steel fiber reinforced concrete (SFRC) [58] and the use of large-sized trough ribs/deck plates have been considered as the two possible solutions to prevent cracking. However, the technological constraints and high maintenance costs decided the problem cannot be solved essentially for the OSDs in operations.

### **1.3.5 Finite element method**

Due to the time-consuming and high costing of fatigue tests and field measurement, the parametric analysis were mostly carried out by FE analysis. The Finite Element Analysis can also get the local stress where the position is difficult to be measured in test. For a structural detail such as the weld root tip of rib-to-deck connection, its stress is hard to be evaluated via fatigue tests. Various structural details and parameters could be considered in FE analysis [45]. Analytical studies usually focused on the local stress around the weld joint such as rib-to-deck connections [59]. However, the stresses in a FE model are singular in a sharp notch, the obtained values could be questioned. Thus different stress evaluation methods were investigated. For the fatigue assessment of welded structures, different concepts are applied: nominal stress, structural stress, local stress and fracture mechanics concepts [60].

The nominal stress method for fatigue evaluation is dominant in the steel bridge fatigue design

specifications [21,29,62]. However, the nominal stress and the corresponding strength are difficult to evaluate the complex OSDs. The hot spot stress (HSS) method comes to be used in ships and offshore structures in recent years [51]. The HSS of a welded joint owing to the structural geometry and the applied loads are included in the stress analyzing model while the notch effect and the defects due to welding are determined by the fatigue tests of the welded joint. Compared with the nominal stress method by Liu et al., the HSS definition and the analysis models seem to be more explicit and operable for the complex details of OSDs [62,63]. The nominal as well as the HSS concepts consider local effects on fatigue strength and using detail dependent design curves. In addition, the notch stress method is by applying reference radii at slit notches, only a single design curve was necessary based on a local material and stress concentration [64]. The reference radii can also be used for the evaluation of weld toes with significantly lower stress concentrations than slit notches. However, achieve the grid precision within the limitation of element numbers is a problem of notch stress method in large FE models.

Furthermore, the fatigue strength for bending is evaluated by using one-millimeter stress method recommended by Yamada et al. [46]. The method is based on the computed stress value 1-mm below the surface in the direction corresponding to the expected crack path. The total stress distribution along the crack path direction is considered to be the sum of the geometric stress caused by the structural geometry change and the non-linear local stress produced by the weld itself. The linear elastic fracture mechanics (LEFM) is used to correlate the total stress based crack propagation life and the local stress based crack propagation life to explain the geometric stress evaluated 1-mm below the surface [65].

Above all, a large amount of studies were conducted to assess the fatigue damage of OSD components by FE methods. The representative scholars including F.B.P de Jong in Holland, K. Yamada in Japan, Adolf F. Hobbacher in Germany and so on. The relative research cases, for example, a study investigated the fatigue strength of welded joints of OSDs using basic theories on the linear elastic fracture mechanics (LEFM) by assuming different depths of weld penetration [8]. The influence of fatigue cracks of U-ribs on deflection and stress of orthotropic steel decks has been partially elucidated by numerical shell models. [16]. However, these studies were either only applicable for local areas, or did not include simulation of welded joints. Until now, crack patterns and combinations of rib-to-rib connections have not been comprehensively studied, and the relationship between multiple rib cracks and their corresponding structural responses is still unclear.

## **1.4 Outline of dissertation**

As the cases of fatigue cracks occurred at root tip of rib-to-deck connection and butt joint of U-ribs, usually the engineers have questions like:

- *How does the root-deck cracks initiate and propagate?*
- *What is the most beneficial structural characteristics for crack prevention and performance improvement?*
- *Whether we can predict fatigue cracks at welded joint of OSD?*

- *What would be changed after crack occurred? The durability of other weld details? Or the whole structural properties?*

Based on these questions, the dissertation is mainly divided into two parts. Figure 1.9 gives a diagrammatic overview of the thesis.

In **Chapter 1**, the background and topic review was described, and structure of dissertation was presented.

In **Chapter 2**, the fatigue damage cases and related theoretical foundation was clarified.

The part I focused at certain location of orthotropic steel deck and conducted with crack behavior analysis which taking into account structural parameters and fabrication process. This part including three sub-objectives in Chapter 3, 4, 5.

In **Chapter 3**, the fatigue behaviors of rib-to-deck welded joints were experimentally evaluated according to the most adverse loading position. Typical crack patterns were obtained from fatigue tests by cutting and MPT inspection. The relationship between reference stress condition and crack depth of specimens could be understand, according to six types of structural parameters.

In **Chapter 4**, the cause identification of the crack initiation of this structural detail were clarified by analyze on the fatigue test results. The effect of weld residual stress on root crack initiation were clarified by using a cutting method and thermo-elastic-plastic FE analysis. The fatigue cracking patterns and their influence factors were discussed by comparing the crack sizes and crack angles in the cross section.

In **Chapter 5**, the cracking mechanism and stress responses around root tip were analyzed by establishing the matching FE models, to verify with fatigue tests results. The effect of root gap shapes, weld penetrations, and plate thicknesses on crack initiation were discussed. Besides, various root crack depths were simulated in models to clarify the stress variations occurring during the propagation stage under cyclic loading.

The part II focused on the stress responses in different locations of orthotropic steel deck which including various crack combination, and investigated the structural characteristics and mechanical properties of structure. This part was investigated in chapter 6 and chapter 7.

In **Chapter 6**, to investigate the effect of rib fractures, and the combination of rib crack and rib-to-deck cracks, the field tests results were compared with FEA by simulating the long artificial cracks. The structure responses and stress behaviors were analyzed, the effects of asphalt stiffness and various loading positions were also discussed.

In **Chapter 7**, the FEA on three-span steel deck was conducted to investigate the stress characteristics of structure with artificial crack combinations. By establishing the solid-shell hybrid models, the interaction between rib cracks and other weld details were clarified. Thus not only the local stress around crack position, but also the crossbeam response was evaluated by hot spot stress method.

In **Chapter 8**, it summarized the conclusions of the obtained results for the experimental and numerical studies.



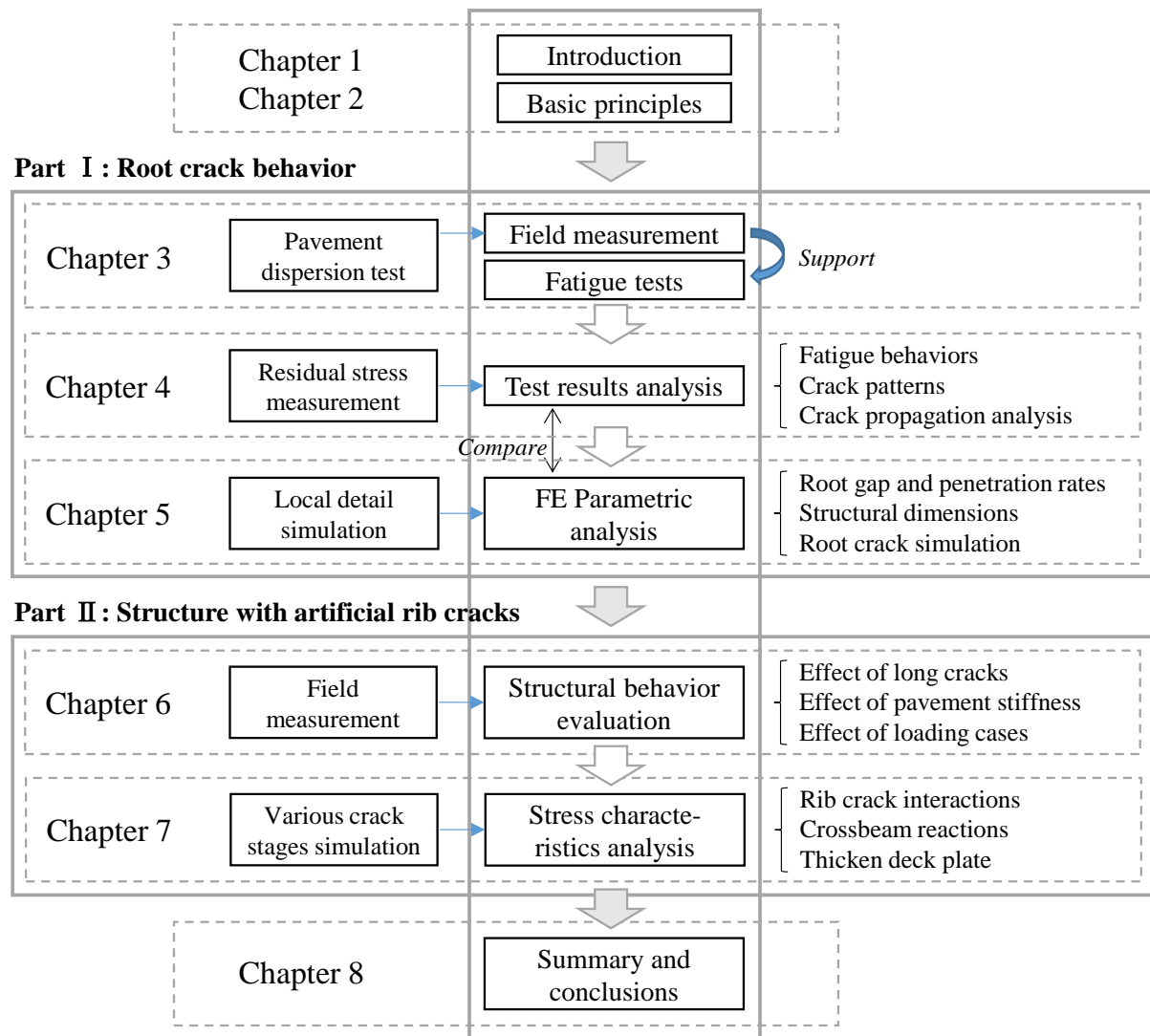


Figure 1.9 Scheme of this study

## Chapter 2 Fatigue damages and mechanisms

### 2.1 Introduction

Fatigue is defined as damage accumulation due to oscillating stresses and strains in the material. Fatigue occurs when a material is subjected to repeat loading and unloading. Its mechanical characteristics are different from static failure as following:

- ① Fatigue can be occurred even if elastic stress region. The nominal maximum stress values that cause such damage may be much less than the strength of the material typically quoted as the ultimate tensile stress limit, or the yield stress limit.
- ② If the loads are above a certain threshold, microscopic cracks will begin to form at the stress concentrators. But the crack propagation will take a long time before failure.
- ③ Eventually, after a crack will reach a critical size, the crack will propagate suddenly even if the plastic material, and the structure will fracture [66].

Fatigue failures in service were already observed in the 19th century. In 1837, Wilhelm Albert publishes the first article on fatigue. He devised a test machine for conveyor chains used in the Clausthal mines [67]. In the 20th century, it has been observed that repeated load applications can start a fatigue mechanism in the engineering material. For example, Sir James Alfred Ewing demonstrates the origin of fatigue failure in microscopic cracks in 1903. L. F. Coffin and S. S. Manson explain fatigue crack-growth in terms of plastic strain in the tip of cracks in 1954. P. C. Paris proposes methods for predicting the rate of growth of individual fatigue cracks in the face of initial scepticism and popular defense of Miner's phenomenological approach in 1961. The fact that most mechanical failures are associated with fatigue is also testified by the results of an extensive study reported in 1983 by Battelle Columbus Laboratories in conjunction with the National Bureau of Standards (currently NIST, National Institute of Standards and Technology) [68]. It is reported that 141 out of the 230 failures (nearly 61%) were associated with fatigue and three main causes of fatigue are improper maintenance, fabrication defects, and design deficiencies.

The measurements on existing bridges showed that the orthotropic steel bridge deck is the element most liable to have fatigue problems, since it is submitted to the direct action of the traffic wheels and thus to the highest stress variations and large number of cycles [10]. The fatigue damage in steel bridges belongs to high-cycle fatigue that deformation is primarily elastic. In addition, the fatigue cracks can easily occur in welded joints of orthotropic steel decks because they were subjected to residual stress and large localized bending moments from the directly applied wheel loads [15]. The fabrication defects of welded joint are also unable to avoid completely. Besides, the fatigue maintenance on the bridges are facing difficulty especially in some important transportation routes with the frequent passage of overloaded transport vehicles. Moreover, the design deficiencies of bridges might arise with the increase of traffic volume. Although new OSD structure has been continuously optimized in design, they were

hard to apply to most of the bridges have been built many years ago. Safety analysis on durability is tend to be one of the most important work.

In this chapter, the fatigue cases in OSDs were discussed, and the fatigue mechanism and evaluation principals were clarified.

## **2.2 Fatigue cases in orthotropic steel bridge decks**

Fatigue is one of the main causes involved in fatal mechanical failures of a wide range of structures and infrastructures, such as aircrafts, ships, vehicles, offshore structures, pipelines, machinery, pressure vessels, cranes, power turbines, transmission towers, bridges, or other engineering structures of high visibility. Such devastating events occur suddenly and result in heavy losses of life and property. The Health and Safety Executive, UK, has listed the main causes of structural damage (1974-1992) for installation in the North Sea as: fatigue 25%; vessel impact 24%; dropped objects 9%; corrosion 6% [69]. It shows fatigue problem is the main cause of damage. For steel bridges and other metallic structure areas, although no exact percentage is available on the mechanical failures due to fatigue, many studies have suggested that 50 to 90 percent of all mechanical failures are fatigue failures [70]. American Society of Civil Engineers (ASCE) Committee on Fatigue and Fracture Reliability stated that about 80 to 90 percent of failures in metallic structures are related to fatigue fracture [71].

The fatigue problem in steel bridge was first reported in Britain. The Severn Bridge, sometimes also called the Severn-Wye Bridge, was opened on 8 September 1966. The bridge is a suspension bridge of conventional design: 1600-m long, consisting of a 988-m central span between the towers and the two 305-m side spans. After operation of five years, three types of fatigue cracks were occurred in OSD. The maintenance and reinforcement costs on fatigue damage were about 2.5times of the bridge construction costs. Obviously, the detection and repair of fatigue damages in OSDs were not only difficult but also cost high. Some inner cracks of OSD were hard to be inspected by visual inspections and Non-Destructive Testing, which might lead to serious implications to bridge security. If large numbers of the fatigue cracks initiated at weld defects of steel bridges, that can be disastrous.

At present, the fatigue problems were reported in OSD all over the world. In Japan, various types of fatigue cracks have occurred in the welded details of OSDs in heavily loaded highways [17], this problem has been recognized as a major concern in OSDs of the Hanshin Expressway and Shuto Expressway [72]. Five typical cases of bridge damages in Japan [73], as shown in Table 2.1.

In these bridges, deck plate thickness was changed over 12mm in some section. It is seen that fatigue cracks were found at the site of 12mm-thick deck plate. In addition, it has been confirmed that many damages and repair traces existed in asphalt pavement. It was also found the penetrated cracks occurred at normal part of deck plate in S Bridge. Actually, the penetrated crack was considered as a most dangerous crack. Before 1999, the root trough-deck cracks occurred at eight bridges in Japan. Recently, even the long through-thickness cracks have been detected and are gradually increasing in occurrence [13,22], as shown in Figure 2.1(a, b).

Table 2.1 Typical cases of bridge damages in Japan [73]

	C Bridge	S Bridge	K Bridge	H Bridge	A Bridge
Operation year	1978	1986	1987	1993	1996
Large vehicles /day	5668	2617	11921	5234	5489
One side lanes	3	1	4	2	2
U-rib thickness	8mm	8mm	6mm	6mm	6 mm
Thickness of pavement	75mm	70mm	80mm	65mm	75mm
Spacing of crossbeams	1.2m/2.5m	2.75m	2.1m	3.0m	2.0m
Damage of pavement	Repaired	Repaired	Repaired a lot	A few	Less
Damage positions	Normal part	Penetrated crack at normal part	Crossing of ribs/ Normal part	Crossing of ribs	Crossing of ribs
Others	The deck plate of 12mm-thick had the fatigue damage occurred				



(a) Root-deck crack

(b) Root-bead crack

(c) Rib cracks

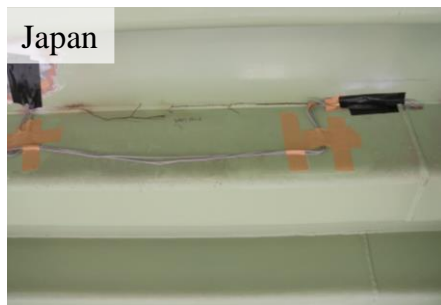
Figure 2.1 Fatigue cracks of steel bridge in Japan [18]

Furthermore, the longitudinal ribs were usually connected by field welding, most of the rib cracks were found in the welding material, along the lines of the butt welds [8], as shown in Figure 2.1(c). Thus the quality of butt welded joint which depend on the site fabrication might be not so stable relative to the shop welding. Besides, the bottom of ribs mainly subjected to the tensile stress in service time, the rib-to-rib cracks might propagated to be a large crack or extend to adjacent ribs once this type of crack occurred.

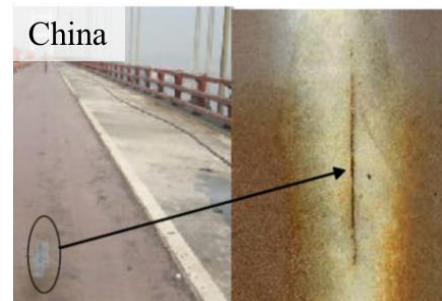
The fatigue cracks were influenced largely by structure dimensions and large vehicles volume. Besides, other influence factors such as pavement damage and corrosion damage would also reduce bridge durability. For instance, Yokohama Bay Bridge is a cable stayed bridge in Yokohama, and it crosses Tokyo Bay with a span of 460 meters. It is part of the Bayshore Route of the Shuto Expressway and opened in 1989. Most of the fatigue damages in Yokohama Bay Bridge were occurred at the positions where pavement cracked. It might because the infiltrating rainwater from the cracked pavement lead to deck plate corrosion and aggravated the fatigue cracking.

In Japan, steel bridges were mostly located near the coastal lines, which would be a great influence factor on fatigue durability. The steel corroded due to salt spray might occurred together with fatigue damage, which might lead to serious implications to bridge security. Especially for the case that the rib cracks had propagated into long fracture section along the weld line, as shown in Figure 2.2(a).

In China, the situation of high proportion of large vehicles could also lead to serious fatigue problems. The recent case is the Guangdong Humen Bridge which main span is 888m. It opened from 1997, and the fatigue cracks occurred after 6 years in service. Although localize spot repairs were conducted repeatedly, the fatigue problems were still serious. The deck propagated cracks were visible at topside of deck plate, when the damaged pavement were replaced, as shown in Figure 2.2(b). The through-deck root crack was firstly confirmed in Viaduct Bridge in France, 1977. After that, the crack type has also been detected in several bridges in other countries.

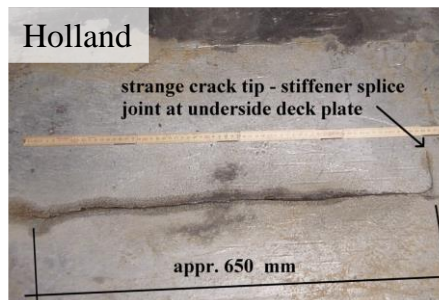


(a) Longitudinal bead crack at rib-to-deck connection

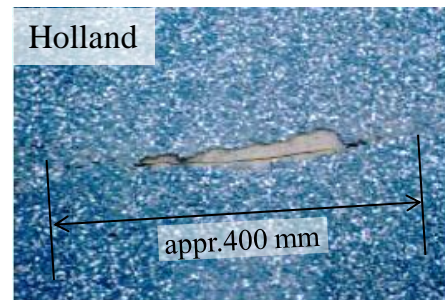


(b) Propagated trough-deck crack (Humen Bridge) [74]

Figure 2.2 Crack visible at downside and upside of deck plate



(a) Root-deck crack (Hagestein Bridge)



(b) Root-deck crack (Van Brienoord Bridge)

Figure 2.3 Root crack visible under wearing course [24]

In Holland, the fatigue cracks in OSDs were also reported by scholars of Delft University, Figure 2.3 (a) shows a crack tip at the right side of the photo. It turned out that a stiffener splice joint is located on the underside of the deck plate at this position. Due to this joint a discontinuity occurs in the deck plate, which is responsible for the strange crack tip. After the removal of the asphalt structure and blasting the deck plate the crack was visible. The length of this crack was 650 mm. As shown in Figure 2.3 (b), it is a well-known example of a movable bridge suffering from fatigue: the bascule bridge Van Brienoord

in the harbor area of Rotterdam [75,76]. Seven years after completion serious cracks in the deck plate have been discovered. Cracks had grown in the deck plate at the intersection of the trough and the crossbeam. The locations of the trough webs under the deck plate at a center-to-center distance of 300 mm are clearly visible. The deck through crack is also reported in other bridges in the Netherlands. It has already been observed in the Galecopper Bridges, Caland Bridges, Hagestein Bridge, Scharberg Bridge and several others, as shown in Table 2.2.

Table 2.2 The cases of through-deck crack of steel bridges in Holland [77]

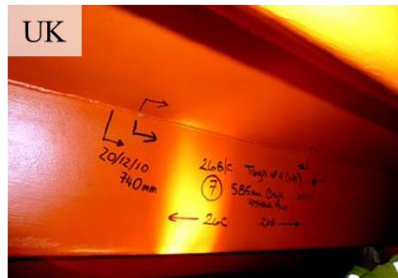
Bridge name	Types	Opened years	Damage reported years
Van Brienoord	Movable	1990	1997
Ketel	Movable	1968	1998
Caland	Movable part	1969	1998
Juliana	Movable	1966	2001
Moerdijk	Fixed	1976	2001
Scharsterrijn	Movable	1972	2002
Caland	Fixed part	1969	2002
Hagestein	Fixed	1980	2002
Galecopper	Fixed	1971	2002
Scharberg	Fixed	1973	2003

The root-bead crack is also a type of fatigue crack that most frequently occurred at OSDs. The through-bead cracks are usually caused by the increased large vehicle traffic volume, quality of welding defects, thin deck plate and so on. Many of the bead through cracks progress along the welding line, some of which would be changed the direction and propagated into the web of the closed ribs.

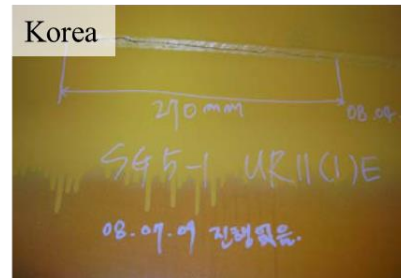
For instance, the Severn Bridge in UK, after 11 years' service from the completion of 1966, the through-bead cracks have been observed in 68 locations in 1977 [78]. Another case in UK, the Erskine Bridge was opened on 2 July 1971. It is a multi-span cable-stayed box girder bridge, with a 305 m main span and two 110 m approach spans. The bead cracks reported in Erskine Bridge as shown in Figure 2.4. This bead crack propagated along the weld line even after reaches a certain crack length, which is different from that damage in Japan. In Korea, the Namhae Bridge is a typical suspension bridge that connects Hadong Noryang and Namhae Noryang, South Korea. The bridge, completed in 1973 has a total length of 660 meters. The through-bead cracks has been found in 32 places after 24 years, as shown in Figure 2.4 (b).

The fatigue cracks in the trough splice joint were observed in Muiden Bridge in 1985 firstly. A fatigue crack in the stiffener splice joint occurs sometime during the lifetime of the bridge structure. This indicates that the crack growth is sensitive to the quality of the weld. The possible cracking at this field welded joint as shown in Figure 2.5. Moreover, driving safety might not be much affected by fatigue cracks at U-ribs when they occurred at bottom of U-ribs, and it might not be a good way for all of rib

cracks that repaired immediately once they were detected, which might lead to cracking again at same loading position. If the reinforcement of the cracked ribs could be delayed as long as the fatigue damage were predictable, it will bring efficient, safe, and great economic benefit that to repair the crack in the most appropriate period.

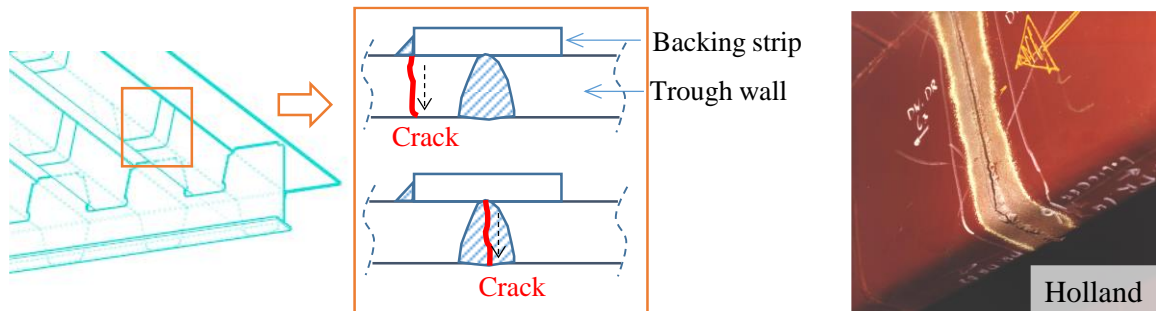


(a) Root-bead crack  
(Erskine Bridge)



(b) Root-bead crack  
(Namhae Bridge)

Figure 2.4 Root cracks in other countries [79]



(a) The possible crack types at field welded joint

(b) Crack in the rib splice joint  
(Muiden Bridge) [24]

Figure 2.5 Crack occurred at the rib splice joint

## 2.3 Fatigue mechanisms of welded joint

### 2.3.1 Fatigue life evaluation

Fatigue is defined as a damage process in the metal due to fluctuating stresses and strains. For structures in service, the damage accumulation may take several years to reach a critical level with resulting failure. ASTM defines fatigue life  $N_f$ , as the number of stress cycles of a specified character that a specimen sustains before failure of a specified nature occurs [80]. For some materials like steel and titanium, there is a theoretical value for stress amplitude below which the material will not fail for number of cycles, called a fatigue limit, endurance limit, or fatigue strength [81].

However, the fatigue strength of a welded joint is significantly lower than a smooth un-welded specimen, perhaps as low as 10% of the fatigue strength of un-welded plate material [82]. The total fatigue life of a welded detail is dominated by the propagation phase due to the presence of the inherent weld flaws. These flaws act as stress raisers, creating regions of high stress concentrations, particularly

at the plate surface close to the weld toe [83]. The fatigue life is usually including two parts as the Eq. (2.1):

$$N_f = N_{\text{total}} = N_{\text{initiation}} + N_{\text{propagation}} \quad (2.1)$$

Two approaches are commonly employed for fatigue damage evaluation and life prediction of bridge structures. The first approach is the traditional  $S-N$  curve method (also known as a Wöhler curve), in which the relationship between the constant-amplitude stress range ( $\sigma$ ), and the number of cycles to failure  $N$ , is determined by appropriate fatigue experiments and described by a  $S-N$  curve. In 1945, M.A. Miner popularized a rule that had first been proposed by A. Palmgren in 1924. This rule variously called Miner's rule or the Palmgren-Miner linear damage hypothesis [84]. It extends this approach to variable-amplitude loadings. In general, the  $S-N$  curve method being used at the bridge design stage or preliminary evaluation of fatigue life, and the fracture mechanics approach for more refined crack-based remaining fatigue life assessment or effective decision-making on inspection and maintenance strategies [85]. As shown in Figure 2.6.

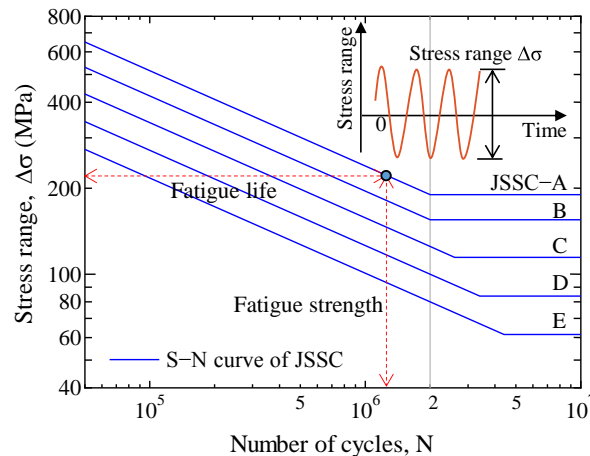


Figure 2.6 Fatigue strength and S-N curve of JSSC specification

Table 2.3 Review of range of detail categories in different codes

Constructional detail	JSSC No.32 (1995)	BS EN 1993-1-9 (2005)	CEN/TS 13001-3-1 (2004)
Base material	100 to 190 (m=3)	90 to 160 (m=3)	200 to 315 (m=5)
Welded built-up sections	100 to 155	71 to 125	80 to 180
Transverse butt joints	65 to 155	50 to 112	63 to 140
Longitudinal butt joints	50 to 155	50 to 112	80 to 180
Cruciform and tee-joints	40 to 100	36 to 80	63 to 125
Out of plane gusset	50 to 80	71 to 80	50 to 125
In plane gusset	40 to 100	50 to 80	50 to 125
Cover plates and plate girders	50 to 100	36 to 56	63 to 125
Overlapped welded joints	40 to 80	40 to 80	50 to 80

\*CEN/TS: European Committee for standardization/Technical Specifications



Based on various fatigue test results, the fatigue strength range corresponding to 2 million cycles of detail categories in different specifications as shown in Table 2.3. We can see, the welding technology is different in different countries. JSSC specification contains some weld details with post-processing, so its fatigue strength is relatively high.

The second method is the fracture mechanics approach which is dominantly dedicated to exploring the features and disciplines of crack initiation and growth in consideration of stress field at the crack tip. This method usually used to evaluate the fatigue propagation process.

### 2.3.2 Fatigue cracking process

In the case of a welded joint, a fatigue limit or a ‘safe life’ is specified, often at 2 or 10 million cycles. The fatigue process is usually divided into four phases:

1. Crack nucleation;
2. Stage I: Crack initiation;
3. Stage II: Crack growth;
4. Stage III: Final fracture.

Crack propagation starts from the “initiation” phase (sometimes called “stage I” and mainly being “short crack” propagation) and continues with the “propagation” phase of stage II (where the Paris law is supposed to hold [86]), up to stage III (fast crack propagation) leading to final failure. For example, as a root crack at rib-to-deck welded joint, the crack initiated (Stage I) at the root of the longitudinal fillet weld between the U-rib and the deck plate. After initiation the crack growth is in a vertical direction from the underside to the top of the deck plate (Stage II). After the crack has grown through the deck plate it grows in the longitudinal direction (Stage III).

Turning to the case of cracked specimen, LEFM applies, and fatigue life (often denominated residual) is mostly given by stage II propagation, generally by the celebrated Paris’ law (Paris and Erdogan, 1963). The Paris law gives the advancement  $da$  of fatigue crack per unit cycle  $dN$ , as a function of the amplitude of stress intensity factor  $DK$ , as shown in Figure 2.7:

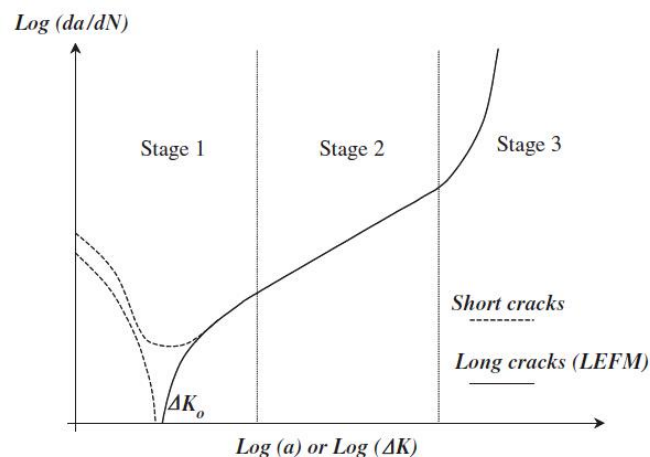


Figure 2.7 A schematic of the typical fatigue growth behavior of cracks

### 2.3.3 Design philosophy and assessment

The design philosophy can be considered as the synthesis of the multiple considerations that are the basis of the design of a structure. A structure shall be designed based on the following principals: I. It resists the design loads during its design life; II. The deformations which occur cause no hazard to the users.

The first requirement can be related to the “Ultimate Limit State” (ULS), which represents the behavior at collapse of the structure and its component parts. The second requirement relates to the “Serviceability Limit State” (SLS) beyond which the structure as a whole and its component parts are subjected to a degree of deformation inappropriate to their intended function [87]. Therefore, the design against fatigue-failure as following:

#### (1) Unlimited fatigue life design

This unlimited fatigue life design implies that the component is designed such that under all stress cycles there is no fatigue damage. The design should meet the condition Eq.(2.2):

$$\sigma < \sigma_f \quad (2.2)$$

In general, the infinite fatigue life was considered as  $N_f > 10^7$ . However, the infinite life design may no longer be valid if the vehicle loads increase during service life.

#### (2) Safe-life design

In order to maintain the designed safety, structure are designed to survive a specific design life with a chosen reserve. Safe-life design should always conformed the Miner's rule and S-N curve method. The drawback is that products designed with a safe-life approach are over-built or allocated more resources than they are expected to need, which may be uneconomical. To counter these drawbacks, alternative design philosophies like fail-safe design and fault-tolerant design were developed.

#### (3) Damage tolerance design

Based on damage tolerance theory, the structural engineer no longer assumes a perfect structural part, like for a safe life component, but rather an initial damage that is allowed to propagate. Fracture criterion and the crack propagation rate are the basis of damage tolerance design.

Instruct the user to inspect the part periodically for cracks and to replace the part once a crack exceeds a critical length. This approach usually uses the technologies of nondestructive testing and requires an accurate prediction of the rate of crack-growth between inspections.

#### (4) Durability design

The goal of durability design is to control the economic lifetime of structure. Therefore, not only several sensitive details or single cracked component need to be mentioned. These include technical considerations, such as design life, design loads, static strength, fatigue strength, inspect-ability, maintainability, and possibilities for repair, durability, and reliability. It takes into account restraining boundary conditions such as economic aspects and the specific wishes of the future owner. (Often the

design loads or use conditions are changing during the service life of a structure.)

Based on the design philosophy above, the assessment approach of welded joint were also sustained developed after a long progress. For the welding details in OSD, the local approach evaluation is the mainly used. The local approaches assessment of structures were received the following essential development:

At the middle of 19th century, scholars evaluated the fracture surfaces including fatigue fracture versus static final fracture. After the fatigue phenomena was noticed by people, in Germany, Pelikan et al. (1957) were aware that the fatigue strength plays a role in addition to the static strength.

Neuber's macrostructural support formula published in 1960, the application of the notch stress theory was started from 1937. Then the fracture mechanics by Paris' equation for crack propagation proposed in 1963.

Fisher et al. gave an overview of details susceptible to fatigue in 1977, which are still very common today. The AASHTO and the AREA fatigue specifications were presented together with the fatigue strength detail classes. Attention was drawn to the fact that the stress ratio approach which was used at that time, might have to be replaced by the stress range approach.

BS 5400 (1980) gives a fatigue assessment procedure including loads and details, however this does not cover the fatigue classification of details of orthotropic steel decks, which means that additional analyses are needed.

Yamada et al. showed a fatigue assessment procedure for several details in 1990. In this publication, the damage for a known vehicle spectrum was calculated with the detail classifications from EN 1993-1-9. A parameter study was carried out for the effect of different trucks.

Maddox gave a fatigue assessment procedure using the "Palmgren-Miner" rule and presented in addition a method using fracture mechanics in 1991 [88]. The short crack fracture mechanics and notch stress intensity factor were developed from 1990 to 1995.

At present, the design philosophy and assessment procedure of OSDs were according to these theories. The theoretical methods about fatigue were close to maturity, fatigue assessment procedures and crack growth procedures are given in various publications. However, there are still many problems in practical application. For an OSD structure, the mechanical properties are very complicated, while the fatigue strength of these welded joints are not addressed in detail until now.

Fatigue design recommendations for steel structures by Japanese Society of Steel Construction (JSSC) was published in 1993(Japanese Version) and 1995(English version). Fatigue resistance in terms of fatigue strength curves for standard details applicable to nominal stresses. The assessment methods presented in this thesis use the nominal stress and geometric stress in evaluation based on the previous theories and specifications, as shown as the model type C/D in Table 2.4. In addition to the theoretical research, the application of the finite element method in structural design based on appropriate computer technology since 1970. The manual calculation was usually based on model type A in structural mechanics. The Model type B/C/D were normally used for stress evaluation of OSDs in recent years.

Table 2.4 Type of stress for fatigue assessment

Model type	Stress raisers	Determined stress	Assessment method
A. Beam model	General analysis of sectional forces using beam theory	Nominal stress range	Nominal stress: Not applicable for assessment
B. Shell model	A + Macro-geometrical effects due to the design of the component	Modified nominal stress range	Modified nominal stress approach: Increased by concentration factor
C. Solid or Shell model	A + B + Structural discontinuities due to the structural detail	Geometric stress range	Geometric stress: the maximum principal stress is used generally
D. Solid detailed model	A + B + C + notch stress concentration	Range of elastic notch stress	a) Fracture mechanics approach b) Effective notch stress approach

\*Fatigue assessment according to ECCS publication (based on equivalent stress range)

### 2.3.4 Other influence factors

The fatigue process is quite complex and is influenced both by the nature of the external loading, the geometry of the structural item and its material characteristics. The following conditions and parameters are important to the damage process:

#### (1) Residual stress at welded joint

Residual stresses can be defined as those stresses that remain in a material or body after manufacture and processing in the absence of external forces or thermal gradients. It has been recently recognized that the residual stress distribution in welded joints is an important factor that affects both the fatigue and brittle fracture of structures [89]. The welding process creates high residual stress in the weld joint (causes shrinkage of the weld metal which may cause additional locked-in stresses). Therefore, the importance of the welding residual stress distribution to the reliable design of welded structures was emphasized [90,91].

The magnitude of the peak residual stress may correspond to the yield point. Thus, it would seem that the stress range, and not the magnitude of the structural stress, determines the fatigue life. Even if the structural stress range is entirely compressive, the effect of the welding residual stress makes the structure susceptible to fatigue failure [92]. As shown in Figure 2.8, the residual stress can increase the range of effective stress intensity factor above the threshold value of  $K$ .

At present, some post-weld treatments have attracted much attention, which is beneficial for the improvement of fatigue strength, by eliminating the tensile residual stresses and generating compressive residual stresses. For a welded detail with post-weld treatment, the total stress is obey the follow Eq. (2.3):

$$\sigma_{\text{total}} = \sigma_{\text{applied}} + \sigma_{\text{re,weld}} + \sigma_{\text{re,treatment}} \quad (2.3)$$

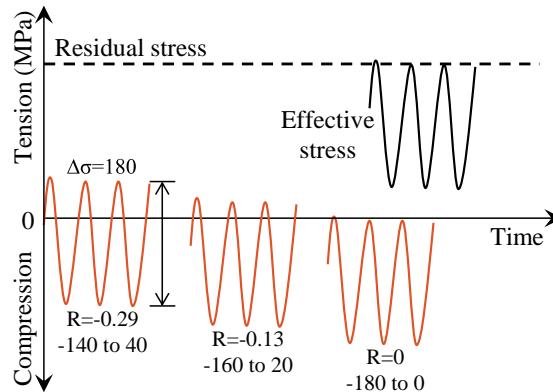


Figure 2.8 Effective stress at the weld joint [10]

### (2) Stress concentration (Geometric properties)

In bridge structures, fatigue is initiated from stress concentrated part of welding joints. Strongly dependent on geometry of welding details. Fatigue strengths are determined by considering the constructional detail together with its metallurgical and geometric notch effects. The shape of the structure will significantly affect the fatigue life; square holes or sharp corners will lead to elevated local stresses where fatigue cracks can initiate. Round holes and smooth transitions or fillets will therefore increase the fatigue strength of the structure. Therefore, the Local geometry at potential crack locus, such as welded toes, some post fabrication processing methods were usually used to prevent the crack initiation. The geometry or global geometry of the item were usually optimized by reduce the welding joint and improve the rationality of structure.

### (3) Loading and environment

Traffic load is certainly the most important influence factor of fatigue problems of OSD. It would lead to the external fatigue cycle directly. Therefore, only analyze on traffic flow volume and loading magnitude is not enough. The time history of the external forces and loading mode with reference to the actual structural item are all important parameters. By the way, the environmental conditions of OSD during service could also effect on structural durability.

In addition, as a complex steel structure with various welded joints, the mechanical behaviors of orthotropic steel deck under wheel loading are always related to the fatigue cracks.

## **2.4 Mechanical behavior of orthotropic steel deck**

### **2.4.1 Deformation of rib and deck plate connection**

The structural behavior of steel orthotropic decks is characterized by the complex interaction between its components (deck plate, ribs and crossbeams) and also by the interaction between the structure, the pavement and the vehicle's tires [93]. The traffic loads are distributed in two-dimension, and the actual stress state is hard to predict because of different stiffness properties and deflection induced secondary stresses. The stresses are also governed by the dimensions and geometry of the members of the structure

as well as the distribution area of the load [94].

The load transferred from the deck plate to the longitudinal ribs, and the local deformation of the deck plate from the wheel load results in transversal flexural stress in the deck and longitudinal rib. Transverse bending stress in deck plate, and local effects on ribs and rib to deck plate connection as shown in Figure 2.9.  $M_g$  is the moment in the deck plate in one rib,  $M_d$  is the moment in the deck plate between two ribs. As a result of transverse load distribution in the orthotropic deck, the ribs will experience local out-of-plane deformation causing transverse flexural stresses in the walls of the ribs.

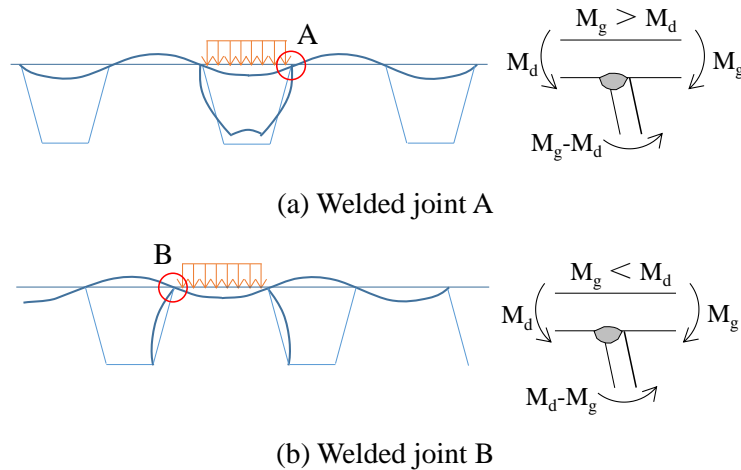


Figure 2.9 Local effects on rib-to-deck connection from wheel loading

When the wheel is positioned direct above the rib wall the highest stress will be found in the deck, if the wheel is placed between the ribs the maximum stress will occur in the rib. At the location of the supports the ribs will be subjected to negative flexural moments from the traffic load generating compressive stresses in the base of the rib [95].

There are several reported fatigue failures in the connection between the longitudinal stiffener and deck plate [16]. For the stress state at root tip of rib-to-deck connection, the compressive stress would occurred when wheel load as shown in Figure 2.9(a). However, the transverse location of the wheel load move from (a) to (b) would lead to adverse stress condition at root tip. When the vehicle pass over in longitudinal direction, an adverse transverse distribution would lead to a larger stress range or tensile stress at details.

#### 2.4.2 Mechanical behavior of the rib splice joint

Significant bending moments arise in the U-rib profile due to the passing vehicles and its axles resulting in considerable longitudinal bending stresses in the cross-section of ribs, as shown in Figure 2.10 [24]. The location of the splice joints in the trough profiles is normally to be the region with the lowest bending moment ranges.

However, there are still considerable stress ranges. These stresses in combination with the presence of a backing strip, lack of weld penetration and misalignment result in high stress concentrations. Fatigue cracks initiate at the locations of these stress concentrations. The crack growth rate is strongly dependent

on the type and the quality of the weld between two ribs [96].

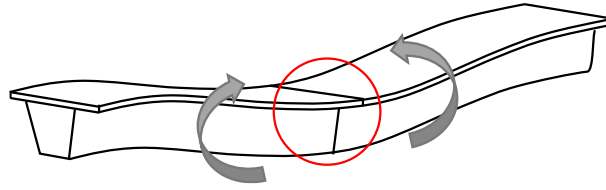


Figure 2.10 Mechanical behavior of the rib splice joint

### 2.4.3 Mechanical behavior of other sub-systems

The interaction between the components in the OSD are complicated under traffic flows, the deck acts as a structural unit and has to accomplish numerous functions simultaneously. Besides the rib and deck plate connections, an OSD have numerous welded joints with complex structural behavior, geometry and load situation [97]. To understand the mechanical behavior of different parts and simplify the structural response, the deck could be divided into sub-systems, as shown in Table 2.5. Besides, the global deformation of OSD cannot be ignore, including the axial, flexural and shear stresses from deformation of supporting main girders.

A full interaction model could be established and analyzed with finite element methods, and the separated sub-system method is possible to use for the limit state calculations and then combined by linear superposition.

Table 2.5 Assembly and description of orthotropic deck systems and their behavior [4]

System illustration	Action and result
	Deck plate deformation: Transverse deck stress from differential displacement of ribs.
	Crossbeam in-plane bending: Bending and shear in crossbeam acting as a beam spanning between the main girders.
	Crossbeam distortion and rib rotation: Out-of-plane bending of crossbeam web at rib due to rib rotation.
	Rib distortion: Local bending of rib wall at crossbeam cut-outs.

## **Chapter 3 Experimental analysis on fatigue behavior of rib-to-deck weld joint**

### **3.1 Introduction**

Currently, the cracking behaviors of rib-to-deck cracks were studied by several researchers. The local stress around rib-to-deck welded joints had been investigated based on experimental and numerical analysis results, and the fatigue strength had been evaluated. Until now, fatigue cracking from the weld root has not been reported in thicker deck plates. There has been a tendency to use thicker plates as preventive measures to avoid fatigue cracking in new orthotropic steel bridges. However, the root crack mechanism and behaviors are still not understood in sufficient detail in relation to parameters such as the rib thickness and weld penetration rate.

Root-deck crack is very hard to identify during the inspection at the initial crack stage because of the hidden locations. The previous studies mostly focused on an overview of macroscopic cracking and the fatigue strength assessment of the rib-to-deck welded joints of orthotropic steel decks. Because of the special location of root cracks, an analysis of crack propagation is usually difficult. The relative research about root crack behavior still insufficient and ambiguous.

In this study, the fatigue behaviors of the rib-to-deck welded joints with PJP (partial joint penetration) and full penetration were experimentally evaluated. The stress responses near the weld joints were examined using field measurements and fatigue tests. The fatigue behaviors of the structural detail were investigated by performing 19 full-scale fatigue tests, diverse stress conditions and one adverse transverse position were considered under the single and double tire loading. These fatigue tests were conducted on six types of orthotropic steel decks with different structural parameters.

### **3.2 Field loading test of orthotropic steel bridge**

A1 Bridge is located in the heavy traffic route of the Tokyo Metro bay area in Japan, which started service from 1980. A1 Bridge consists of two simple box girder bridges and a three-span continuous box girder bridge with orthotropic steel decks. Large vehicles account for 45.2% of the daily traffic volume. The dimensions of the orthotropic steel deck are given in Table 3.1. Asphalt pavement damage in A1 Bridge was visually inspected in 2004, and severe root cracks were observed during the re-paving construction process in 2005. The root cracks occurred around the intersections of the U-rib at the weld joints between crossbeams, and the maximum length of cracks was over 400mm.

Based on A1 Bridge, the field measurement focused on the rib-to-deck weld joint where the root cracks had been observed. A field loading test was conducted in August (2005)[41] when the influence of the asphalt pavement was most negligible at high temperatures. The mid-span of the U-rib was set as



the target section, and the measured transverse stresses near the target used as “reference stress”, which were 5 mm away from the weld toe at the bottom of the deck plate. In the dynamic loading test, a large vehicle with three-axles was used as the test truck which was moved on the target section. The measured reference stress range was about -40 MPa to 6 MPa under the rear tires, as shown in Figure 3.1. Although the tensile stress was much lower than the compressive stress, it has the potential to open the weld root gap, and lead to the initiation and propagation of the root cracks. In this study, an absolute value of stress ratio  $\sigma_{t,max} / \sigma_{c,max}$  equal to 0.13 was obtained from field measurement data.

In addition, the stress range of A1 Bridge was determined by a stress histogram measurement, which was carried out for three-days by using the rain-flow method, as shown in Figure 3.2. The maximum stress range was over 170 MPa [41,98]. These results were used in the following fatigue tests.

Table 3.1 Dimensions of the orthotropic steel decks of A1 Bridge

Structural components	Dimensions (mm)
Thickness of asphalt pavement	75
Thickness of deck plate	12
Dimension of U-rib	340×284×8
Spacing of the transverse rib	3000
Spacing of U-rib	680
Spacing of web of girder	2800
Distance between crossbeams	5600

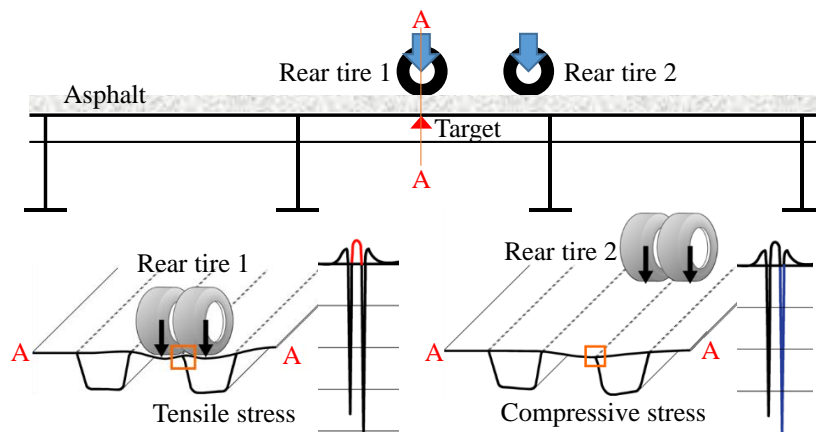


Figure 3.1 Field measurements in loading test of orthotropic deck bridge

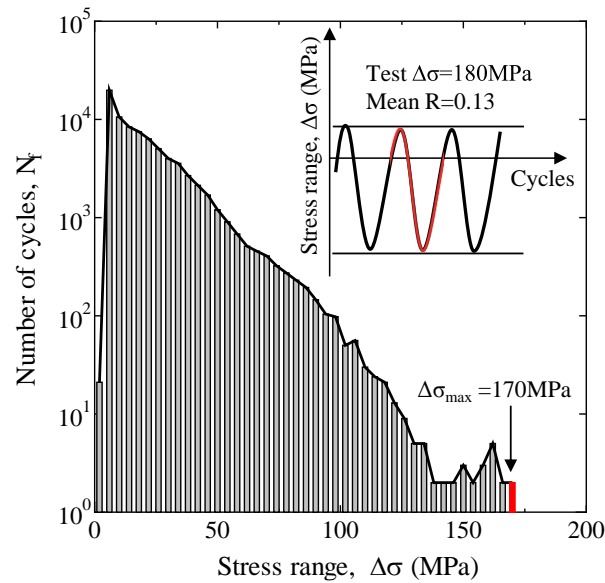


Figure 3.2 Field stress histogram measurement for three-days

### 3.3 Fatigue test

#### 3.3.1 Test specimen

A total of 19 fatigue tests were conducted on full-scale orthotropic steel deck specimens. Each specimen was 1400 mm wide and consisted of two U-ribs of 2000 mm span between two cross beams, three views of specimens as shown in Figure 3.3. The sizes of U-rib are 320×240×6(8) mm, which was same as the rib dimensions in A1 Bridge. Steel grade of JIS G3106 SM400A [99] was used for the fabricated specimens, whose chemical composition and mechanical properties are listed in Table 3.2.

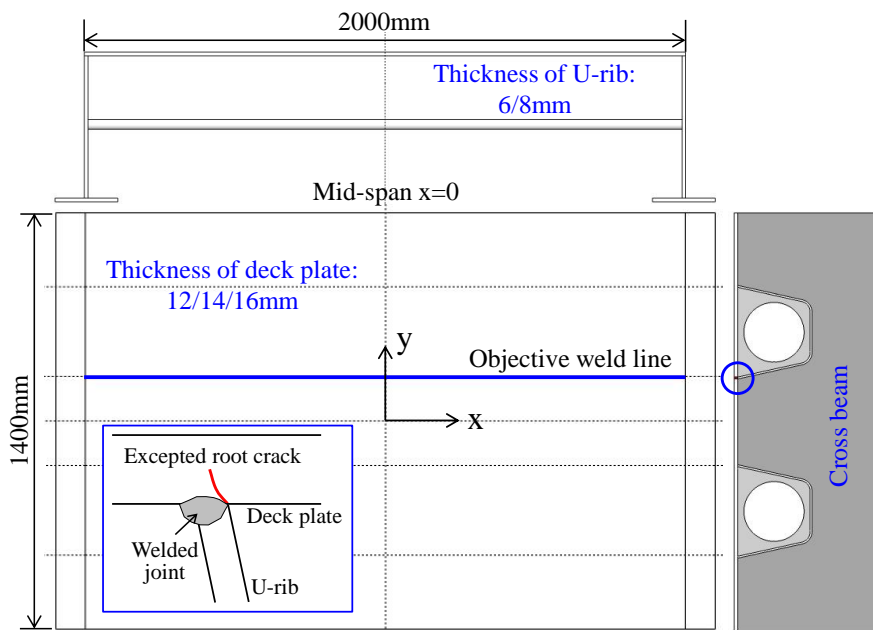


Figure 3.3 Three views of specimens

Table 3.2 Chemical composition and mechanical properties

(a) Specimen of fatigue test and residual stress measurement test

Yield point (MPa)	Tensile strength (MPa)	Elongation (%)	C (%)	Si (%)	Mn (%)	P (%)	S (%)
302	423	30	0.16	0.05	0.78	0.014	0.004

(b) Rubber plate

Yield point (MPa)	Tensile strength (MPa)	Elongation (%)
1.2	3.2	250

A total of 19 full-scale specimens were used in fatigue tests. The specimens were fabricated with 12, 14, and 16mm thick deck plates and 6 and 8mm thick U-ribs. The 12mm thick deck plate and 6mm thick rib are here referred to as D12U6 (the D and U values are the thicknesses of the deck plate and U-rib, respectively). The other combinations included D12U6, D16U6, D14U6, and D12U8. Three types of D12U6 specimens were fabricated, with 0%, 75%, and 100% weld penetration rates at the U-rib-to-deck connection, the photographs of the weld joints of the specimens after etching by a 5% nitric acid solution are shown in Figure 3.4. In the figure, the heat affected zone caused by the welding process can be observed. The welding area varies between the specimens with different penetration rates. The D12U8 specimens were fabricated with 50% penetration, and the D14U6 and D16U6 specimens were all fabricated with 75% penetration.

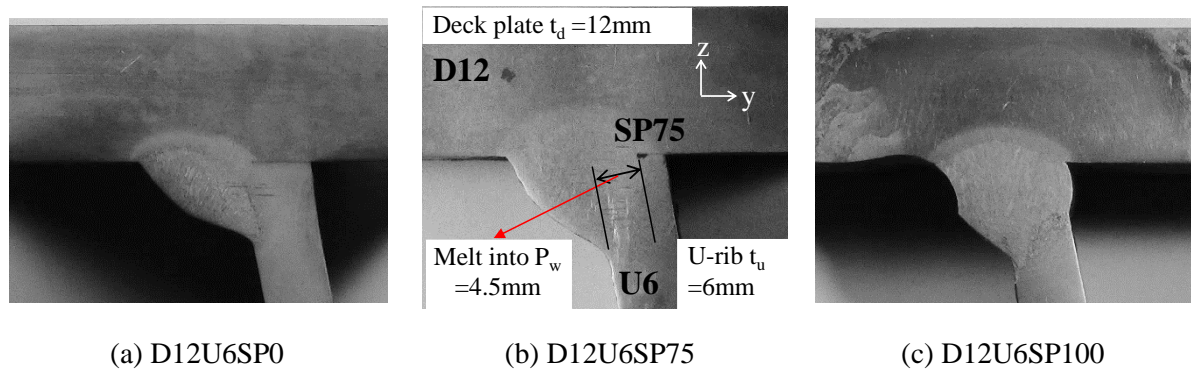


Figure 3.4 Weld joint photos of specimens in etching test

Table 3.3 Welding conditions of specimens

Specimen	Current (A)	Voltage (V)	Speed (cm/min)	Number of passes
D12U6SP0				
D12U6SP75	220~280	28~30	30~39	
D12U6SP100				
D12U8SP50	200~280	25~30	35~45	2
D14U6SP75	280	32	45	
D16U6SP75	280	32	45	

These rib-to-deck fillet welds were all welded using a semi-automatic CO<sub>2</sub> welding process with two passes, the welding conditions as shown in Table 3.3. Therefore, and weld penetration rates are abbreviated to SP0, SP50, SP75, and SP100. Based on these dimensions and welding conditions, the specimens could be divided into six types, as listed in Table 3.4.

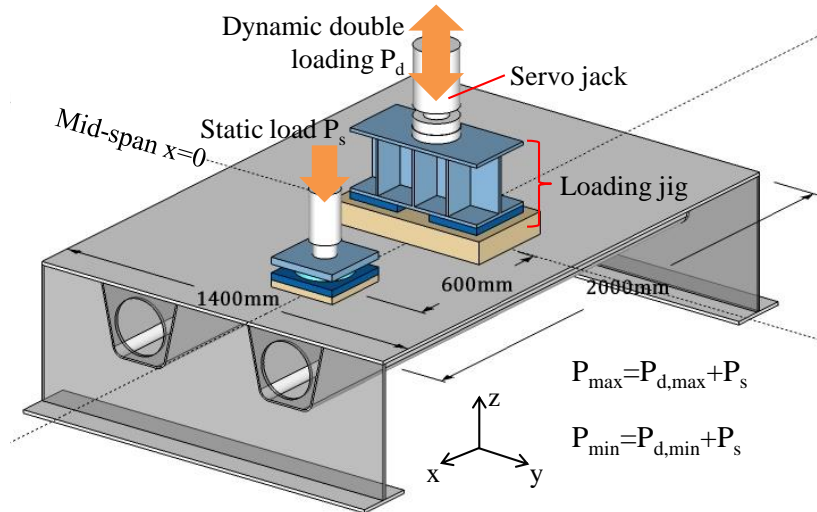
Table 3.4 Dimensions of specimens

Specimen	Thickness (mm)		Penetration depth $P_w$ (mm)	Penetration rate $P_w/t_u$ (%)	Tested amount
	Deck $t_d$	U-rib $t_u$			
D12U6SP0			0	0	4
D12U6SP75	12	6	4.5	75	5
D12U6SP100			6	100	3
D12U8SP50	12	8	4	50	3
D14U6SP75	14	6	4.5	75	2
D16U6SP75	16	6	4.5	75	2

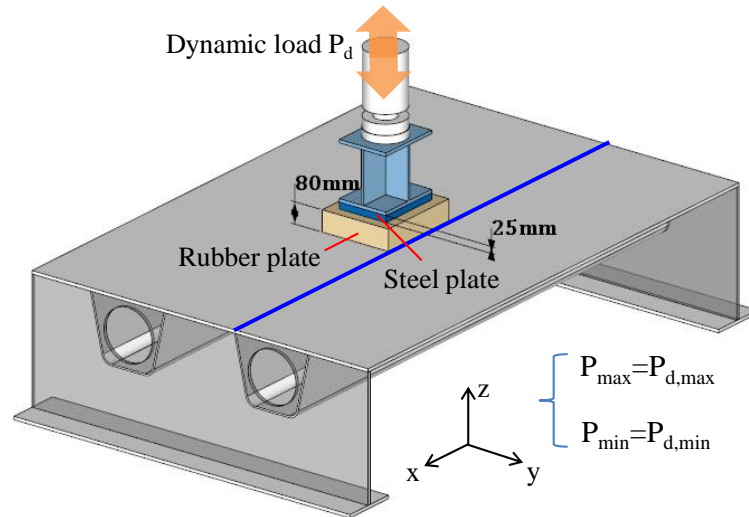
### 3.3.2 Test set-up

This experimental setup could provide static loading  $P_s$  and dynamic loading  $P_d$  using two hydraulic jacks during the test [98]. The three dimensional view of the specimens and setup with double/single-tire loading positions are shown in Figure 3.5 (a, b). During the double-tire loading tests, dynamic loading located at mid-span provided the alternative stress, the amplitude of test set-up provided sine wave with frequency of 2Hz. The static loading contributed to the tensile stress at mid-span which set at 600mm away from mid-span cross section. Both the dynamic loading and tire area of the single test were set at half the corresponding values of the double tire test. A single loading plate was placed between two U-ribs at the mid-span.

The test coordinates were set at the mid-span of a longitudinal U-rib ( $x=0$ ), and the static load side was the positive  $x$  direction. The blue line in Figure 3.5 (b) shows the target welded joint that was the focus of this study. The loading jig consisted of a loading brick, steel plate, and rubber plate. Double tire load was simulated by two 25mm-thick steel plates. The area size of tires are dependent on the pressure area of the actual tires 195mm×250mm [98], and there is a 130mm-width gap between the two plates. Below these steel load plates, the asphalt pavement of bridge was replaced with rubber plates, which edges were about 30mm beyond the borders of double tire. The rubber plate was used to ensure effective load dispersion, as shown in Figure 3.6. The properties of the rubber plates are summarized in Table 3.2 (b).



(a) Double-tire loading test



(b) Single-tire loading test

Figure 3.5 Test setup and loading cases

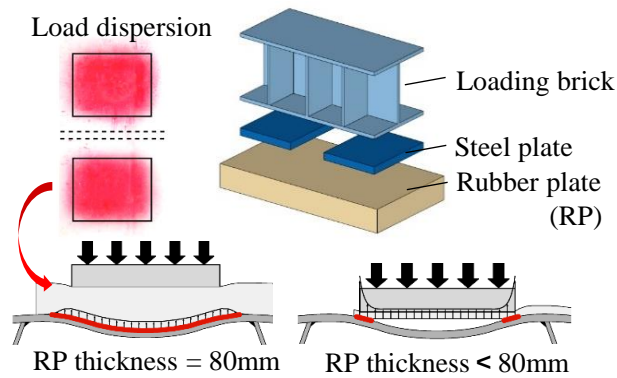


Figure 3.6 Loading jig and wheel load dispersion

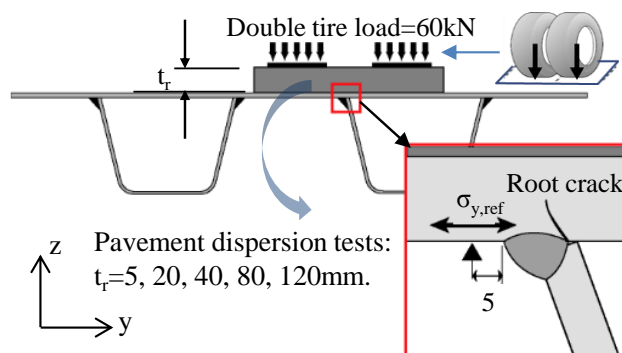
In order to accurately simulate the wheel load dispersion of an actual bridge during the fatigue loading test, the fatigue tests were conducted with rubber plates by the static loading test (vertical load=60kN). To examine the relation between dispersion effect and thickness of the rubber plate, the pressure-

sensitive paper was placed between the rubber plate and the top surface of the deck. The thickness of rubber were tested as 5mm, 20mm, 40mm, 80mm, and 120mm, as shown in Figure 3.7(a). The pressure distributions under different rubber thicknesses were compared. The pressure-sensitive paper test with the 20mm- and 80mm-thick rubber plate is shown in Figure 3.7(b).

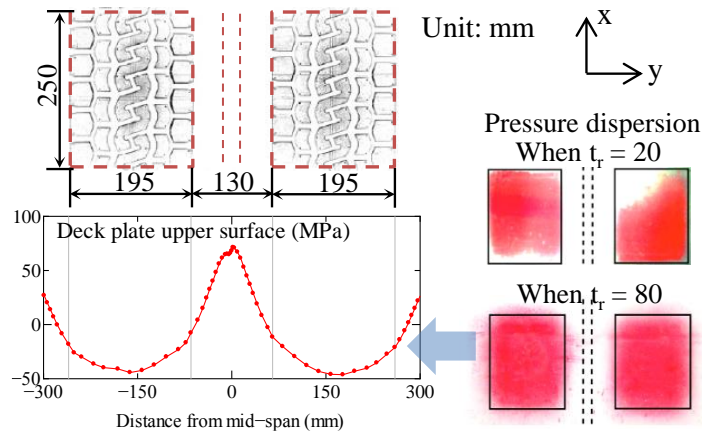
Inokuchi, Kainuma and Kawabata et al. (2008) analyzed the reference stress by FE analysis [100]. The thickness of rubber were tested as 5mm, 20mm, 40mm, 80mm, and 120mm, tests and FE results show that rubber thickness increased from 40mm to 120mm with the reference stress increases conversely, and load dispersion was effective when 80mm thick has been chosen. Finally, it was considered the 80mm thick rubber plate could be used to effectively simulate the load dispersion of asphalt pavement, as its stress waves were smooth enough at edges of tire borders.

Because the stress at the weld root tips could not be directly measured, strain gauges were attached at a location 5mm away from the weld toe of the target weld line, and the measured transverse stress was considered to be a reference stress. The relationship between the stress at the root tip and stress at a location 5mm away from the weld toe was determined a high-correlation coefficient 0.943 by Inokuchi et al. (2011). Uniaxial strain gauges (FLA-1-11) were attached at reference points that 5mm away from weld toe of the objective welded line, every 50 or 100mm spacing distance in a range of 150mm to 600mm away from mid-span in the x direction. The transverse stresses of points that were 5 mm away from the weld toe in the objective weld line were considered as the reference stresses.

The standard loads 10 tonf (98kN) were imposed to test specimen at these two loading positions respectively, the measured reference stress waves as shown in Figure 3.8. The static loading  $P_s$  could usually provide a tensile stress for mid-span. During fatigue testing, these two loading jacks worked together to provide the controllable stress range at mid-span. The single-tire tests were conducted using a dynamic load  $P_d$  alone in the middle of two U-ribs at mid-span, and having a magnitude half of the double tire loading.



(a) Loading test with different thick rubber



(b) Loading areas and dispersion test results [98]

Figure 3.7 Loading dispersion static tests

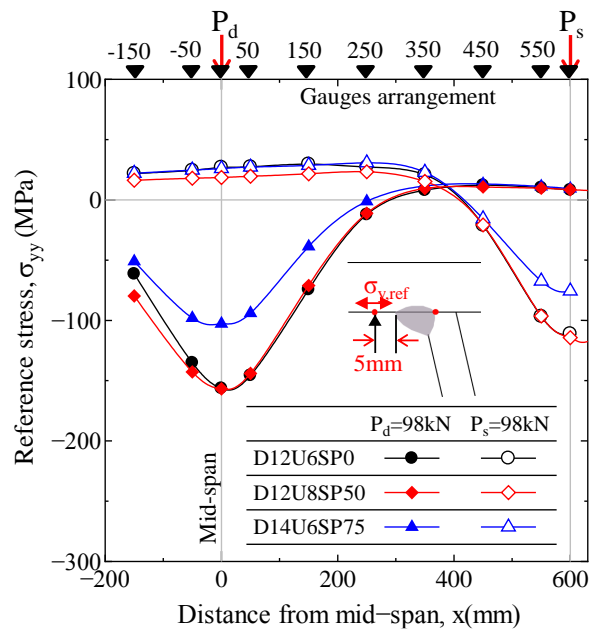


Figure 3.8 Reference strain distributions of static loading tests

### 3.3.3 Loading condition

Based on field measurement results of A1 Bridge, the test primary stress range of the mid-span reference point of basic specimens was controlled at 180 MPa. The tested primary reference stress at the mid-span was considered as the stress condition for each specimen. The basic fatigue test set the maximum compressive stress at -160 MPa and the maximum tensile stress at 20 MPa because the measured stress ratio of A1 Bridge was 0.13. The stress ratio  $R$  is defined as the algebraic ratio of absolute value of minimum stress to maximum stress. The other stress range conditions and different stress ratios were used for comparison tests. The maximum value of tensile stress was considered as an important factor for crack initiation, and the effects of stress ratio for a given stress range were explained,

e.g., the stress range of -140 MPa to 40 MPa.

In addition, the reference strains of specimens with different plate thicknesses under the same loading were different because the structural rigidity changed. Therefore, before the fatigue tests, a single static loading of 98kN was independently applied to the  $P_s$  and  $P_d$  locations. D12U6SP0-1 was set as the basic specimen. D14U6SP75-1 and D12U8SP50-1 were contrast specimens, and their reference stress distributions are shown in Figure 3.8. Even though the penetration rate of these three specimens were different, it was considered different penetration rate of welded joint could only effect the peak stress at root tip but not structural responses. Figure 3.8 also shows that D12U8 had almost the same stress range as D12U6. Thus it was considered the U-rib thickness also cannot change the reference stress range of specimens. However, the maximum tensile strains of D14 and D12 were nearly the same, while the maximum compressive strain of D12 was about 52% larger than that of D14 at mid-span.

In the fatigue tests, the D14U6SP75-1 was carried out with the same double tire loading condition as D12U6SP0-(No.4):  $P_{d,min}=-118\text{kN}$ ,  $P_{d,max}=-11.8\text{kN}$ ,  $P_s=-218\text{kN}$ . For D12U6SP0-(No.4) the stress range was 40~-140MPa, and D14U6SP0 was 46~-78MPa. The stress range conversion of D12 and D16 with the same loading condition was calculated by using another method. This paper referred the field measurement results (D12U6) [41], and built the contrast FE model D16U6 with same loading and boundary condition.

The conversion and calculation process as following:

1) D12U6 reference stress from field measurement: Tensile strain= $29\mu\epsilon$ , Compressive strain= $200\mu\epsilon$ , stress ratio  $R=0.145$ , Strain range= $229\mu\epsilon$ .

2) D16 FE Model analysis: Tensile strain= $34\mu\epsilon$ , Compressive strain= $95\mu\epsilon$ , Stress ratio  $R=0.358$ , Strain range= $128\mu\epsilon$ .

$$\frac{\Delta\sigma(D16)}{\Delta\sigma(D12)} = \frac{229}{128} = 1.78$$

Basic test stress range  $\Delta\sigma_{test}(D12)=180\text{MPa}$   $\Delta\sigma_{test}(D16)=180/1.78 \approx 101\text{MPa}$

When D16 stress ratio  $R = 0.358$

$\Delta\sigma_{test}(D16) = \sigma_t + \sigma_c$  ( $\sigma_t/\sigma_c=0.358$ )  $\sigma_t=26.6\text{MPa}$ ;  $\sigma_c=74.4\text{MPa}$

Therefore, the stress range of specimen D16U6SP75-1 was set at 26.6 to -74.4MPa during the fatigue test. It was equivalent to the D12 specimens with stress range of 180MPa under the same loading. It was obvious that an increase in the deck plate thickness from 12mm to 16mm led to a decrease in stress range, whereas it had the opposite effect on the stress ratio. Above all, the primary stress range 180MPa as basic test stress range for D12 specimens; stress range of D14 set as 46~-78MPa which was equivalent to 40~-140MPa of D12, and D16 set as 26.6~-74.4MPa which was equivalent to 20~-160MPa of D12.

The list of tested specimen-(No.) and their corresponding test conditions as shown in Table 3.5. Three million cycles were applied to all specimens in the first loading stage. If there was no crack initiation, additional 1.5 million cycles were applied to continue the testing. A single tire loading was applied to



D12U6SP75-1 and D12U6SP100-2/-3 specimens.

The test primary stress distribution of specimens D12U6SP0/SP75 in the longitudinal under dynamic loading as shown in Figure 3.9 (a, b). The reference stress ranges at mid-span were measured during fatigue test, as shown in Figure 3.10. The data for D12 and D16 showed no obvious fluctuations with an increase in the load cycles, because no cracking occurred at mid-span. On the other side, the stress range of the D14 specimen decreased at 1.22million cycles, it shown to be fatigue crack occurred. Its rate of decline tended to be slower from 2.33million cycles, which meant the crack propagation process seemed to stop.

Table 3.5 Stress conditions of all specimens

Specimen-No.	Primary stress (MPa)		Primary stress range $\Delta\sigma$ (MPa)	Load cycles ( $\times 10^4$ )	
	$\sigma_{\max}$	$\sigma_{\min}$		Double tire	Single tire
D12U6SP0-1	20	-160	180	300	0
D12U6SP0-2	20	-100	120	300+150	0
D12U6SP0-3	20	-70	90	300	0
D12U6SP0-4	40	-140	180	300	0
D12U6SP75-1	20	-160	180	300	600
D12U6SP75-2	20	-100	120	300	0
D12U6SP75-3	40	-140	180	300	0
D12U6SP75-4	0	-180	180	300+150	0
D12U6SP75-5	40	-140	180	300	0
D12U6SP100-1	40	-140	180	300	0
D12U6SP100-2	40	-140	180	300	300
D12U6SP100-3	40	-140	180	300	600
D12U8SP50-1	20	-160	180	300	0
D12U8SP50-2	0	-180	180	300+150	0
D12U8SP50-3	20	-160	180	300	0
D14U6SP75-1	46	-78	124	300	0
D14U6SP75-2	46	0	46	300	0
D16U6SP75-1	26.6	-74.4	101	300	0
D16 U6SP75-2	26.6	-74.4	101	300	0

\* A part of experimental data in this table was come from the reference [41].

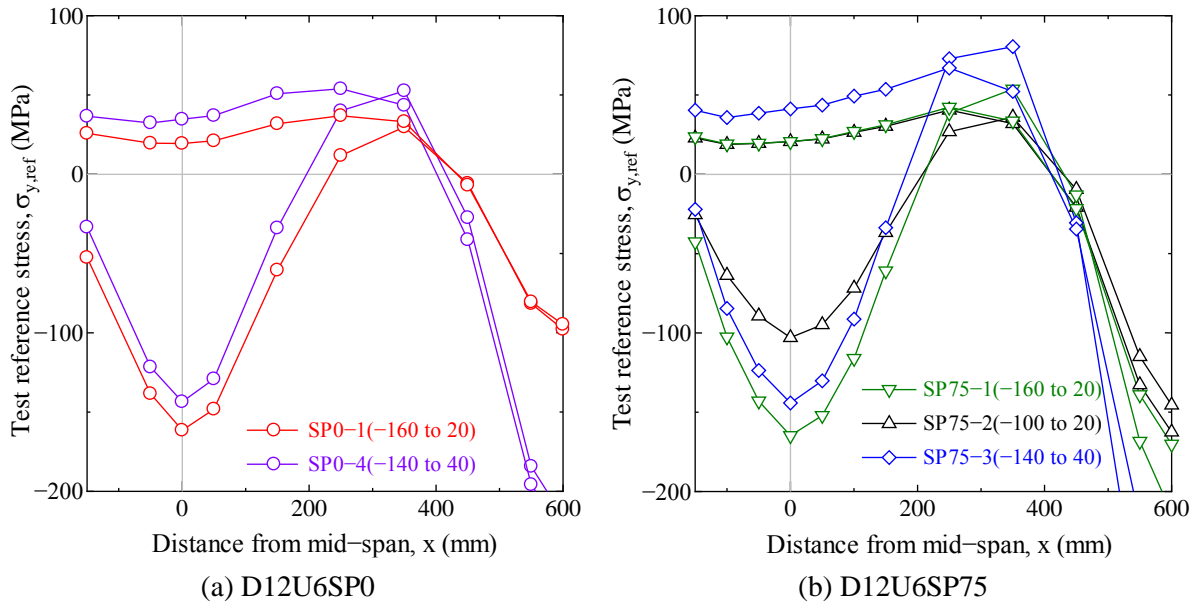


Figure 3.9 Measured reference stress range of specimens

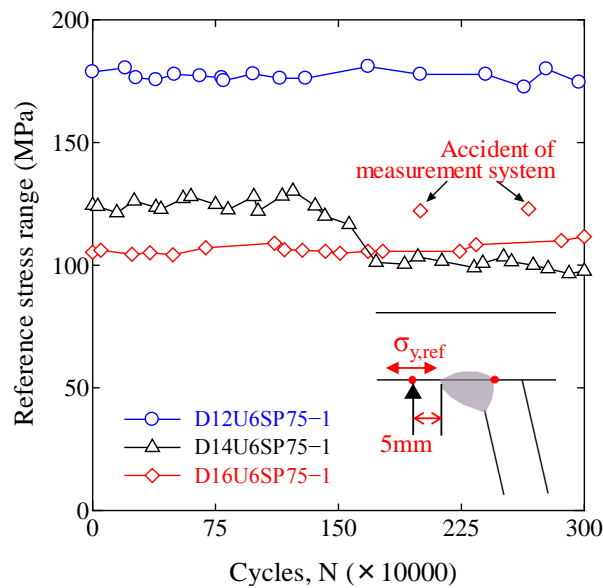


Figure 3.10 Reference stress ranges and cycles during fatigue loading tests

### 3.4 Test process and results

#### 3.4.1 Test process

The following test implementation process was used for the six types of specimens.

1) Four D12U6SP0 specimens were tested. D12U6SP0-1 adopted the basic stress range. SP0-2 was carried out with the two-thirds of the basic stress range, and SP0-3 was conducted with half of the basic stress range. SP0-4 considered whether the maximum tensile stress value could also be a contributory factor in the crack initiation and propagation, which was investigated by contrast tests with a stress range

of 40 to -140MPa.

2) Five D12U6SP75 specimens were tested with different stress ranges. In addition, D12U6SP75-1 was retested twice by 3million cycles of single-tire loading after the double-tire loading at first stage. The stress range of specimen under the single-tire loading is about -6 to -60MPa.

3) Three D12U6SP100 specimens were tested with stress range of 40 to -140MPa in the first stage. Then, D12U6SP100-2 and D12U6SP100-3 were subjected to an extra 3million cycles and 6million cycles of single-tire loading, respectively. Moreover, the grinding treatment was performed at the weld toes of SP100-2 and -3 specimens before the double tire testing to prevent the initiation of toe cracks. (Grinding treatment” is a post-welded treatment to change the geometry at welded joint.)

4) Three D12U8SP50 specimens were tested. D12U8SP50-2 was set as a contrast test, with a stress range of 0 to 180MPa, to explore the effect of the compressive stress on the root crack. In addition, press straightening was carried out in the fabrication process of D12U8SP50-3 to handle the deformation of the deck plate after welding. The residual stress at root tip would be changed by press straightening treatment, which totally could influence the root crack behavior.

5) Two D14U6SP75 specimens were tested. The calculated and converted stress range of 46 to -78MPa was used for D14U6SP75-1, and the tensile part of this stress range (46 to 0MPa) was used for D14U6SP75-2 as a contrast test.

6) Two D16U6SP75 specimens were tested, with a stress range of 26.6 to -74.4MPa.

After all of the fatigue tests were completed, the length of surface cracks were detected by magnetic particle testing (MT) method. The cracks were mainly existed in the range of  $\pm 200$ mm along the welding line from the mid-span. And then, the specimens were cut with 25mm intervals in longitudinal to measure the crack details in cross sections by MT again. All four crack patterns are shown in Figure 3.11. Typical fatigue crack category should be (1)/(2)/(3).

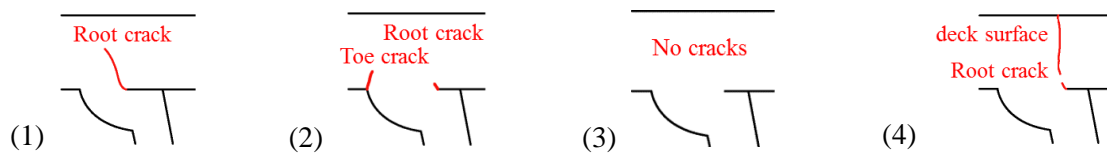


Figure 3.11 Typical crack patterns of test results

### 3.4.2 Crack category

The test results showed three types of crack categories: 1) the occurrence of root cracking only, 2) the occurrence of both toe cracking and root cracking, and 3) non-crack initiation. The crack shapes and stress ranges are summarized in Table 3.6.

Crack type (1) showed that the basic stress range easily led to root cracking, as planned. It was revealed that the tensile stress and crack length of the SP0 specimen were larger than those of the SP75

and SP100 specimens for the same stress range. However, the stress range and crack depth of the SP75 specimens did not show a correlation because of the differences in the geometry of the root gap. The root crack length of SP100 and SP0 were almost half of deck thickness under the stress condition of -140 to 40 MPa. The root crack depths of the specimens were very different with diverse penetration rates, even under the same stress range. For specimens of the same type, either a larger stress range or larger tensile stress would lead to a larger crack depth. The stress condition of D14U6SP75-2 showed the important influence of the tensile stress on the fatigue crack initiation, because its stress range was much smaller than the others. However, root cracks still occurred under a large tensile stress. Meanwhile, a maximum root crack depth comparison of SP100-2 and SP100-3 showed that the additional 3million single loading cycles only led to a propagation of about 0.8% in the through-deck direction. Thus, the single loading was not considered to play a major role in the rib-to-deck crack propagation.

Crack type (2) showed that both toe and root cracks would initiated under a relatively high tensile stress. The crack was easily initiated at the weld toe under a high stress ratio. In particular, the toe crack depths were mostly larger than the root crack depths in the same cross-section. A toe crack also occurred in D12U8SP50-1 under the basic stress range. This might have been due to the geometry of the weld toe, which led to a high stress concentration. The difference in the radius and flank angles of the weld toe between D12U6 and D12U8 will be discussed later in this paper. Some reports have suggested that both root and toe cracking occurred during the fatigue tests of orthotropic steel decks. The past full-scale orthotropic steel deck fatigue tests proved that toe cracking would occur with a high tensile stress [15,34]. However, there has been no report of toe cracking in actual orthotropic steel decks with 12 mm deck plates in Japan.

The type (3) (non-cracking) specimens showed that three parameters should be considered to prevent weld cracking: the deck plate thickness, stress range, and maximum tensile stress. Two of the D16U6SP75 specimens showed no cracking after 3 million cycles. This showed the significant improvement in fatigue durability when the deck plate thickness was increased from 12mm to 16mm. The D12U8SP50-2 specimens showed that fatigue cracks did not occur where the stress ranges were purely compressive even under the basic stress range of 180 MPa, it was considered the welded joint might under the relative lower tensile residual stress so that effective tensile stress range would be smaller than others. At the same time, a one-third or one-half decrease in the stress range while maintaining the same tensile stress could also enhance the fatigue life. This means both the tensile stress and stress range control the fatigue life before crack initiation.

Finally, there are two special cases D12U6SP0-4 and D12U8SP50-3P, the deck crack occurred from upper side of deck surface, as shown in Figure 3.12. In the case of SP0-4, the root crack had a relatively small depth at the location where the deck crack propagated rapidly. The crack occurred on the upper surface of the deck plate because the steel reached the yield strength during the fatigue test. This crack was perpendicular to the deck plate. It was thought that this type of deck crack tends to propagates

through the root crack. From the perspective of bridge structural safety, this case would be worse than when only root cracking occurs. These two specimens was still classified as Crack type (1) because these deck crack should not be the fatigue crack. There are no in-depth study for deck crack in following discussion about test results.

Table 3.6 Relationship between stress condition and crack depth

Category	Specimen-No.	Tensile stress (MPa)	Stress range (MPa)	Crack depth (mm)		Crack depth percentage (%)	
				$a_r$	$a_t$	$a_r/t_d$	$a_t/t_d$
1) Root crack	D12U6SP0-1	20	180	3.2		26.7	
	D12U6SP0-4	40	180	5.4		45.0	
	D12U6SP75-1	20	180	1.5		12.5	
	D12U6SP75-2	20	120	3.2		26.7	
	D12U6SP100-2	40	180	6.0	/	50.0	/
	D12U6SP100-3	40	180	6.1		50.8	
	D12U8SP50-3	20	180	1.3		10.8	
	D14U6SP75-1	46	124	6.4		45.7	
D14U6SP75-2	46	46	0.7		5.0		
2) Toe and root cracks	D12U6SP75-3	40	180	3.2	4.5	26.7	37.5
	D12U6SP75-5	40	180	4.6	5.7	38.3	47.5
	D12U6SP100-1	40	180	2.2	3.4	18.3	28.3
	D12U8SP50-1	20	180	4	4.6	33.3	38.3
3) No crack	D12U6SP0-2	20	120				
	D12U6SP0-3	20	90				
	D12U6SP75-4	0	180	/	/	/	/
	D12U8SP50-2	0	180	/	/	/	/
	D16U6SP75-1	26.6	101				
D16U6SP75-2	26.6	101					

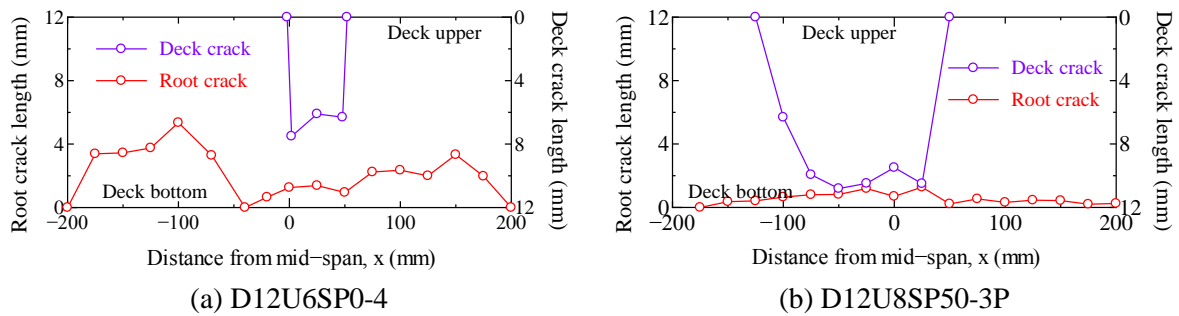
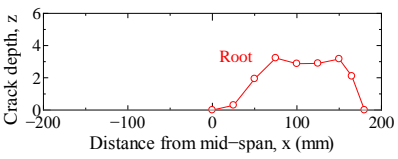
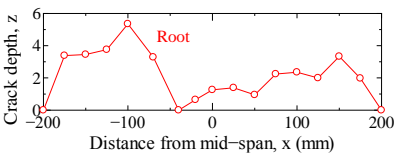
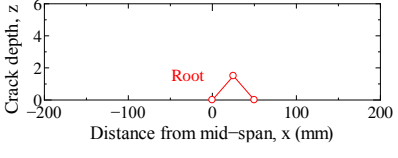
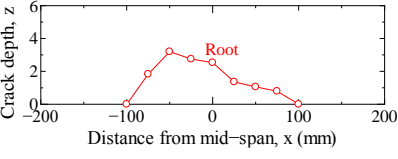
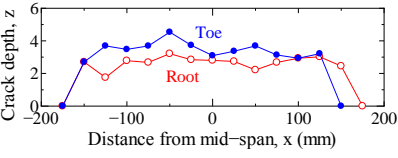
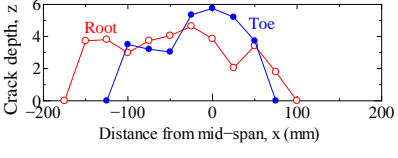
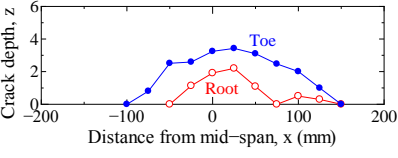


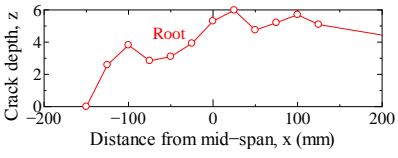
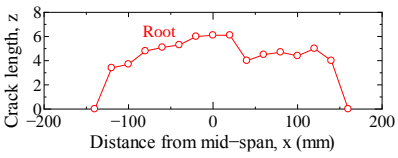
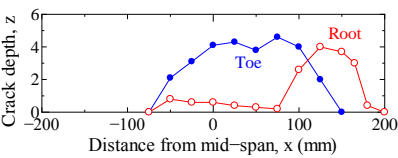
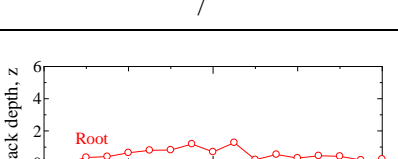
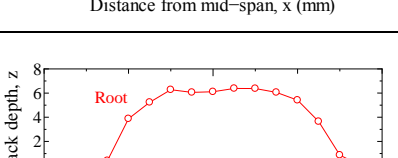
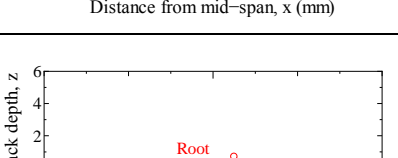
Figure 3.12 Crack depth distribution of deck/root cracks

The specimens ID, corresponding stress conditions, maximum crack depth, and crack depth diagrams in x direction, are provided in Table 3.7.

Table 3.7 Test stresses and the measured crack depth

Specimen	No.	Stress			Maximum crack depth, a (mm)	Image of crack depth (mm) and scope
		$\sigma_{max}$	$\sigma_{min}$	$\Delta\sigma$		
D12U6 SP0	1	20	-160	180	$a_r=3.2$	
	2	20	-100	120	Non-crack	/
	3	20	-70	90	Non-crack	/
	4	40	-140	180	$a_r=5.4$	
D12U6 SP75	1	20 -6(S)	-160 -60(S)	180 56	$a_r=1.5$	
	2	20	-100	120	$a_r=3.2$	
	3	40	-140	180	$a_r=3.2$ $a_t=4.5$	
	4	0	-180	180	Non-crack	/
	5	40	-140	180	$a_r=4.6$ $a_t=5.7$	
D12U6 SP100	1	40	-140	180	$a_r=2.2$ $a_t=3.4$	

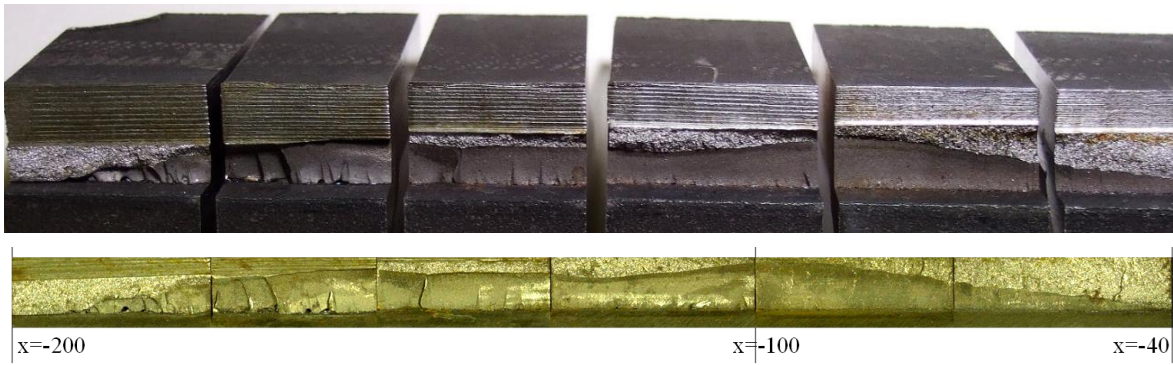
Follow the last page:

D12U6 SP100	2-G	40 -6(S)	-140 -60(S)	180 54	$a_r=6$	
	3-G	40 -6(S)	-140 -60(S)	180 54	$a_r=6.1$	
D12U8 SP50	1	20	-160	180	$a_r=4$ $a_t=4.6$	
	2	0	-180	180	Non-crack	/
	3-P	20	-160	180	$a_r=1.3$	
D14U6 SP75	1	46	-78	124	$a_r=6.4$	
	2	46	0	46	$a_r=0.7$	
D16U6 SP75	1	26.6	-74.4	101	Non-crack	/
	2	26.6	-74.4	101	Non-crack	/

\* $a_r$ : maximum crack depth of root crack; \* $a_t$ : maximum crack depth of toe crack;

\*n-G: Specimen ID-Grinding treatment; \*n-P: Specimen ID-Press straightened

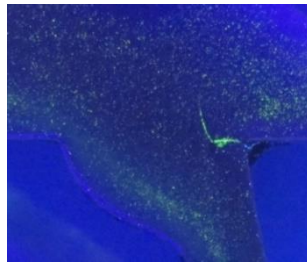
The root crack fracture surface of D12U6SP0-4 in longitudinal is shown in Figure 3.13 (a). The fracture surface consists of some discontinuous fractures that could be multi-cracks initiated by the root crack and eventually forming a large crack. The corresponding crack patterns of other specimens by MPT inspection are shown in Figure 3.13.



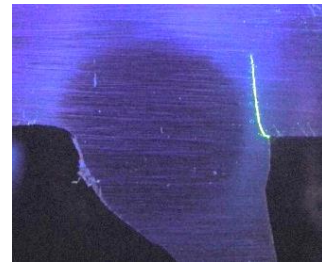
(a) Fracture longitudinal section of D12U6SP0-4 from -200 to -40 mm



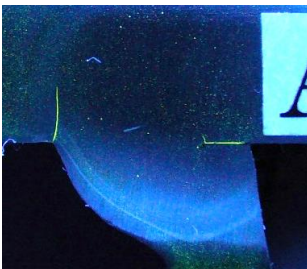
(b) D12U6SP0-4; x=-100mm



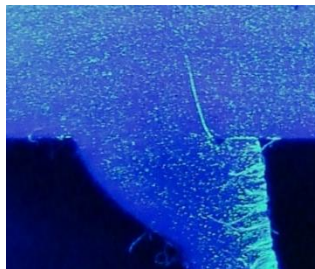
(c) D12U6SP75-2; x=0mm



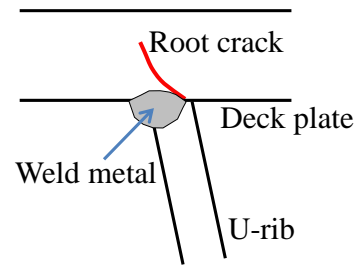
(d) D12U6SP100-3; x=120mm



(d) D12U8SP50-1; x=0mm



(e) D14U6SP75-1; x=0mm



(f) Image

Figure 3.13 MT inspections of typical cracking specimens [100]

### 3.5 Summary

This study focused on the fatigue behavior of weld root using an experimental investigation method. The structural responses of the reference points near the weld joints were examined using field measurements and fatigue tests. A total of 19 full-scale specimens with diverse loading cases were carried out. Six types of specimens were fabricated with different plate thicknesses and weld penetration rates. The cracks were mainly existed in the range of  $\pm 200$ mm along the welding line from the mid-span. The crack projected depth are measured by MPT inspection in cross sections with 25mm intervals in longitudinal. The results are summarized as follows:

(1) The field loading test focused on the rib-to-deck weld joint were carried out in an actual bridge. The maximum stress range was over 170 MPa, which was carried out for three-day stress histogram



measurement by using the rain-flow method. An absolute value of stress ratio equal to 0.13 which obtained from field loading test.

(2) The fatigue test specimens were fabricated with six types of structural dimensions. The experimental setup simulated the single and double tire loading at mid-span of specimens, and provided the alternative stress for at least 3 million cycles. Root cracks tend to initiate easily in the basic stress range -160 to 20 MPa under double tire loading, and the single tire loaded above the welded joint is not easy to cause the root crack extension in the deck vertical direction.

(3) The test results showed three types of crack categories: 1) the occurrence of root cracking only, 2) both toe crack and root crack occurred, 3) non-crack initiation. The fatigue test results also demonstrated that fatigue cracks did not occur where the stress ranges were purely compressive, it was considered the welded joint might under the relative lower tensile residual stress so that its effective tensile stress range would be smaller than others.

(4) Finally, a one-third or one-half decrease in the stress range while maintaining the same tensile stress could also enhance the fatigue life. This means both the effective tensile stress range and the whole stress range would affect the fatigue life before crack initiation.

## Chapter 4 Residual stress test and crack behavior analysis

### 4.1 Introduction

In a previous study, one sectional full-scale specimens of OSD under diverse loading cases were carried out. After the fatigue tests, all of the fatigue cracks were detected by magnetic particle testing (MPT) and measured in different directions. Based on the fatigue test results, the crack category and patterns showed diversity based on different influence factors. Moreover, the residual stress cannot be avoided during welding process. The residual stress at welded joint is one of the most complicated factors.

Moreover, even if the structural stress range is entirely compressive, the effect of the welding residual stress makes the structure susceptible to fatigue failure [101]. The residual stress can increase the range of effective stress intensity factor above the threshold value of  $K$  [102]. According to previous studies by other scholars, it is possible to determine the residual stress in the weld joints by means of experimental measurement as well as FE analysis.

In this chapter, firstly, the residual stress distribution in vertical of model specimens with or without weld penetration and root gap were measured using the cutting method. In addition, thermo-elastic-plastic finite element analyses were carried out on parametric models of actual welded joints. The effect of residual stress on root crack initiation and propagation were clarified.

And then, based on the six types of specimens which were fabricated with different plate thicknesses and weld penetration rates, the test parametric analysis on fatigue crack behaviors were carried out. The comparison of the crack sizes, crack propagation angles in the cross-sectional and longitudinal directions were investigated.

### 4.2 Experimental measurement of welding residual stress

#### 4.2.1 Three-scale specimens and cutting method

Residual stress measurements were mainly carried out using the hole drilling method [103], cutting method [104], and X-ray diffraction method [105]. In this study, the cutting method were used to measure the welding residual stress in the weld root of the deck plate and U-rib connection. The cutting method was employed to investigate the residual stress distribution along the path of the root crack propagation.

A standard steel deck composed of 12-mm-thick deck plate, 6-mm-thick U-rib, and 6 mm welds was used. However, it is difficult to measure the residual stress because of gage length and the number of strain gages. In order to examine the specific residual stress distribution, the specimens (deck plate thickness: 36 mm, U-rib thickness: 18 mm, welding size: 18 mm) were fabricated three-times with standard dimensions. The test specimens were manufactured according to the Japanese Industrial

Standard (JIS G3101) [106] and consisted of a steel plate of SM400 with 260 mm length and 120 mm width. The deck plate and U-rib were fillet-welded using semi-automatic CO<sub>2</sub> gas metal arc welding. Table 4.1 lists the welding conditions of the tested specimens. Figure 4.1 shows the shape, dimensions, and cutting position of a large-scale specimen.

The deck plate thickness  $t_d$  and U-rib thickness of the specimen were 36 mm and 18 mm, respectively. To clarify the effect of the residual stress considering the weld penetration rate and the root gap of the deck plate-to-U-rib joint, the specimens were fabricated with weld penetration rates of 0% and 75% and a root gap of 2 mm. The test specimens were sliced at 15 mm intervals to manufacture a large specimen by machining, and surface-polished to a thickness of 10 mm as shown in Figure 4.2, where  $D$  denotes the design deck plate thickness,  $U$  is the design U-rib thickness,  $SP$  is the weld penetration rate, and  $G$  is the root gap.

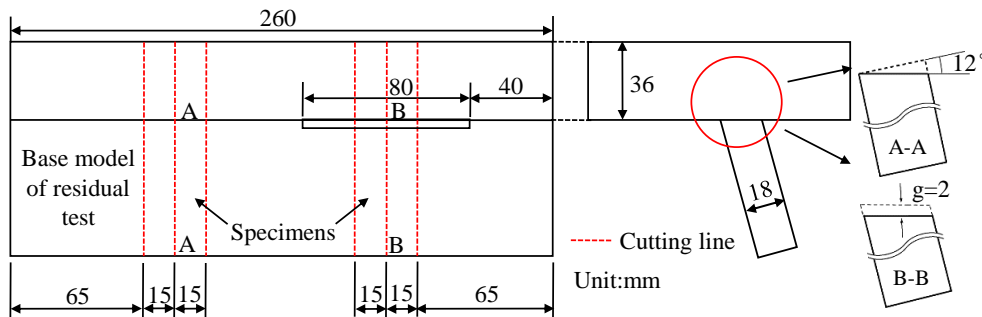
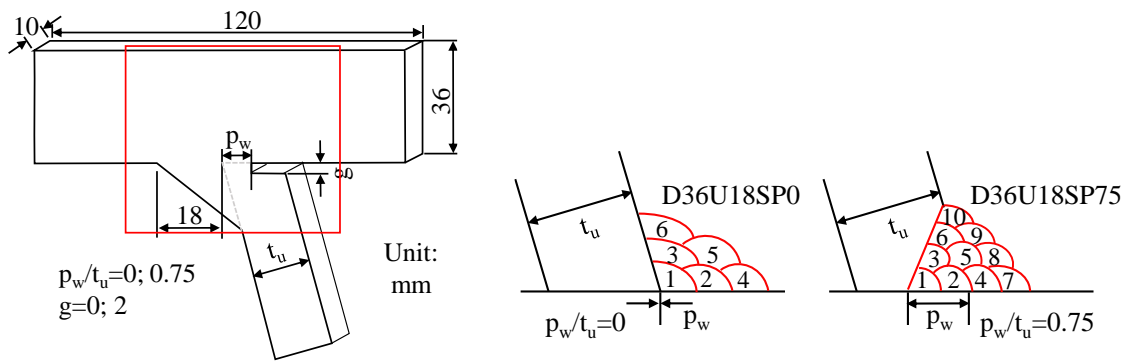


Figure 4.1 Dimensions and cutting positions of specimen



(b) Three views of specimen

(c) Welding passes of three-times welded joints

Figure 4.2 Dimension of specimens and welding joints

Table 4.1 Welding conditions of three-scale specimens

Specimen	Welding method	Current (A)	Voltage (V)	Speed (cm/min)	Number of passes
D36U18P0	Semi-automatic CO <sub>2</sub>	240	30	30~39	6
D36U18P75		240	30	24~42	10

Strain gages (gage length = 0.3 mm) were attached to the deck plate to measure changes in strain on both sides of the specimen, as shown in Figure 4.3 (a). The residual stress was calculated from the

change in strain before and after the cut. The first cutting and second cutting as shown in Figure 4.3 (b, c). The cutting blade thickness is about 1mm, as shown in Figure 4.4 (a), and a case of measured residual stress results as shown in Figure 4.4 (b).

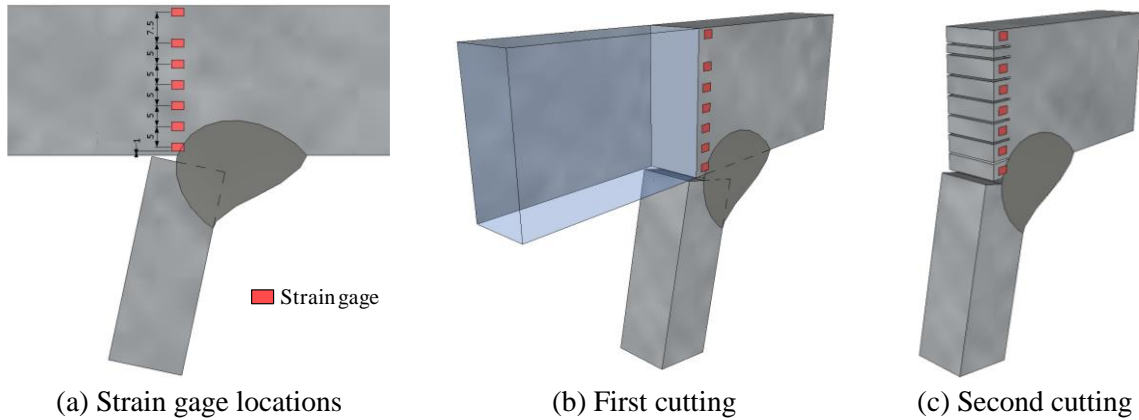


Figure 4.3 Location of strain gages in the cutting method (unit: mm)

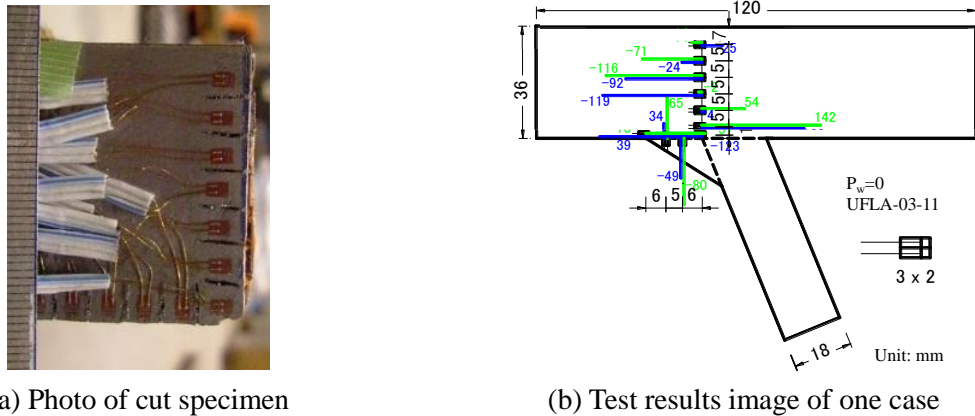


Figure 4.4 Residual stress distribution comparison

#### 4.2.2 Test and FE results comparison on residual stress

Because experimental methods need special equipment and long time to be executed, many results have been reported based on thermal elastic-plastic analyses using commercial finite element codes [107,108]. To verify the reliability of the analysis results, it is necessary to compare the results with experimental data.

A two-dimensional FE analysis model was built using Marc mentat, a commercial FE analysis code. The weld joints of the deck plate and U-rib were modeled using plane strain elements with four or three nodes. The shape and dimensions of the FE model were selected to account for the weld penetration rate and the root gap. Figure 4.5 shows the FE analysis model and mesh of the weld root. The minimum mesh size of the weld root was set to  $0.6 \times 0.6$  mm.

The following sequence was used for the analysis. First, a thermal conductivity analysis was performed by supplying instantaneous heat at 873 K to the welded portion of the specimen [109]. The obtained temperature distribution was regarded as the heat load. An elastic-plastic stress analysis was

then performed under plane strain conditions. These analyses were repeated until the entire model became isothermal. The model was then cooled down to an external temperature of 288 K, and the welding residual stress was determined from the final stress state. Figure 4.6 shows the temperature dependencies of the thermal and mechanical properties. However, this analysis was not considered for welding sequence and penetration of the base material. The stress-strain relationship subsequent to yield was regarded as linear. The von Mises criterion for yield was used to calculate the yield stress of the material.

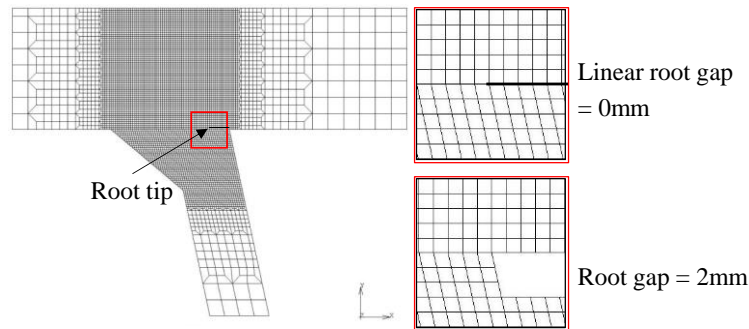


Figure 4.5 FE analysis model and root gaps

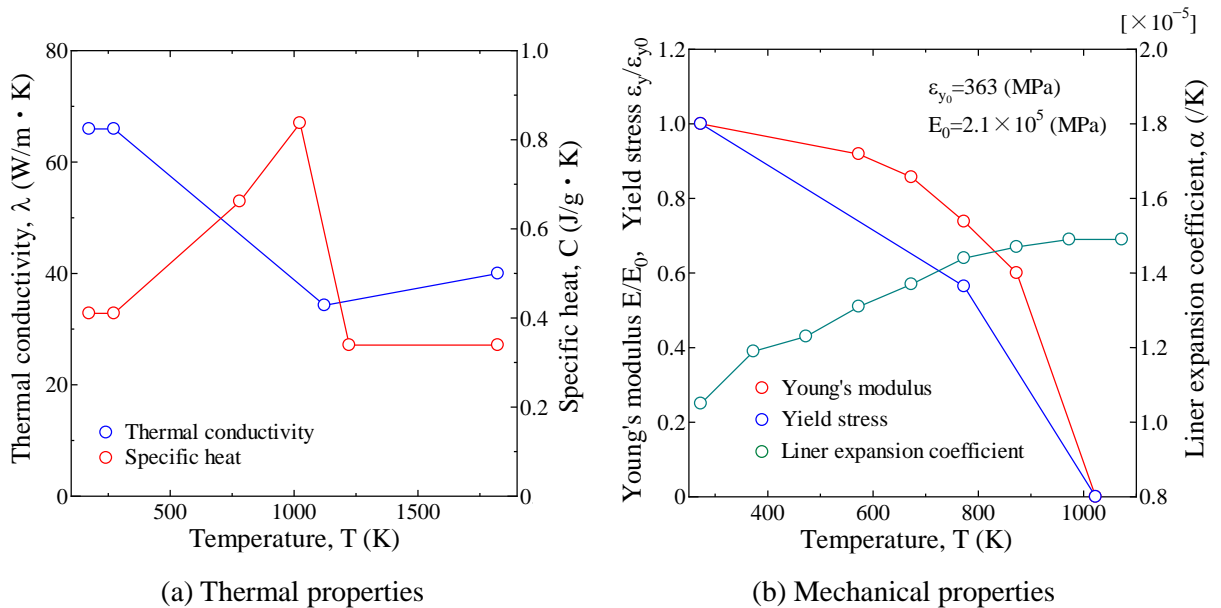


Figure 4.6 Temperature dependencies of the thermal and mechanical properties

To measure the residual stress between the deck plate and U-rib of an orthotropic steel deck, the respective stress distributions calculated from the experimental measurement and FE analysis were evaluated and compared based on changes in the weld penetration rate and the root gap. The residual stress distributions from the experimental measurement as shown in Figure 4.7 (a). The average experimental values of each type were compared with those from the FE analysis, as shown in Figure 4.7 (b). It is difficult to compare the residual stress; however, the stress distribution from the experimental measurement exhibited a similar trend to that from the FE analysis. The residual stress near the weld root was measured as high tensile residual stress and approached zero at about 3 mm from

the root. In addition, the section of about 3-25 mm from the root tip had compressive residual stress.

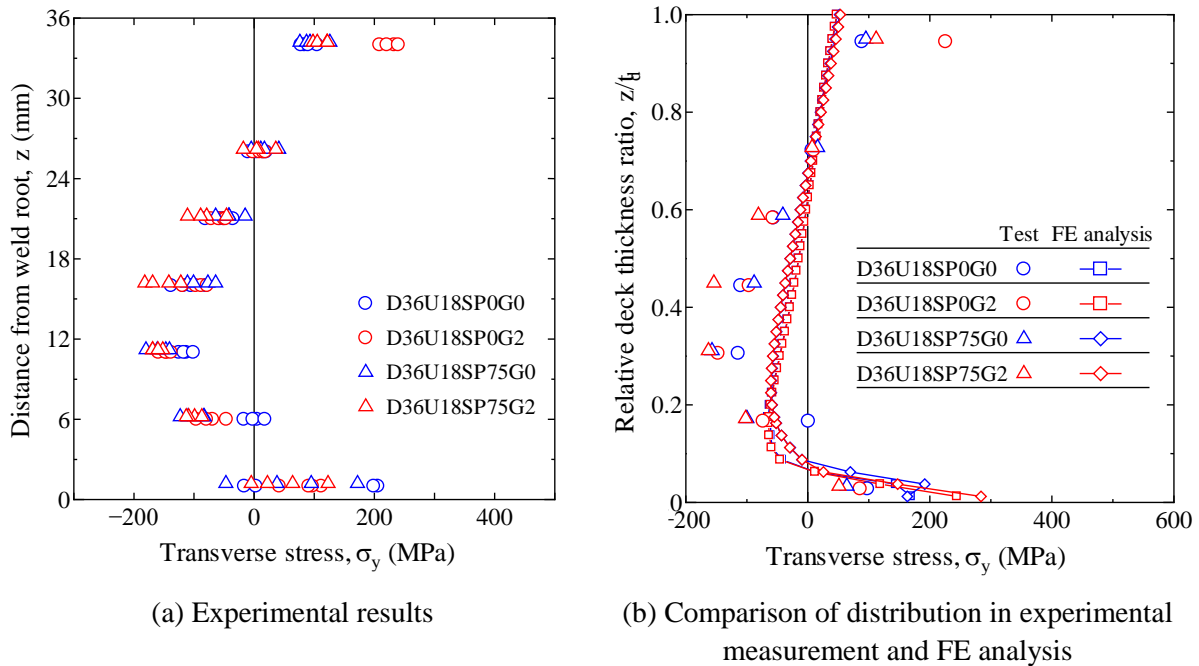


Figure 4.7 Residual stress distribution in deck plate to U-rib

### 4.2.3 Welding residual stress of FE partial models

To verify the welding residual stress and compare the results of the experimental measurement and FE analysis for large-scale specimens, analysis models were composed of a single U-rib, as shown in Figure 4.2(a). FE analysis models are summarized in Table 4.2. A total of 12 FE models were constructed for two deck-plate thickness model cases. In the FE analysis, the U-rib thickness, the weld penetration rate, and the root gap were determined considering the actual orthotropic deck plate. Using a three-dimensional solid element, the minimum element size was set to  $0.3 \times 0.3$  mm. The analysis was also conducted considering the length of the orthotropic deck plate in the bridge direction, and the analytical method was same in prior section.

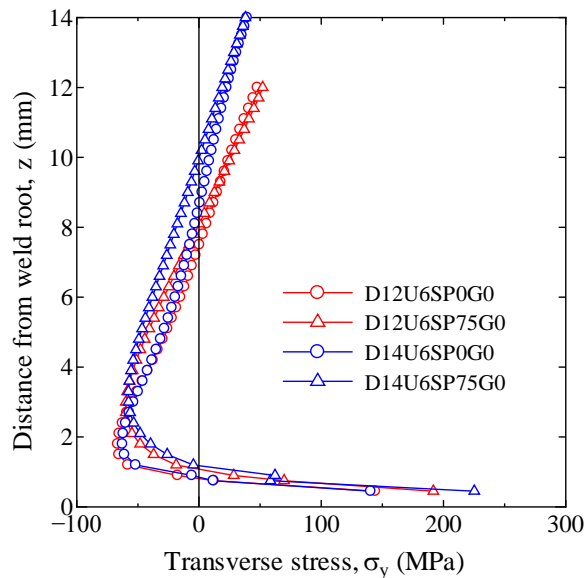
Figure 4.8 compares the effect of the thickness of the deck plate and U-rib, the weld penetration rate, and the root gap on the residual stress distribution at the root tip. The results showed that a tensile field existed from the root tip to 1 mm, compressive field existed from 1 mm to 8 mm, and then tensile stresses existed beyond 8 mm. Moreover, the maximum compressive residual stress was located away from the weld root, thus increasing the tensile stress in the root tip. As shown in Figure 4.8 (a), the tensile residual stress near the root tip for the deck plate of 12 mm was similar to that of the 14 mm deck plate; however, the tensile residual stress of the model with 75% weld penetration rate was 30% to 50% higher than that with 0% because of the heat input from welding. In Figure 4.8 (b), a comparison of the effect of the U-rib thickness shows a similar trend to the effect of the weld penetration.

It is difficult to compare the residual stress in the weld root because the shapes of root tip are different depending on the presence or absence of the root gap. However, the results of the analysis model show

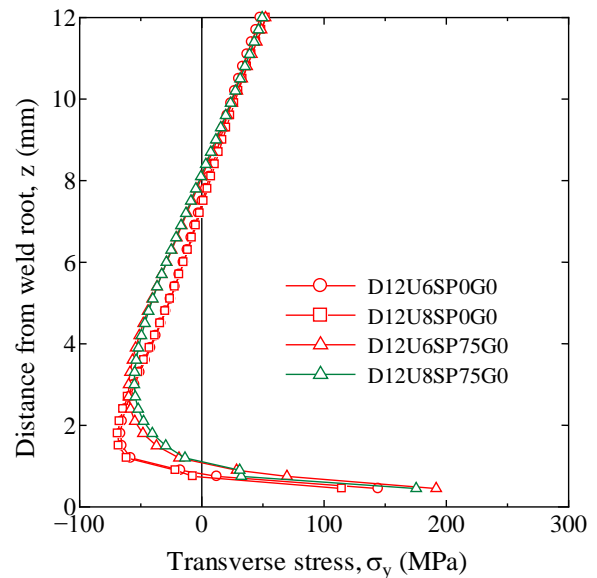
that the root gap has less influence on the residual stress, as shown in Figure 4.8 (c). To compare the effect of weld penetration rate without the root gap on the residual stress, the tensile residual stresses were observed for weld penetration rates of 75%, 50%, 25%, and 0%, as shown in Figure 4.8 (d). It was observed that the residual stress of the analysis model with 75% weld penetration rate was 35% higher than that with 0% penetration rate, 25% higher than with 25% penetration rate, and 15% higher than with 50% penetration rate.

Table 4.2 Parameters of FE analysis models

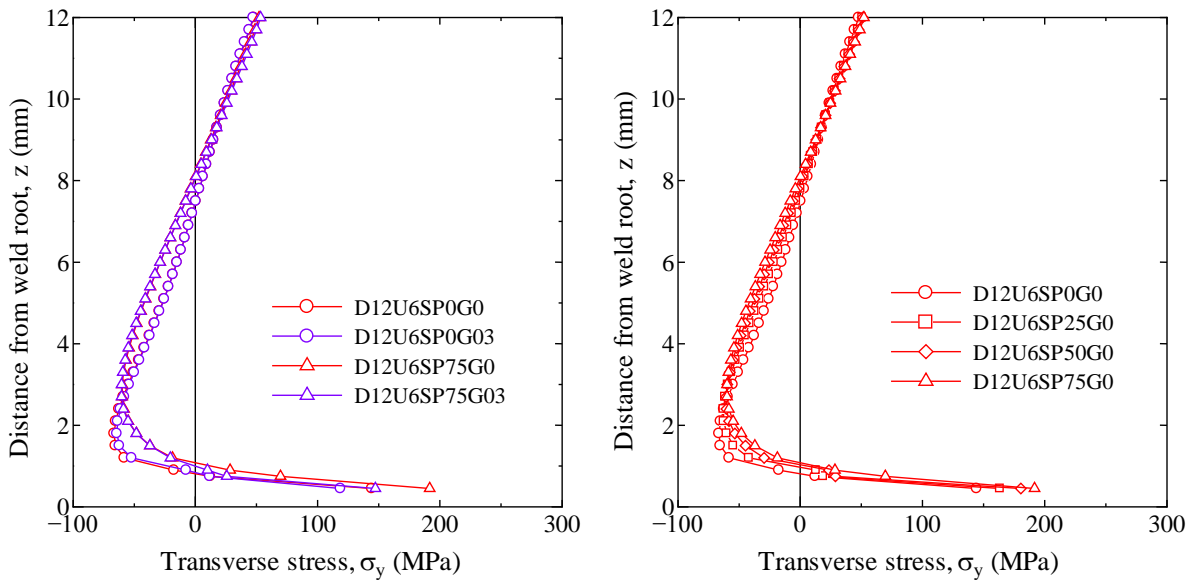
FE models	Deck plate thickness(mm)	U-rib thickness (mm)	Weld penetration rate (%)	Root gap (mm)
D12U6SP0G0	12	6	0	0
D12U6SP0G03				0.3
D12U6SP25G0			25	0
D12U6SP50G0			50	
D12U6SP75G0			75	
D12U6SP75G03			8	6
D12U8SP0G0	0			
D12U8SP75G0	75			
D14U6SP0G0	14	6	0	0
D14U6SP75G0			75	



(a) Effect of deck plate thickness



(b) Effect of U rib thickness



(c) Effect of root gap

(d) Effect of weld penetration rate

Figure 4.8 FE analysis results

Figure 4.9 shows the principal stress in the standard orthotropic steel deck (deck plate = 12 mm, U-rib = 6 mm, weld penetration = 75%, and root gap = 0 mm), which was calculated from the analysis results [27]. The tensile residual stress near the root tip was located at approximately 45° and was similar to the crack initiation and propagation in actual orthotropic steel decks. The tensile residual stress in the deck surface was slightly higher than that in the central part, and the angle of the principal stress was 45°. Thus, the principal stress was similar regardless of the thickness of the deck plate and U-rib, the weld penetration, and the root gap.

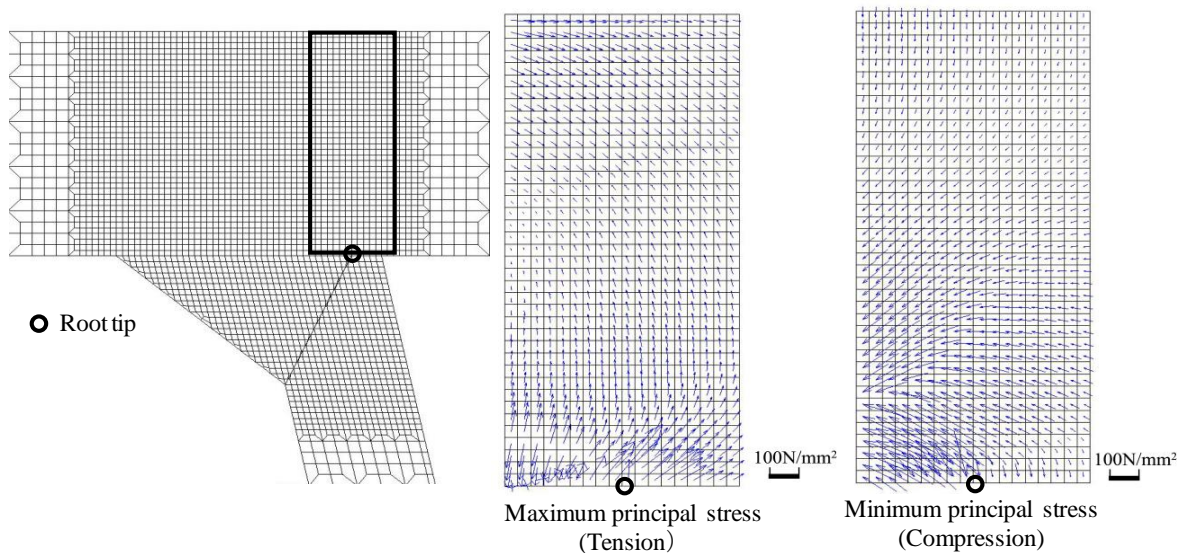


Figure 4.9 FE analysis on principal stress of D12U6SP75G0



#### 4.2.4 Effect of residual stress on full-scale specimen

To evaluate the welding residual stress of original test specimen, the residual stress of cutting out pieces of D12U6SP0-1 and D12U8SP50-1 were measured. The location of the cut out pieces of specimen is shown in Figure 4.10. Although residual stress values were different for each specimen, it was obvious that stress trends were similar in the vertical direction of the deck, even for specimens with different penetration rates and structural dimensions.

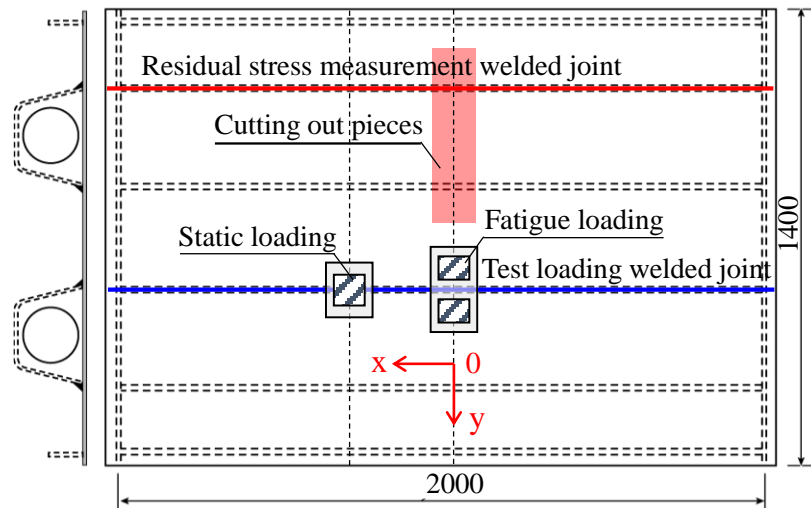


Figure 4.10 The location of cut out pieces of specimen

The stress distribution of the tested three-scale specimens was similar to the results from the residual test of full-scale specimen, as shown in Figure 4.11 (a). In particular, residual tensile stress always existed at about 10~20% of the thickness of the deck plate from the root tip. Based on the residual stress test results shown in Figure 4.11 (a), the values of residual stress near the root tip were confined to 60 to 100 MPa, while the actual residual stress of the root tip should be higher. Superposition of the tensile stress and residual stress would make the structure susceptible to fatigue failure [101].

However, the residual tensile stress would be released after crack initiation and propagation. The structural stress distribution in z direction of deck plate was calculated according to the basic specimen, as shown in Figure 4.11 (b). It was compared with the FE and measured initial residual stress of this structural detail in deck thickness direction, the residual stress occurs could lead to increase the maximum tensile stress value of effective stress. Compressive stress areas of initial residual stress near the neutral axis ( $z=6\text{mm}$ ) also proved the tensile stress in crack top may be offset and lead to crack propagation stop.

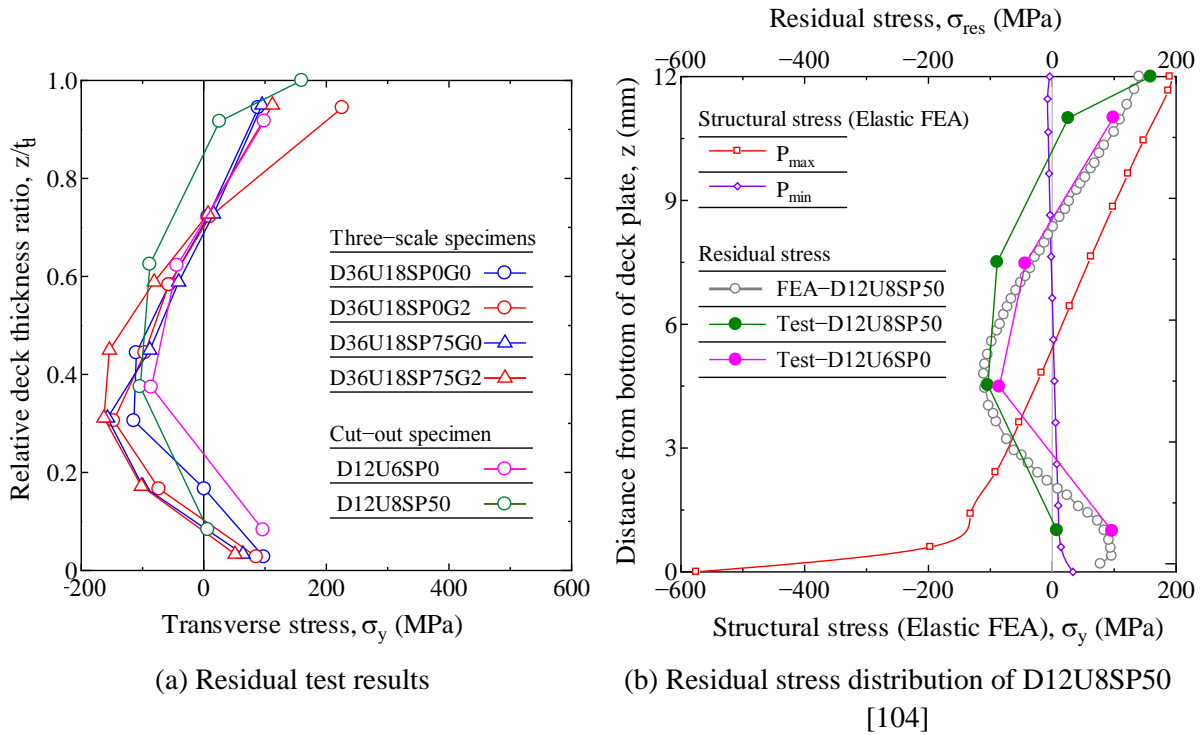


Figure 4.11 Residual stress distribution comparison

The crack depth of each tested specimen was usually smaller than half of deck thickness, as shown in Chapter 3. The D12 specimens showed that the root-to-deck cracks mostly stopped propagating after they reached the neutral axis of the deck plate thickness. It might be because of the root crack appear to close after the residual stress was released, and finally stopped the crack propagation.

A past fatigue test on fillet-welded cruciform joint under compressive cyclic stress also concluded that the fatigue root cracks propagated to a length of 4 mm (1/3 of plate thickness) and then ceased to grow [110]. It was suggested that the tensile stress range would affect crack propagation instead of the stress range. However, either the tensile stress around the crack tip was not large enough to reach the stress intensity factor, or the stress range provided only by the tensile stress was smaller than the constant amplitude of the fatigue limit stress range, which stopped the fatigue crack propagation [45].

Figure 4.12 shows the measured reference stress and relative reference stress range of the SP75 specimens. These figures show that the maximum stress range and maximum compressive stress of all specimens were located in the mid-span, and the maximum tensile stress point should be between the dynamic and static loading positions.

According to the residual stress measurement and analysis, the theoretical crack initiation point should obey the following formulas:

- (1)  $\sigma_{res} \leq \sigma_{max,c}$  Maximum tensile point
- (2)  $\sigma_{max,c} \leq \sigma_{res} \leq \sigma_y - \sigma_{max,t}$  Maximum tensile point
- (3)  $\sigma_y - \sigma_{t,m} \leq \sigma_{res}$  Mid-span (Maximum stress range point)

where  $\sigma_{res}$  is the residual stress of the weld root tip,  $\sigma_y$  is the yield strength of base metal,  $\sigma_{max,t}$  and  $\sigma_{max,c}$  are actual tensile/compressive stress at the root tip, respectively, and  $\sigma_{t,m}$  is the tensile stress at the mid-span under minimum fatigue load.

Root cracks of tested specimens were mostly initiated at the mid-span, which was consistent with the case of (3). The crack depth distribution of the D12U6SP0 specimens was different from others, as shown in Table 3.7, the deep cracks of D12U6SP0-1 were observed in the range  $x=50$  to 150 mm. Because the origin of fatigue failure changed with the magnitude of the stress range owing to the welding residual stresses in the weld root. The residual stress of the D12U6SP0-1 specimen seemed to be smaller than those of the SP75 and SP100 specimens. Thus, the crack was initiated at the maximum tensile point and not at the mid-span.

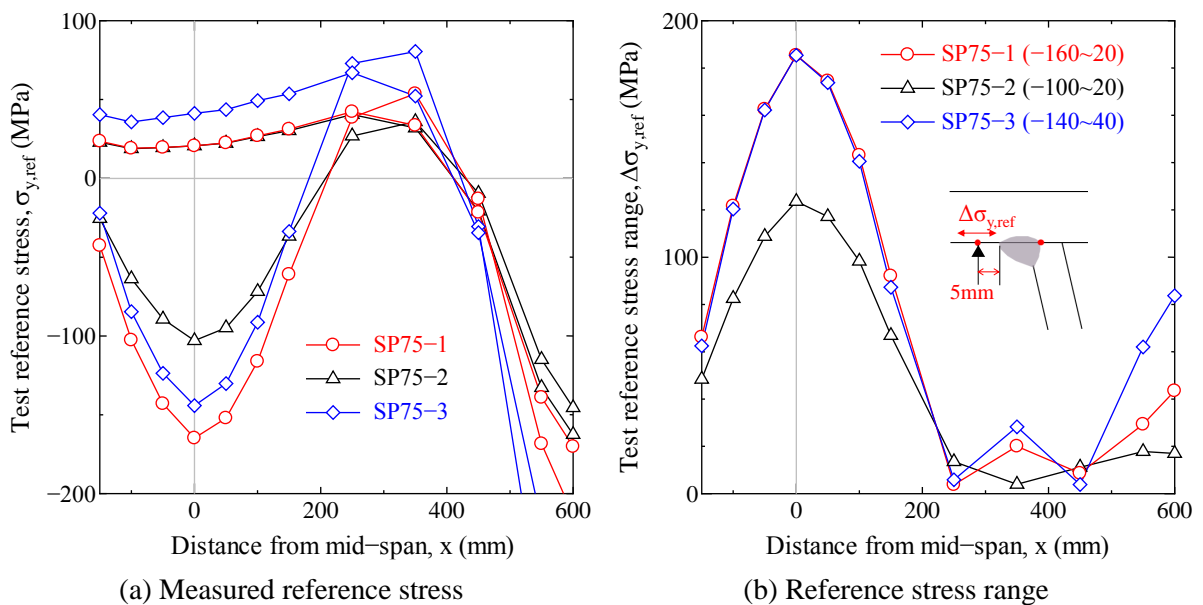


Figure 4.12 Measured reference stress of D12U6SP75

### 4.3 Parametric analysis of fatigue crack sizes

#### 4.3.1 Crack sizes comparison

In order to investigate the fatigue behavior of root cracks, cracking positions, crack depth/width/length, and propagation angles were analyzed. The fatigue crack of cross-sections were measured to investigate the crack propagation behaviors. Fatigue test results analysis were carried out, the crack sizes at mid-span in three-dimensional directions were compared. The crack length in the longitudinal direction is denoted as “x,” likewise, crack sizes in transverse and vertical directions are denoted as “y” and “z”, respectively. Crack sizes were defined in accordance with global coordinates, as shown in Figure 4.13(a).

This study also measured the root crack depth in one cross-section at intervals of 0.1mm in the transverse direction. Thus, the crack angles of every propagation stage could be calculated, defined as

crack propagation angle  $\theta_p$ . At the same time, the crack tip angle was defined as  $\theta$ , as shown in Figure 4.13 (b). The local coordinate origin was located at the crack initiation point.

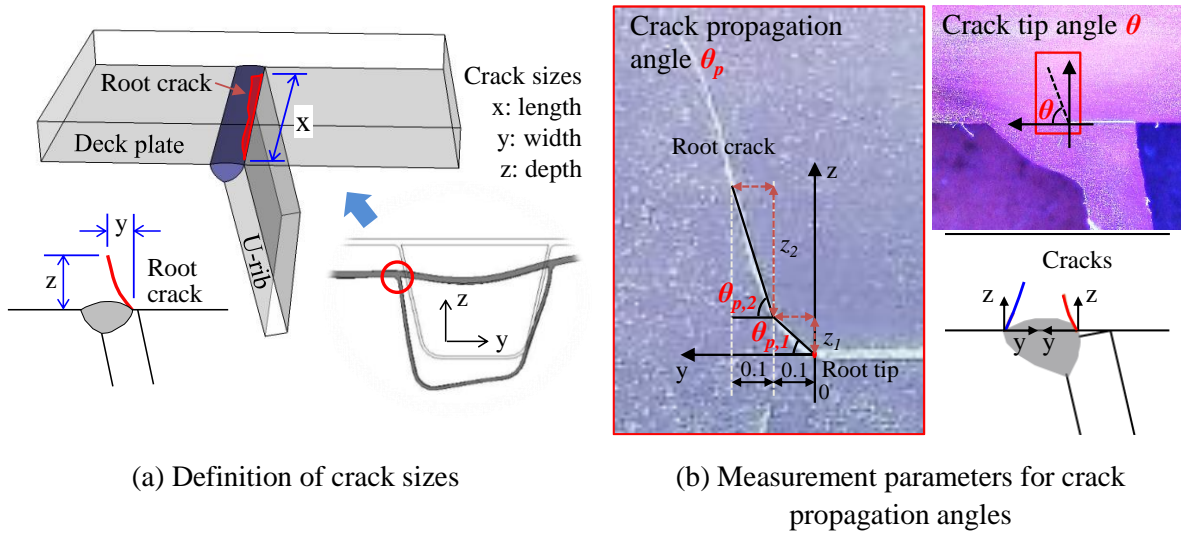


Figure 4.13 Definition of root crack parameters

To investigate the relationship between the crack length and maximum crack depth, the measured data of the cracking specimens are plotted in Figure 4.14, and the confidence limits are plotted at a distance of two distance deviations ( $\pm 2s$ ) from the mean. Most of the data for the tested specimens were distributed between the confidence limits. The crack depth was in proportion to the crack length, at about 65-times the mean. Thus, the crack length should be inversely proportional to the crack depth for the same structural details under the same stress condition. In addition, two of the specimens that fell outside of the scope of the confidence limits were been press straightened and groove treated, respectively. Meanwhile, the root crack depth usually smaller than mean value when both toe and root crack occurred. Besides, due to the limited number of D14 specimens, it cannot be concluded whether  $z/x$  ratio would be affected by the deck plate thickness.

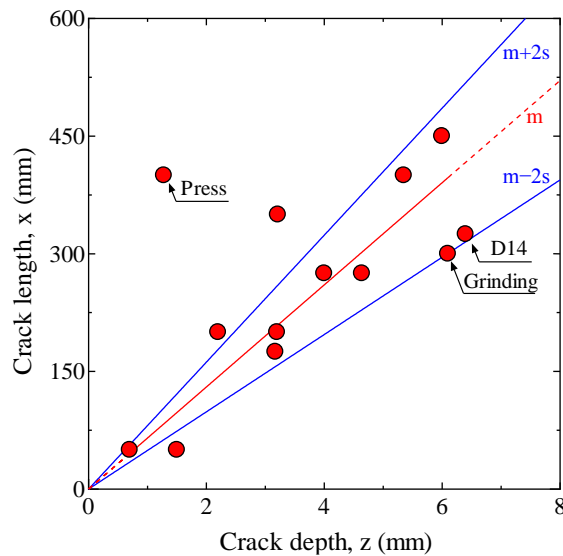


Figure 4.14 Measures data of root cracks of all specimens

The effect of the weld penetration rate on the crack propagation of the D12U6 specimens is shown in Figure 4.15 (a). The average crack depth began to approach the maximum crack depth after the small and multiple cracks coalesced together to form long semi-elliptical cracks. However, the average crack depth was not in proper proportion to the maximum crack depth in some cases where deck or toe cracks existed. For instance, D12U6SP0-4 was a case where a deck crack occurred from the upper deck surface, which might have led to a change in the stress flow near the root tip. In addition, D12U6SP75-2 had the smallest stress range, and its cracking degree was nearly the same as D12U6SP0-1 in this figure, which might have been due to the same tensile stress. Moreover, compared with D12U6SP100-1, in which both toe and root cracks occurred, D12U6SP100-3 had only root cracking because of the groove treatment at the weld toe. The results showed that the root crack depth and length of SP100-3 were larger than those of SP100-1 when the toe cracking was avoided.

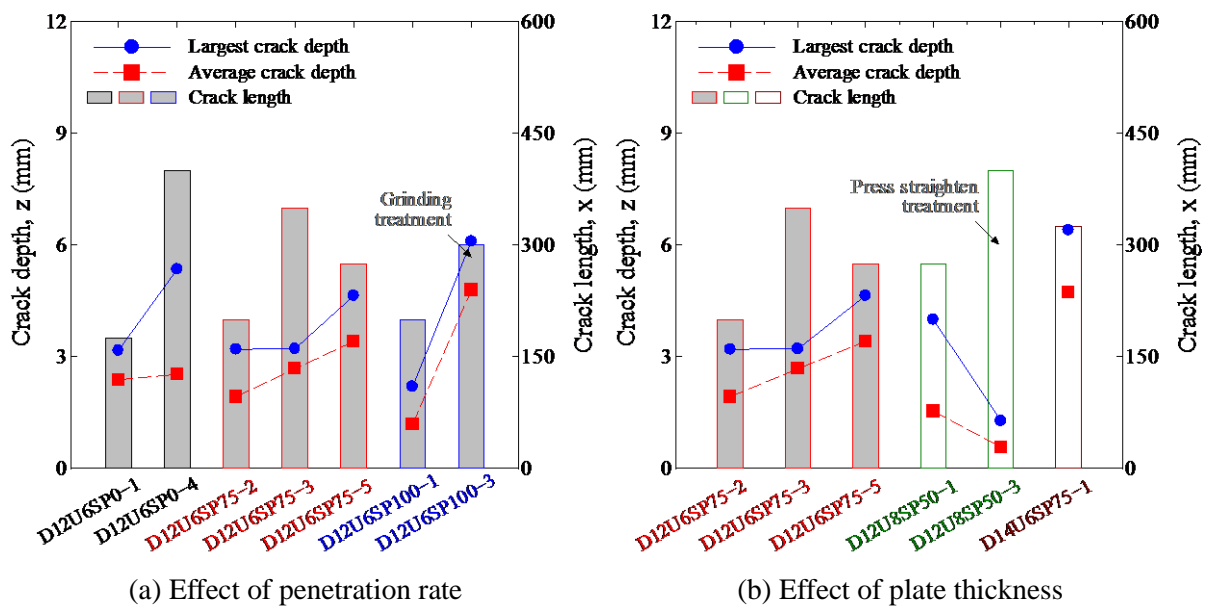


Figure 4.15 Effect of structural parameters on root crack propagation

The effect of the plate thickness on the crack propagation is shown in Figure 4.15 (b). First, D12U8SP50-3 had the maximum crack length and minimum crack depth because its deck plate had been press straightened after fabrication. This led to a small root crack depth, but extended the length in the longitudinal direction. Further, the crack lengths of D12U8SP50-1/-3 were inversely proportional to their crack depths under the same stress range. Under the same test conditions, D12U6SP75-3/-5 also showed this phenomenon. Therefore, the fatigue crack damages could not be accurately assessed by only crack length  $x$ , even with the same structural details for a steel bridge.

Moreover, D14U6SP75-1 had the largest root crack depth, while no cracking occurred for D16. The static loading test results suggested that increasing the thickness of the deck plate could decrease the local stress range under the same loading conditions. Thus, the relatively higher fatigue life in the test results of D16 compared to those for D12 was reasonable. However, the crack depth of D14 was larger than those in other specimens, which might have been due to its high tensile stress. The test results

showed the crack patterns were susceptible to change with change in the magnitude of the stress range; and the crack depth seems could be affected easily by the structural parameters.

### 4.3.2 Effect of stress range on crack propagation

#### (1) Specimens under stress range of -140 to 40MPa

Figure 4.16 (a) shows the crack sizes at mid-span of D12U6 specimens with penetration rates of 0%, 75%, and 100%. The crack depths are very different due to the effect of penetration rate. In Figure 4.16 (b), the maximum crack depths with higher penetration rate were shown to be smaller than those of SP0, the higher penetration rate can prevent or slow down the growth of root cracks. Previous analytical study also suggested that an increase in the penetration rate (up to 75%) would produce a lower stress at the weld root, which results in a higher fatigue resistance.

However, there were also the contract results obtained by related experiments in past studies. Small-scale specimens of a rib-to-deck welded joint with no restraint on the ribs were tested by Yamada et al. [45], it reported that the fatigue resistance of a 100% penetration weld was slightly lower than that of an 80% PJP weld. We considered that a penetration rate in the range of 0% to 75% is desirable for fatigue durability of this structural detail. However, for the welded joint with full penetrated, it might have an opposite effect than 75% penetration rate. It was considered the root tip geometry of full penetrated welded joints were different from that of partial joint penetration, the fatigue strength of specimen with full penetration depending on the welding technology and geometrical properties at root tip.

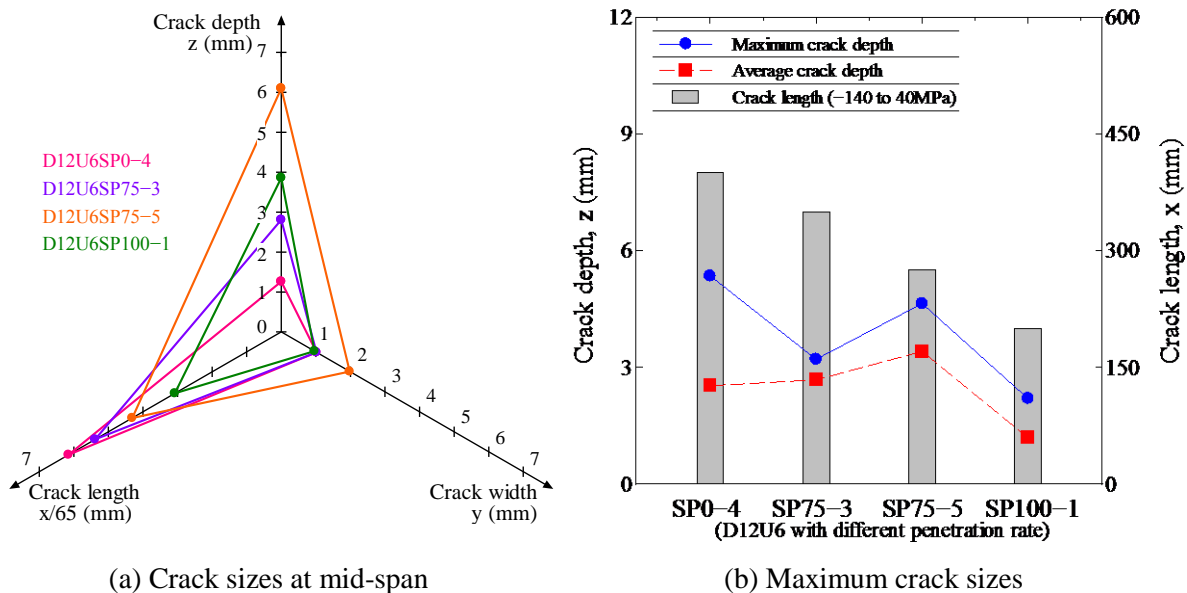


Figure 4.16 Effect of weld penetration rate on crack propagation

Based on the calculated mean and confidence limits of Figure 4.14, the crack length and depth of specimens with a tested stress range of 40 to -140MPa, are plotted in Figure 4.17. It is obvious that both the crack depth and crack length decrease with an increase in the penetration rate in the case of a high stress ratio.

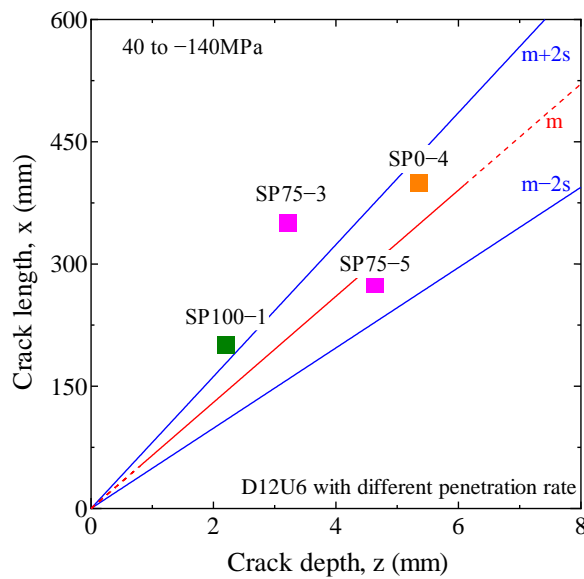


Figure 4.17 Relationship between crack depth and length (Effect of penetration rate)

## (2) Specimens under stress range of -160 to 20MPa

The crack depths were compared for two groups of specimens: under the same stress range of -160 to 20MPa and under the same loading conditions. The crack sizes at mid-span varied considerably due to the different structural parameters, as shown in Figure 4.18. The crack behavior of D12U6SP0-1 was shown to be different than the behaviors of other specimen. The root crack was in the range from 0 to 175 mm in longitudinal direction, therefore the crack depth at mid-span was 0 for D12U6SP0-1. This behavior may be attributed to the low penetration rate and low residual stress. It should be noted that D12U6SP0-4 and D12U8SP50-1 have deck and toe cracks respectively, occurring along with the root cracks, which was disadvantage. Thus Figure 4.18 showed that an increase in the thickness of U-rib is invalid for preventing root cracks.

Based on the calculated mean and confidence limits of Figure 4.14, the crack length and depth comparison of specimens with different plate thicknesses as shown in Figure 4.19. Firstly, the crack depths and lengths of D12U6SP0-1 and D12U8SP50-1 under 20 to -160MPa showed that they were closed to average. Moreover, under the same loading, D12U6SP0-4 and D14U6SP75-1 showed that the maximum root crack depth of D14 was larger than that of D12, but their crack depth percentages were nearly the same at around 45% of the deck plate thickness. It is well known that the stress range plays a major role before crack initiation because of the effect of residual stress. However, the residual tensile stress would be released after the crack initiated. Thus, the maximum tensile stress would play a decisive role, instead of the stress range during crack propagation. The D14 specimen was tested with a large tensile stress, which contributed to its crack depth. Overall, an increase in the deck plate thickness was beneficial to the fatigue durability before the crack initiation, but thickening the U-rib had no obvious effect in the prevention of root cracking.

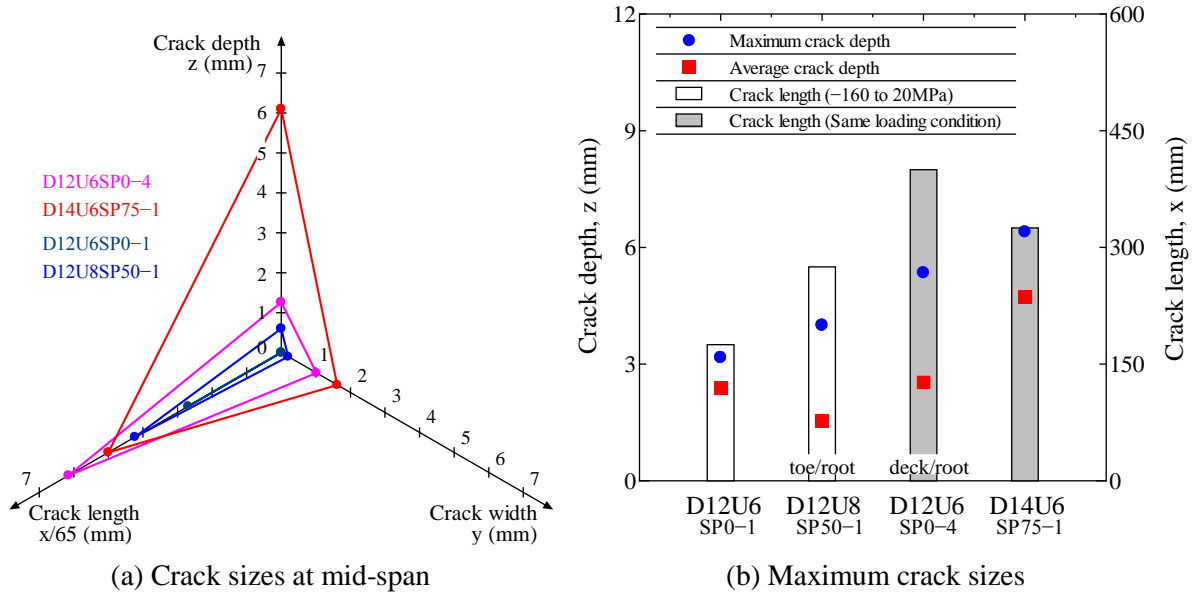


Figure 4.18 Effect of weld penetration rate on crack propagation

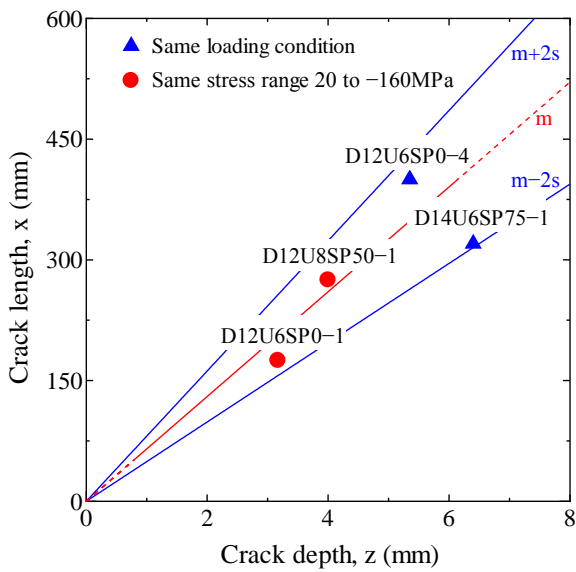


Figure 4.19 Relationship between crack depth and length (Effect of plate thickness)

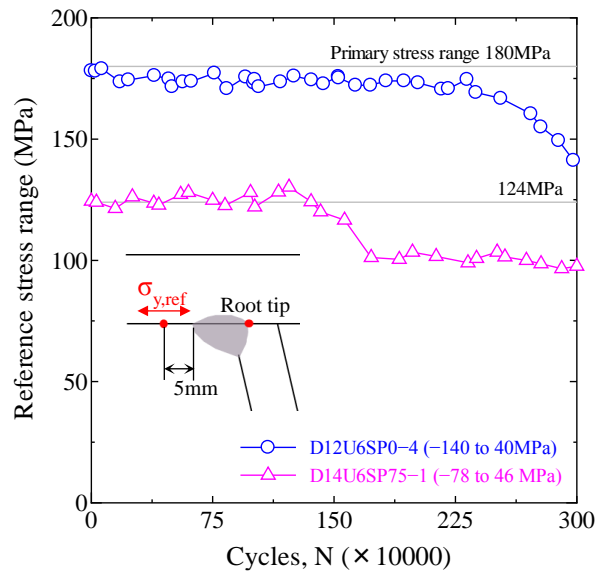


Figure 4.20 Dynamic reference stress range at mid-span

The dynamic reference stress responses at mid-span of these two specimens are shown in Figure 4.20. Even though the stress range of D14 is smaller than D12 under the same loading conditions, the crack initiation (after 1.22 million loading cycles) life of D14 is significantly smaller than that of D12 (after 2.32 million loading cycles). However, no crack was observed in the specimen D16U6SP75-1 (under the same loading as D12U6SP75-1), which showed a good performance in fatigue durability.



## 4.4 Crack propagation analysis

### 4.4.1 Crack propagation directions

The crack propagation angle distributions of D12U6SP0-1 are shown in Figure 4.21. A root crack occurred in range of 0 to 200mm in the x direction, and the scope of the larger-than-average crack depth was +50mm to +150mm, with the maximum crack located at x=150mm. However, the propagation angles of adjacent cracks were different, even though they had nearly the same crack depth. Thus, it was considered that more than one crack initiation point existed.

The root crack shapes of tested specimens D12U6SP0-1 and D12U8SP50-1 were measured at intervals of 0.2mm in the transverse direction, as shown in Figure 4.21. Disparity existed around the initial crack angles of the two specimens. This was mainly due to the different penetration rates and U-rib thicknesses, which caused a geometric difference at the root gap. However, the basic expansion tendencies were similar when  $y \geq 0.3$ mm. The crack angles propagated from small to large and tended to be stable at  $70^\circ$  to  $80^\circ$ . It was reasonable that the crack tip angles were only affected by the maximum principal stress. Even though some local parameters (residual stress, geometry of root gap et al.) were different at welded joint, the propagation angle of all specimens always tend to be a stable value when under the similar test conditions.

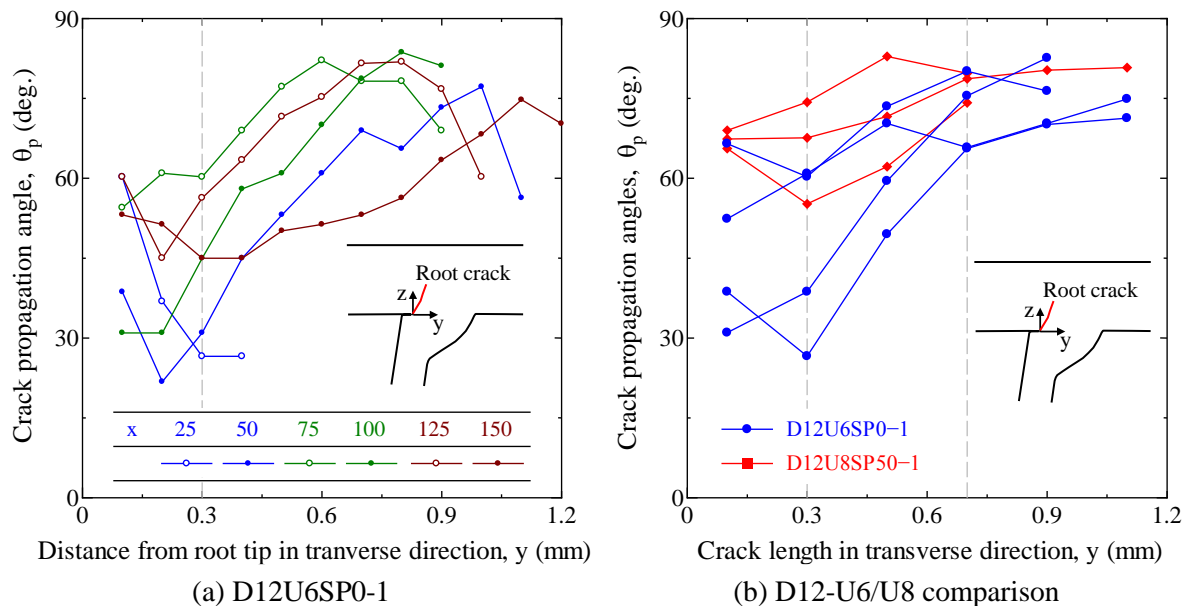


Figure 4.21 Root crack propagation angles of cross-sections

To explain the crack process of D12U6SP0-1, the crack depth was measured in the y and z directions in each cut section as shown in Figure 4.22 (a). The red and blue lines indicate that the trends of root crack propagation were opposite, and the crack depth in the z direction varied notably even for a given y value. Crack propagation angle and the related depths was shown in Figure 4.22 (b). It is clear that crack angles at x=125 were very different from those at other sections because the crack propagation angle was larger than that of other cross sections. The fatigue cracks were usually observed as small

semi-elliptical cracks at multiple points along the weld line, and then the small fatigue cracks propagated and coalesced into a larger crack. Thus, the cross-section between peak values was probably near the confluence of two small cracks.

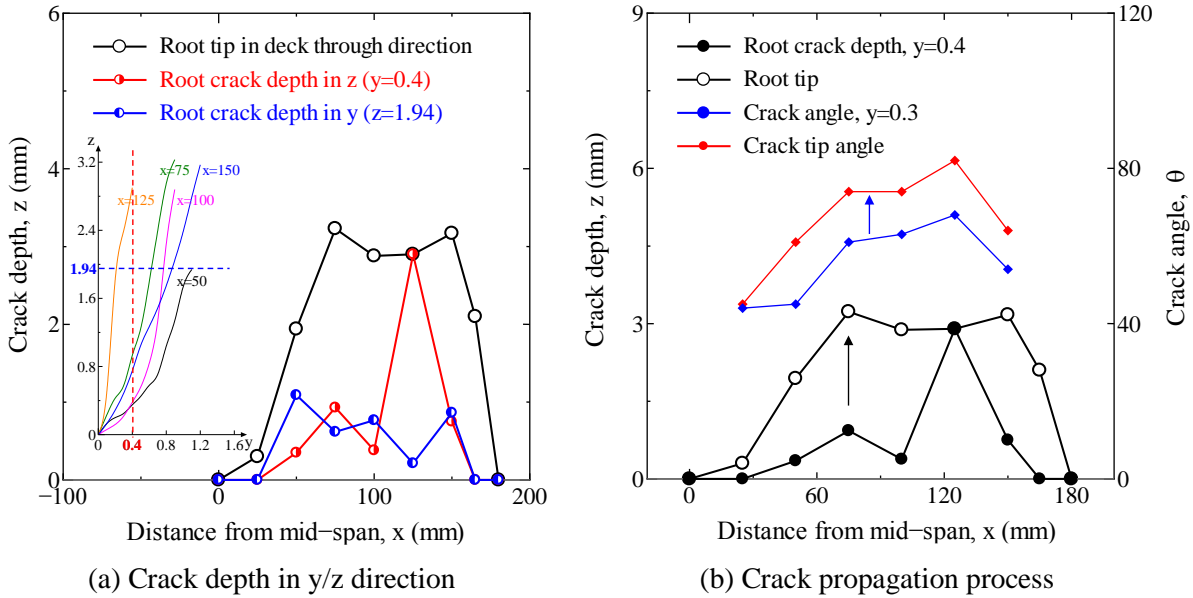


Figure 4.22 Crack depth comparison of D12U6SP0-1 cross sections

#### 4.4.2 Effect of penetration rate on crack angles

The crack angles of specimens SP0-4, SP75-3, SP75-5, and SP100-3 were compared. These four specimens were under the same stress range (-140 to 40 MPa). The root tip was set as the origin coordinates as mentioned in Figure 4.13 (b). Figure 4.23 shows the crack tip angles of all cross sections of these four specimens.

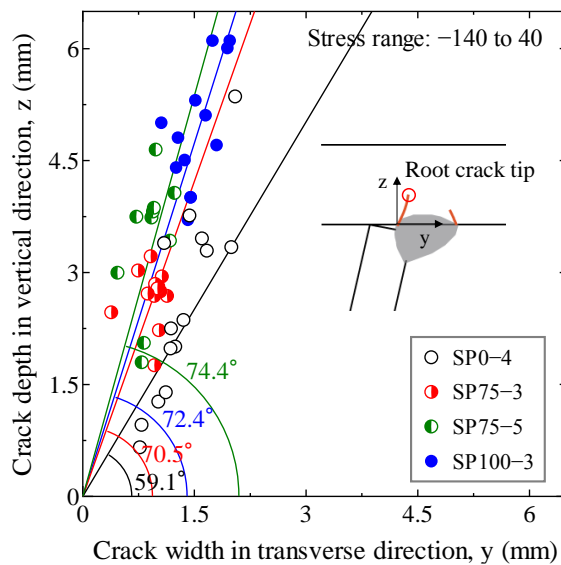


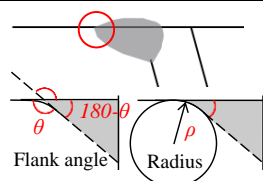
Figure 4.23 Average crack tip angles of specimens under -140 to 40 MPa

The SP0 specimens have the smallest crack angles, and the average cracking angles of the SP75 and SP100 specimens are nearly the same. The SP0 specimens had more oblique cracks, which might have been caused by the geometric shape of the root gap.

#### 4.4.3 Effect of weld toe on root crack

There are four specimen with both of root and toe crack occurred during the fatigue test. As we all know, the fatigue cracking at weld toes precipitate from inherent micro-discontinuities such as slag inclusions; in the presence of high tensile welding residual stresses; and the stress concentration due to the weld geometry. Because the fabrication process of the specimens were totally same, and the micro-discontinuities and residual stresses were hard to be detected accurately, the geometric parameters of the weld toes of D12U6SP0 and D12U8SP50 were measured, as listed in Table 4.3.

Table 4.3 Geometry of weld toe

Specimen	No.	Flank angles of the weld toes $\theta$ ( $^{\circ}$ )	Radius of the weld toes $\rho$ (mm)	Measurement method
D12U6SP0	-1	128	1.13	
	-4	129	1.10	
D12U8SP50	-1	102	0.47	
	-2	107	0.46	

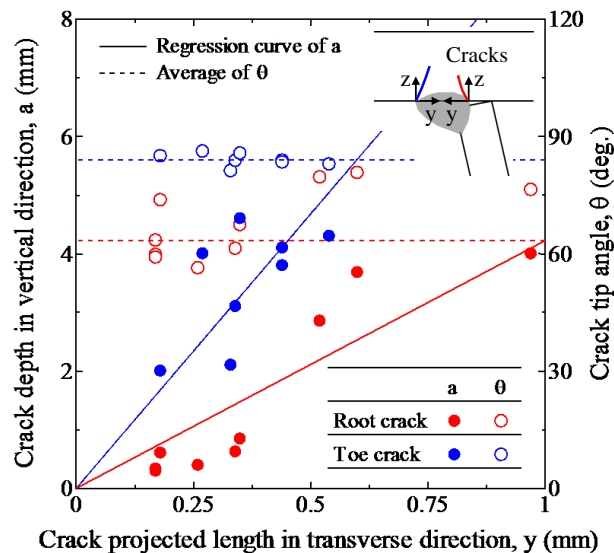


Figure 4.24 Comparison of root and toe crack tips of D12U8SP50-1

Previous studies have shown that cracks originate from the weld root when the weld leg length (or weld size) is small and from the weld toe when the length is large [111]. In a fillet welded joint, a specimen with a larger radius at the weld toe usually had a smaller stress concentration, which would provide a better fatigue resistance. The radius of the weld toe of D12U6SP0 was much larger than that of D12U8SP50. Test results of D12U6SP0-1 and D12U8SP50-1 also showed to be the toe crack were easier occurred at U8 specimen. It was considered the stress concentration of U8 should be larger than

that of U6 specimens when under the same stress condition. The geometry of weld toe could be one of critical factors for toe crack initiation. The toe and root crack tips of D12U8SP50-1 were compared to investigate their relationship. The depths and angles of the crack tips in cross-sections are shown in Figure 4.24.

The crack tip points were fitted by the least square method. Both the angles and depths of the weld toe cracks were larger than those of the weld root cracks. In addition, the root and toe cracks of D12U6SP75-3/D12U6SP100-1 were also compared as shown in Figure 4.25. For these two specimens under the same stress conditions, the root crack depth were smaller than toe crack depth. It seemed that the stress around the root tip was affected by a toe crack. The stress of the root crack tip might tend to be weaker after the toe crack initiated. In another way, the root and toe crack tip angles of these two specimens tended to be nearly the same. Even though the geometry of the root/toe tip of the full penetration specimen was different from that of a PJP specimen, this would only lead to a difference in the initial cracking directions. However, the average crack tip angles were only affected by the maximum principal stress.

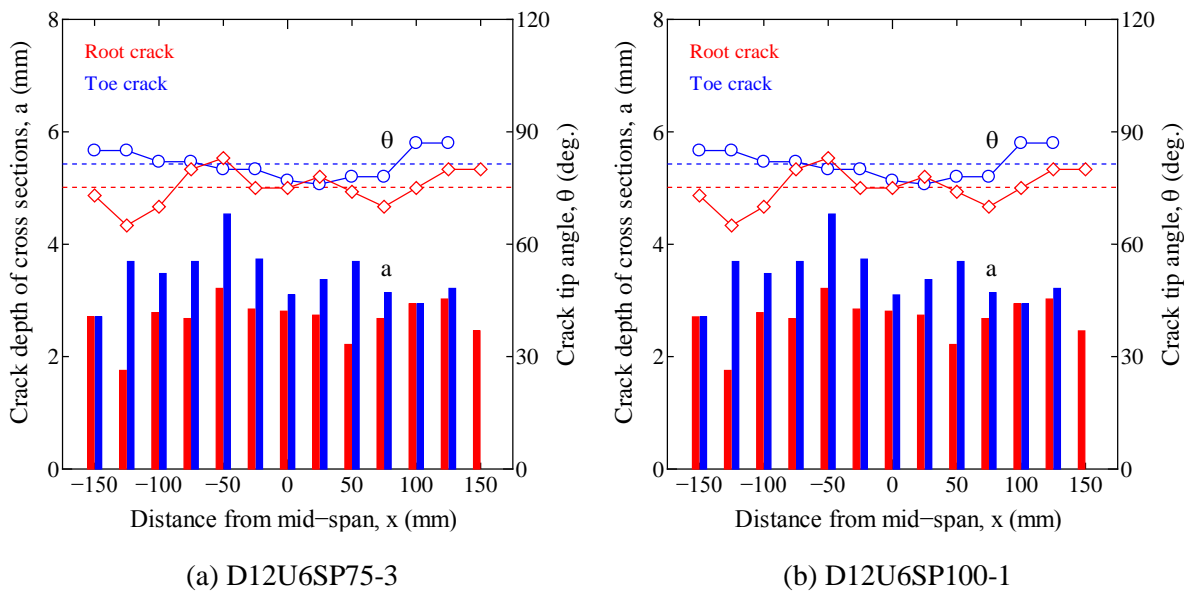


Figure 4.25 Comparison of toe and root cracks (40 to -140MPa)

## 4.5 Summary

To clarify the behavior of formation of the root crack in the deck plate-to-U-rib connection, the welding residual stress was measured using the cutting method. The residual stress in the weld root was examined to quantitatively investigate. Moreover, the fatigue cracking patterns and their influence factors were also discussed by comparing the crack sizes and crack propagation angles at cross sections. It was explained the cause identification of the crack initiation of this structural detail by parametric analysis based on fatigue test results, summarized as follows:

(1) The residual stress near the weld root was measured to be high tensile residual stress, and the experimental results showed a similar trend to the FE analysis results. It was identified the residual stress distribution in an orthotropic steel deck depending on partial penetration weld. The tensile residual stress for the analysis model with 75% weld penetration was 1.35-times larger than that with 0% penetration rate.

(2) Based on the measurement of the welding residual stress and fatigue test results, the cracking behavior of the weld root were investigated by considering the effective stress. The magnitude of tensile stress would play a decisive role during the root crack propagation after the residual stress was released around the root tip.

(3) The crack length of this structure detail should be about 65times larger than crack depth. This ratio usually accordance with the root crack behavior of this structural detail, without special treatment in welded joint. For instance, the grinding at weld toe could avoid crack at toe but might lead to a deeper root crack, and the press straighten could be an effective treatment for preventing root cracks propagating in depth in actual bridge.

(4) The crack depths with higher penetration rate were shown to be smaller than those of SP0, the higher penetration rate can prevent the root cracks. However, the fatigue durability of specimen with full penetration was hard to judge because its special geometrical properties at root tip. Besides, an increase in the deck plate thickness was beneficial to the fatigue durability before the crack initiation, but thickening the U-rib had no obvious effect in the prevention of root cracking.

(5) The cases with the occurrence of both toe and root cracks were discussed, by comparing the geometric parameters at the weld toes of 6mm- and 8mm-thick U-rib specimens. The radius of the weld toe of U6 was much larger than that of U8 specimens. Test results also showed to be the toe crack were easier occurred at U8 specimen under this loading case. Therefore, besides the inherent micro-discontinuities and the presence of welding tensile residual stresses, the geometry of weld toe could be one of critical factors for toe crack initiation.

## Chapter 5 Numerical analysis of rib-to-deck weld joint with artificial root cracks

### 5.1 Introduction

The structural parametric effects and the position of wheel load were considered in previous numerical studies [15,17]. It is considered that the crack initiates from the weld root and propagates through the weld throat. This propagation can be prevented with sufficient or full penetration [112,113]. Thus, Japan Road Association (JRA) [21] specifies a minimum penetration of 75% of rib wall; additionally, the LRFD Bridge Design Specifications (AASHTO 2004) [29] suggest a minimum penetration of 80%. Recently, series test results showed that increasing the penetration rate is also beneficial for the prevention of root cracks. However, some researchers found that the fatigue performance of the rib-to-deck weld is not directly related to its penetration [114]. The effect of the fabrication process and weld penetration on root crack initiation were investigated in the previous research [33], however the correlation is still unclear. Besides, it was summarized that the use of thick deck plate (~16 mm) might improve the fatigue durability of the rib-to-deck joints, whereas it was found that the fatigue strength gradually decreases as the deck plate thickness increases [45]. However, the effect of plate thickness on fatigue durability of cracked specimens is still insufficient and unclear. Above all, the root crack mechanism is still not understood in sufficient detail with regard to parameters such as the weld penetration rate, shape of root gap, and plate thickness.

Based on the previous test results of sectional specimens, this chapter focused on the root crack mechanism at rib-to-deck welded joints, conducted with structural parameters analysis on the matching FE models under the basis stress condition. The fatigue behaviors of structure detail were investigated by considering the effect of root gap shapes, weld penetrations, and plate thicknesses on crack initiation. Moreover, to understand the cause of root crack propagation, various root crack depths were simulated in the crack models. The structural responses of artificial fatigue crack in models were evaluated, and the crack tip stress variations occurring at the different propagation stage under cyclic loading were clarified.

### 5.2 FE models

#### 5.2.1 FE models with non-crack

In order to investigate the fatigue behavior and stress response at root tip, the Sectional OSD models were built by the analysis program MARC mentat 2012, as shown in Figure 5.1 (a). These elastic FE models were set the same boundary conditions as the fatigue tests. The main deck plate, U-ribs, and rubber were simulated using eight-node solid elements. The elastic modulus (E) and Poisson's ratio were set to be 206,000MPa and 0.3, respectively, for the steel's material properties. The dimensions of the

root gap and mesh refinement are shown in Figure 5.2.

For an elastic model, the mesh refinement could lead to more accurate stress distribution and infinite concentrated stress value even exceed the yielding strength. So to ensure the correct stress distribution at stress concentrated location, the minimum mesh size was determined to be 0.2mm in the welded joint.

Different plate thickness and penetration rates were considered, the boundary conditions of D12U6SP75 model were set as the same primary loading conditions of its corresponding specimen. In the presence of a flaw or slots at the root gap, the direction and value of maximum principal stress near root tip could be totally influenced [109]. There are linear and triangular shaped root gaps that exist in the tested specimens. In this study, elastic models were simulated with for the abovementioned two kinds of root gaps at partial joint penetration, hereafter referred to as “line-gap” and “tria-gap” models. The root gap shapes and welded joint dimensions were simulated as illustrated in Figure 5.2 (a, b).

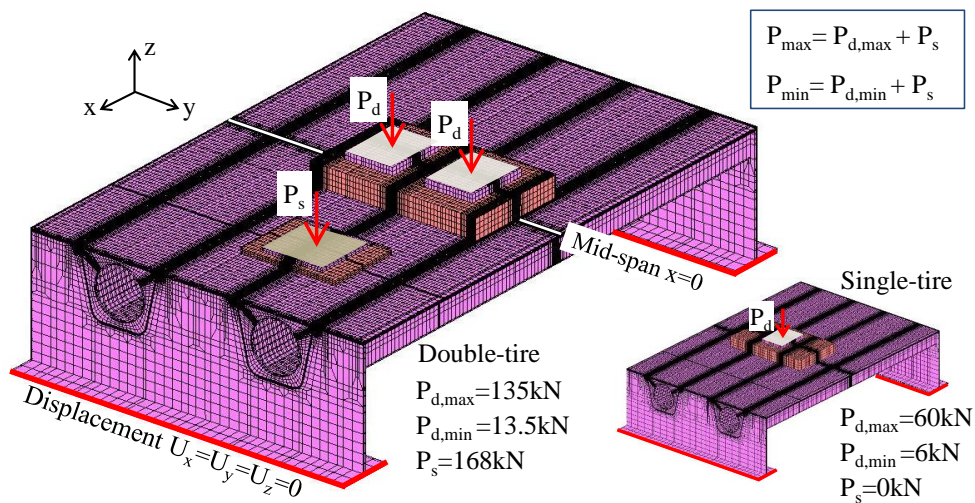
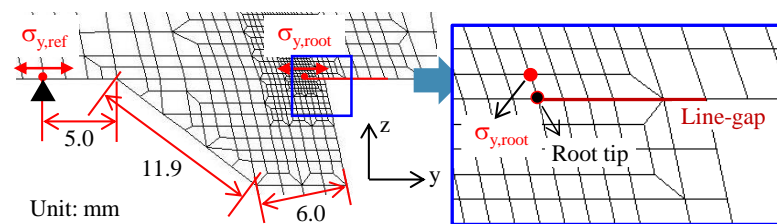
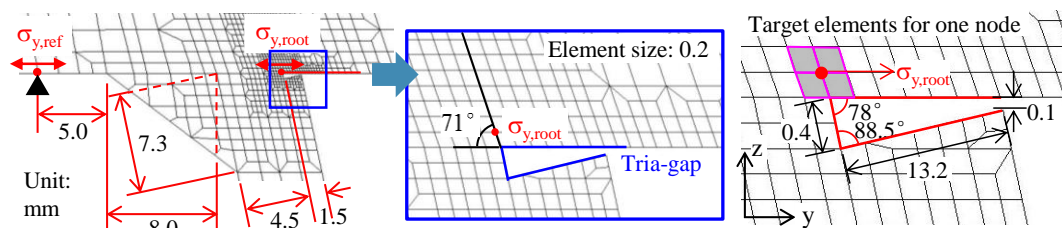


Figure 5.1 FE models and the loading conditions



(a) Linear root gap

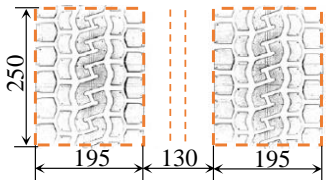
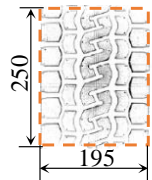


(b) Triangular root gap

Figure 5.2 Basic FE model and the dimensions of root gaps (D12U6SP75)

The reference stress range of D12U6SP75 at mid-span was controlled between -160 to 20 MPa in FE analysis, which was same as the stress conditions in the test. Loading conditions of other FE models were set identical to the loading conditions of D12U6SP75. The maximum principal stress determined the cracking direction, whereas the principal stress was not a constant but changed for the different loading cases. Thus, the FE models only considered the most unfavorable loading cases of the fatigue tests:  $P_{\max}$  and  $P_{\min}$ , as shown in Table 5.1.

Table 5.1 Loading cases of FE models

Loading cases	Double tire load		Single tire load	
$P_{\max} = P_{d,\max} + P_s$	$P_{d,\max} = 135\text{kN}$	$P_s = 168\text{kN}$	$P_{d,\max} = 60\text{kN}$	$P_s = 0\text{kN}$
$P_{\min} = P_{d,\min} + P_s$	$P_{d,\min} = 13.5\text{kN}$		$P_{d,\max} = 6\text{kN}$	
Dimensions of loading tires (Unit: mm)				

Based on the FE model of D12U6SP0-1 and D12U6SP75-1, with a reference stress range of 20 to -160MPa, Figure 5.3 shows that the results of the FE analyses and tests had similar stress distributions at reference points in the traffic direction. The stress of the root tip at mid-span was the tensile stress under  $P_{\min}$  and tended to be the compressive stress under  $P_{\max}$ . In addition, there was a high stress concentration at the root tip compared to the reference point.

Figure 5.4 shows that  $\sigma_{y,\text{root}}$  was about 1.7times larger than  $\sigma_{y,\text{ref}}$  under  $P_{\max}$ . When the tensile stress of the reference point at mid-span increased from 20MPa to 40MPa, the stress of the root tip increased by about 2~3times. The stress at root tip and the stress at the reference point were determined to be high-correlation, as shown in Table 5.2 [115]. The reference stress could also be considered as the nominal stress of root tip. As the case of D12U8SP50 model, the stress distribution from weld toe to root gap at bottom of deck plate, as shown in Figure 5.5. Obviously, the stress at deck plate bottom would be tensile stress under  $P_{\min}$  and be compressive stress under  $P_{\max}$ . The tensile stress at root tip is less than 10% of compressive stress there.

Table 5.2 The correlation coefficient between root tip and reference stress

The location of reference point	Correlation coefficient
At deck plate-10mm away from weld bead	0.883
At deck plate-5mm away from weld bead	0.943
At rib-5mm away from weld bead	0.396
At rib-10mm away from weld bead	0.409
At deck plate of rib inside-5mm away from weld root	0.951
At upper side of deck plate above the root tip	0.996
At bottom of rib	0.695



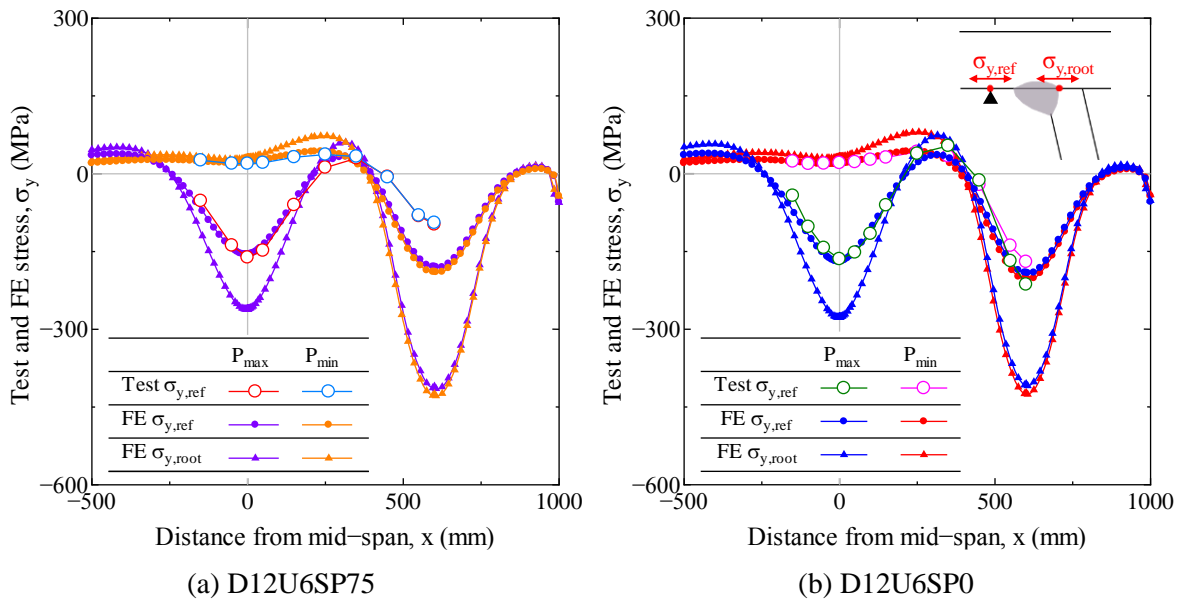


Figure 5.3 Stress distributions of specimens in longitudinal direction

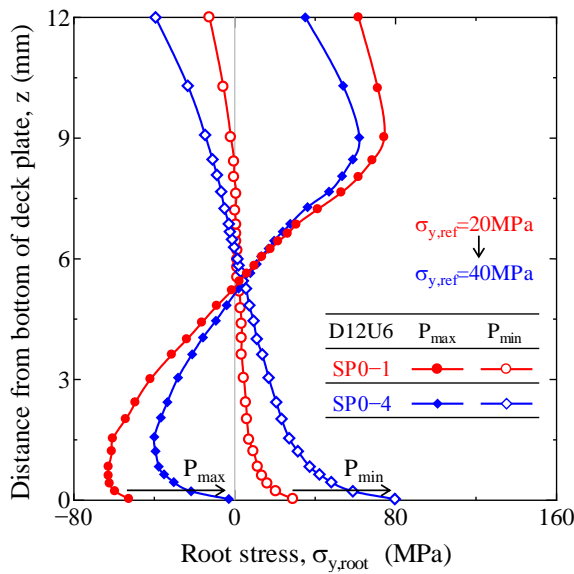


Figure 5.4 Relationship between reference stress and root stress

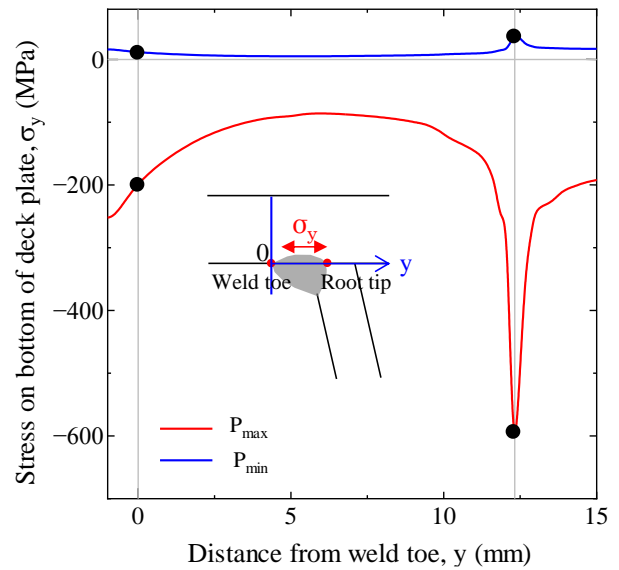


Figure 5.5 Stress distribution at welded joint of model D12U8SP50

### 5.2.2 FE models with artificial root cracks

Researchers have studied the effect of root gap on the root crack propagation of load-carrying fillet-welded cruciform joints [33]. Although the residual stress at rib-to-deck weld root is different from welded cruciform joint, and cannot be considered in elastic analysis, it was still a valid argument that the higher tensile stress might occur at the root tip because of the geometry of line-gap, thereby affecting the cracking process. Therefore, line-gap was simulated in basic models of D12U6SP75. The loading conditions were set the same as its non-crack model.

To examine the stress response in rib-to-deck joint after the root crack occurred, artificial root cracks with projected depths of 0.2/2/4/6/8 mm that based on the root crack measurements of tested specimens, were simulated in FE models D12U6SP75, as shown in Figure 5.6. The finite element analyses were performed on the basis of the contact analysis model.

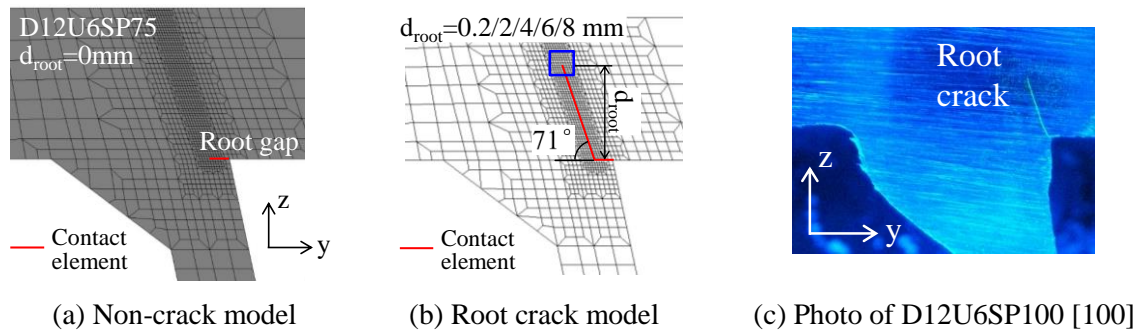


Figure 5.6 Definitions of FE Analytical model

Although the 8mm-crack has not occurred in fatigue tests due to the limitation of boundary condition, the through deck root cracks had been reported a lot in decades, so the stress response of 8mm-crack model was considered in FE analysis as a kind of adverse case. Besides, the initiation angles of fatigue crack were significantly different; however the propagating angles were proved to be similar, regardless of the root gap shape and welding details.

For all these crack models, the stress of adjacent node above crack tip was considered as the concentrated stress at crack tip surrounding, which belongs to elastic zone. To explain the visible relationship between crack depth and applied stress response, the artificial crack was only simulated in elastic FEA. The following parameters did not considered here.

1) The residual stress effect did not considered.

Not only the actual residual stress values are different from one to another, but also the dynamic redistributions need a large number of verifications base on the corresponding tests [116].

2) The friction between cracked surfaces did not considered.

Because of the irregular cracked surface, the friction factor would not be a constant. The artificial root crack was simplified as linear shape with smooth cracked surface, with friction factor 0.

3) Neither crack tip plastic zone nor plasticity-induced crack closure did not considered.

The researches about plastic zone around crack tip are generally used to determine the crack propagation rates and crack mechanism [117,118]. However, in this study, the crack propagation rate is not the aim. In addition, plastic zone usually very small and continued changing. We don't know the crack tip plastic zone area, and hard to be simulated due to the mesh size limit. Therefore, stress at crack tip surrounding is a kind of supplement for crack behavior evaluation, but not the actual crack tip stress.

4) The dynamic crack propagation process was not established.

The dynamic crack propagation process was replaced by several static crack stages of different crack depth. It is effective to clarify the crack behaviors by investigating static state of crack stages.

The transverse stress distribution under maximum and minimum loading cases in cracking direction as shown in Figure 5.7 (a, b).

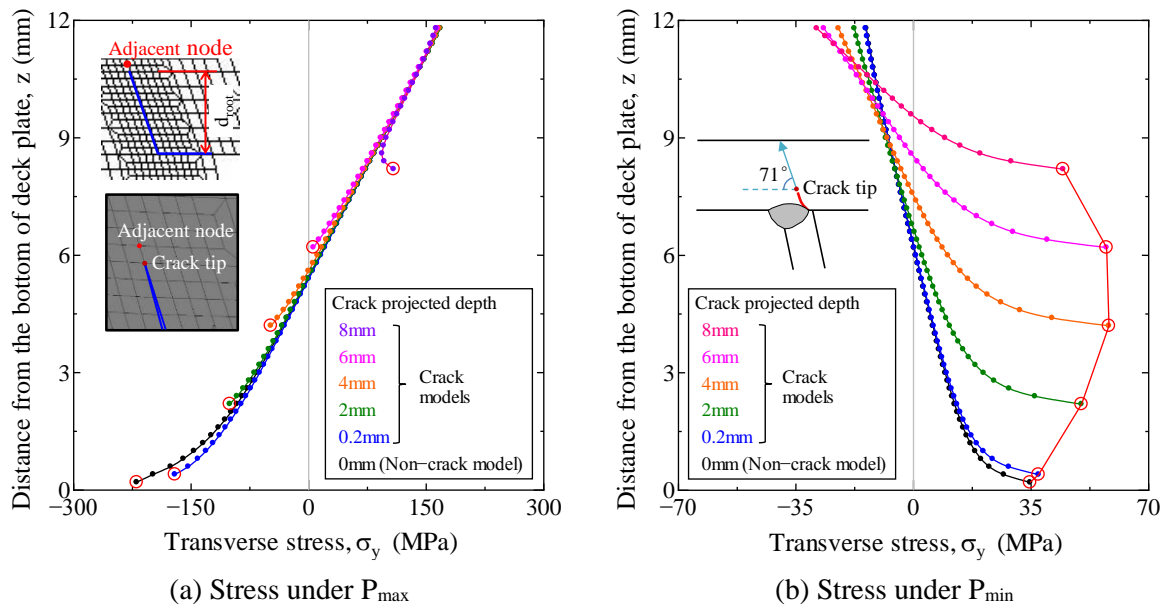


Figure 5.7 Transverse stress of models in cracking direction with artificial root cracks

### 5.3 Parametric analysis on non-crack model

#### 5.3.1 Effect of root gap shapes

The node stress at root tip cannot be used as peak stress because of the stress sensitivity around root tip. Thus, the node stress of  $N_1$  and  $N_2$  near the root tip with tria-gap model was compared, as shown in Figure 5.8. The transverse stress  $\sigma_y$  were approximated, while the principal stress  $\sigma_1$  of  $N_1$  was observed to be larger than that of  $N_2$ . In addition, the principal stress of element 1 represented the maximum element stress near root gap, and its direction is almost perpendicular to the root cracking direction of the test results. Element 1 is a neighboring element of  $N_1$  node.

For the two types of root gap models, the stress at adjacent node ( $N_1$ ) above the root tip was used for the stress response evaluation. FE models with 6 mm-thick U-rib were simulated with the triangle root gap at PJP, and models with 8 mm-thick U-rib were built with line-gap, based on the inspection of cross-sections of the cut specimens.

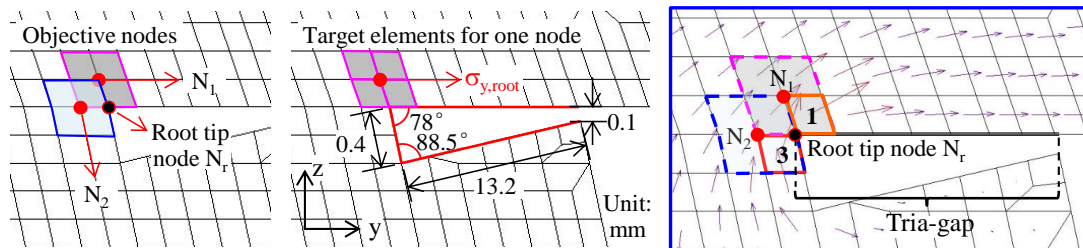


Figure 5.8 Details of tria-gap of model D12U6SP75

In general, the structural stress  $\sigma_s$  is comprised of membrane stress and bending stress. According to [51], the root stress at actual weld root tip should also consider the nonlinear stress peak due to the notch effect, which was in self-balance and determined by the gradient of the bending stress. The actual weld root tip stress considering the notch effect could comply with Eq. (5.1)

$$\sigma_k = \sigma_m + \sigma_b + \sigma_{nl} \quad (5.1)$$

Where  $\sigma_k$  is actual stress;  $\sigma_m$  is membrane stress, equal to the average stress calculated through the thickness of the plate;  $\sigma_b$  is bending stress, linearly distributed along the thickness direction;  $\sigma_{nl}$  is nonlinear stress peak.

Figure 5.9(a) shows the stress distributions at root gap of D12U6SP75 in the longitudinal direction. Reference stress distributions of the experimental test and FE analysis results were shown to be similar. However,  $\sigma_{nl}$  was dependent on root gap shapes; hence, the root tip stress range of tria-gap model was larger than that of line-gap. In other words, the root tip takes into account the higher stress-raising effects due to the triangular shape of the gap.

There must be a point where nonlinear stress is equal to zero, owing to the self-balance in vertical direction. The transverse stress and principal stress of the nodes in the simulated cracking direction are shown in Figure 5.9 (b). All of the stresses tend to be nearly the same at the node that is 1 mm away from the bottom of deck plate, therefore only structural stress exists (nonlinear stress approaching 0). Moreover, it is considered that the local stress distribution within a scope of 1 mm could be affected by root gap shapes.

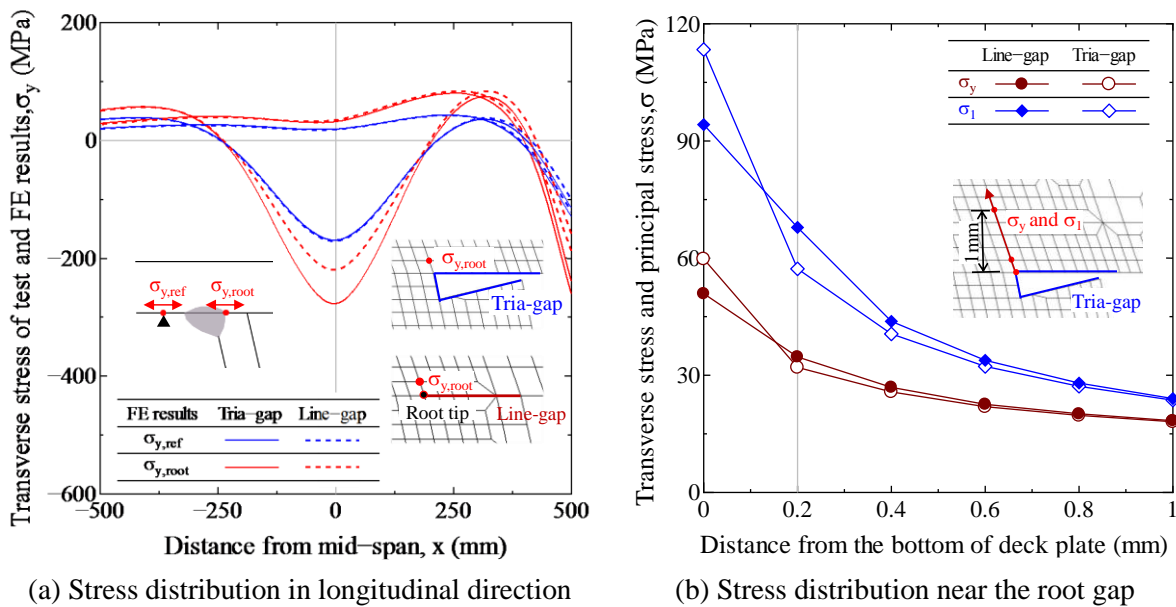


Figure 5.9 Comparison of models with different root gap geometry (D12U6SP75)



Figure 5.10 Major principal stress contours

Major principal stress contours of two kinds of models with different shape-gaps are shown in Figure 5.10. The stress distributions near the weld joint are almost same within the same stress range as the distributions under maximum and minimum loading cases. In addition, it was suggested that the geometrical characteristics and various penetration rates of weld joint, including the weld process and flaws, could affect the initiation angle of root crack (when the projected crack depth in transverse direction  $\leq 0.3$  mm). On the contrary, the tendency of crack propagating angles was shown to be a similar when the crack tip is situated away from the root gap. Therefore, the gap shape has little impact on the direction of root propagation.

### 5.3.2 Effect of weld penetration

Based on the test results, we confirmed that higher penetration rate of D12U6 is advantageous for the prevention of crack propagation. However, SP100 showed differing geometric characteristics at the root tip. Therefore, the effect of penetration rate on fatigue behavior was evaluated on the major principal stress under  $P_{\max}$  and  $P_{\min}$ , as shown in Figure 5.11. The principal stress distributions of three models in the simulated cracking direction are also shown in Figure 5.11. The absolute value of principal stress at root tip always reduced as penetration rate increased. The major principal stresses of SP100 were about 9% to 12% smaller than SP0.

The effect of penetration rate on the stress response of D12U8 models is discussed as an extension of the fatigue test. Owing to the 8 mm-thick rib, root gaps of U8 specimens resembled a linear shape. Therefore, the line-gap was used for the simulation of three models: (D12)U8SP50, U8SP75, and U6SP75. The transverse stress and relative rate were compared. Figure 5.12 (a) shows that the transverse tensile stresses of U8 are nearly same under  $P_{\min}$  with different penetration rate, while Figure 5.12 (b) shows that the stress range increased with a change in the penetration rate from 50% to 75%.

Figure 5.13 showed the stress distribution at bottom of deck plate of three models with tria-gap: (D12)U6SP0, U8SP50, and U6SP75. The peak stress of U6SP0 and U6SP75 were tend to be similar, the penetration rate seems regardless of the root tip stress but only the distribution tendency. The penetration rate would affected the stress distribution but has little influence on peak stress. D12U6SP75

has the largest  $\sigma_y$  at root tip and even reached 1.8 times larger than that of U8SP50. It was considered that increasing the thickness of U-rib could reduce the tensile stress peak value.

No matter for U6 or U8 specimens, different penetration rate would lead to the stress range fluctuates at root tip. The tendency of penetration rate effect could also be changed by the geometry of root gaps. Therefore, the penetration rate could affect the fatigue life of the structure, up to a point. However, relative to the rib-to-bead crack, the larger penetration rate were not the crucial factor for rib-to-deck cracking.

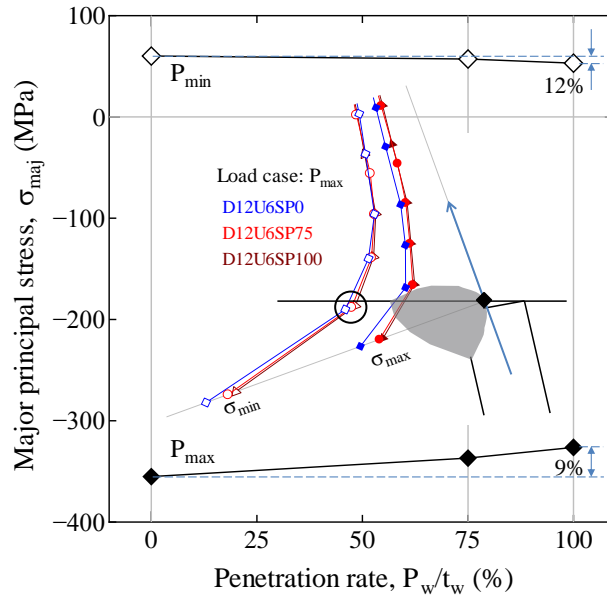


Figure 5.11 Effect of weld penetration rate on root tip stress of D12U6

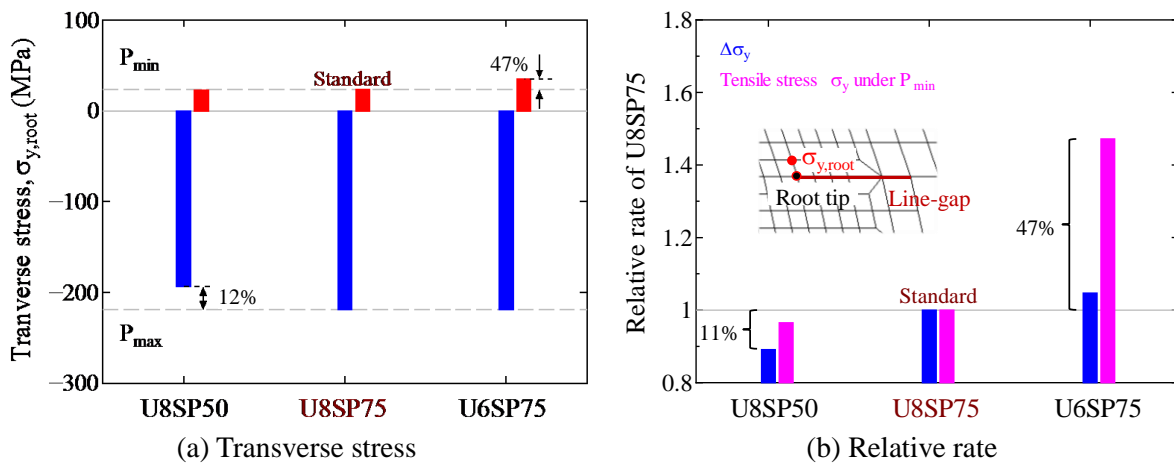


Figure 5.12 Stress comparison of (D12) U8SP75/U8SP50/U6SP75

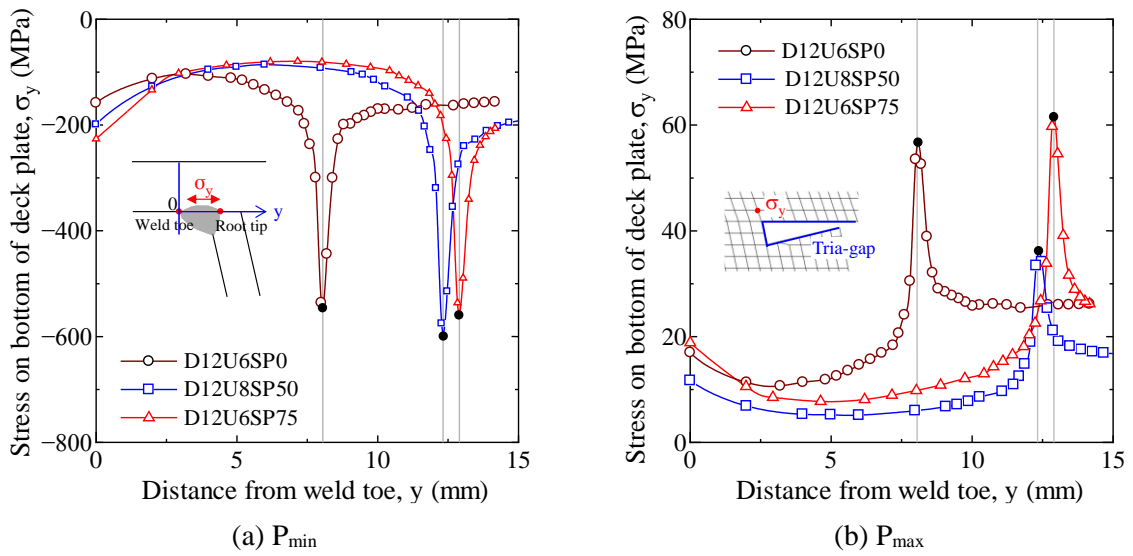


Figure 5.13 Stress distribution in y direction at mid-span

### 5.3.3 Effect of plate thickness

Figure 5.14 shows the stress response of models in longitudinal direction. All of the models used here were built with tria-gap. Increasing the thickness of deck plate could reduce the stress range at mid-span effectively, while increasing the thickness of the U-rib appears to have small effect on the stress range. However, the tensile stress decreased by approximately 47% under  $P_{min}$ , when U-rib thickness increased from 6 to 8 mm, as shown in Figure 5.14. The inertial axis of deck plate and U-rib changed with variation in the stiffness of structure. Hence, the 8 mm-rib could effectively reduce the tensile stress of the welded joint. The tensile stress tends to be a more effective factor as compared to the stress range for crack growth after the residual stress released at crack tip. Therefore, a larger maximum tensile stress of U6 had adverse effects on fatigue propagation.

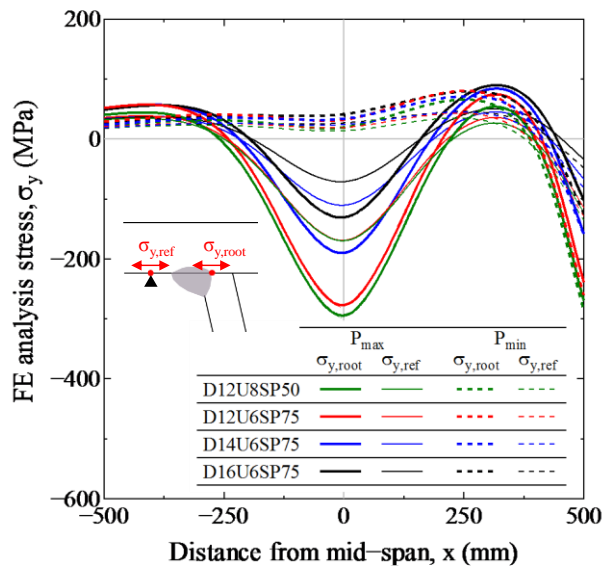


Figure 5.14 Stress response of models in longitudinal direction

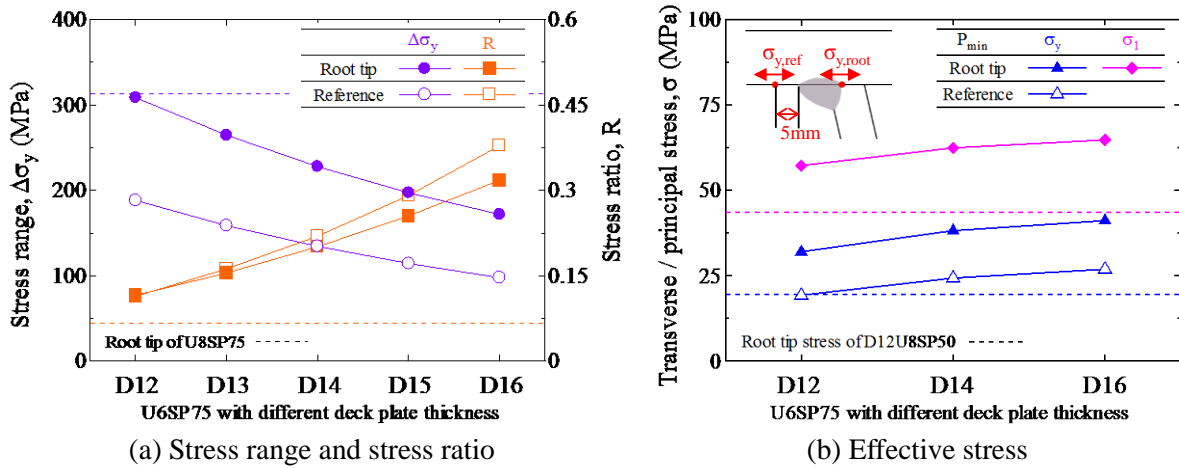


Figure 5.15 Effect of deck plate thickness on stress

The relationship between stress range/ratio and deck plate thickness was compared using five FE models; these models were established with 6 mm-thick U-rib and 75% penetration rate under the same loading conditions, as shown in Figure 5.15(a). The stress range of root tips were gradually decreased according to thickness of deck plate changed from 12 mm to 16 mm, but the stress ratios were increased. The transverse tensile stress and maximum principal stress were compared considering the effective stresses during the root crack propagation, as shown in Figure 5.15(b). The tensile part of stress range was shown to be larger when the deck plate thickness was increased; this can be indicated as an adverse effect of thick plate on root crack behavior.

Figure 5.16 shows the unit stress distributions of the models with different deck plate thicknesses, assuming the root tips were under the same stress condition. Although the stress gradient of thin plate is larger than that of thick plate, the stress of inner point, which is equally distant from the plate surface, increased in the order of deck thickness as 12 mm, 14 mm, and 16 mm. Therefore, the fatigue strengths gradually decreased with the increase in deck plate thickness, which can be attributed to the effect of thickness. The welded joints with thick deck plates tend to have lower fatigue strengths than those of thin deck plates; this was consistent with the FE results analyzed by Ya et al. [17].

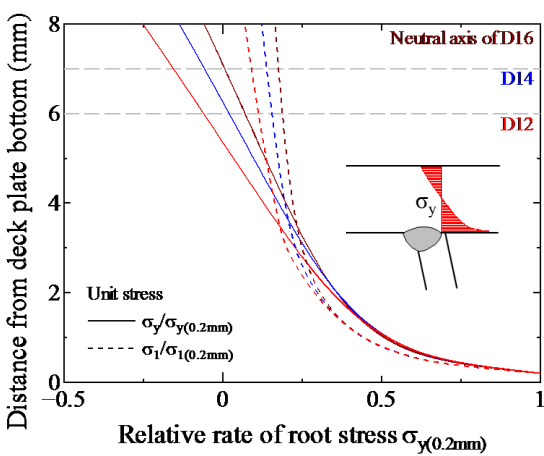


Figure 5.16 Unit stress comparison of D12/D14/D16 deck plate under  $P_{max}$

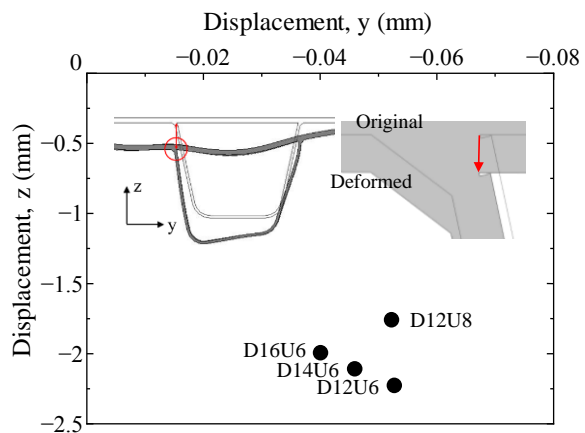


Figure 5.17 Displacements of root tips in y and z directions



Based on these analyses, the test results of control groups D12U6SP0-4 and D14U6SP75-1 could be explained (Chapter 4). The root cracking degree of D14 has no additional advantage over that of D12, which may be attributed to the high tensile stress. Although the stiffness increased with increase in the plate thickness, the fatigue life might be reduced owing to the low fatigue strength of the thick deck plate.

The effect of plate thickness on displacement at root tip were compared, as shown in Figure 5.17. Increasing the U-rib thickness could reduce the vertical deformation of the structure, and increase the stiffness of OSD. Increasing the thickness of deck plate could reduce the structure deformation in both y and z directions.

The structural deformations and principal stresses of D12U6SP75 under the double-tire loading cases are shown in Figure 5.18 (a). Based on the stress flow near the root tip under loadings of  $P_{max}$  and  $P_{min}$ , all of the tensors showed that the tensile-compressive stress cycles existed near the root tip, which would cause the fatigue cracking at the rib-to-deck welded joint. This was consistent with the test results. Figure 5.18 (b) shows the deformation and principal stress tensor of the D12U6SP75 model under the single-tire loading. The structural deformation of this loading case was relatively smaller than that of the double-tire loading. The peak tensile stress occurred below the element near the weld root tip as a result of the bending of the deck plate. The theoretic cracking direction of a root crack should always be perpendicular to the principal stress. Thus, the single-tire loading made no obvious contribution to the root-deck cracking, but may have caused the bead cracking. In an actual bridge, more experimental research and investigation are needed to determine whether this loading would lead to bead cracking.

Figure 5.19 (a, b, c) show the structural deformation of other dimensional models. The principal stress around root tip at mid-span cross section under double tire loading of different models were slightly different. Obviously, the thickened plate could increase the structural rigidity and reduce the deformation.

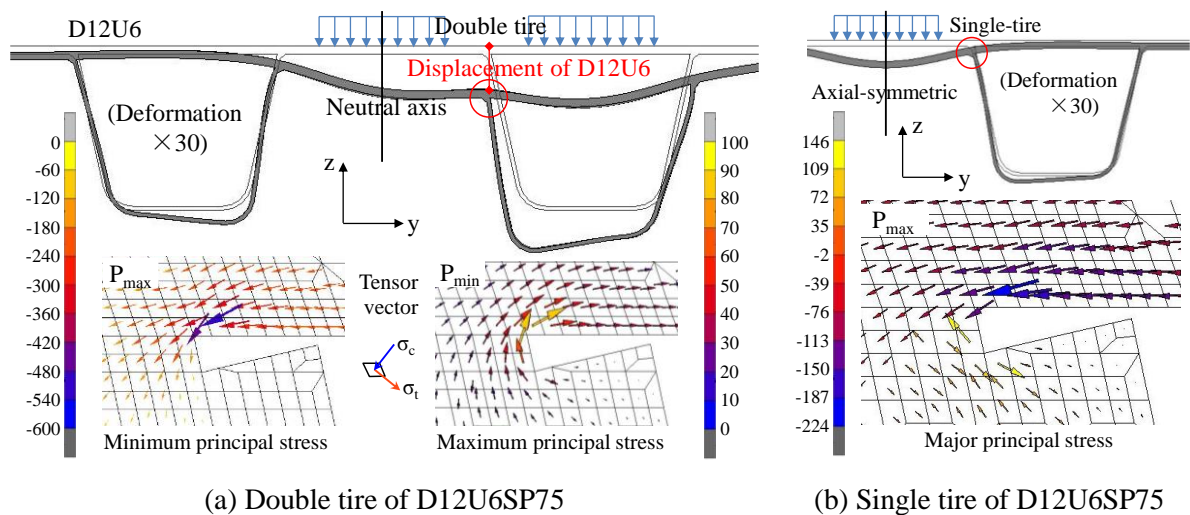


Figure 5.18 Structural deformation and principal stress of root tip at mid-span

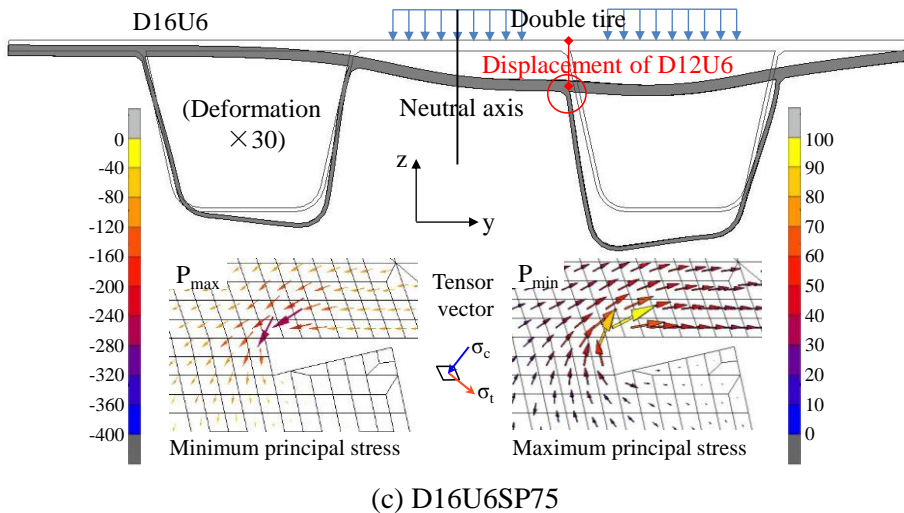
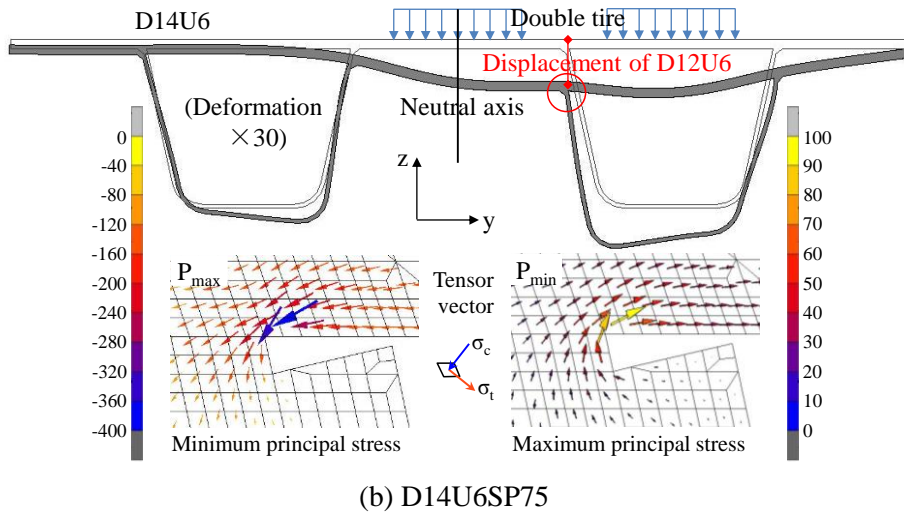
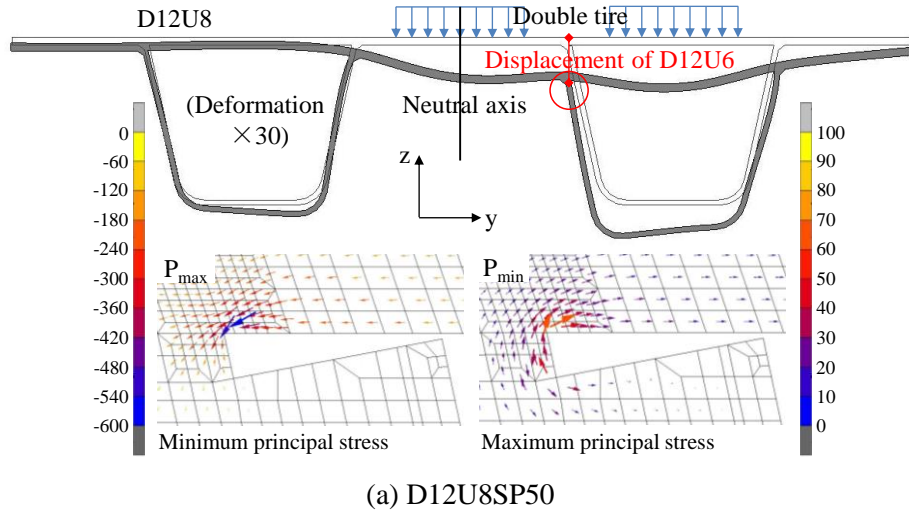


Figure 5.19 Structural deformation and principal stress of root tip at mid-span

## 5.4 Stress analysis of models with artificial root cracks

### 5.4.1 Effect of crack depth on stress response

The stress distributions including the node stress at cracked surface and the remaining sections are shown in Figure 5.20. For the models with root crack that projected depth between 0 to 6mm, the stresses of crack tip surrounding shown to be compressive stress under  $P_{\max}$ , as shown in Figure 5.20(a). The tendency for stress states was similar to compare with the non-crack and crack model. The neutral axis would not move because the crack closed in compression zone and the structural bearing capacity unchanged when the root crack propagated from 0 to 6mm. However, the stress concentration cannot avoid after the crack tip extend into tensile zone. Thus in the case of 8mm-crack, the stress concentration occurred after the crack tip extended into the tensile zone.

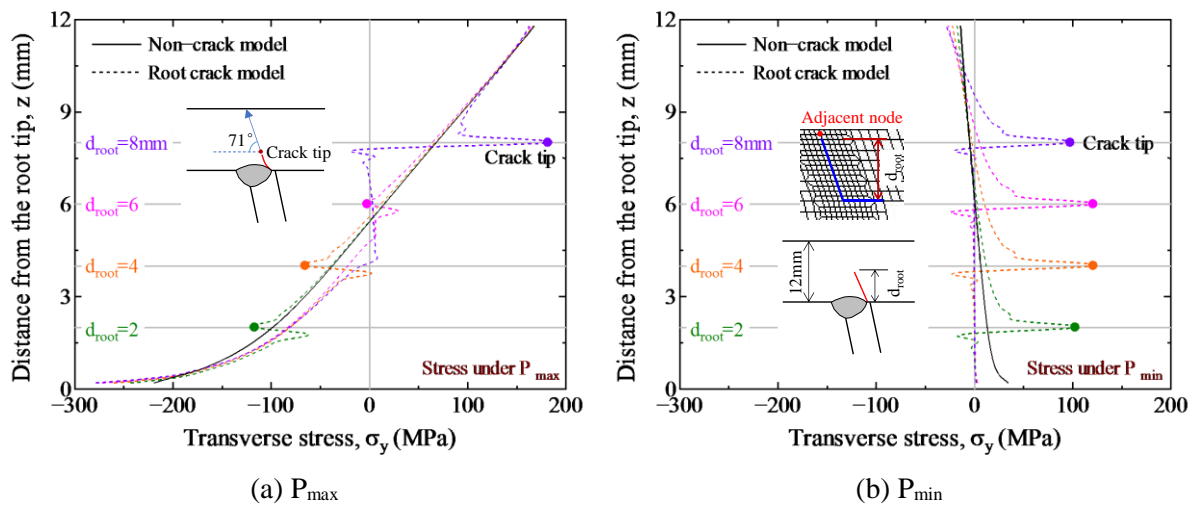


Figure 5.20 Stress variations in deck plate thickness

On the other hand, a tensile stress zone existed below the neutral axis of deck plate when models under  $P_{\min}$ . In this case, the stress redistribution in deck thickness during the whole cracking process, as shown in Figure 5.20(b). The cracked section cannot afford the tensile stress, the crack tip tend to be open, and the neutral axis moving up continues during the crack growth.

Figure 5.21(a) shows the transverse stress variations at crack tip surrounding of these crack models under the half cycle loading. In case of crack length from 0.2 to 6mm, the transverse compressive stress tend to reduce under  $P_{\max}$ . However, the tensile stress has not changed much under  $P_{\min}$ . 8mm-crack model shows the tensile stress always around its crack tip under the whole loading cycle. The tensile stress value for  $P_{\max}$  on 8mm crack length is about 1.86-times larger than those of  $P_{\min}$ . It was considered the crack tip would forms tensile stress under the whole cycle of loading when a root crack propagated over half of deck plate thickness.

Besides, the maximum principal stress at crack tip surrounding in these models also showed a similar tendency from  $P_{\min}$  to  $P_{\max}$  in Figure 5.21(b). The stress condition around crack tip of 8 mm-crack model are serious than other crack models for high stress concentration under  $P_{\max}$ . The tensile stress value for  $P_{\max}$  on 8mm crack length is about 2.34-times larger than those of  $P_{\min}$ . In case of crack depth from 6 to

8mm under  $P_{max}$ , the concentrated stress around crack tip tend to be 2.27-times larger. It was considered the crack tip would forms tensile stress under the whole cycle of loading when a root crack propagated over half of deck plate thickness. In this case, with the crack extending, the loading value  $P_{max}$  would be a dominant factor for crack propagation instead of  $P_{min}$ , and lead to a larger principal tensile stress at crack tip surrounding. Above all, the promoting effect between crack growth and principal stress might result in a significant reduction in the residual life of this structure.

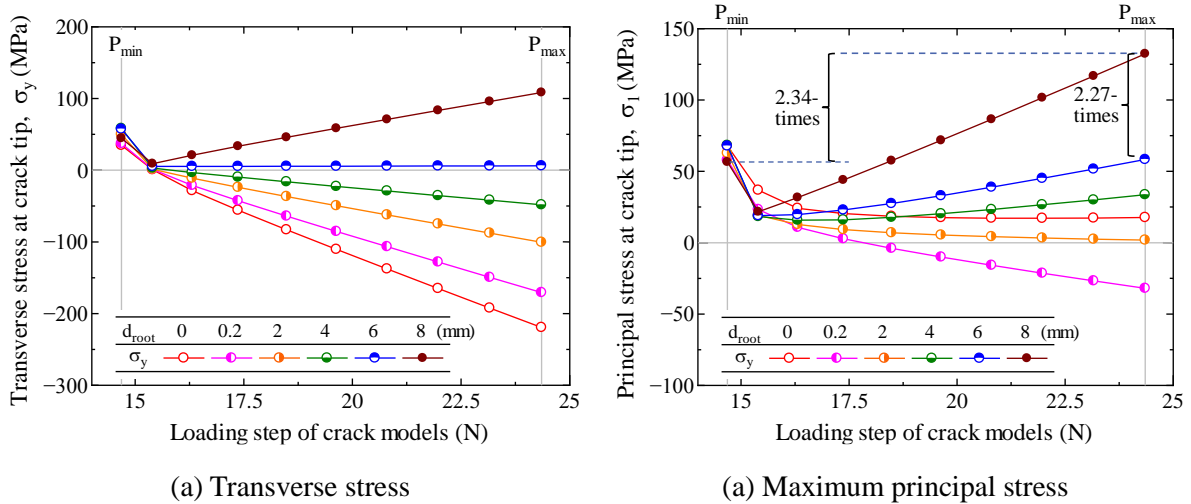


Figure 5.21 Stress variations at crack tip surrounding under half loading cycle

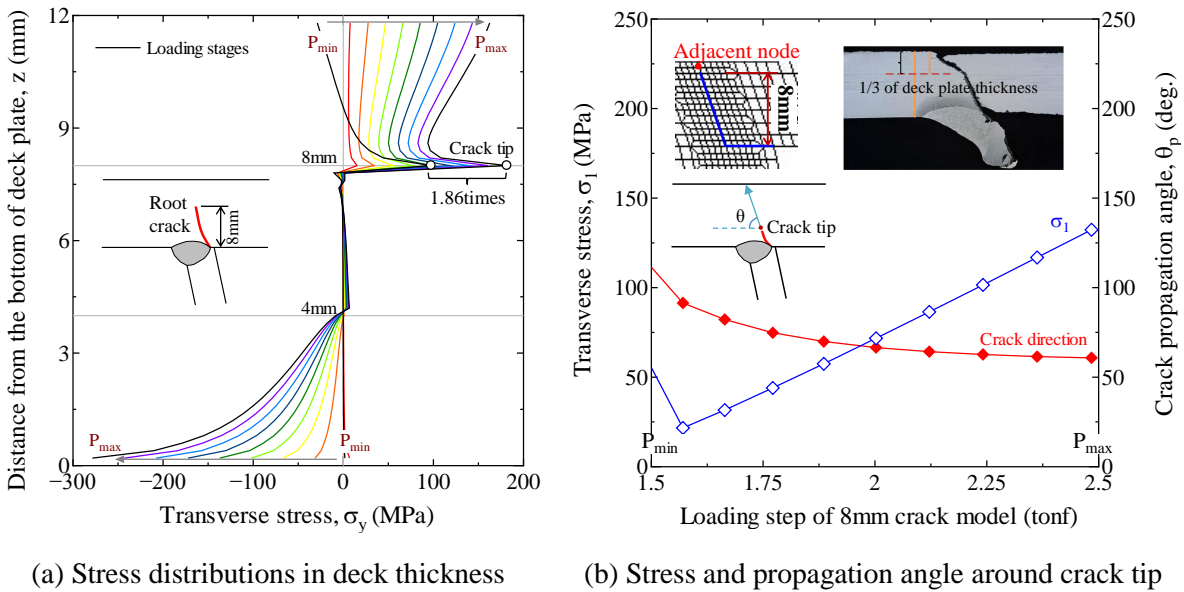


Figure 5.22 8mm-crack models during half cycle

Figure 5.22 (a) shows the transverse stress distribution in deck plate thickness of 8mm-crack model under cyclic loadings. The upper one-third thickness of deck plate suffered the tensile stress, whereas the cracked part in range of 4mm distance from bottom of deck plate were in a state of compression under any loading steps. Figure 5.22 (b) shows the concentrated stress and propagation angle around crack tip under cyclic loadings. Obviously, not only the stress around crack tip would be changed, but

also the propagate direction also be changed during fatigue cycles. The crack propagation angle under  $P_{\max}$  tend to be smaller than that under  $P_{\min}$ , which is consisted with the fracture mode of through deck root cracks in actual bridge.

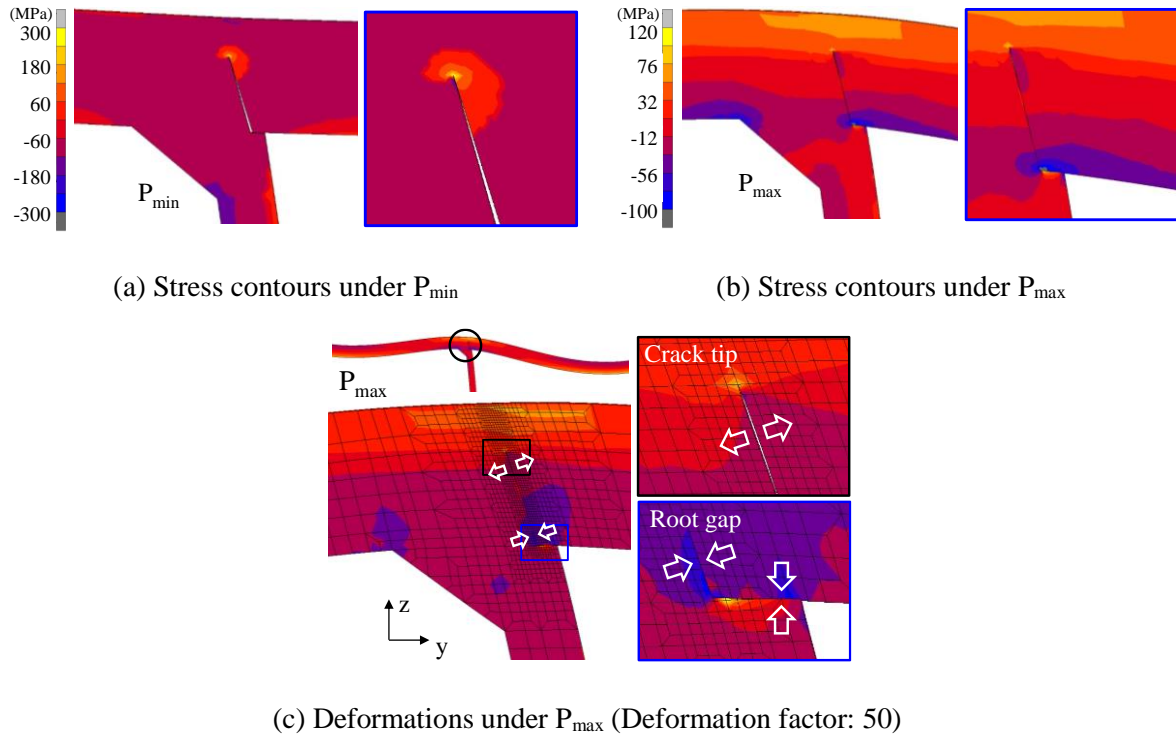


Figure 5.23 Major principal stress contours of 8 mm-crack model

The stress contours and deformations around root tip of 8 mm-crack model were shown in Figure 5.23. It can be seen that the crack tip and the remaining un-cracked section are always in a state of tension, a tensile stress zone leads to the crack tip opening even when the crack is closed at the bottom of deck plate.

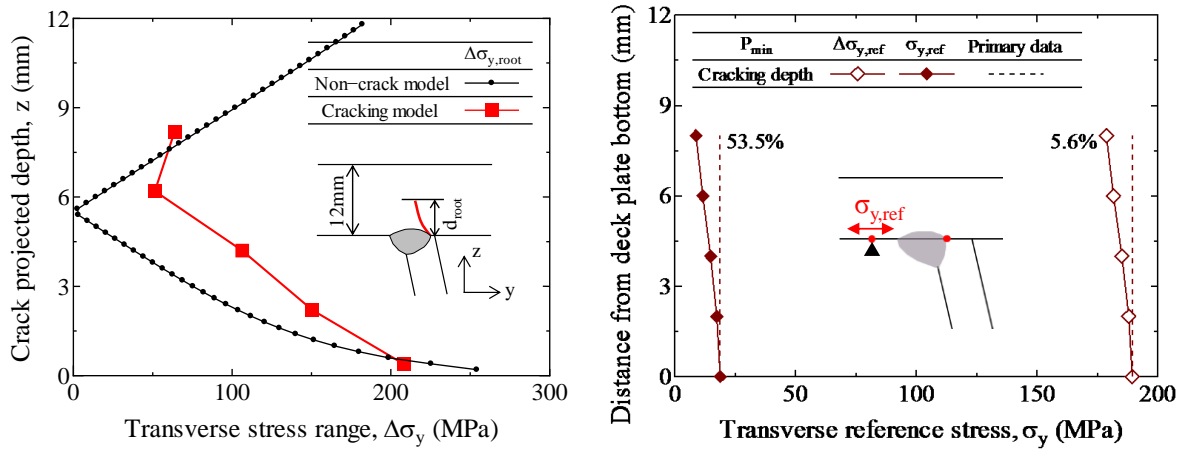
In Chapter 4, we had known the compressive residual stress usually existed at middle of deck plate. In practically, crack propagation rate would not instantly be accelerated once reach to the middle axis. However a tensile residual stress zone existed at the upper part of deck plate. Therefore, even taking into account the effect of residual stress and stress redistribution during crack extend, there is always a critical crack depth which might cause a rapid fracture of root crack. In actual bridges, the fracture mode and the critical crack depth would also change depending on the magnitude of traffic loading, structural dimensions and so on.

## 5.4.2 Other influence factors

### (1) Stress range comparison

During the root cracking process, stress range of non-crack model in simulated root crack path and the stress range at crack tip surrounding are shown in Figure 5.24(a). The stress range at crack tip surrounding of crack models were observed to be larger than that of the non-crack model. The reference

stress range of tests and FE analysis results were compared in Figure 5.24(b). Reference stress ranges were decreased due to the decrease in tensile stress, which were depend on crack patterns and properties.



(a) Stress range of crack tip surrounding

(b) Stress range of reference point

Figure 5.24 Stress range comparison of reference point and crack tip surrounding

### (2) Effect of penetration rates

Figure 5.25 shows the effect of penetration rates on the stress distribution around crack tips for different crack depths. Herein D12U6 model with weld penetration rate 0%, 75% and 100% penetration were considered. The stress distributions of the models with different weld penetration were similar under  $P_{min}$ , however, they were slightly different under  $P_{max}$ . According to the preceding analysis, the stress around crack tip in the compression zone should be approximated to the corresponding stress in non-crack model, and the compressive stress zone around crack tip almost has non-effect on crack growth. Therefore, it was suggested that the crack propagation process seems to be independent of the penetration rate if their residual stress are same in deck plate thickness.

### (3) Effect of structural dimensions on fatigue strength

Experimental studies such as plate fatigue tests with small-scale specimens were usually used to obtain the basic fatigue test data. Simplified small-scale specimens representing the rib-to-deck welded connection were tested at Nagoya University until early 2009[11]. Ya et al. computed the fatigue strengths of the rib-to-deck joints at  $2 \times 10^6$  cycles. The fatigue strengths were determined by regression analysis assuming the slope of S-N diagram as 3 (denoted as Ya curve). Therefore, the reference stress range of full-scale tests in this study were verified with the S-N curves of small-scale fatigue tests. Assuming the fatigue strength curves of small-scale specimens were applicable to the FE analysis results herein, the equivalent fatigue life were calculated according to corresponding S-N curves for the specimens with different dimensions, as shown in Figure 5.26.

The test data of nominal stress and its number of cycles represents the fatigue strength before root crack initiation. It shows the fatigue strength of D12 quite coincident with Ya curve, whereas the fatigue strength of D14 is smaller than Ya curve and almost fit with D16 regression curves. It was found there

are significant difference in fatigue strength between full-scale and small-scale specimens when the thicker plates were used, due to the residual stress or other external factors.

Moreover, the root stresses of FE models in this paper were including part of the stress peak, so their equivalent fatigue lives are much smaller than test results. It shows the fatigue life of U8 might be prolonged slightly relative to that of U6. The effect of deck plate thickness on fatigue strength shows that the fatigue strength at root tip of thick plate does not increase significantly compared to the strength of 12mm-thick deck plate.

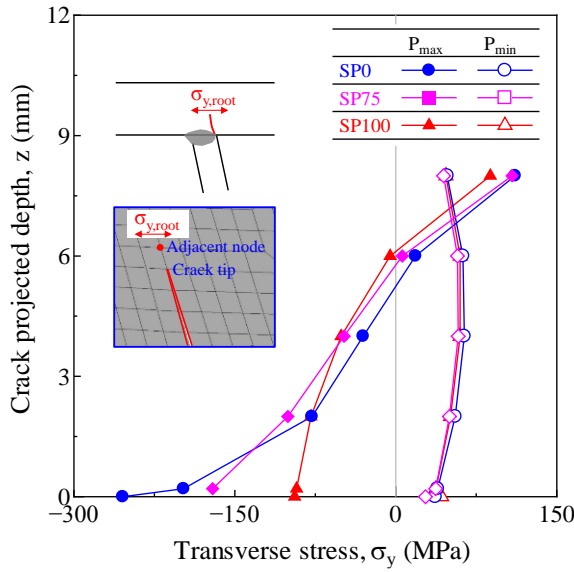


Figure 5.25 Effect of penetration rate on stress during crack propagation.

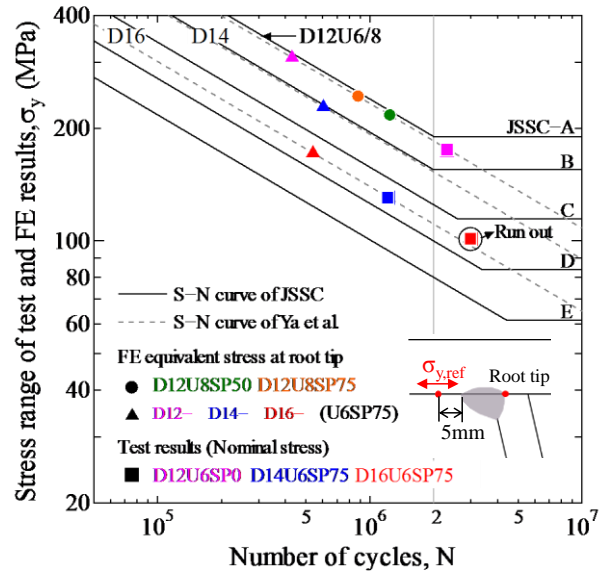


Figure 5.26 Effect of structural dimensions on fatigue strength.

### 5.5 Summary

Based on the previous test results, the fatigue behaviors of rib-to-deck welded joints were investigated by establishing the matching finite element models. Experimental specimens with two kinds of root gap shapes were simulated and evaluated in FE analysis. Various structural dimensions and root crack depths were also simulated in the models. The fatigue behaviors of structure detail were investigated by considering the effect of weld penetrations, plate thicknesses, and crack depth on crack propagation. The structural responses of artificial fatigue crack in models were evaluated, and the stress variations around crack tip occurring at the different propagation stage under cyclic loading were clarified. The results are summarized as follows:

(1) The test and FE results were compared, the FE analyses and test results had similar stress distributions at reference points in longitudinal direction. Based on the stress flow near the root tip under double tire loadings, the principal stress tensors showed that the tensile-compressive stress cycles existed near the root tip, which would cause the fatigue cracking at the rib-to-deck welded joint. This was consistent with the test results. However, the single-tire loading made no obvious contribution to

the root-deck cracking, but may cause the bead cracking.

(2) The root gap shape and penetration rate have an impact on the root cracking direction and fatigue life at the initiation stage, but seem not directly related to the crack propagation mechanism; the higher penetration rate is advantageous for the prevention of root crack initiation. However, compared to the fatigue life of 12mm-thick deck plate, that of thickened deck plate does not increase significantly before root crack initiation. Whereas the U-rib thickness has limited effect on the stress response of the root tip.

(3) The significant difference between the 8mm-crack model and other crack models is the high stress concentration around the crack tip. In practice, crack propagation rate would not be accelerated instantly once it reaches the middle axis due to the compressive residual stress. However, there is a residual tension zone at the upper part of the deck plate, the critical crack depth would cause a rapid fracture of the root crack. In actual bridges, the fracture mode and the critical crack depth would also change depending on the magnitude of traffic loading, structural dimensions and so on.



## Chapter 6 Structural behavior of orthotropic steel decks with artificial cracks in longitudinal ribs

### 6.1 Introduction

Longitudinal ribs are usually connected via field welding, so most rib cracks have been found within the welded material, along the lines of the butt welds [23]. Since the butt welded joints of these ribs are often fabricated on-site, they prone to being of lower quality than shop welds, as shown in Figure 6.1.



(a) Field assembly

(b) Cross section of U-ribs

Figure 6.1 Field welding of trough splice joints [10]

The occurrence of fatigue cracks in field-welded U-ribs has been shown to account for approximately 5.7% of the total damage to orthotropic steel decks [14]. Even though they did not comprise the largest proportion of fatigue cracks, it is one kind of fatigue cracks that most likely to extend into large size. The bottoms of the ribs are subjected to tensile stress at the time of service, and thus, rib-to-rib cracks might propagate to rapidly form a large crack once this type of crack occurs. Additionally, longitudinal ribs are usually connected via field welding, so most rib cracks have been found within the welded material, along the lines of the butt welds [41]. Since the butt welded joints of these ribs are often fabricated on-site with incomplete penetration, cracks would be easy to initiate from the stress concentrated points. The root crack was prone to occur from the root tip of butt joint and cannot be detected easily.

In this study, to investigate the effect of rib fractures, and the combination of rib crack and rib-to-deck cracks, the field tests were carried out at an actual bridge in previous study. The artificial cracks were set at the cross section of mid-span by gas-cut from the rib bottom. Moreover, FE models with the combination of artificial rib crack and rib-to-deck cracks were established. Based on the field measurement and FE analyze results, the structural responses of orthotropic steel deck were compared which caused by the rib crack initiated from mid-span and quarter span. Besides, the torsional rigidity of ribs with butt weld crack were investigated via quantitative analysis. The effects of multiple ribs

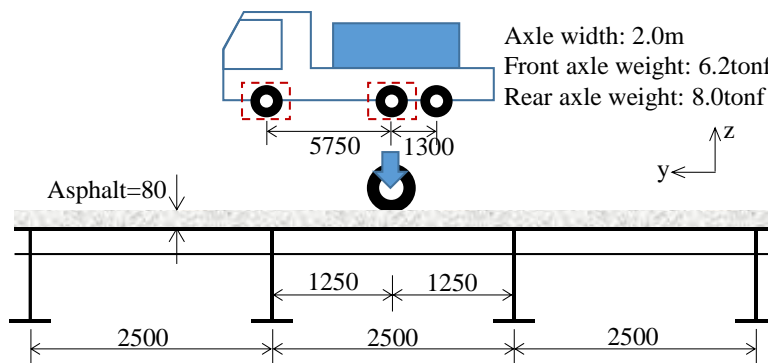
fracture on structural responses were also discussed by considering various crack combinations and three type of typical transverse load positions. Finally, the effect of asphalt pavement having different Young's modulus on structure stiffness was considered under different temperatures.

## 6.2 Field measurements

In actual bridge, to consider the construction convenience and avoid the largest bending moment occurred at welded joint, the butt welded joints of ribs are usually set at the quarter span. In this study, to investigate the stress responses of structure with artificial rib cracks, the field test was carried out by considering the most adverse crack position—the artificial cracks were set at the cross section of mid-span by gas-cut. Therefore, the complicated growth path of root-to-deck crack in longitudinal direction could be simplified as symmetric. When the rib crack occurred at mid-span, the displacement of deck plate and the torsion of ribs would be the largest, and the loading at cracked section would be a most adverse case in longitudinal.

The objective bridge used for field measurements was an orthotropic steel bridge in the national Expressway. The total length of the main girder is 99 m, and the transverse spacing between girders is 3.5 m. The distance between the two crossbeams is 2.5 m. The orthotropic steel deck consisted of a 12 mm-thick deck plate, 6 mm-thick U-rib, and 12 mm-thick crossbeam. The dimensions of the longitudinal U-rib is 320×240×6 mm and the thickness of the asphalt pavement is 80 mm, as shown in Figure 6.3.

Field static testing of the actual bridge was conducted in November. The loading truck used was a three-axle truck with a total weight of 217.6kN (22.2tonf) and an axle width of 2m. The second and third axles both weighed 78.4kN (8.0tonf). The wheel base of first and second axles is 5.75m. The rear wheels were all double tires and the wheel base is 1.30m. The tire area, transverse loading positions, and the strain locations, as shown in Figure 6.3(b, c). In longitudinal direction, loadcase1 is the loading at mid-span, and loadcase2 is the loading at quarter span. The biaxial strain gauges were attached to the bottom of the deck plate to measure the longitudinal and transverse stress, and a uniaxial strain gauge was attached to the bottom of the U-rib to measure the transverse stress.



(a) Front/rear tire loading and the side view of bridge deck (Unit: mm)

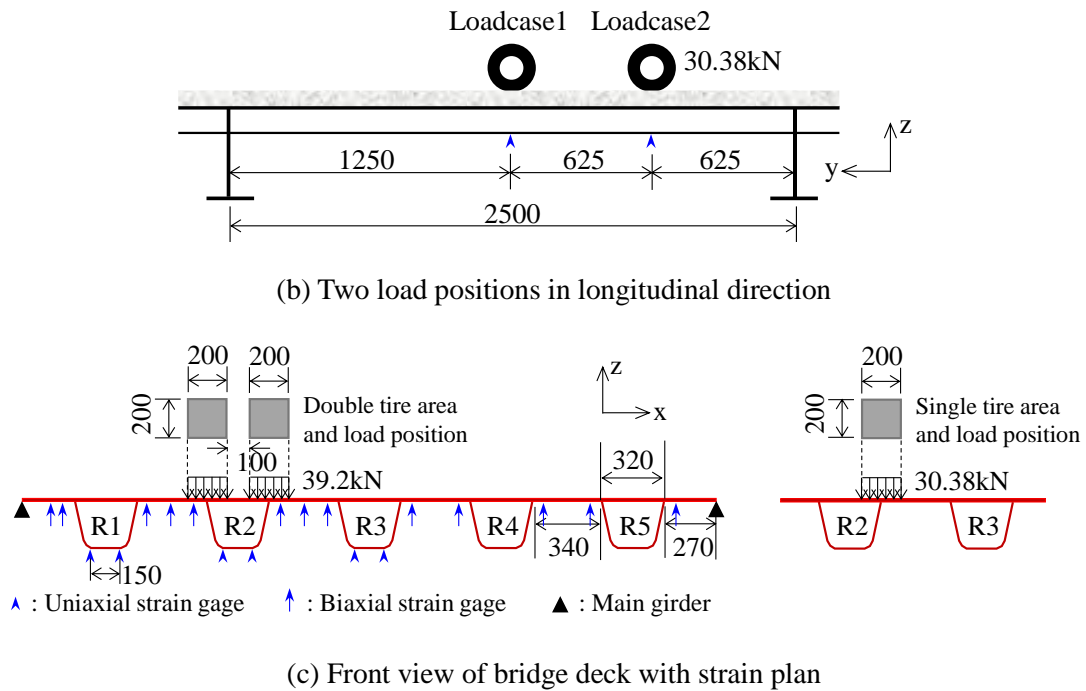


Figure 6.2 Loading cases of field measurement (Unit: mm)

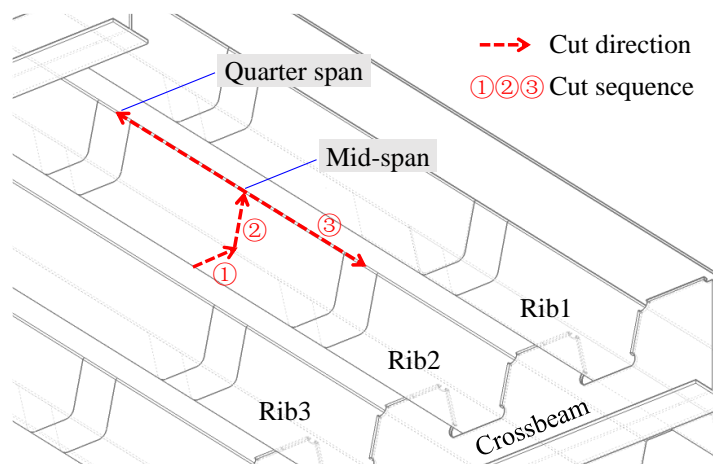


Figure 6.3 Artificial cracks by gas-cut in actual bridge

As the safety consideration for the test bridge, the rear tire loading test was only carried out on the non-crack structure. The front tire loading tests was conducted on the structure before and after the artificial cutting process. The location of artificial cracks by gas-cut in actual bridge as shown in Figure 6.3. The cut sequence obey the general initiation and propagation process. The cut direction was along the butt weld ①② and rib-to-deck weld ③. The bead crack at rib-to-deck welded joint were easy to occur due to the effect of fractured ribs and incomplete penetration. The rib-to-deck artificial cracks propagated in both of longitudinal directions, which cracked from mid-span to quarter span. The stresses were measured at mid-span and quarter span at several cracking stages.

### 6.3 Comparison of field results and FEA

#### 6.3.1 FE models

The FE models of a one-span orthotropic steel deck between two girders were built according to the standard dimensions of an actual bridge in Expressway. The elastic models by comprising the solid elements and rigid loading surfaces were established by Marc mentat 2012. A Young's modulus of 206,000 MPa and Poisson's ratio of 0.3 were applied as the steel material properties. All of the welded joints and cope holes were simulated in models using a minimum mesh size of  $1 \times 1$  mm. The aspect ratio of elements are closed to 1.0 at refined mesh locations. The boundary conditions, element mesh division, the load positions of single tire at mid-span and quarter span are shown in Figure 6.4(a). The model was fully-constrained at the connection to the main girders. In addition, the stress interaction between the transverse and longitudinal wheels should be small, thus it was ignored in this study, and only the one side tire of the first/second axle was simulated as a loading surface in the models. The loading area of one tire was simulated by a rigid body with an area of  $200 \times 200$  mm (double tire area is  $200 \times 200$  mm  $\times 2$ ). The load positions are shown in Figure 6.4(b). This model was named as model N (non-crack model).

The rib crack would decrease the bending moment capacity of orthotropic steel deck. In order to compare the field measurement and FEA results, the crack simulation of FE model was correspond to the artificial gas-cut cracks in field test. This model was named as model D. It fractures throughout the mid-span section of rib2 and half-span of rib-to-deck weld joints. The image of crack path as shown in Figure 6.5(a). The artificial rib-to-rib crack and rib-to-deck crack were simulated by contact elements, with friction factor of 0. The structural details and contact surface of artificial cracks as shown in Figure 6.5(b). According to the gas-cut cracks in field test, the fracture cross-section of bead crack was set as horizontal to avoid the transverse deformation constraint. This study focused the structural response of orthotropic steel deck because stress of crack tip was difficult to be evaluated in the full-scale FEM model. The fatigue crack of FE model was simulated to use the contact element method considering the behavior of closed and opening crack.

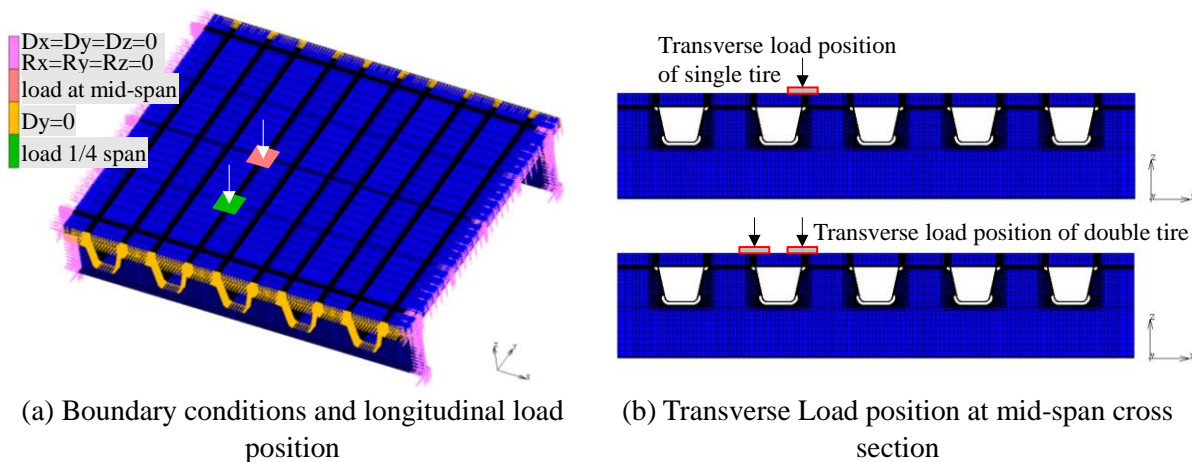
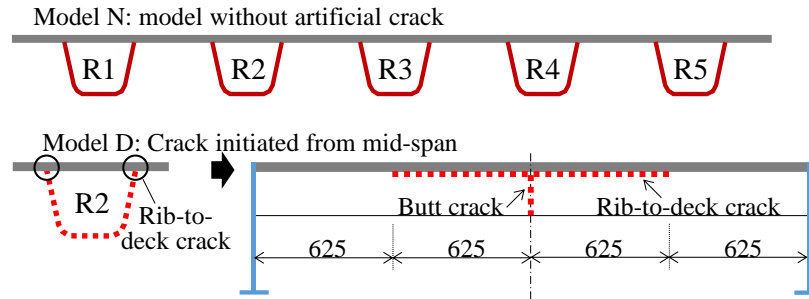
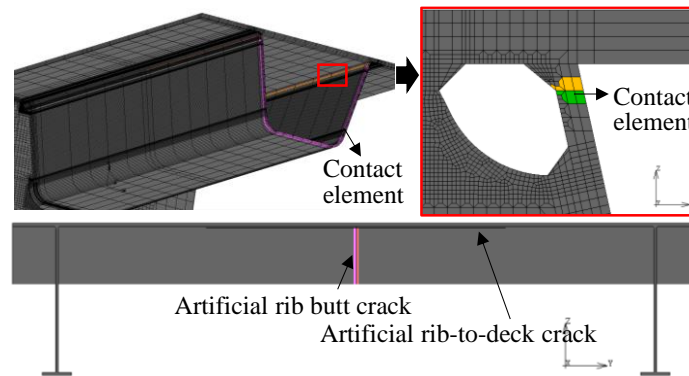


Figure 6.4 FE model of solid elements



(a) Model ID and the image of crack path



(b) FE simulation of gas-cut cracks in field tests

Figure 6.5 FE models with artificial cracks

This study also investigated the effects of stiffness of asphalt pavement on structural responses in different seasons. For the simulation of asphalt pavement, the membrane between the asphalt layer and the steel deck was considered acts as a fixed surface under static loading, by node connection. A Poisson's ratio of 0.35 was used, and its elastic modulus was determined from Eq. (6.1), as suggested by a previous investigation of the effects of asphalt pavement on an orthotropic steel deck [119].

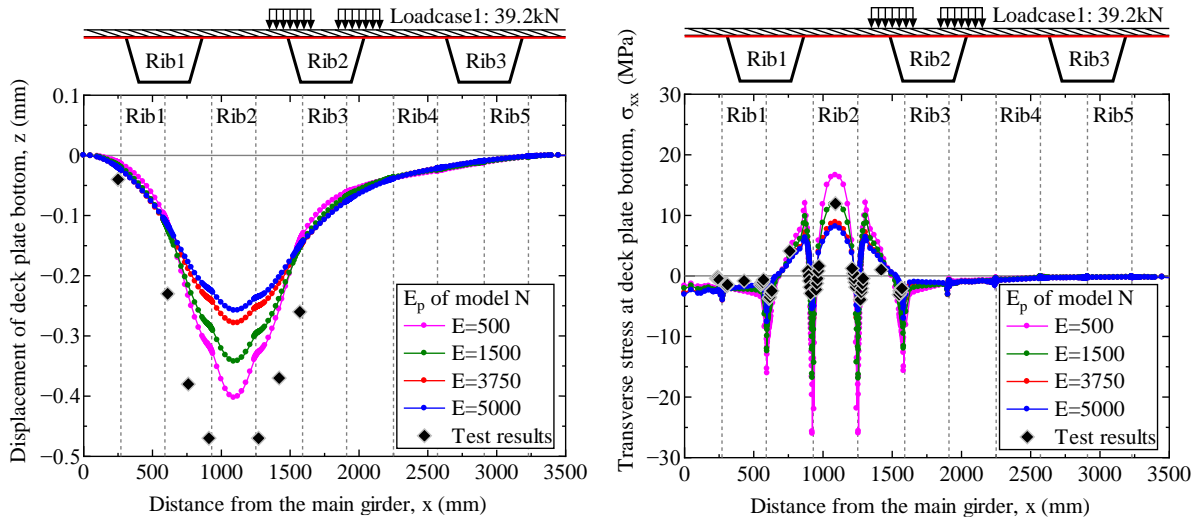
$$E_p = 10^4 e^{-0.07T} \quad (6.1)$$

where  $E_p$  is the elastic modulus of the asphalt pavement, and  $T$  is the atmospheric temperature ( $^{\circ}\text{C}$ ). The atmospheric temperature below the deck plate during the field measurement is  $14^{\circ}\text{C}$ . Therefore, the Young's modulus of the asphalt pavement was about 3750MPa. In addition, depending on the seasonal temperatures in summer ( $40^{\circ}\text{C}$ ), spring/ autumn( $30^{\circ}\text{C}$ ), and winter( $10^{\circ}\text{C}$ ), the Young's modulus of the pavement was set to be  $E_p=500, 1500, \text{ and } 5000\text{MPa}$  in FE models, respectively.

### 6.3.2 FEA and field measurement comparison of double tire load tests

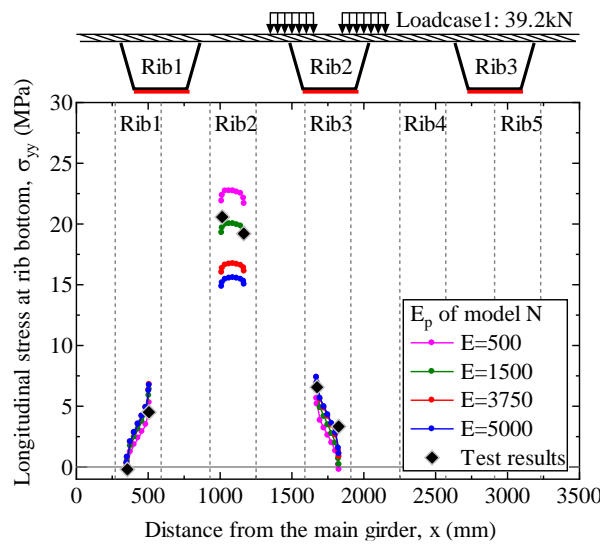
The deformations and the uniaxial stresses at mid-span by FEA analysis and field measurements, as shown in Figure 6.6. The model was under the longitudinal loadcase1, and the transverse loading above the rib2. The deformation measured from the test results was larger than the numerical results due to the simplified loading case: only one side of axle load was simulated in the FEA but not the three-axle vehicle load. Thus only the local deformation could be measured, the vertical deformation of the whole

structure was ignored because the fatigue stress usually related to the local deformation. Some previous study suggested that the interaction effects between wheels could be ignored, because the stress influence lines of load tires are really short in orthotropic stress decks [120]. Therefore, the wheel load simulation in this study is considered acceptable. Besides, the enlarged deformation by manual cut in actual bridge might also lead to the difference between FEA and field test.



(a) Deformation of the deck plate bottom

(b) Transverse stress at the deck bottom



(c) Longitudinal stress at the rib bottom

Figure 6.6 Test results and FEA comparisons

The transverse stress  $\sigma_{xx}$  at bottom of the deck plate is shown in Figure 6.6(b). Compared with the stress situation at bottom of the deck plates, the maximum principal stress at rib was depend on the longitudinal stress because of the orthotropic mechanics mechanism. Thus the longitudinal stress  $\sigma_{yy}$  at the bottom of the ribs in the mid-span was as shown in Figure 6.6(c). Their stress distributions are basically consistent, but FEA results were slight smaller. Field test in the actual bridge was conducted

with the atmospheric temperature 14°C, its corresponding  $E_p$  of the asphalt pavement is about 3750MPa. However, the calculated stress by FEA shows the field test results are more similar to the case with the asphalt  $E_p$  of 1500MPa (atmospheric temperature 30°C). On the one hand, FEA results are more conservative than field measurement. On the other hand, the temperature difference might exist between the air and asphalt. Ahmed (1995) carried out a research investigating the relationship between air temperature and pavement temperature and from measurement results at one road segment, results of the research indicated that a difference exist between the air temperature and pavement temperature sometimes may up to 5 degrees [121].

### 6.3.3 FEA and field measurement comparison of single tire load tests

The single tire loading equals to 30.38kN for the model N and D, and its transverse position was just above the rib2, the fractured location at rib2 as shown in Figure 6.4(b). The pavement stiffness were according to the actual and set  $E_p=3750\text{MPa}$ . The longitudinal loadcase1 was loaded at mid-span, and loadcase2 was loaded at the quarter span. The structural responses at two cross-sections were measured and compared base on FEA method and field test results.

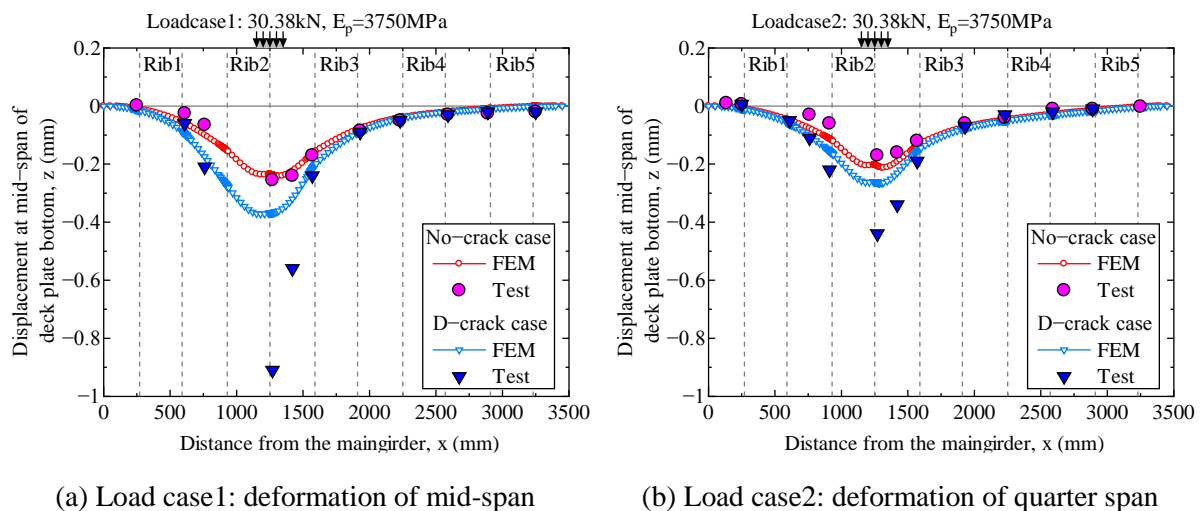


Figure 6.7 Displacement of deck plate bottom

The comparison of the deformations at deck plate bottom by FEA and field tests, are shown in Figure 6.7. For the model N, the tested deformations were consistent with the FEA results under both of the loadcase1 and loadcase2. For the model D, the measured displacement of field tests at cracked rib2 are much larger than FEA results. Based on the test results, after the fatigue damage of structure grew to be long cracks just as the artificial crack of model D, the displacement would reach to about 2~3 times larger than non-crack structure. By the way, the combination of rib-to-rib and rib-to-deck cracks would lead to a large influence on the displacement within longitudinal range.

The transverse stresses  $\sigma_{xx}$  of the deck plate bottom were compared between FEA and field tests, as shown in Figure 6.8. The nominal stresses which 5mm away from weld toe were measured by field test, and these spot all falls on the stress distribution curves of FEA and matched well.

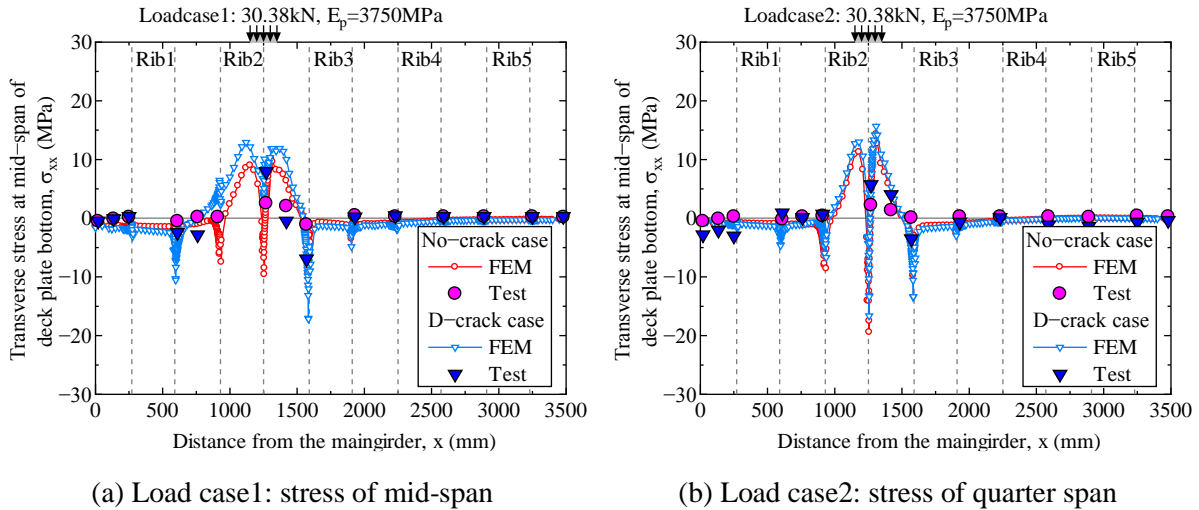


Figure 6.8 Transverse stress of deck plate bottom

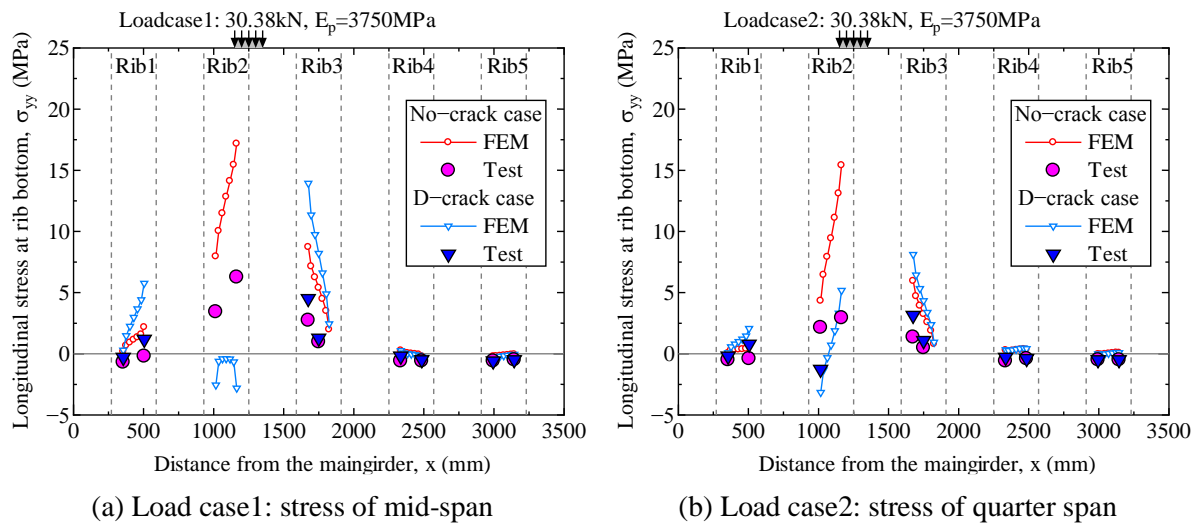


Figure 6.9 Longitudinal stress of rib bottom

Figure 6.8(a) shows that the compressive stress concentration mainly existed at the weld joints in model N. After crack D occurred, the deck plate would bearing the tensile stress instead of the fractured rib, which would also lead to the larger compressive stress condition at adjacent welded joints. It was considered, the contributions of the ribs to the transverse and vertical restraints of deck plate would be reduced after the rib-to-deck crack occurred. In Figure 6.8(b), FEA result indicates that the crack had small effect on the stress distribution of quarter span, while the field test shows the transverse stresses of deck plate at quarter span were sensitive to the rib-to-deck cracks.

Both of the deck plate stress or rib bottom stress would be affected by this crack combination, and the longitudinal stress at ribs would be mainly effected by rib-to-rib cracks. The longitudinal stresses  $\sigma_{yy}$  of the rib bottom were compared between FEA and field tests, as shown in Figure 6.9. The test results are smaller than FEA results. Moreover, the bottom stress of rib1/2/3 would be fluctuated by this loading case. The loading effect can be ignored at the farther ribs. For the D-crack case, after the rib2 cracked at mid-span, it unable to withstand the primary longitudinal stress anymore, so the high tensile stress would



be transferred to the adjacent rib especially the rib3. Figure 6.9(a) and (b) shows, whether cracking or not, the mid-span stress at rib bottom are always larger than that of quarter span.

## 6.4 Comparison of rib fracture locations

### 6.4.1 Effect of the mid-span and quarter span cracks on stress responses

To compare with field test results in 3.2 section, the model D simulated the rib-to-rib crack which initiated from the mid-span. The model D was named to D4-Mid in this section. The Young's modulus of asphalt was set as 500MPa to reduce the effect of pavement stiffness. The same single tire loading 30.38kN was conducted on these models under the same transverse load position as shown in Figure 6.4(b).

In addition, to discuss the difference between mid-crack and quarter crack, other four FE models were established to simulate the combination of 1/4-span rib crack and rib-to-deck cracks with various length. Images of the artificial cracks in five models as shown in Figure 6.10. In this section, the model D4-Mid and D4-Qua were compared to discuss the effect of rib-to-rib crack on structural response.

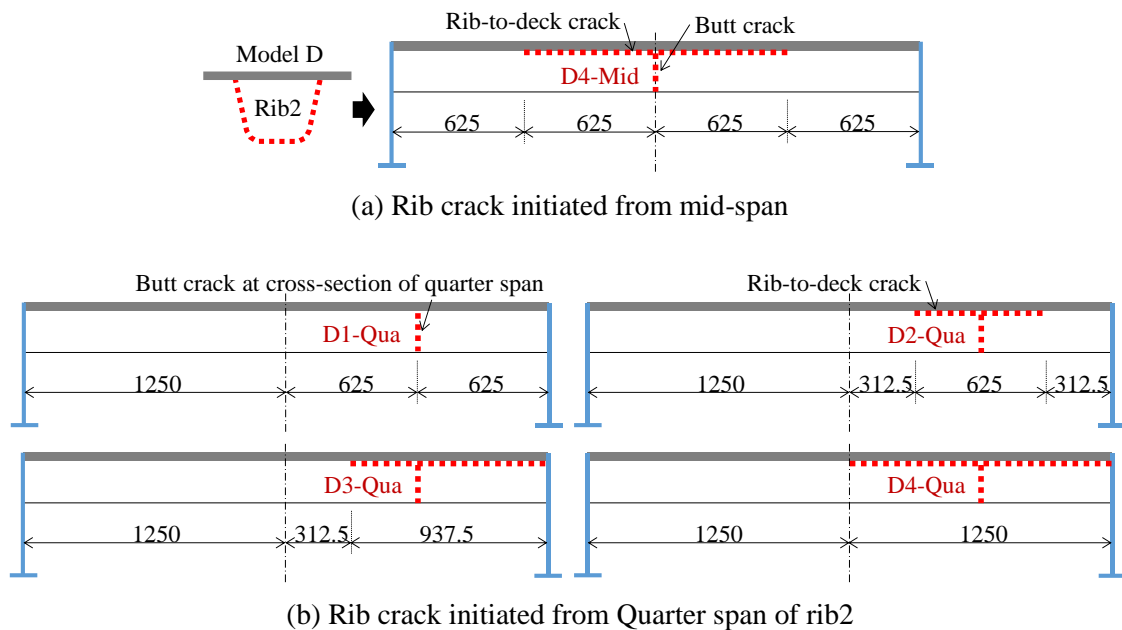


Figure 6.10 Images of artificial cracks in FE models (Unit: mm)

The effect of mid-crack and quarter crack on structural responses were investigated in following aspects: transverse stress at deck plate, longitudinal stress of adjacent rib, rib torsion, crack propagation direction, and the influences on other structure details (adjacent rib stress, crossbeam).

Comparison of the mid-span and quarter span cracks on stress responses are shown in Figure 6.11. The local stress distributions at the deck plate bottom are similar when rib crack initiated from mid-span or quarter span, as shown in Figure 6.11(a). However, it shows a larger stress concentration occurred at welded joint of D4-Qua model, its transverse stress is about 11.7% larger than that of D4-Mid. After the

rib-to-deck crack combined with the butt weld crack at quarter span, the degree of rib torsion would according to the distance between the rib-to-deck crack and crossbeam. Conversely, the rib torsion would lead to the influences on other structure details (adjacent rib stress, crossbeam). For instance, the longitudinal stress of adjacent rib3 as shown in Figure 6.11(b). Obviously, for the case of butt weld crack occurred at mid-span, its tensile stress at the adjacent rib would be about 20% larger than the case of 1/4-span crack. Moreover, the unidirectional stresses are all approach to the major principal stresses in two types of models, as shown in Table 6.1. It was suggested that the transferred stress from fractured structures might be numerically different due to different crack locations, but their cracking modes would be nearly same.

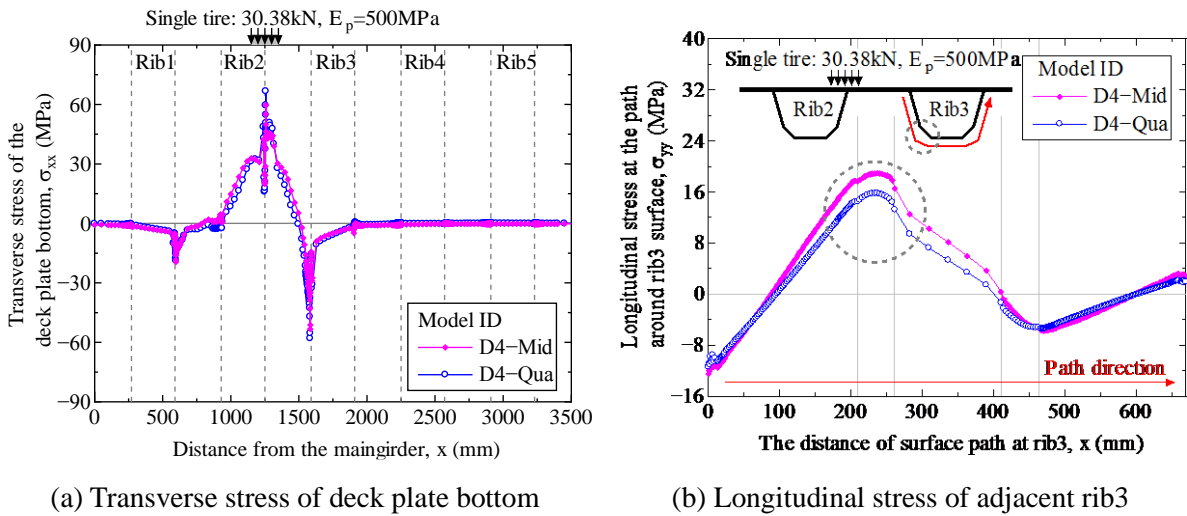


Figure 6.11 Comparison of the mid-span and quarter span cracks

Table 6.1 Effect of the rib-to-rib crack locations on structural responses

Model ID	Deck plate bottom			Rib bottom	
	Displacement $z$ (mm)	Transverse stress $\sigma_{xx}$ (MPa)	Maximum principal stress $\sigma_{max}$ (MPa)	Longitudinal stress $\sigma_{yy}$ (MPa)	Maximum principal stress $\sigma_{max}$ (MPa)
D4-Mid	-0.86	59.70	60.11	18.93	18.93
D4-Qua	-0.92	66.73	67.27	15.79	16.43

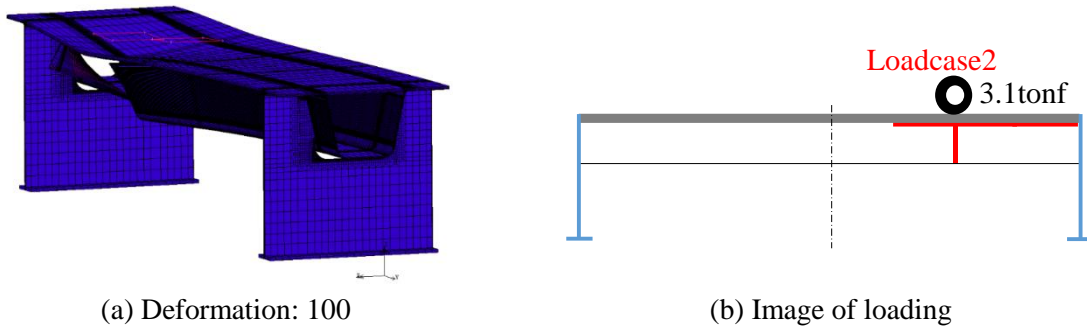


Figure 6.12 Deformation of D3-Qua model

For example: the deformation of model D3-Qua as shown in Figure 6.12. In this case, the effect of rib rotation on stress at crossbeam cannot be ignored. It is evident that the rib-to-deck crack which more closed to crossbeam might lead to large deformation easily.

#### **6.4.2 Torsional rigidity of rib with butt weld crack at quarter span**

As we all know, the rib-system in the orthotropic steel deck owns high flexural and torsional rigidity, and could result in enhanced load distribution, as well as to minimize the differential deflection [1]. Therefore, the structure with fractured ribs would always accompanied by the stress transfers and stiffness declines. U-rib is a typical closed rib which mainly responsible for the longitudinal stress and part of transverse stress. The combination of rib-to-rib crack and rib-to-deck cracks would lead to the fractured U-rib losing its contribution to load capability in both directions. Here based on four models with butt weld crack at quarter span, the torsional rigidity variation of ribs were clarified depending on the rib-to-deck crack length. The single tire of loadcase2 was conducted in FE analysis, the dimension of artificial cracks as shown in Figure 6.10(b).

The torsional rigidity of the rib still play a role before the rib-to-deck weld cracking, but it would be reduced gradually according to the rib-to-deck crack length and its distance from the crossbeam. When the rib-to-deck crack extending approached to the crossbeam, such as the crack mode in models D3/D4-Qua, the fractured ribs cannot bear the structure torsion anymore, thus this distortion effects would be passed to the crossbeam. As shown in Figure 6.13, in-plane distortion from horizontal shear was increased significantly because of two cracks combination. Furthermore, for model D4-Qua, the combination of butt weld crack and rib-to-deck crack also made it difficult for vertical loads to pass to the crossbeam effectively, that's why its in-plane distortion from vertical displacement was reduced than that of model D1-Qua.

According to the above mechanical analysis, to compare the localize stress responses at cross section of quarter span, the maximum principal stress of deck plate bottom and adjacent rib3 was compared as shown in Figure 6.14. Both of the unidirectional stresses and the major stress directions would be changing during the crack propagation process, therefore the maximum principal stress was compared here. Figure 6.14(a) indicates that the localize stress of deck plate is largely depend upon the rib-to-deck crack length, in another word is the load distribution situation. The local stress of deck plate bottom in D3/D4-Qua models are nearly same, because it is hard to transfer their vertical load to the nearest crossbeam in the fractured rib2 location. Figure 6.14(b) shows the similar stress situation. After the butt weld crack occurred, the stress at adjacent would be slightly increased. Whereas the rib-to-deck crack propagation from crack mode from D2 to D3 (and D3 to D4), would result in a significant increase in stress of adjacent ribs. Above all, it was considered that the concentrated loading could transfer to adjacent ribs in transverse, but tend to be hard to transfer to crossbeam after serious fracture occurred.

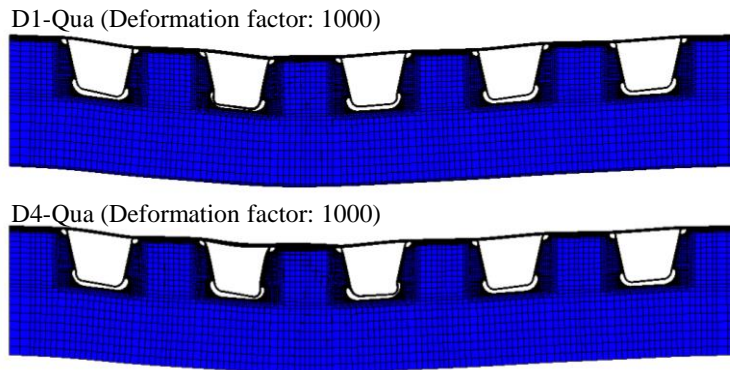


Figure 6.13 Crossbeam deformation of the models with quarter crack under loadcase2

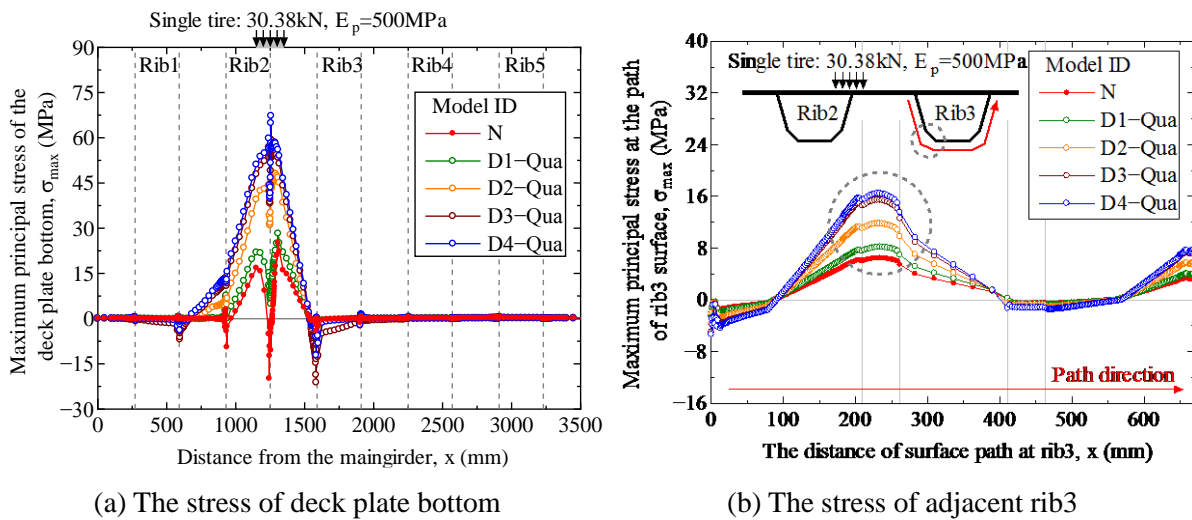


Figure 6.14 Stress responses with rib-to-rib cracks at quarter span

## 6.5 Structural responses when multiple ribs fractured

### 6.5.1 FEA analysis under double tire loading

According to the stress analysis above, although the effect of crack initiation positions on structural response is different, the local stress distributions are similar for Mid- and Qua-case. Even when the rib crack of butt weld combined with large rib-to-deck cracks, the difference of maximum principal stresses at local deck plate bottom is about 10.6%; the difference of stresses at adjacent rib bottom is about 13.2%. Moreover, the propagate direction of long cracks could always be affected by various factors such as running position of traffic vehicle, roughness of fatigue cracked fracture surface, etc. For the models with Qua-crack, their rib-to-deck crack propagation (length and direction) will be totally different in longitudinal direction, which is hard to be simulated in FEA. Therefore, in this section, the butt weld crack at mid-span could be considered as a simplified case, and most adverse stress situation, to investigate the effect of multiple rib cracks on structural responses. The model D4-Mid was denoted as model D in this section, which owns a symmetrical root crack.

In this section, we discussed seven-types of FEA model under the double tire loading at mid-span. Model N/D were established in the section 6.4. Other five models were established as shown in Figure 6.15, denoted as model A/B/C/E/F herein. The artificial rib cracks are all located within the mid-span, and the dashed lines represent the cracked sections. Model A simulated a crack existing at the bottom of rib2 with a length of 150 mm; model B simulated a crack at half the height of rib2; model C simulated fractures throughout the mid-span section of rib2; model E simulated the simultaneous cracking of the butt welds of rib1/rib2 in the mid-span. Likewise, the artificial crack of model F was same as model C, but with triple rib cracks.

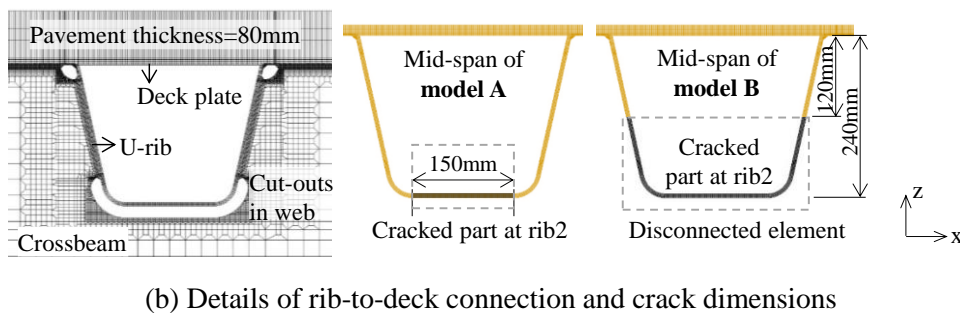
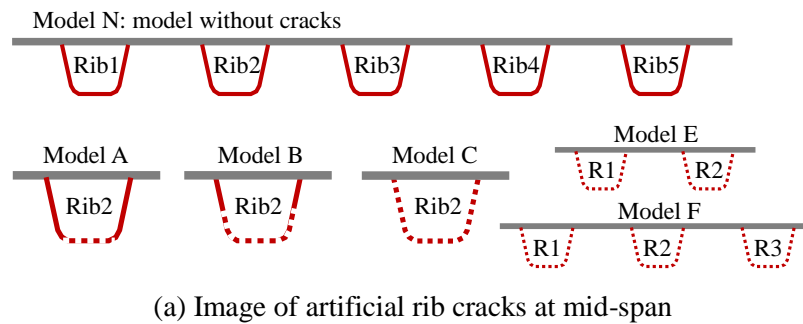


Figure 6.15 Details of various models with artificial crack combinations at mid-span

## 6.5.2 Structural responses under various transverse load cases

Three transverse load positions of double tire above the mid-span were investigated via quantitative analysis. The transverse load positions of double tire, as shown in Figure 6.16. The prototype of double tire loading is the rear tire load in field tests, which weighed 39.2kN (4.0tonf). In previous study, only one loading position was tested in the static field measurement, named as “t1”. Additional transverse loading positions “t2” and “t3” were discussed in the following numerical analysis, the transverse loads of t2 and t3 were relocated 160 and 330 mm from t1. For model N with asphalt pavement  $E_p=500\text{MPa}$ , diagrams of the transverse loading positions and corresponding deformations at mid-span of model N were shown in Figure 6.16(a). Obviously, different loading position would result in varying degrees of rib torsion.

For the models with various artificial cracks under Load position t1, the displacements of deck plate bottom at mid-span cross section were shown in Figure 6.16 (b). During the propagating process of a

rib crack initiates from the rib bottom to approach the deck plate at one rib, its final deflection tended to be about two times larger than the initial deflection. There is a significant increase in deformation when the rib crack propagated from stage A to C, in which case the maximum displacement of model C reached 1.9 times that of model A. However, the deformation of the deck plate did not change much when cracks occurred in adjacent ribs, which could potentially be attributed to the support of the main girders. Moreover, if a longitudinal crack occurred at the rib-to-deck connection at the same time, the corresponding structural deformation should increase depending on the length of the bead cracks. Herein, the maximum displacement of model D reached approximately 1.2 times larger than model C.

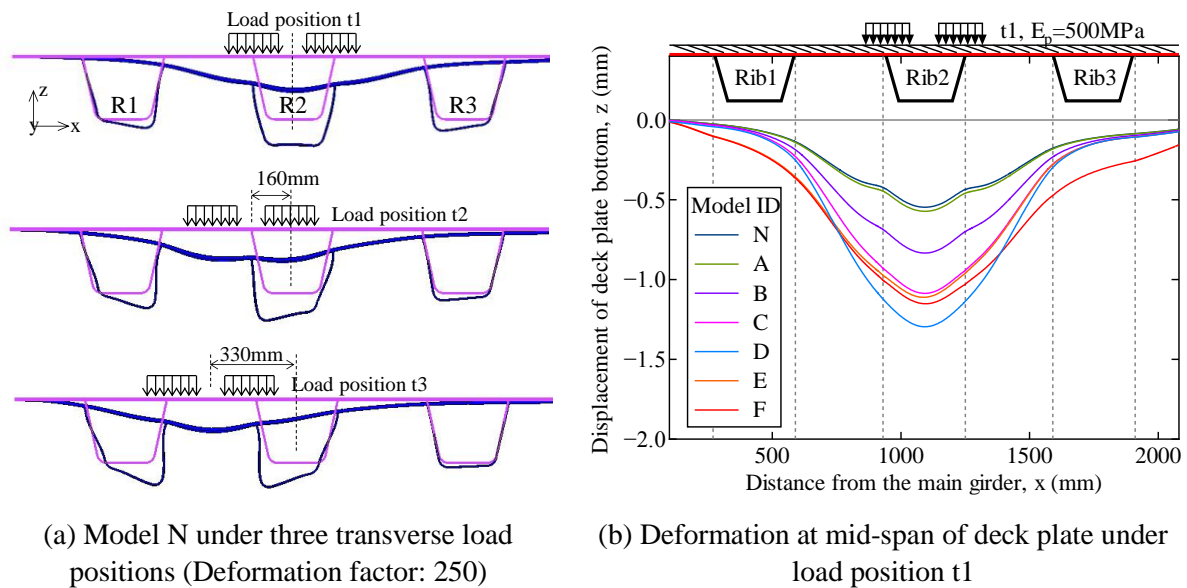


Figure 6.16 Deformations at mid-span of models

Based on the model N, transverse stress distribution at the bottom of the deck plate under three loading positions was compared in Figure 6.17(a). The wheel loads t2 caused the maximum bending moment and stress concentration of the rib-to-deck welded joint, it was because the double tire directly loaded on deck plates but not loaded above the welded joint, which lead to a larger transverse bending moment. Figure 6.17(b) shows the longitudinal stress distribution around rib2 cross section. The stress distributions were different according different load position, and the maximum tensile stresses were approximately the same depending on transverse loading position. Generally, the maximum tensile stress existed at the bottom of the rib, but the different transverse load position might affect the initiation point at rib butt weld.

In addition, the longitudinal stress distributions at the rib bottoms under three load positions were shown in Figure 6.17(c). The stress of rib bottom was sensitive to the different loading positions, and these stress distributions followed the same tendency in all models with artificial cracks. The wheel load position t3 was located between two adjacent ribs and was considered to be the most likely responsible for cracks initiated at double ribs bottom.

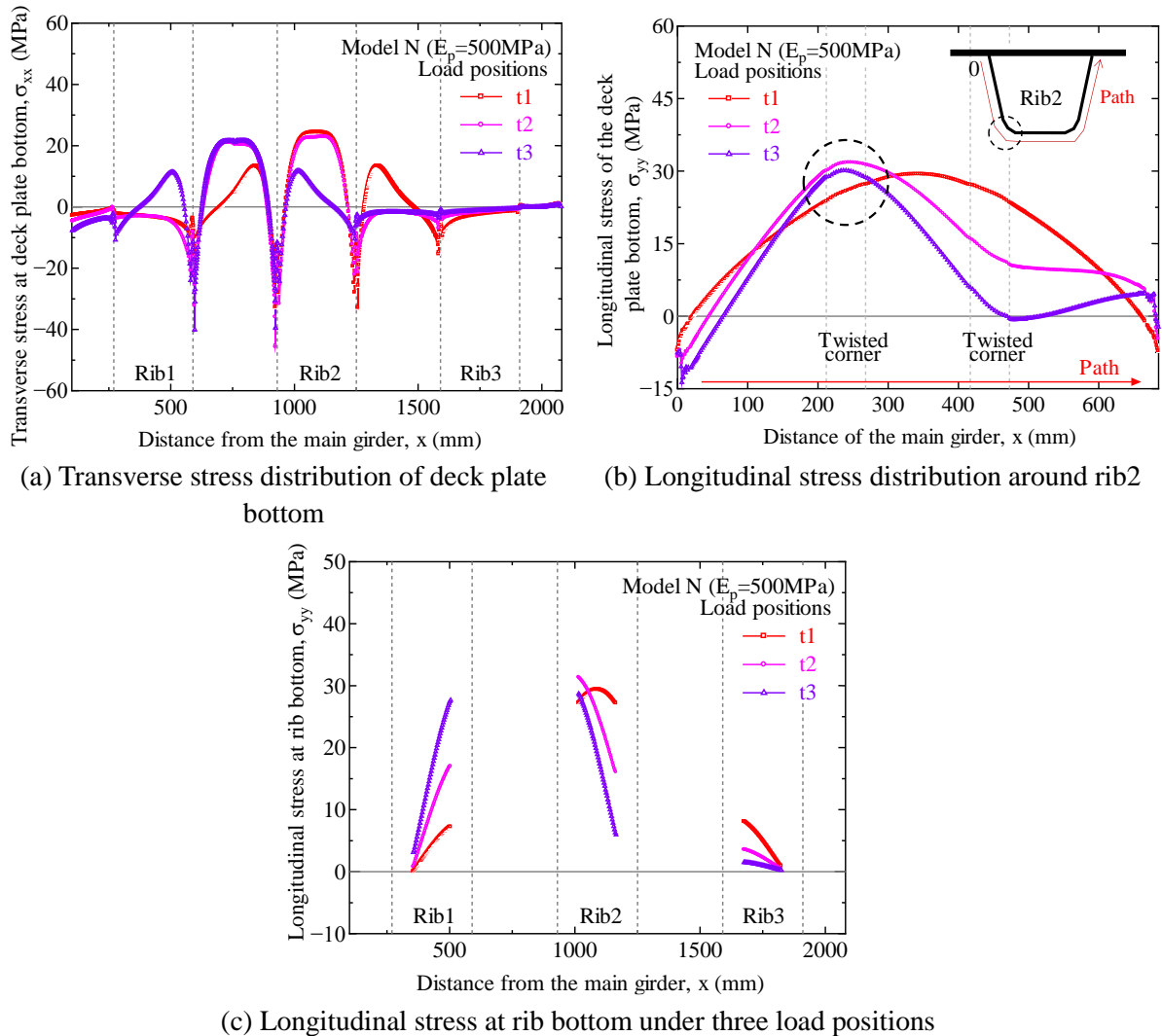


Figure 6.17 Stress distribution at mid-span under three loading positions of model N

### 6.5.3 Effect of rib cracks on stress ranges at adjacent rib

For crack models (A/B/C/E/F), each artificial crack type could be recognized as the five stages during rib crack propagation. When under the transverse load position t3, the longitudinal stress distributions at the rib bottoms of these cracked models, as shown in Figure 6.18. The stress of rib bottom was also sensitive to the different crack combinations. For cracked models under t3, the maximum tensile stress was primarily located at the rib twisted corner that close to the loads. The rib withstood the increasing longitudinal tensile stress when the crack propagating along the adjacent ribs (crack stages A through C). From this, it could be speculated that the effect of the interactions between multiple cracked ribs on the fatigue problem at the butt weld could not be ignored.

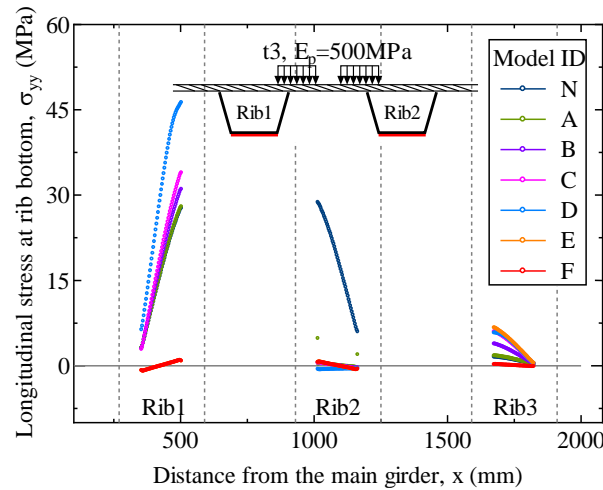


Figure 6.18 Longitudinal stress of rib bottom under the load position t3

Aimed at the interaction between cracked ribs, it could be evaluated by the equivalent stress range of various transverse loads. The wheel position t3 exerted its load precisely between ribs rib1 and rib2 on the deck plate. The maximum stresses at rib1 and rib2 were nearly the same in the model N, but once a crack occurred at rib2, the maximum stress at rib1 of models A, B, C, and D rose in varying degrees. In this study, the occurrence frequencies of a stress range corresponding to a loading position came from the statistics results of wheel lateral positions in an actual bridge [23]. Based on the Palmgren-Miner Rule, the equivalent conversion of the fatigue stress amplitude under different loading positions can be calculated by Eq (6.2):

$$\Delta\sigma_{eq} = \left( \frac{\sum_{i=1}^n p_i \Delta\sigma_i^3}{\sum_{i=1}^n p_i} \right)^{1/3} \quad (6.2)$$

Where  $\Delta\sigma_{eq}$  is an equivalent stress range,  $p_i$  is the frequency of occurrence corresponding to a stress range of  $\Delta\sigma_i$ , and  $n$  is the number of cycles.

Table 6.2 Maximum stress range at the bottom of rib1 and equivalent conversion

Model ID	Maximum stress range at rib1 bottom (MPa)			Equivalent stress range $\Delta\sigma_{eq}$ (MPa)	Percentage
	$\Delta\sigma_{t1}$ , $p1=0.29$	$\Delta\sigma_{t2}$ , $p2=0.29$	$\Delta\sigma_{t3}$ , $p3=0.29$		
N	7.23	17.00	27.66	19.39	100%
A	7.63	17.34	27.94	19.66	101%
B	11.70	20.94	31.02	22.65	117%
C	15.66	24.47	33.91	25.66	132%
D (D4-Mid)	21.62	33.97	46.25	35.27	182%

For each crack model, the maximum stress range at bottom of rib1 and the equivalent stress amplitude of three transverse loading positions, as shown in Table 6.2. Compared with the equivalent stress range of model N, the relative percentage of crack model D shows an equivalent stress range of approximately



1.82 times that of the standard value of the model N. Additionally, the other crack models A/B/C also demonstrated growths of 1%, 17%, and 32%, respectively. Therefore, the fatigue strength recommended by the specifications might not applicable for the evaluation of butt welds when adjacent rib cracks occurred. The interactions between multiple U-ribs could result in decreasing fatigue strength of the structural detail. Especially for the combination of cracks propagating in different directions, the strength reduction of the structure could seriously compromise the bridge safety.

### 6.5.4 Stress variations depending on pavement stiffness

The deck plate stiffness is related to the asphalt pavement stiffness which changing depending on the seasonal temperature. Therefore, the stress variations of some details depending on pavement stiffness were clarified. When under the transverse load position t1 at mid-span, the center point of rib2 at deck plate bottom owns the largest deformation in vertical. The effect of asphalt temperature on the transverse stress at this point as shown in Figure 6.19(a). For all these models, the pavement stiffness at winter would strengthen the structure effectively, and different rib crack mode would lead to a similar tendency for stress variation related to variable pavement stiffness. Model D has a large bead crack at rib-to-deck welded joint combined with a rib-to-rib crack at mid-span, thus its deck plate bearing the large tensile stress directly and be more sensitive to structure stiffness than other models. Here we focused on the stress at the center point of rib2 of the models, and corresponding pavement  $E_p=500$  MPa was set as standard, as shown in Figure 6.19(b). When Young’s modulus of pavement increased from standard value to 1500MPa/5000MPa, the target stress would decrease to about 68% or 40% of standard stress on average.

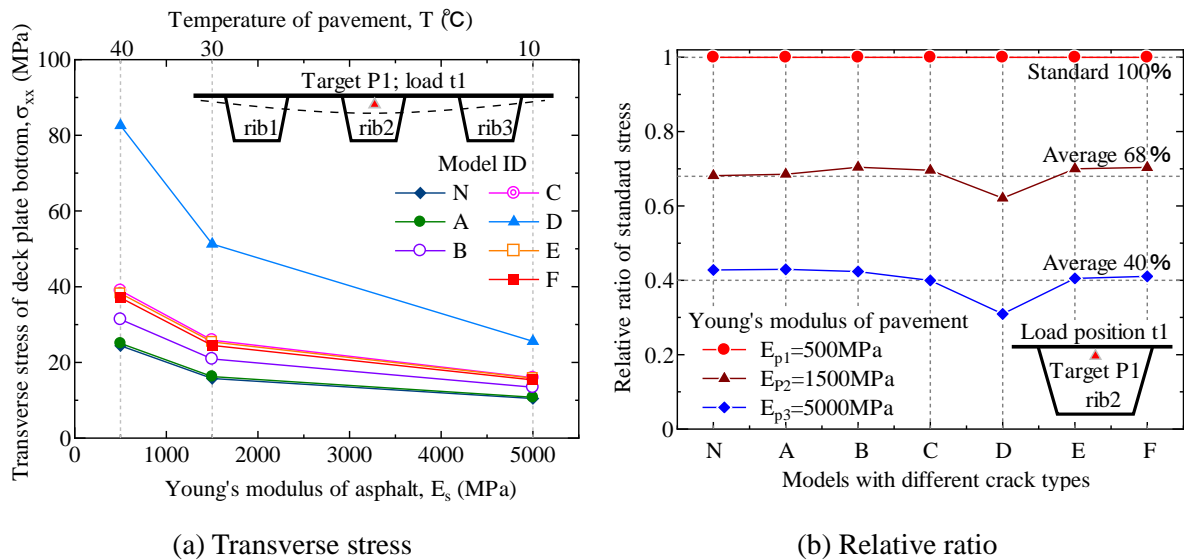


Figure 6.19 Effect of pavement stiffness on structural response at certain location

Based on the model N, Figure 6.20(a) shows the stress distribution near the rib-to-deck weld toe. The weld toe stress was almost same as the stress 1 mm away from the weld toe. Thus, the stress 1 mm away from weld toe was considered to be the peak stress, and denoted as “Toe1”. Meanwhile, “Toe2” is the

weld toe at right-side of rib2; “P1” represents the middle point of the deck plate bottom inside of rib2; and “P2” represents the middle point at the bottom of rib2.

The stress of the models with pavement  $E_p=500$  MPa was set as standard. Compare with standard stress, the relative stress ratio of locations Toe1 and Toe2 depending on the Young’s modulus of the pavement as shown in Figure 6.20(b). Obviously, the influence of changing the stiffness of pavement on the weld toe stress was largest under the wheel load of the t2 position. The stress ratio of Toe1 under t2, would decrease from 100% to 7% when the  $E_p$  of the pavement increased from 500 MPa to 5000 MPa (corresponding to a temperature decrease from 40°C to 10°C). The stress concentration caused by geometry mutations could be reduced significantly with improvements in pavement stiffness. In the case of structure with minimum pavement stiffness, evidently the asphalt pavement at low temperatures could enhance structural durability. Figure 6.20(c) shows the rib bottom stress was affected minimal by pavement stiffness among the details, deck plate bottom follows by, and the stress concentration position at deck plate is most affected by the pavement stiffness.

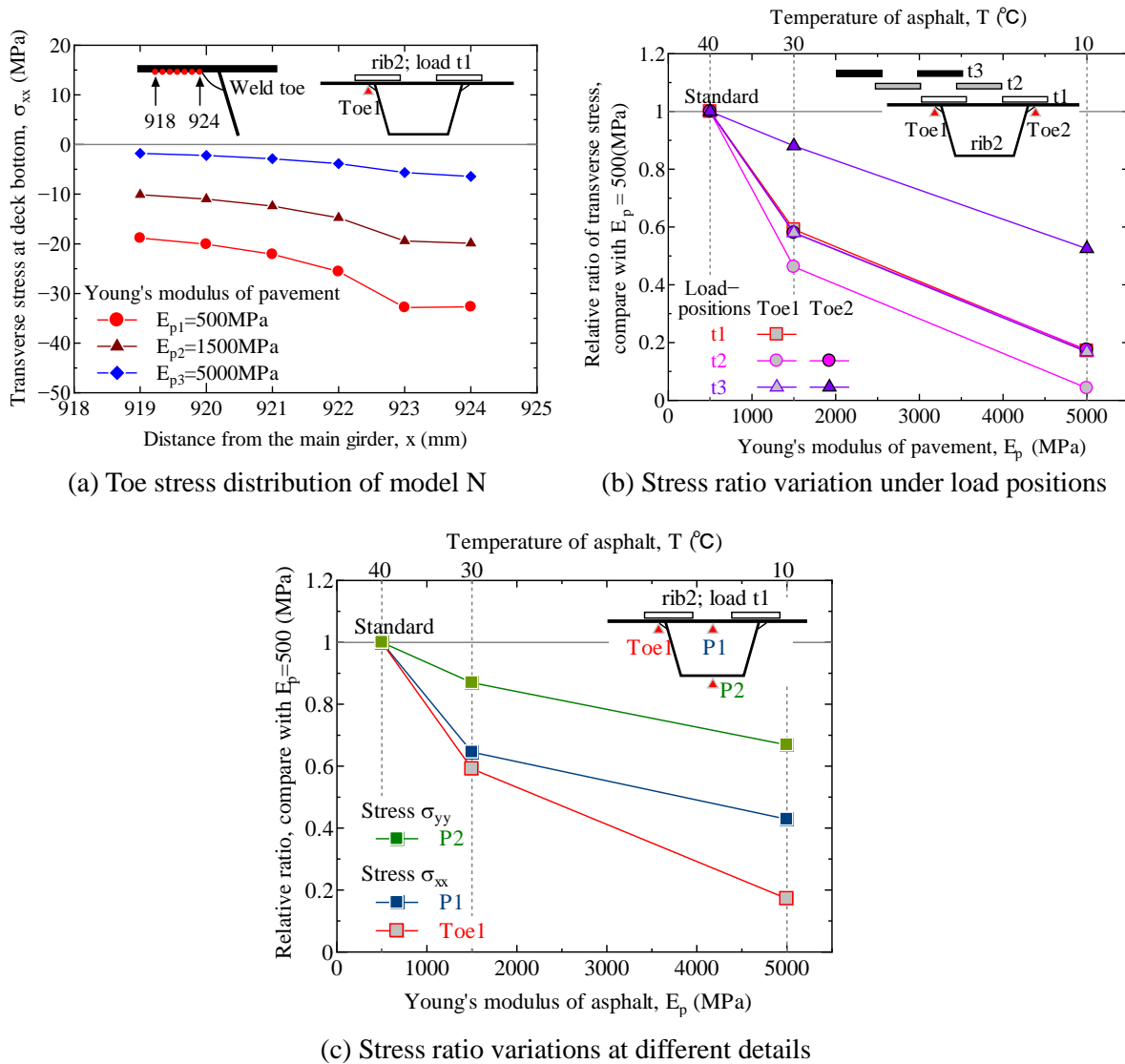


Figure 6.20 Stress and stress ratio variations depending on the pavement stiffness

## 6.6 Summary

To investigate the effect of rib fractures, and the combination of rib crack and rib-to-deck cracks, the field tests results were compared with FEA by simulating the long artificial cracks. The structure responses and stress behaviors were analyzed, the effects of asphalt stiffness and various loading positions were also discussed. The results are summarized as follows:

(1) For the non-crack structure, the tested deformations and stress distributions were consistent with the FEA. For the structure with artificial long cracks, the measured displacement would reach to about 2~3 times larger than non-crack structure. The measured stresses of deck plate bottoms were in good agreement with FEA results, except the fractured rib part.

(2) Once the fatigue cracks occurred at butt weld of ribs, the longitudinal stress withstood by the stiffener would be transferred to the localized deck plate. The combination of rib-to-rib and rib-to-deck cracks would lead to adverse effects on the displacement and stress response within longitudinal range, because the contributions of the ribs to the transverse and vertical restraints of deck plate were weakened. One rib fracture would lead to stress fluctuated at deck plate nearby within three-rib ranges in transverse, the loading effect on the farther ribs can be ignored.

(3) The butt weld crack occurred at rib would also result two important consequences: one is the effect of rib rotation on out-of-bending at crossbeams, another is the interaction between adjacent ribs. The interactions between multiple U-ribs could result in decreasing fatigue strength of the structural detail, especially for the combination of cracks propagating to different directions, the strength reduction of structure could seriously compromise the bridge safety.

(4) Pavement stiffness variation caused by seasonal temperature has similar influence on the stress responses of the cracked or non-crack structures. The deck plate stress in winter would decrease to about 40% of maximum stress (in summer) on average. In particular, it greatly reduced the stress concentration caused by geometric mutation of the welded joints. Obviously the asphalt pavement at low temperature could enhance the structural durability.

## Chapter 7 Stress characteristics of deck plate and crossbeam with butt weld crack combinations

### 7.1 Introduction

Based on the Chapter 6, we could know the occurrence of fatigue cracks at U-ribs might lead to an adverse effect on the deformation and stability of the structure, which could seriously compromise the durability. Furthermore, rib cracks are arguably the causation of fatigue cracks in other positions, which caused by the stress redistribution of the structure. For instance, the large crack at butt welded joint might lead to the rotation of ribs, and out-of-bending at crossbeams. Besides, for the fatigue problem existed at rib-crossbeam or rib-deck welds, the coexistence of various rib cracks might be highly dangerous. Thus it is critical to consider the coexistence of large cracks at multiple U-ribs, to predict and assess the best response to preserve structure integrity.

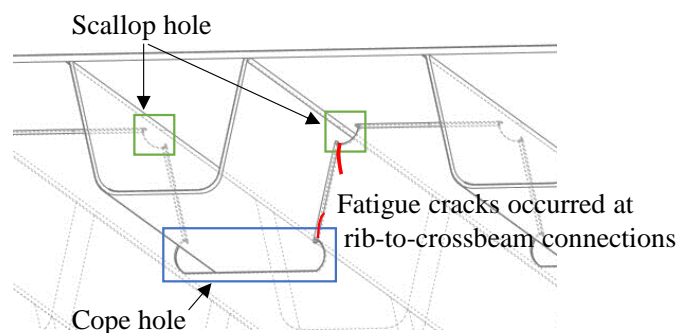


Figure 7.1 The cut-outs and typical cracks at crossbeams

According to statistics of fatigue cracks on the major expressways in Japan, the weld toe crack which located at the rib-to-crossbeam connection, especially occurred at the scallop and cope holes are most general type, as shown in Figure 7.1. It accounted for more than one-third of the total fatigue cracks. The crossbeams were usually applied to the out-of-plane flexure by the traffic flows in longitudinal direction. The rib to crossbeam details is influenced by three local effects [4]: Firstly, out-of-plane distortion of the crossbeam from rib rotation; secondly, in-plane distortion of the crossbeam from horizontal shear. Finally, the in-plane distortion from vertical displacement of the free edge of cut-outs. Therefore, the stress state of cut-outs in the crossbeam was combined between their in-plane and out-of-plane stresses. Besides, the shape of welded joints at scallop and slit would lead to high stress concentration, and it was hard to ensure the weld quality at round welding. The fatigue problems at the nearby of cope hole would be sensitive to structural stiffness and vehicle loadings. For instance, if rib cracked at butt joint in a cross section between crossbeams, the rib rotation and distortion would lead to a significant increasing in local stress at cope holes.

The long crack cases at rib butt weld, as mentioned in chapter 6, might affecting a wide range on the

orthotropic steel structure. Especially, the crossbeam stress cannot be evaluated well depending on a single-span model. Therefore, according to the solid models and crack types in chapter 6, this chapter refined and built the solid-shell hybrid models with three-span section to investigate the whole structural response and stress characteristics of crossbeam and other details. This chapter only considered double tire loading and cracks located at mid-span. The local stress variations from non-crack stage to multiple-crack stages were analyzed, and the stress characteristics of rib-to-crossbeam connections were also conducted. Besides, the sensitive points at cope holes of crossbeam were evaluated by hot spot stress method. Finally, the effect of various crack combinations on thickened deck plate structure was also discussed by stress evaluation.

## 7.2 FE analysis of rib crack combinations

### 7.2.1 FE models





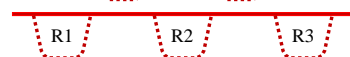
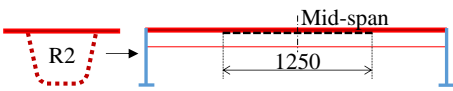
The solid-shell hybrid FE models of three-span OSD between two girders were built using same dimensions as those in Chapter 6, which according to the standard dimensions of actual bridge in the Expressway. As we discussed in previous chapter, the butt welded joints of ribs are usually set at the quarter span in actual bridge, to consider the construction convenience and avoid the largest bending moment occurred at welded joint. Therefore, when butt weld crack combined with rib-to-deck cracks in actual bridge, the rib-to-deck crack propagation (length and direction) will be totally different in opposite longitudinal directions, which is hard to simulate the various actual cases in FE models. When the rib-to-deck long crack propagated close to the scallops of crossbeam, the structural local buckling might occurred. In addition, the butt weld crack initiated from mid-span would lead to a larger out-of-plane bending moment of crossbeam than the quarter crack case, which could be considered as a simplified and extreme situation. In this section, the butt weld crack at mid-span was discussed, to investigate the adverse mechanical condition of crossbeam, and avoid the complex local deformation such as the buckling near cut-outs due to the artificial crack.

The element mesh division and boundary conditions are shown in Figure 7.2. The model was fully-constrained at the connection to the main girders. Only the double tire at one side of the second axle was simulated as a loading surface on the models. The loading area of the rear wheels was simulated by a rigid body with an area of  $200 \times 200 \times 2 \text{ mm}^2$ , and the corresponding load is 39.2kN [122]. The solid and shell elements were connected by nodes as shown in Figure 7.2(b). Contact elements were used to simulate the artificial cracks. The connect detail of rib-to-deck weld of Model D as shown in Figure 7.2(c).

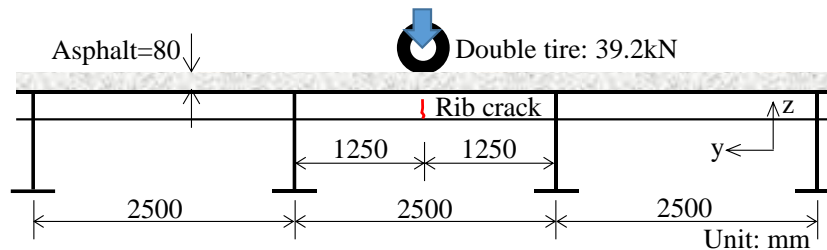
Models were denoted as model-n /a /b /c /d /e /f, the artificial crack dimensions and structure details of solid part were similar as the models in chapter 6, as shown in Table 7.1. The dispersion effect of asphalt was considered in summer, which corresponding Young's modulus of pavement was set as  $E_p=500\text{MPa}$ .



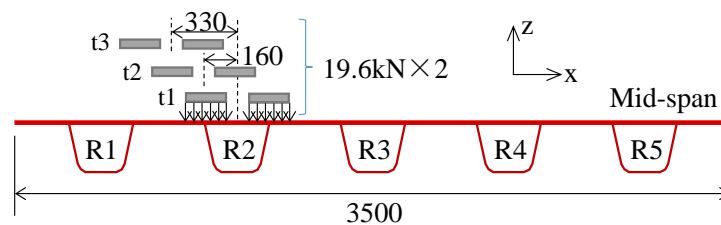
Table 7.1 The models with artificial cracks at ribs

Model ID	Image of models	Crack positions	Rib-to-deck connection	Other connections
(n)	Non-crack	/		
(a)		Cross section of mid-span	Including welded joint (6mm)	Including welded joint (6mm)
(b)				
(c)				
(e)				
(f)				
(d)		Mid-span and $\pm 625$ mm in longitudinal	No welded joint	

The loading condition and mid-span cracks of FE model as shown in Figure 7.3(a). Three transverse load positions of double tire above the mid-span were also discussed, as shown in Figure 7.3(b). Figure 7.4 shows the major principal stress contours at mid-span of all models under the load case t1. It can be know that the stress distribution of rib bottom with model-n was mainly subjected to tensile stress, thus the rib-to-rib cracks might occurred at bottom of ribs firstly and propagate rapidly caused by the tensile stress at crack tips. After the rib crack occurred, the stress concentration at crack tip mainly bearing the tensile stress instead of cracked part. And finally, the local deck plate would undertake the loading in both transverse and longitudinal directions.



(a) Load position of double tire in longitudinal



(a) Load position of double tire in transverse

Figure 7.3 Loading conditions of FE models

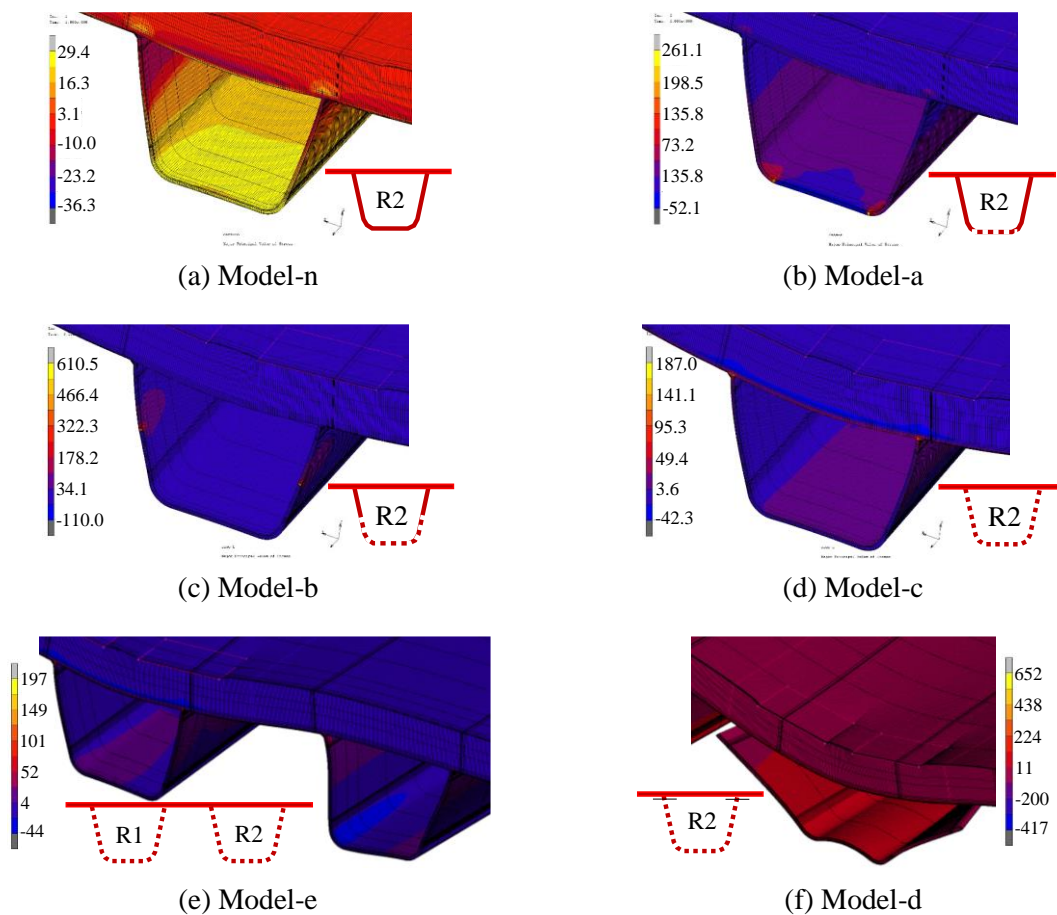


Figure 7.4 Major principal stress contours of models under t1 (Deformation: 100)

### 7.2.2 Local deformations at crack cross section

To investigate the different effects of crack combinations on structure integrity, six models were established with artificial cracks for comparison with model-n. Model-d included two kinds of serious fatigue damage resulting from rib crack propagation. The Young's modulus of the pavement of all models was set to 500 MPa.

The displacements of the deck plate bottom at the mid-span were as shown in Figure 7.5. Although the displacement distributions of the models were different when subjected to different transverse loading positions, the tendency of deformations were similar when the area of the cracked section changed at the mid-span. The rib crack was found to have a significant effect on the deflection of the deck plate. For instance, a rib crack initiating from the bottom of the deck plate and propagating to the butt weld disconnected completely in the mid-span. Its final deflection tended to be over two times larger than the initial deflection. Specifically, this led to a significant increase in deformation when the rib crack propagated from stage (a) to (c) especially under t1 load, in which case the maximum displacement of model-c reached 1.9 times that of model-a. Moreover, if a longitudinal crack occurred at the rib-to-deck connection at the same time as a rib crack, the corresponding structural deformation increased depending on the length of the bead cracks. Herein, the maximum displacement of model-d reached



approximately 1.2 times that of model-c. However, the deformation of the deck plate did not change much when cracks occurred in adjacent ribs, which could potentially be attributed to the support of the main girders.

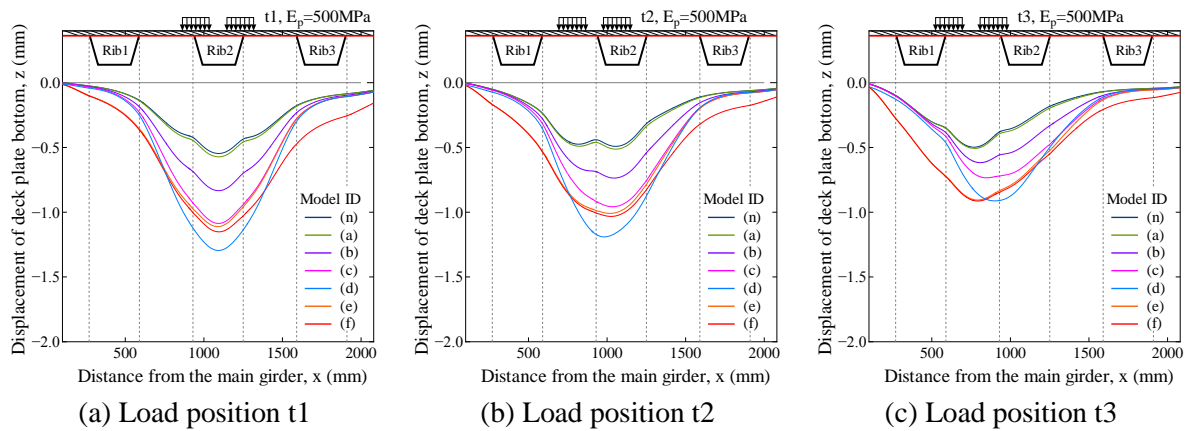


Figure 7.5 Deformation of the deck plate

Table 7.2 Criteria for deflection of orthotropic plate decks

Load positions	Limitation
Vehicular loads on deck plates	Span/300
Vehicular loads on ribs of orthotropic metal decks	Span/1000
Vehicular loads on ribs of orthotropic metal decks: extreme relative deflection between adjacent ribs	0.10in (2.54 mm)

Table 7.3 The relative displacement and allowable deflection of deck plate

Model ID	Young's modulus $E_p$ (MPa)	Load positions		
		t1 (span/1000)	t2 (span/300)	t3 (span/1000)
(n)	500	$0.030 < 328/1000$	$0.115 < 328/300$	$0.127 < 328/1000$
(a)		0.031	0.115	0.128
(b)		0.032	0.110	0.126
(c)		0.029	0.101	0.120
(e)		0.025	0.094	0.116
(f)		0.023	0.093	0.116
(d)	500	$1.009 > 988/1000$	$0.844 < 988/300$	$0.469 < 988/1000$
	1500	0.569	0.477	0.296
	5000	0.256	0.217	0.153

There were many provisions regarding the maximum deflection of steel bridges. The criteria for deflection of orthotropic plate decks in AASHTO are suggested in Table 7.2. The extreme relative deflection between adjacent ribs met all requirements. The relative displacements of the deck plate were compared in Table 7.3. Most of the models did not exceed the allowable deflection, with the exception

of model-d under the t1 wheel load with pavement  $E_p=500$  MPa. Therefore, the combination of rib-to-deck bead crack and rib crack most adversely affected the bridge integrity. However, for the case in which cracks only occurred at the butt weld of a rib splice, even if a crack occurred at multiple ribs, the deformation of structure was not found to compromise bridge security. From these results, a daily round check and maintenance plan could be optimized based on the different crack types and pavement stiffness dependent on the seasonal temperature.

### 7.2.3 Local stress variations at crack cross section

The transverse stress distributions of the deck plate bottom at the mid-span are shown in Figure 7.6, and the three loading positions were also considered and compared in this section. The figure shows that the weld toe stress tended to increase once a fatigue crack occurred at the U-rib, and gradually changed from compressive stress to tensile stress. This meant that the deck plate might have to bear the tensile stress instead of the U-rib in the case of a severely cracked rib. For model-d, which simulated both a rib-to-deck crack and rib crack, the maximum tensile stress at deck plate was even larger than the concentrated stresses of the other models, since its deck plate was partially disconnected from rib2. Therefore, only the deck plate between rib1 and rib3 was used to bear the bending moment caused by the wheel loads. Although the maximum stress of model-d was slightly reduced when under load position t3, it led to an occurrence of larger compressive stress concentration in the adjacent rib-to-deck welded joints. It is commonly accepted that the amplitude and maximum of cyclic load are the most important factors affecting fatigue life. Thus, model-d did not only cause the largest tensile stress at the deck plate, but also likely caused fatigue cracking at the nearby stress concentration zone.

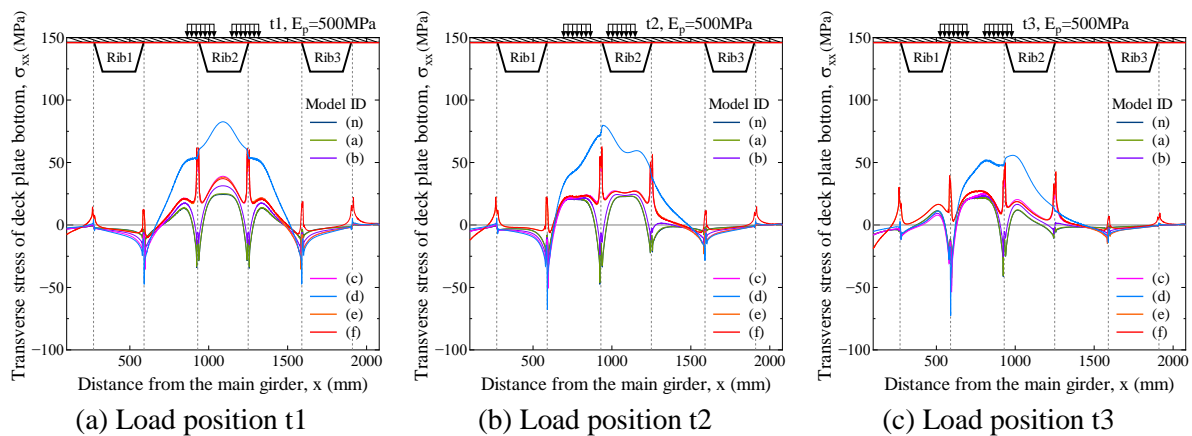


Figure 7.6 Transverse stress distribution at the bottom of the deck plate

For other crack models-a /b /c /e /f, the artificial cracks of each model could be categorized into five stages during rib crack propagation. The stress at the weld toe of the rib-to-deck welded joint changed substantially when the transverse load position changed from t1 to t3. These weld toe stress values, notably the absolute stress values at rib3, were reduced, and those at rib1 were increased. Furthermore, the localized deck plate withstood the tensile stress instead of the ribs at the mid-span once the rib stiffener cracked. This shows that the stresses at weld toes of rib2 significantly increased from stage (b)

to (c). The stress of rib2 from crack stage (c) to (f) showed that the localized toe stress was largely unaffected by adjacent rib cracks. Above all, the local stress at the welded joint, which was connected to the cracked ribs, was found to increase; thus, a crack spanning multiple ribs might have induced tensile stress at many welded joints of the deck plate. However, the toe stress was largely unaffected by adjacent rib cracks, and the interactions between multiple cracked ribs on localized weld toe stress could be ignored.

The longitudinal stress distributions at the bottom of the ribs for three load positions were as shown in Figure 7.7. The stress at bottom of the ribs was sensitive to the loading position and different crack combinations. The maximum tensile stress was primarily located at the rib corner close to the loads. The maximum stress values at the corners of the rib bottoms were compared. The results showed that the rib withstood the increasing longitudinal tensile stress as the crack propagated along the adjacent ribs (crack stages (a) through (c)). From this, it could be speculated that the effect of the interactions between multiple cracked ribs on longitudinal stress at the butt weld could not be ignored.

The wheel position t3 exerted its load precisely between ribs rib1 and rib2 on the deck plate. The maximum stresses at rib1 and rib2 were nearly the same in the non-crack model, but once a crack occurred at rib2, the maximum stress at rib1 of models-a /b /c, and -d rose in varying degrees.

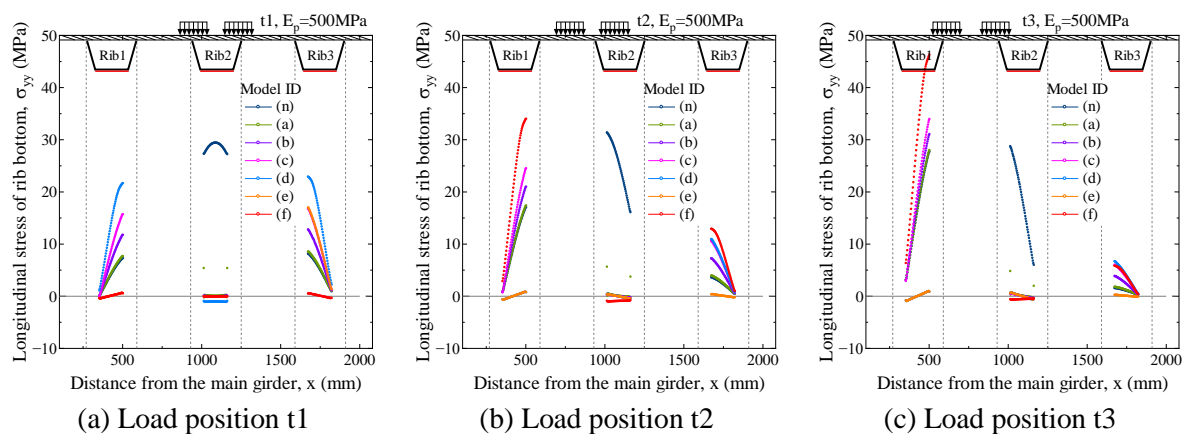


Figure 7.7 Longitudinal stress distribution at the bottom of ribs

## 7.2.4 Stress response of other structural details

To evaluate the effect of different rib crack combinations on stress variations at welded joints, the stress analysis were conducted under the transverse load position t1. Figure 7.8 shows the principal stress distribution of rib-to-deck welded joint from mid-span to crossbeam. For the weld toe stress at rib or at deck of the rib-to-deck welded joint, it seems to be that the stress of crossbeam would not be affected large by rib cracks at mid-span, although the toe stress distributions near the mid-span are different depending on crack types.

The tensile stress occurred at weld toe of rib near crossbeam, as shown in Figure 7.8 (a). Three uniaxial stresses are approximate at this path, and the maximum principal stress near crossbeam is determined by vertical stress  $\sigma_{zz}$ , as shown in Figure 7.9 (a). Their peak principal stresses of all models

are around 20MPa. Figure 7.8 (b) shows the weld toe stresses at deck, the toe stress at deck plate is much larger than those of ribs at mid-span. However, its maximum principal stress value is close to 0MPa near crossbeam because the maximum principal stress at deck toe was determined by longitudinal stress instead of transverse stress where far from mid-span.

The maximum principal stresses at the middle-axial plane of rib2 left-side scallop are shown in Figure 7.10(a). The stress distributions are almost same in different crack models. Meanwhile, the maximum principal stresses at the middle-axial plane of rib2 cope hole are shown in Figure 7.10(b). When the structure under the loading t1 at mid-span, it shows the rib torsion occurred when the rib crack and load positions are asymmetric in model-e. The cope hole stress of model-e is much larger than that of other models, but the scallop stress is similar with others. Moreover, it was considered the structure torsion would also be affected by transverse load position.

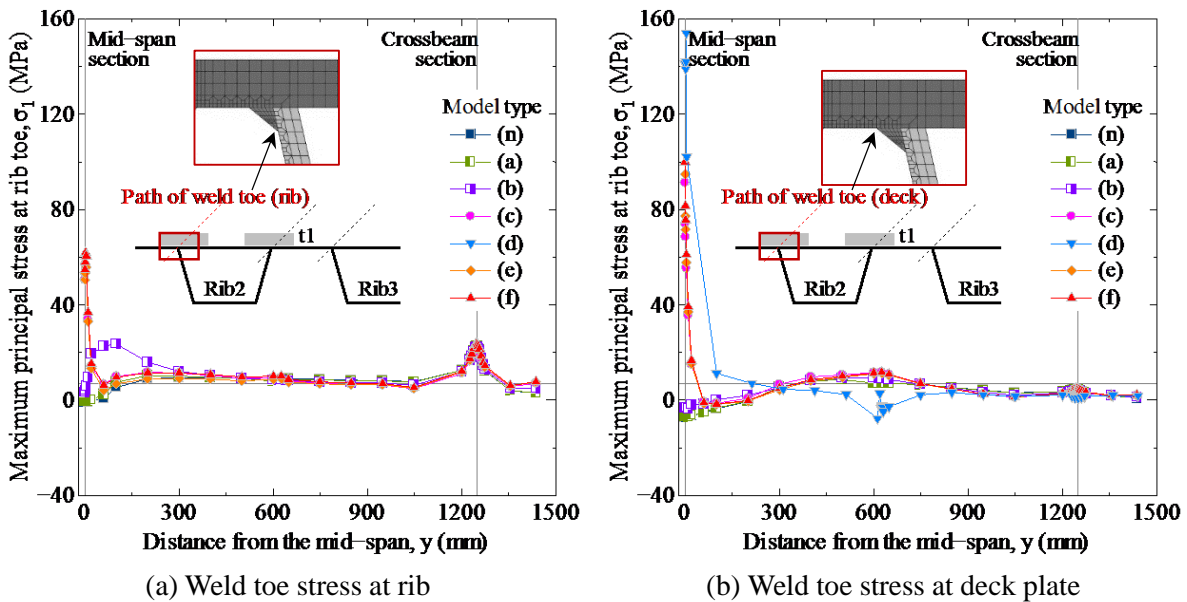


Figure 7.8 Stress distributions at rib-to-deck connections in longitudinal direction

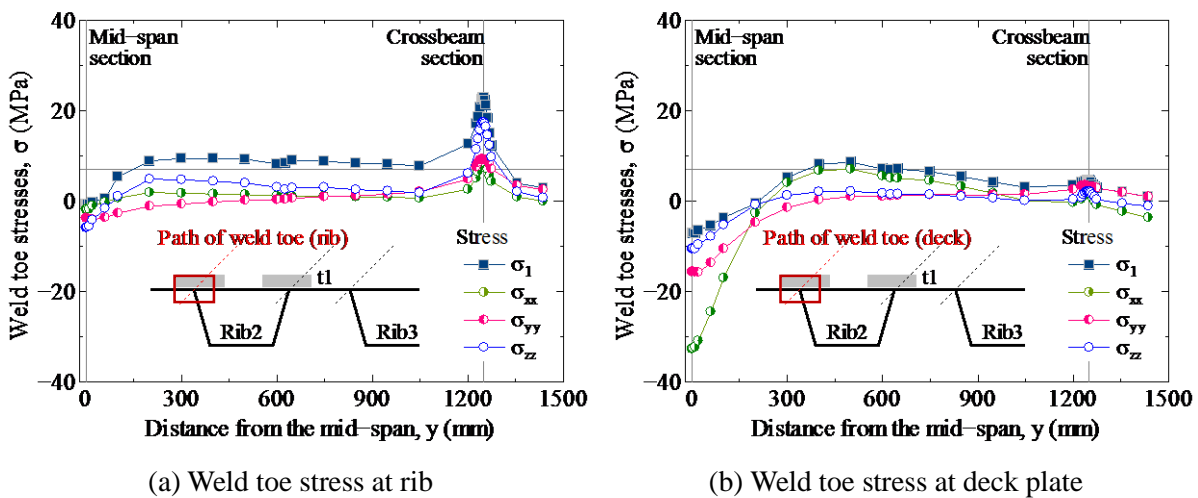
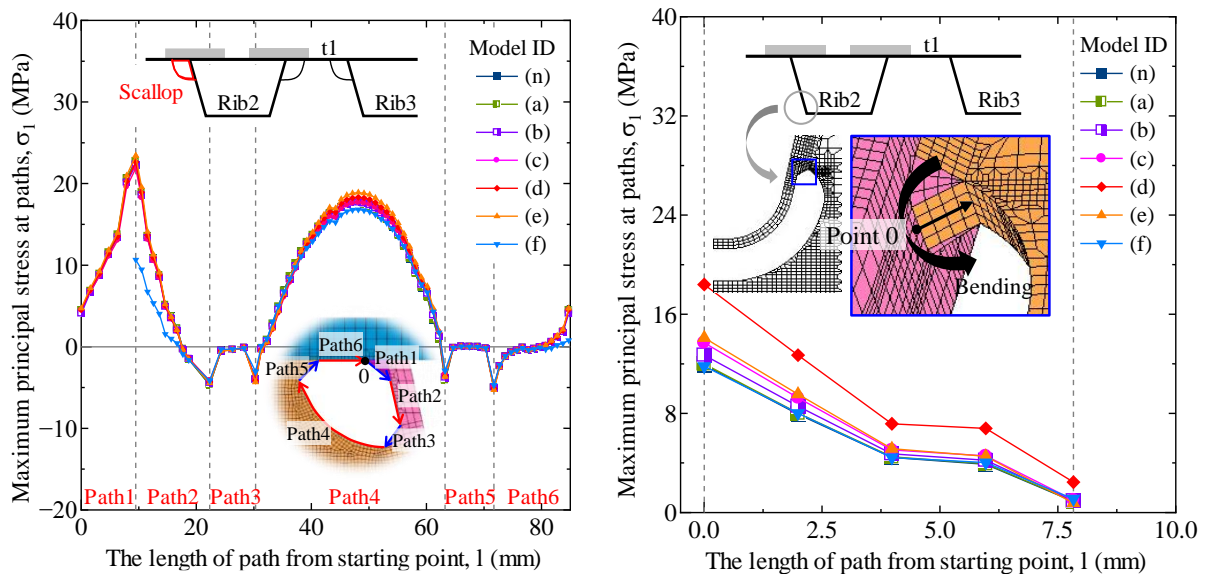


Figure 7.9 Toe stresses at rib-to-deck connections in longitudinal direction



(a) Maximum principal stress at scallop

(b) Maximum principal stress at cope holes

Figure 7.10 The crossbeam stress of rib2 under transverse loading t1

### 7.3 Stress characteristic of rib-to-crossbeam connections

#### 7.3.1 Effect of transverse loading on cut-out stress

Based on the previous section, we could know the multiple rib crack might lead to serious rib torsion. In model-e, three transverse loading positions t1/ t2/ t3 were conducted at mid-span in FE analysis. Figure 7.11(a, b) shows the maximum principal stress at middle-axial plane of rib1 /rib2 scallop. The stress distribution under different transverse loading positions is totally different. In addition, the adjacent rib1 stress is smaller than rib2 stress at scallop. Figure 7.11(b) shows the peak stress under t1 occurred at rib-to-deck welded joint (path 1), but welded joint stress at path3/ 5 was showed in all compressive stresses. For the case of t2, its peak stress is smaller than those of other loading positions, but the tensile stress existed at all of the welded joints. This might because the load case t2 loaded above the scallop directly.

Figure 7.11(c) shows the maximum principal stress at welded joint of rib1/rib2 cope holes. The stress tendency is similar to change the load position. Besides, due to the main girder and bending effects in transverse, the adjacent rib1 stress is larger than rib2 stress. Obviously, the in-plane and out-plane deformation of crossbeam would be effected by the combination of rib cracks and different load cases. The effect of transverse load positions on cope hole stress and scallop stress are also different. The stress near the cope hole would be magnify due to the slit, and the localized bending at cope holes are more sensitive to fatigue loadings than scallops.

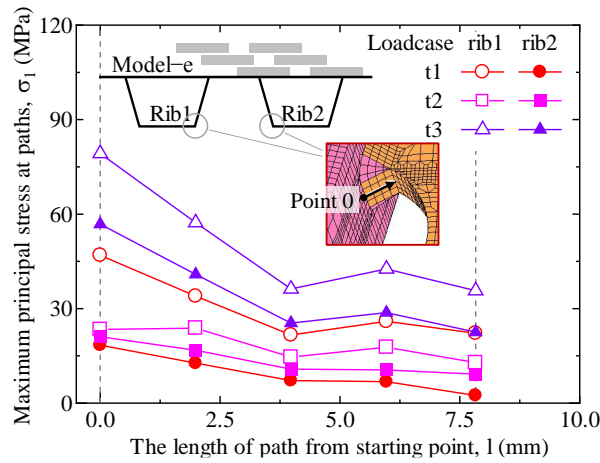
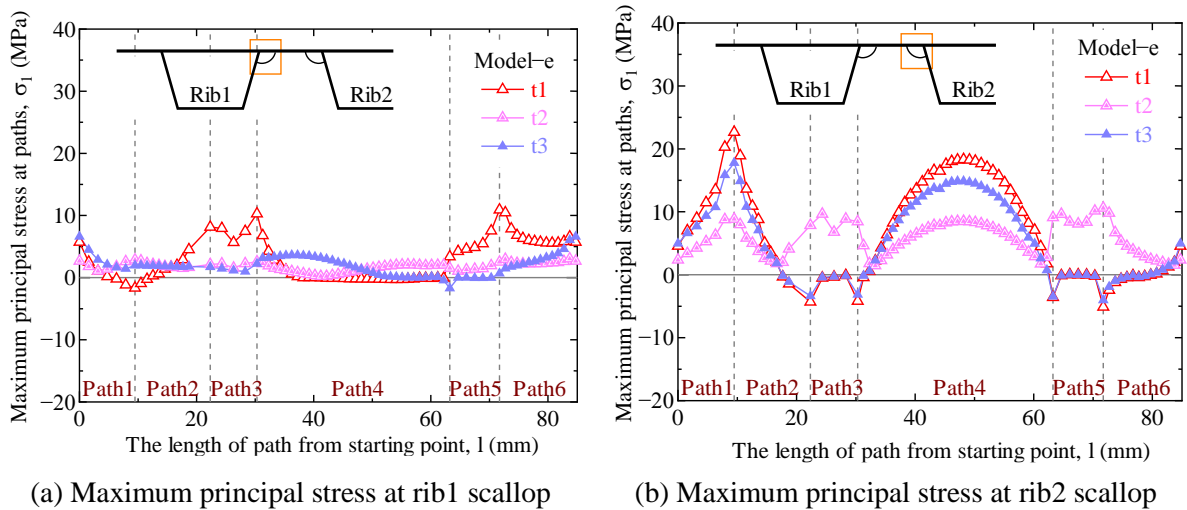
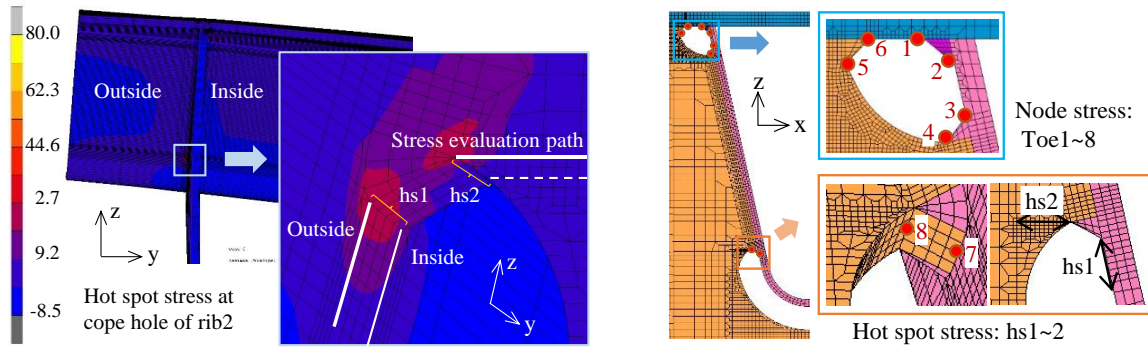


Figure 7.11 Stress distributions at middle axial plane of cut-outs in model-e

### 7.3.2 Effect of longitudinal loading on cut-out stress

Model-f would be most affected by the longitudinal loading because of its triangular cracked butt weld at mid-span. To investigate the stress characteristics around scallop and cope holes, weld toe stress of cope holes were evaluated and compared by node stress and hot spot stress. In this section, model-f with five longitudinal load positions were discussed under transverse load t2. The out-of-plane distortion of crossbeam caused by the rib rotation is illustrated in Figure 7.12(a). It also showed the stress evaluation paths of hot spot stress at inside and outside surface of crossbeam. The stress contour at termination of cope hole was showed that the stresses of outside surface of target crossbeam are usually larger than those of inside surface. The toe stress at cope hole were denoted as hs1/2, which calculated by hot spot method. The node stress of weld toes at cut-outs of crossbeam in middle-axial plane were denoted as toe 1~8, as shown in Figure 7.12(b).



(a) Out-of-plane distortion of crossbeam due to rib rotation (Deformation: 200) (b) Definitions of stress points at scallop and cope holes in crossbeam

Figure 7.12 Crossbeam details of FE models

In addition, the crossbeam stress could also be directly affected by longitudinal location of wheel load, thus, the five longitudinal loading positions were also simulated under model-f. The target crossbeam and the loading positions were shown in Figure 7.13. The distance of 1/6 span was set as loading spacing between each load step in longitudinal. The traffic direction was considered as the vehicle drives away from target crossbeam.

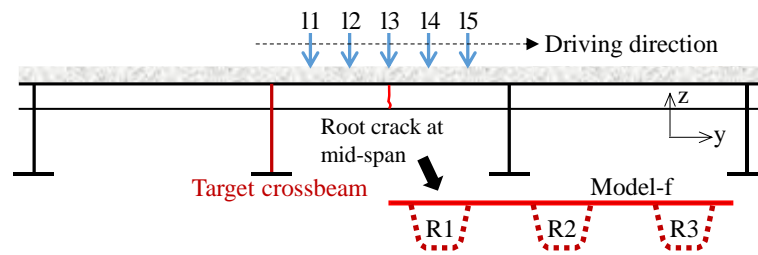


Figure 7.13 Target crossbeam and five longitudinal loading positions

Based on model-f under transverse load position t2, the toe stresses at cut-outs of rib2 were compared with that of rib1 at middle-axial plane, as shown in Figure 7.14. The influence of longitudinal loading positions on weld toe stress was different. The maximum principal stress at scallop was increased as wheel loading pass away from target crossbeam; however, the stress at cope hole was decreased in general. The numerical values were showed that the stress of cope should be larger than those of scallop. Toe 7 might be the most sensitive location to t2 loading case, and the principal stress of Toe 7 in adjacent rib1 is larger than those of Toe 7 in rib2, it might be the in-plane distortion of the crossbeam from horizontal shear.

In case of Toe 7 stress under t2, the stress of three locations was evaluated in tensile stress, as shown in Figure 7.15. The stress of rib1 is much larger than those of rib2 and rib3. When double tire loading change from 11 to 15, the tendency for tensile stresses of Toe 7 at three ribs are always increase firstly and then decrease. The largest tensile stress range was showed near the mid-span because of the artificial rib cracks there. Depending on the longitudinal loadings, the case of model-f shows that the stress range at rib1 is about 1.3-times larger than those of rib2, and 2.4-times larger than those of rib3. Moreover, the

stress tendency of model-n is similar with that of model-f at these locations. The comparison between model-n and -f shows that the stress range would increase about 130%, 129% and 164% at rib1/ rib2/ rib3 respectively, once the multiple cracks occurred at adjacent ribs.

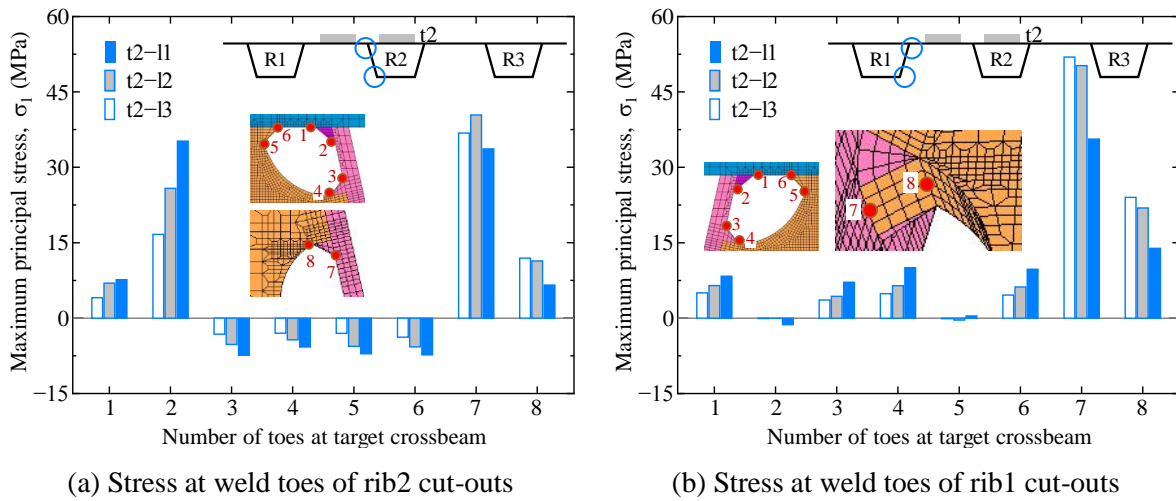


Figure 7.14 Maximum principal stresses of model-f crossbeam

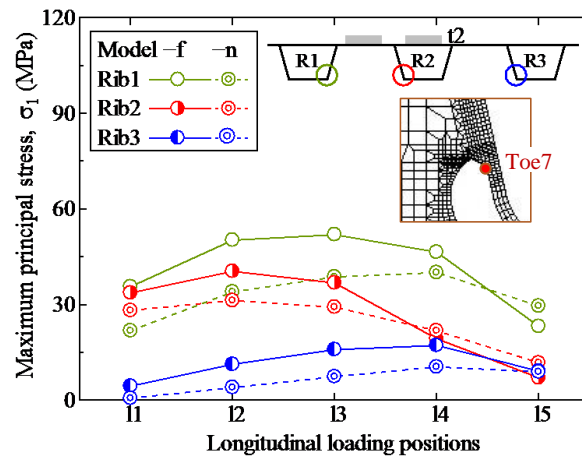


Figure 7.15 Maximum principal stresses at Toe7 of cope holes

### 7.3.3 Evaluation on cope hole stresses by hot spot method

Due to the limitation of mesh sizes, and the influence of geometric characteristics of grid, the stress singularity often occurred at geometric mutation point. At present, hot spot stress were usually used for fatigue strength evaluations. The hot spot stress  $\Delta\sigma_{hs}$  is usually determined by linear or quadratic surface stress extrapolation method. For the cope hole details in orthotropic steels, the IIW recommend the hot spot points “type b”, which could be calculated by the extrapolation method which is given in Eq. (7.1).

$$\Delta\sigma_h=1.67\Delta\sigma_{0.4t}-0.67\Delta\sigma_{1t} \quad (7.1)$$

The symbols  $\Delta\sigma_{0.4t}$  and  $\Delta\sigma_{1t}$  represent the surface stress at a distance of 0.4t (t is the thickness of



base plate) and 1t to the weld toe respectively. For hs1 point, the  $\sigma_{zz}$  in extrapolation path were used for calculation; for hs2, the  $\sigma_{xx}$  in path were used to calculate the hot spot stress.

When the wheel loading at mid-span (same as l3), the hot spot stress at hs1 and hs2 as shown in Figure 7.16 (a). For hs1 point, the outside stresses are slightly larger than that of inside stress. For hs2, the inside stress are all compressive stress under t1/ t2/ t3, but the corresponding outside stress are all tensile stress. Obviously, the rib rotation was caused by loading position and the outside stress range represents the maximum stress range of the structural detail. The comparison of three loading positions shown that the corresponding stresses are totally different. For the case of t3, the outside stress of hs1 is about 1.09-times larger than the inside stress of hs1 and 2.15 and 3.94-times larger than those of hs2 and hs3. It was considered both of the in-plane distortion from horizontal shear and out-of-plane distortion from rib rotation existed.

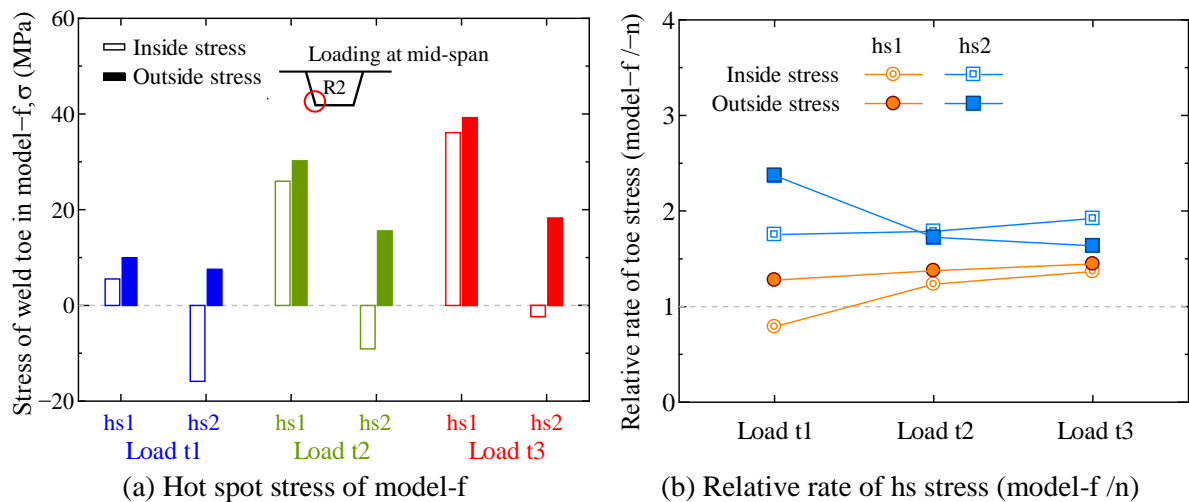


Figure 7.16 Comparison of inside and outside stresses at rib2 by hot spot method

To compare the model with artificial rib cracks, the non-crack model should be less affected by rib rotation based on the tensile stress results, as shown in Figure 7.16 (a). The relative rate of hot spot stress of model-f was compared with those of model-n, as shown in Figure 7.16 (b). The rib crack between crossbeams always lead to an evident increasing (about 1.3~2.5 times larger) in outside stress at cope holes connection. And the outside stress of hs2 would be more sensitive to rib cracks than hs1, which might be because the transverse stress at crossbeam increased much more than vertical stress at ribs near the rib-to-deck connection.

To evaluate the outside stress at cope holes of model-f, changed loading positions were considered. The distributions of hot spot stress hs1/hs2 and uniaxial node stress at weld toe (node1 corresponding to hs1, node2 corresponding to hs2) were compared, as shown in Figure 7.17. It shows that the node2 stress is larger than those of node1 in any loading position. However, the calculated hot spot stresses of hs1 and hs2 are in an opposite tendency.

In order to figure out the relationship between two kinds of stress evaluation method, the stress distribution of hs1 and hs2 at extrapolation paths and the extrapolated value of hot spot stress were

compared. The model was loaded under the transverse t2 at mid-span (13) position, as shown in Figure 7.18. It can show that the calculated hot spot stress  $hs1 > hs2$ , but the node peak stress  $node2 > node1$ . The hot spot stress has considered the slope of stress distribution curves but cannot account for the peak stress at weld toe due to different geometry shapes. Thus the crack initiating at  $hs2$  might be easier than at  $hs1$ . Based on hot spot stress method, the fatigue evaluation is hard to access the stress concentration at weld detail, where is sensitive to local geometrical discontinuity. The crack initiation and propagation could be effected by both of the peak stress at weld toe and the stress distribution around welded joint. Therefore, the fatigue evaluation on structural details should not only consider the nominal stress or hot spot stress when the geometrical shape of welded joint might be the main factors for crack initiation.

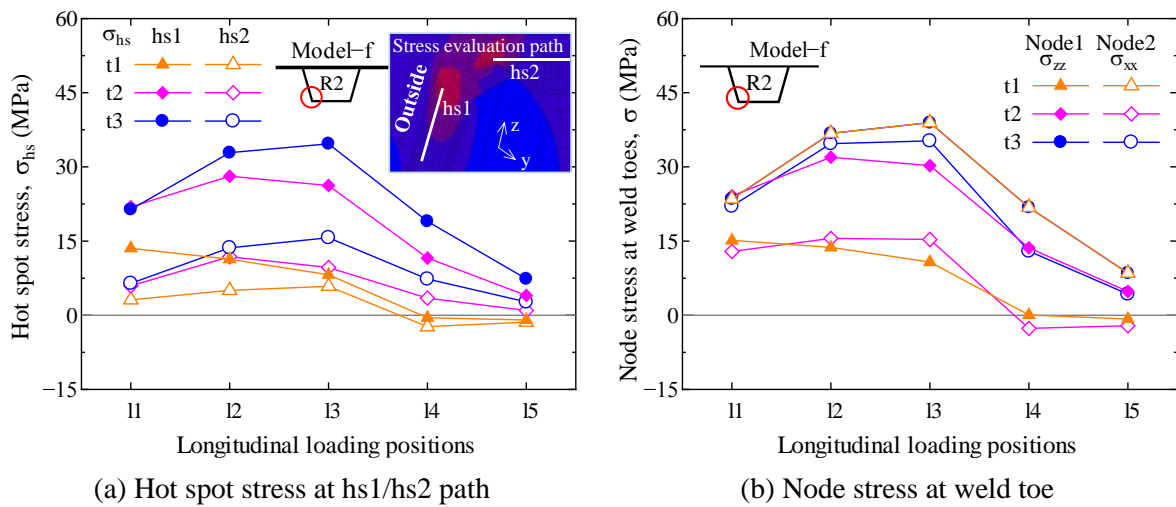


Figure 7.17 Node stress and hot spot stress  $hs1/2$ (outside) of crossbeam

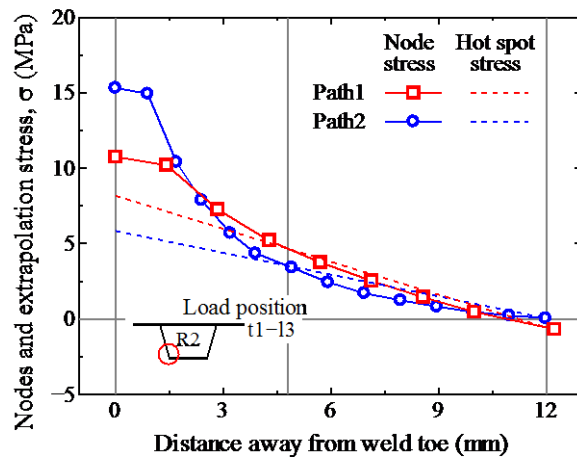


Figure 7.18 Comparison of node stress / hot spot stress at cope hole path

## 7.4 Stress characteristics of structure with 16mm-deck plate

### 7.4.1 Effect of rib cracks on stress ranges at adjacent rib

For a non-crack model with 16mm-thick deck plate, the stress characteristics should be similar with those of 12mm-thick model at details. However, after crack occurred, the structural response might be different, moreover, it is also unclear that whether the stress at crossbeam would be reduced effectively by thickening the deck plate. The FE models of 16mm-thick deck plate with artificial rib cracks at mid-span were denoted as model-n16 /a16 /c16 /e16 /f16. In transverse, one load case t1 (double tire load above the rib2) was loaded at mid-span. Besides the deck plate thickness, 16mm-models are consistent with the 12mm-models.

Figure 7.19 shows the stress distribution at the external surface around rib1 at mid-span. The maximum tensile stress occurred at the bottom of ribs, which owns a same tendency with that of 12mm-model, as shown in Figure 7.19. The maximum tensile stress values at rib1 external surface of crack models are different. Rib1 tensile stress significantly increased at the bottom when the adjacent rib crack propagated. Thus the rib2 cracking might lead to the cracking at bottom of the rib1, and then rib1 might also lead to the other adjacent rib fracture.

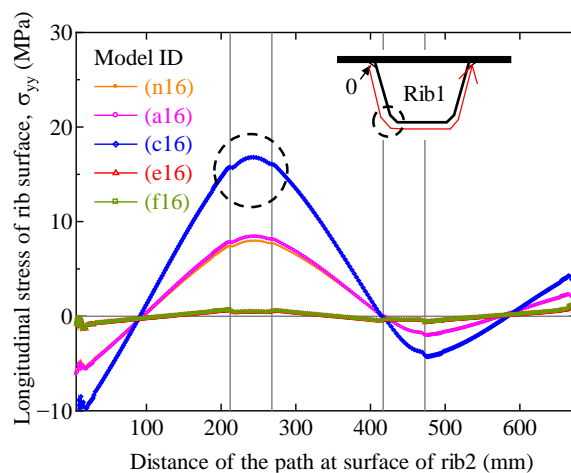

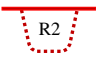

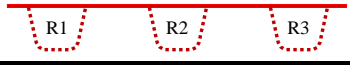


Figure 7.19 Longitudinal stress distribution of rib1

Table 7.4 The maximum stress range and the amplification of rib1

Model ID	Crack types	Stress range $\Delta\sigma$ (MPa)	Percentage
n16	Non-crack	7.96	100%
a16		8.40	106%
c16		16.80	211%
e16		0.44	6%
f16		0.45	6%

The maximum stress range and amplification of rib1 in some stages of the adjacent rib crack growth, as shown in Table 7.4. The relative percentage of models a16/c16 showed that their stress range would increase to 106% and 211% when comparing with the standard value of non-crack model. Therefore, the interactions between multiple U-ribs cannot be ignore, and it might lead to the decrease in fatigue strength of the rib-to-rib butt welds which was recommended by specifications.

#### 7.4.2 Effect of pavement stiffness on structural response

The deformation and stress response of structure were changed severely from model type a16 to c16, as shown in Figure 7.20. Therefore, the rib crack extent in vertical have an important influence on the structure stress. However, the deformation and stress of deck plate bottom does not changed much when cracks occurred at adjacent ribs, which might due to the support from main girder and rib-to-deck connections.

Figure 7.20(b) shows the stress concentration at weld toe of non-crack model were changed from compressive stress to tensile stress concentration after rib crack occurred. The stress value was changed from -20MPa to over 70MPa. It shows that once the fatigue crack occurred at longitudinal rib, the deck plate nearby would have to bear the tensile stress instead of U-rib. However, in case of the peak stress at weld toe, there is only about 3~6% difference between the cases of whole rib crack occurred at one rib or multiple adjacent ribs. It was considered that the interactions between multiple cracked U-ribs have little impact on the stress response of deck plate.

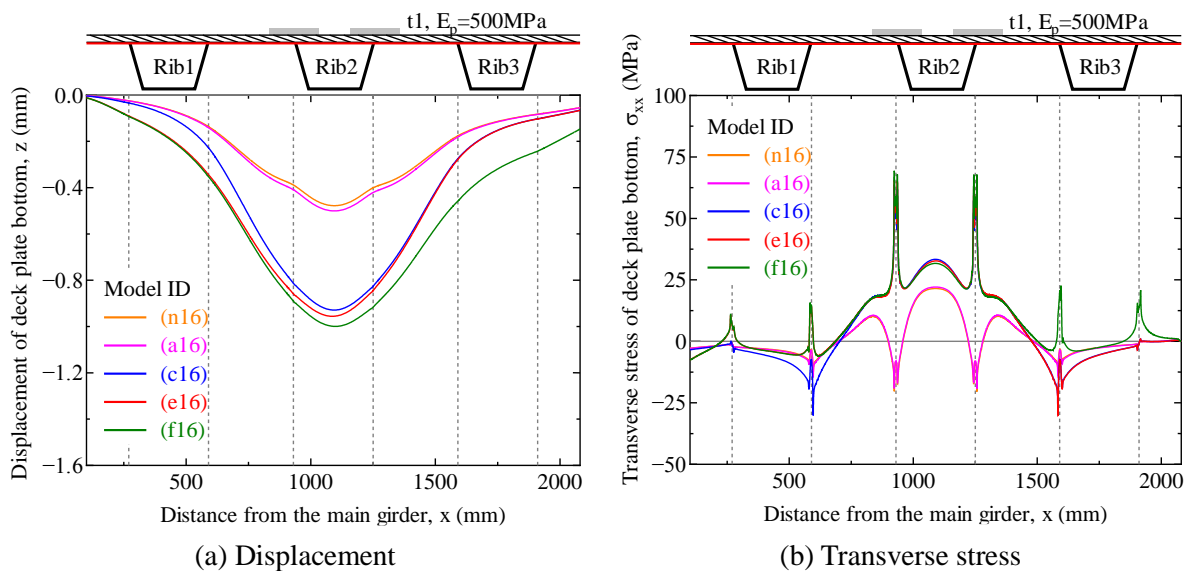


Figure 7.20 The structural response of deck plate bottom at mid-span of 16mm-models

#### 7.4.3 Effect of rib cracks on cut-out stresses

The maximum principal stress distributions at rib2 scallop in the middle-axial plane of crossbeam, as shown in Figure 7.21(a). The stress distributions are similar for different crack models, because the scallop is far away from the cracked cross-section. The maximum tensile stress around scallop located

at rib-to-deck welded joint. Meanwhile, the maximum principal stresses stress of rib3 scallop is much smaller than that of rib2 scallop, as shown in Figure 7.21(b). The fracture of longitudinal rib would cause the rib torsion and out-of-plane deformation of crossbeam. The different cracking degree in rib2 has different effects on stress at rib3 scallop due to the rib torsion. It was considered the crossbeam would subjected to both of in plane stress and out-of-plane stress. But for the transverse and longitudinal loads in different positions, there would be a more complicate influence on the stress at cut-outs of crossbeam.

In addition, the stress values at scallop of 16mm-model seems close to that of 12mm-model, because the stress at crossbeams mainly affected by rib rotation and the crossbeam bending. It seems would not be influenced much by deck plate thickness.

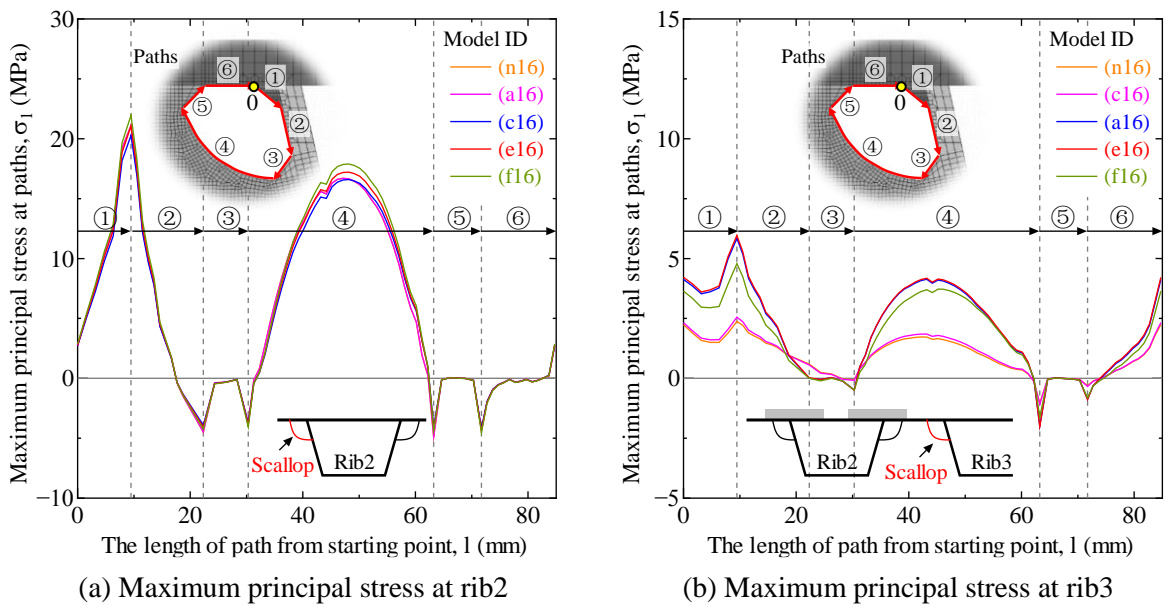


Figure 7.21 The stress distributions at scallops in middle-axial plane of crossbeam

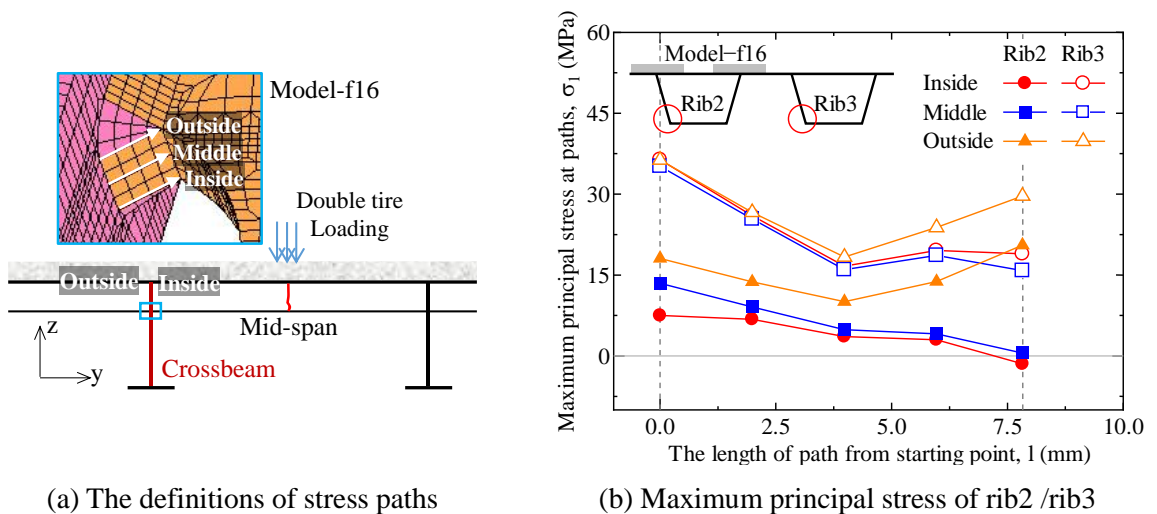


Figure 7.22 The stresses at welded joint of cope holes

Finally, compare with the scallop cut-out, the localized bending at cope holes should be more sensitive to fatigue loadings due to the slit. The maximum principal stress near the cope hole would be magnified by slit due to the loading at mid-span. The cope hole stress of model F16 is much larger than that of other models, because rib bottom of rib1 /rib2 /rib3 cannot afford the tensile stress anymore, and this crack combination would cause a severe rib deflection. Furthermore, there is a difference at the stress values of crossbeam in thick direction, which is caused by the out-of-plane deformation and rib rotation. Three stress evaluation paths at the rib-to-crossbeam connection of cope hole as shown in Figure 7.22 (a). These paths were located at the inside surface/ middle-axial plane/ outside surface of the crossbeam. Inside path located at the surface which closest to the load position. The maximum principal stress at cope holes of rib2 /rib3 as shown in Figure 7.22 (b).

In contrast, the stress at cope hole of rib3 is larger than that of rib2, and a small difference existed between inside and outside stresses of rib3. It shows even though both of the rib rotate (about x axis) and rib3 torsion occurred, the rib torsion is a main factor that causing stress at rib3 cope hole. The rib cracks combined with adverse transverse load position lead to the multifold stress at cope hole. Besides, the stress at cope hole of rib2 shows the outside stress is much larger than the inside stress. Because of the total different geometric properties of two weld toes, the weld toe belongs to crossbeam would be much more affected by out-of-plane deformation.

## 7.5 Conclusions

Based on the previous study, the structure responses and stress behaviors of three-span steel decks were discussed. The effect of loading positions on stress characteristics of structure with different crack combinations were investigated. In addition, the effect of various crack combinations on thickened deck plate structure was also discussed by stress evaluation. The results are summarized as follows:

(1) The crack occurring at the ribs would generated large tensile stress at the welded joints of the deck plate. However, in transverse, the local toe stress was almost unaffected by adjacent rib cracks, and the effects of interactions between multiple cracked ribs on deformation and stress of deck plate could be ignored. Besides, a rib had to withstand the increasing longitudinal tensile stress when the crack propagated along adjacent ribs. Therefore, it could be speculated that the effect of interactions between multiple cracked ribs on longitudinal stress at the butt weld could not be ignored.

(2) Depending on the criteria for deflection for orthotropic plate decks in AASHTO, in the case that cracks only occurred at the butt weld of a rib splice, the structure deformation did not compromise bridge integrity. However, bridge safety was most adversely affected by the combination of rib-to-deck bead crack and rib crack. For the combination of rib-to-deck weld crack and rib crack, both the large deformation and strength reduction of structure might lead to serious safety problems.

(3) The fracture of longitudinal rib would cause the rib torsion and out-of-plane deformation at crossbeam. The effect of rib torsion on stress at crossbeams are significantly. The rib cracks combined

with adverse transverse load position would lead to the multifold stress at cut-outs at crossbeams, and the stress near the cope hole would be magnify due to the slit. The localized bending at cope holes are more sensitive to fatigue loadings than scallops. For the weld toe stresses at rib-to-crossbeam connections, both of the in-plane distortion from horizontal shear and out-of-plane distortion existed.

(4) For a FE model with 16mm-thick deck plate, the stress characteristics should own a same tendency with those of 12mm-thick model, and its structural response should be less than 12mm-model because of the strengthen stiffness. However, the stress values at cut outs of 16mm-model seems close to that of 12mm-model, because the stress at crossbeams mainly affected by rib rotation and the crossbeam bending, and it seems would not be influenced much by deck plate thickness.

## Chapter 8 Summary and conclusions

### 8.1 Summary of works

The purpose of this research is to investigate the fatigue behaviors of major cracks in orthotropic steel decks. Mainly focused on the root crack occurred at rib-to-deck connection, and the butt joint of U-ribs. Therefore, the dissertation is mainly divided into two parts, objective of first part is rib-to-deck welded joint, and the second is field butt weld at longitudinal rib.

In the first part, the fatigue behaviors of the rib-to-deck welded joints with PJP and full penetration were experimentally evaluated through the field measurements and fatigue tests. The fatigue tests were conducted on six types of orthotropic steel decks with different structural parameters. The fatigue behaviors of the structural detail were investigated by diverse stress conditions, and one adverse transverse position were considered under the single and double tire loading.

And then, the cause identification of the crack initiation of this structural detail was explained through the fatigue loading test and residual test results. The fatigue cracking patterns and their influence factors were discussed by comparing the crack sizes, crack propagation angles in the cross-sectional and longitudinal directions. Based on the test results, the cracking mechanism and stress responses around root tip were analyzed by establishing the matching FE models under the basis stress condition. The fatigue behaviors of structure detail were investigated by considering the effect of root gap shapes, weld penetrations, and plate thicknesses on crack initiation. Moreover, various root crack depths were simulated in models to clarify the stress variations occurring during the propagation stage under cyclic loading.

In the second part, to assess and predict the integrity of a structure with large cracks in butt weld of ribs and rib-to-deck cracks, the field measurements in actual bridge was carried out in this study, and simulated the long cracks at rib butt welds and rib-to-deck welded joint by artificial gas-cut. The structure responses and stress behaviors of corresponding bridge decks were established and analyzed by FEA with one-span solid model. Besides, the torsional rigidity of ribs with butt weld crack were investigated via quantitative analysis. Furthermore, the effect of pavement stiffness and different transverse load positions on local structure were also investigated via quantitative analysis.

In addition, the refined and built the solid-shell hybrid models with 3-span section to investigate the whole structural response and stress characteristics of crossbeam and other details. The local stress variations from non-crack stage to multiple-crack stages were analyzed, and the stress characteristics of rib-to-crossbeam connections were also conducted. Besides, the sensitive points at cope holes of crossbeam were evaluated by hot spot stress method. Finally, the effect of various crack combinations on thickened deck plate structure was also discussed by stress evaluation.



## 8.2 Conclusions

### Major conclusions and my innovations:

- I. The high tensile residual stress existed near the root tip. Both the effective tensile stress and whole stress range would affect the fatigue crack behavior.
- II. Larger penetration rate is advantageous for fatigue durability. Besides, fatigue durability could be enhanced by thickened deck plate, but thickened U-rib has no evident contribution on crack growth prevention.
- III. After root crack propagated over half of deck plate thickness, the larger tensile stress at crack tip occurred, which might result in a significant reduction in the residual life.
- IV. Rib fracture would generate large tensile stress at localized deck plate and adjacent ribs. The effect of rib torsion on stress at crossbeams are significant.

### (1) Findings from the experimental fatigue testing on rib-to-deck welded joint are summarized as follow.

The field loading test focused on the rib-to-deck weld joint were carried out in an actual bridge. The fatigue test specimens were fabricated with six types of structural dimensions. The experimental setup simulated the single and double tire loading at mid-span of specimens, and provided the alternative stress for at least 3 million cycles. The basic stress range was set as -160 to 20 MPa under double tire loading, which obtained from field loading test. Root cracks tend to initiate easily under double tire, while the single loading was not considered to play a major role in the rib-to-deck crack propagation.

The test results showed three types of crack categories: 1) the occurrence of root cracking only, 2) both toe crack and root crack occurred, 3) non-crack initiation. The fatigue test results also demonstrated that fatigue cracks did not occur where the stress ranges were purely compressive, it was considered the welded joint might under the relative lower tensile residual stress so that its effective tensile stress range would be smaller than others. A one-third or one-half decrease in the stress range while maintaining the same tensile stress could also enhance the fatigue life. This means both the effective tensile stress range and the whole stress range would affect the fatigue life before crack initiation.

The residual stress near the weld root was measured to be high tensile residual stress, and the experimental results showed a similar trend to the FE analysis results. It was identified the residual stress distribution in an orthotropic steel deck depending on partial penetration weld. The tensile residual stress for the analysis model with 75% weld penetration was 1.35-times larger than that with 0% penetration rate. The test results also showed that the crack depths with higher penetration rate were smaller than those of SPO. The higher penetration rate can prevent the root cracks. However, the fatigue durability of specimen with full penetration was hard to judge because its special geometrical properties at root tip.

Based on the measurement of the welding residual stress and fatigue test results, the cracking mechanism of the weld root were investigated by considering the effective stress. The magnitude of tensile stress would play a decisive role during the root crack propagation after the residual stress was

released around the root tip. Besides, an increase in the deck plate thickness was beneficial to the fatigue durability before the crack initiation, but thickening the U-rib had no obvious effect in the prevention of root cracking.

**(2) Findings from the parametric FE analysis on rib-to-deck test specimens are summarized as follow.**

The test and FE results were compared, the results of the FE analyses and tests had similar stress distributions at reference points in longitudinal direction. Based on the stress flow near the root tip under double tire loadings, the principal stress tensors showed that the tensile-compressive stress cycles existed near the root tip, which would cause the fatigue cracking at the rib-to-deck welded joint. This was consistent with the test results. However, the single-tire loading made no obvious contribution to the root-deck cracking, but may cause the bead cracking.

The root gap shape and penetration rate have an impact on the root cracking direction at the initiation stage, but seem not directly related to the crack propagation mechanism; the higher penetration rate is advantageous for the prevention of root crack initiation. However, although the stiffness increased with the increase in plate thickness, the fatigue life of crack initiation might be reduced owing to the low fatigue strength of the thick deck plate, whereas the U-rib thickness has limited effect on the stress response of the root tip.

The significant difference between the 8mm-crack model and other crack models is the high stress concentration around the crack tip. The stress conditions of root tip would be changed when a root crack propagated over half of deck plate thickness. The promoting effect between crack growth and principal stress might result in a significant reduction in the residual life of this structure. Finally, based on fatigue strength evaluation, the fatigue life at root tip of thicken plate does not increase significantly compared to that of 12mm-thick deck plate before root crack initiation.

**(3) Findings from the structural behavior and stress characteristics of OSD with artificial butt weld crack combinations are summarized as follow.**

For the structure with the combination of butt weld fracture and rib-to-deck cracks, the measured stresses of deck plate bottoms were in good agreement with the FEA. The displacement would reach to about 2~3 times larger than non-crack structure. The crack occurring at one rib bottom would generated large tensile stress at local details of deck plate and adjacent ribs within longitudinal range. In transverse, one rib fracture would lead to stress fluctuated at deck plate nearby within three-rib ranges, the loading effect on the farther ribs can be ignored. The interaction between multiple U-rib cracks could result in decreasing fatigue strength of the structural detail, especially for the combination of cracks propagating to different directions.

Besides the local stress, the butt weld crack of ribs would usually result two important consequences: one is the interaction between adjacent ribs; another is the effect of rib rotation on crossbeam stresses. Firstly, the first rib cracking might lead to the cracking at bottom of the adjacent rib, and then it might

be accelerated the fracture in multiple ribs. Secondly, the effect of fractured ribs on stress at crossbeams are significantly. Moreover, the rib cracks combined with adverse transverse load position would lead to the multifold stress at cut-outs of crossbeams. The localized bending at cope holes are more sensitive to fatigue loadings than scallops. For the weld toe stresses at rib-to-crossbeam connections, both of the in-plane distortion from horizontal shear and out-of-plane distortion existed.

The pavement stiffness would be changed according to seasonal temperature. The deck plate stress in winter would decrease to about 40% of maximum stress (summer) on average. Furthermore, depending on the criteria for deflection for orthotropic plate decks in AASHTO, in the case that cracks only occurred at the butt weld of a rib splice, the structure deformation did not compromise bridge integrity. However, bridge safety was most adversely affected by the combination of rib-to-deck bead crack and rib crack. For the combination of rib-to-deck weld crack and rib crack, both the large deformation and strength reduction of structure might lead to serious safety problems.

### **8.3 Recommendations for future works**

A lot of works had been done in this study, about fatigue crack behaviors in OSD. But there are also something important but cannot be clarified in this study, the limitations of my research as shown follows:

- 1) Experimental study in Chapter 3, only the most adverse loading position was discussed. Among 19 full-scale specimens, some special crack patters need more verification in continued study.
- 2) Field measurement and FEA in Chapter 6, the long crack was simplified as symmetric simulation.
- 3) FE simulation of artificial cracks in Chapter 5, the dynamic crack propagation process was replaced by several static crack stages of different crack depth. Only the visible relationship between crack depth and applied stress response was explained. For typical crack in local model under unidirectional stress, it is common to use Node Release Technique/ Cohesive Element Approach to simulate the crack propagation process [123-126]. However for a large structural under complex loading case, the FEA on elastic shell or solid model is still the major method [127,128].

The following parts are the recommendations for my future works:

- 1) Fatigue strength evaluation: Based on the results of this study, the fatigue strength evaluation should be conducted in the future. So that the effects of this study could be expanded to other research area.
- 2) Multi-scale modeling is favorable for FEA on artificial local cracks by using fracture mechanics approach. Related work will be conducted in future. For instance, three-level models could be used to accurately evaluate the stress-intensity factors at the weld detail [129]. The crack growth could be simulated by numerical integration of the Paris formula.
- 3) Nondestructive testing of residual stress: At present, no matter the residual stress test or FE

simulation, more accurate measurement methods were developed. By the way, the nondestructive testing of residual stress at welds would be more and more important.

- 4) Post weld treatment: The application of the post weld treatment would have a wide prospect in actual bridges. About post weld treatment, only the press strengthen method was discussed in this study. The new detection and maintenance methods are always demanded all over the world.
- 5) Fatigue and corrosion interaction: The fatigue and corrosion problems are always the most significant topics in OSD bridges. The interaction between corrosion damage and fatigue cracks should not be ignore.

---

## Bibliography

- [1] A. Karlsson, C. Wesley, Fatigue analysis for orthotropic steel deck bridges, Chalmers University of Technology, 2014.
- [2] Z.H. Qian, D. Abruzzese, Fatigue failure of welded connections at orthotropic bridges, *Frattura Ed Integrità Strutturale*. 3 (2009) 105–112.
- [3] S.T. de Freitas, Steel plate reinforcement of orthotropic bridge decks, TU Delft Library, 2012.
- [4] R.J. Connor, HDR Engineering, United States, Federal Highway Administration, Office of Bridge Technology, Manual for design, construction, and maintenance of orthotropic steel deck bridges, U.S. Dept. of Transportation, Federal Highway Administration, Washington, D.C., 2012.
- [5] T. Gurney, Fatigue of steel bridge decks, HMSO Publication Centre, Transport Research Laboratory, Department of Transport, London, UK, 1992.
- [6] T.O. Medani, Design principles of surfacings on orthotropic steel bridge decks, Delft University of Technology, 2006.
- [7] T.O. Medani, X. Liu, M. Huurman, A. Scarpas, A.A.A. Molenaar, Experimental and numerical characterization of a membrane material for orthotropic steel deck bridges: Part 1: Experimental work and data interpretation, *Finite Elements in Analysis and Design*. 44 (2008) 552–563.
- [8] W.F. Chen, L. Duan, *Bridge Engineering Handbook*, CRC Press, 1999.
- [9] T. Mori, S. Shigihara, H. Nakamura, Fatigue tests on welded connections between deck plate and trough rib in steel plate deck in consideration of weld penetration, *Journal of Japan Society of Civil Engineers A*. 62 (2006) 570–581.
- [10] M.H. Kolstein, Fatigue classification of welded joints in orthotropic steel bridge decks, TU Delft Library, 2007.
- [11] R. Wolchuk, Orthotropic redecking of bridges on the North American Continent, in: *Structural Engineering International Conference*, Zurich, Switzerland, 1992: 125–130.
- [12] T. Okamoto, M. Hadano, Evaluation of painting life time for steel bridge by paint view system, 2003.
- [13] S. Ya, K. Yamada, T. Ishikawa, Fatigue durability of trough rib to deck plate welded detail of some orthotropic steel decks, *Journal of Structural Engineering, JSCE*. 56A (2010) 77–90.
- [14] Committee on Steel Structures, Fatigue of orthotropic steel bridge deck, *Steel structures* (19), Japan Society of Civil Engineers, 2010. (in Japanese)
- [15] C. Miki, Fatigue damage in orthotropic steel bridge decks and retrofit works, *International Journal of Steel Structures*. 6 (2006) 255–267.
- [16] M.H. Kolstein, European research on the improvement of the fatigue resistance and design of steel orthotropic bridge decks, in: *Advances in Steel Structures (ICASS '96)*, Sacramento, California, USA, 2004.
- [17] S. Ya, K. Yamada, Fatigue durability evaluation of trough to deck plate welded joint of orthotropic

- steel deck, *Journal of Japan Society of Civil Engineers A.* 64 (2008) 603–616.
- [18] J. Murakoshi, Study on fatigue behaviors and maintenance techniques for cracking at rib-to-deck welded joints in orthotropic steel deck, Doctoral Thesis, Nagoya University, 2014. (in Japanese)
- [19] M.C.M. Bakker, F.B.P. de Jong, Ultrasonic underside inspection for fatigue cracks in the deck plate of a steel orthotropic bridge deck, *Heron.* 5, 2003.
- [20] S. Inokuchi, H. Ishii, T. Ishigaki, H. Maeno, T. Sumi, K. Yamada, Fatigue assessment for weld between deck plate and u-rib in orthotropic steel decks with consideration of pavement properties, *Journal of Japan Society of Civil Engineers A.* 66 (2010) 79–91.
- [21] Japan Road Association (JRA), Fatigue design guidelines for steel highway bridges, 2002. (in Japanese)
- [22] Z.G. Xiao, K. Yamada, S. Ya, X.L. Zhao, Stress analyses and fatigue evaluation of rib-to-deck joints in steel orthotropic decks, *International Journal of Fatigue.* 30 (2008) 1387–1397.
- [23] Z.G. Xiao, K. Yamada, J. Inoue, K. Yamaguchi, Fatigue cracks in longitudinal ribs of steel orthotropic deck, *International Journal of Fatigue.* 28 (2006) 409–416.
- [24] F.B.P. de Jong, Renovation techniques for fatigue cracked orthotropic steel bridge decks, TU Delft, Delft University of Technology, 2007.
- [25] E. Ypeij, New developments in Dutch steel bridge building, Amsterdam, Netherland, 1972.
- [26] Japanese Society of Steel Construction, U-shaped rib for steel decks, JSS II 08-2006. (in Japanese)
- [27] Japan Road Association (JRA), Specifications for Highway Bridges, 2002. (in Japanese)
- [28] K Mizuguchi, K Yamada, M Iwasaki, S Inokuchi, Rationalized steel deck structure and large model test for developing new type of structure, *Proceeding of International Orthotropic Bridge Conference, American Society of Civil Engineers, Reston, VA, 2004: 675–688.*
- [29] American Association of State Highway and Transportation Officials, AASHTO LRFD bridge design specifications, 5rd Ed., Washington, D.C., 2010.
- [30] H.B. Sim, C.M. Uang, Stress analyses and parametric study on full-scale fatigue tests of rib-to-deck welded joints in steel orthotropic decks, *Journal of Bridge Engineering, ASCE.* 17 (2012) 765–773.
- [31] R. Wolchuk, G. Baker, Orthotropic deck bridges, *Proceeding of International Orthotropic Bridge Conference, American Society of Civil Engineers, Reston, VA, 2004.*
- [32] C.V. Dung, E. Sasaki, K. Tajima, T. Suzuki, Investigations on the effect of weld penetration on fatigue strength of rib-to-deck welded joints in orthotropic steel decks, *International Journal of Steel Structure.* 15 (2014) 299–310.
- [33] H.B. Sim, C.M. Uang, C. Sikorsky, Effects of fabrication procedures on fatigue resistance of welded joints in steel orthotropic decks, *Journal of Bridge Engineering, ASCE.* 14 (2009) 366–373.
- [34] S. Inokuchi, Wheel trucking test for weld of U-shaped rib and deck plate in the orthotropic deck, *Proceedings of the 23th U.S.-Japan Bridge Engineering Workshop, 2007.*
- [35] S.J. Maddox, Fatigue of welded joints loaded in bending, *Transport and Road Research*

- Laboratory (TRRL), Wokingham, Berkshire United Kingdom, 1974.
- [36] T. Mori, Influence of weld penetration on fatigue strength of single-sided fillet welded joints, *Steel Construction Engineering, JSSC*. 10 (2003) 9–15. (in Japanese)
- [37] B. Baik, K. Yamada, T. Ishikawa, Fatigue crack propagation analysis for welded joint subjected to bending, *International Journal of Fatigue*. 33 (2011) 746–758.
- [38] T. Mori, H. Harada, Fatigue tests and stress analyses on connections between deck plates, transverse ribs and trough ribs in steel orthotropic deck, *Journal of Japan Society of Civil Engineers, Ser. A1 (Structural Engineering & Earthquake Engineering (SE/EE))*. 67 (2011) 95–107. (in Japanese)
- [39] T. Mori, X.L. Zhao, P. Grundy, Fatigue strength of transverse single-sided fillet welded joints, *Australian Civil Engineering Transactions*. 39 (1997) 95.
- [40] J. Murakoshi, N. Yanadori, T. Ishizawa, N. Toyama, T. Kosuge, Study on effect of deck thickness of orthotropic steel deck on fatigue durability, *Steel Construction Engineering, JSSC*. 19 (2012) 55–65. (in Japanese)
- [41] S. Inokuchi, S. Kainuma, A. Kawabata, D. Uchida, Field measurement and development of an experimental system for fatigue-cracking from weld roots between deck plate and u-rib in orthotropic steel decks, in: *Proceeding of 2nd International Orthotropic Bridge Conference*, American Society of Civil Engineers, Sacramento Section, Sacramento, California, USA, 2008: 345–357.
- [42] J.W. Fisher, S. Roy, Fatigue damage in steel bridges and extending their life, *Advanced Steel Construction*. 11 (2015) 250–268.
- [43] S. Inokuchi, D. Uchida, A. Kawabata, T. Tamakoshi, Influence of asphalt pavement failure on local stress of orthotropic steel decks, *Steel Construction Engineering, JSSC*. 15 (2008) 75–86. (in Japanese)
- [44] X. Liu, T.O. Medani, A. Scarpas, M. Huurman, A.A.A. Molenaar, Experimental and numerical characterization of a membrane material for orthotropic steel deck bridges: Part 2: Development and implementation of a nonlinear constitutive model, *Finite Elements in Analysis and Design*. 44 (2008) 580–594.
- [45] S. Ya, K. Yamada, T. Ishikawa, Fatigue evaluation of rib-to-deck welded joints of orthotropic steel bridge deck, *Journal of Bridge Engineering, ASCE*. 16 (2011) 492–499.
- [46] B. Baik, T. Ishikawa, K. Yamada, Fatigue crack propagation behavior of fillet welded joint subjected to bending, *Journal of Structural Engineering A, JSCE*. 55A (2009) 871–879.
- [47] I.T. Kim, Fatigue strength improvement of longitudinal fillet welded out-of-plane gusset joints using air blast cleaning treatment, *International Journal of Fatigue*. 48 (2013) 289–299.
- [48] T. Sakagami, Remote nondestructive evaluation technique using infrared thermography for fatigue cracks in steel bridges, *Fatigue & Fracture of Engineering Materials & Structures*. 38 (2015) 755–779.
- [49] Y. Zhang, Q. Rong, Dynamic monitoring of fatigue crack process of orthotropic steel bridge

- structure with acoustic emission, in: ICF13, 2013.
- [50] M. Sugimoto, M. Kawamura, H. Hayashi, Y. Murayama, Inspection and monitoring of Hanshin Expressway for structural maintenance, SPIE's 5th Annual International Symposium on Nondestructive Evaluation and Health Monitoring of Aging Infrastructure. International Society for Optics and Photonics, 2000: 220–228.
- [51] A.F. Hobbacher, The new IIW recommendations for fatigue assessment of welded joints and components – A comprehensive code recently updated, *International Journal of Fatigue*. 31 (2009) 50–58.
- [52] Z. YuanZhou, B. Ji, Z. Fu, H. Ge, Local stress variation in welded joints by ICR treatment, *Journal of Constructional Steel Research*. 120 (2016) 45–51.
- [53] P.K. Tateishi, M.T. Hanji, M.S. Hanibuchi, Improvement of extremely low cycle fatigue strength of welded joints by toe finishing, *Weld World*. 53 (2013) 238–245.
- [54] M.M. Tai, P.C. Miki, Improvement effects of fatigue strength by burr grinding and hammer peening under variable amplitude loading, *Weld World*. 56 (2013) 109–117.
- [55] M. Tai, C. Miki, Fatigue strength improvement by hammer peening treatment—verification from plastic deformation, residual stress, and fatigue crack propagation rate, *Weld World*. 58 (2014) 307–318.
- [56] L. Hacini, N.V. Lê, P. Bocher, Evaluation of residual stresses induced by robotized hammer peening by the contour method, *Experimental Mechanics*. 49 (2008) 775–783.
- [57] H.C. Yildirim, G.B. Marquis, Fatigue strength improvement factors for high strength steel welded joints treated by high frequency mechanical impact, *International Journal of Fatigue*. 44 (2012) 168–176.
- [58] J. Murakoshi, N. Yanadori, H. Ishii, Research on steel fiber reinforced concrete pavement for orthotropic steel deck as a countermeasure for fatigue, *Stress*. 1 (2008) 1–13.
- [59] X. Ju, S. Choi, K. Tateishi, Analytical study on crack propagation at rib-to-deck welded joints in orthotropic steel decks, *Steel Construction Engineering, JSSC*. 19 (2012) 85–94.
- [60] D. Radaj, C.M. Sonsino, W. Fricke, Recent developments in local concepts of fatigue assessment of welded joints, *International Journal of Fatigue*. 31 (2009) 2–11.
- [61] European Committee for Standardization, EN 1993-2: Eurocode 3: Design of steel structures - Part 2: Steel bridges, 2006.
- [62] R. Liu, Y. Liu, B. Ji, M. Wang, Y. Tian, Hot spot stress analysis on rib–deck welded joint in orthotropic steel decks, *Journal of Constructional Steel Research*. 97 (2014) 1–9.
- [63] R. Liu, B. Ji, M. Wang, C. Chen, H. Maeno, Numerical evaluation of toe-deck fatigue in orthotropic steel bridge deck, *Journal of Performance of Constructed Facilities, ASCE*. 29 (2015) 1–10.
- [64] C.M. Sonsino, W. Fricke, F. de Bruyne, A. Hoppe, A. Ahmadi, G. Zhang, Notch stress concepts for the fatigue assessment of welded joints – Background and applications, *International Journal of Fatigue*. 34 (2012) 2–16.



- 
- [65] Z.G. Xiao, K. Yamada, A method of determining geometric stress for fatigue strength evaluation of steel welded joints, *International Journal of Fatigue*. 26 (2004) 1277–1293.
- [66] W.H. Kim, C. Laird, Crack nucleation and stage I propagation in high strain fatigue—II. mechanism, *Acta Metallurgica*. 26 (1978) 789–799.
- [67] W. Schütz, A history of fatigue, *Engineering Fracture Mechanics*. 54 (1996) 263–300.
- [68] R.P. Reed, *The Economic effects of fracture in the United States.*, US Department of Commerce, National Bureau of Standards, Washington D.C., 1983.
- [69] T. Lassen, N. Récho, *Fatigue life analyses of welded structures: Flaws*, John Wiley & Sons, 2013.
- [70] H.O. Fuchs, I. Stephens, *Metal fatigue in Engineering*, John Wiley & Sons, New York, 1980.
- [71] T. Moan, K.M. Engesvik, Discussion of “Fatigue reliability: Introduction” by The Committee on Fatigue and Fracture Reliability of the Committee on Structural Safety and Reliability of the Structural Division, *Journal of Structural Engineering*. 110 (1984) 195–196.
- [72] T. Yuge, F. Machida, H. Morikawa, T. Miki, T. Kamiki, T. Masui, Analysis of fatigue damage patterns in orthotropic steel deck of Tokyo Metropolitan Expressways, *Proceeding of International Orthotropic Bridge Conference*, American Society of Civil Engineers, Reston, VA, 2004: 531–542.
- [73] A. Kawabata, S. Inokuchi, D. Uchida, et al. Improvement of fatigue durability in steel deck bridges by thicken deck plate, Japan Bridge Construction Association, 2008. (in Japanese)
- [74] W. Xu, X.N. Zhang, Analysis of distress characters and design of steel orthotropic bridge decks pavement in China, *Proceeding of 2nd International Orthotropic Bridge Conference*, American Society of Civil Engineers, Sacramento Section, Sacramento, California, USA, 2008: 184–192.
- [75] M.H. Kolstein, J. Wardenier, Laboratory tests of the deck plate weld at the intersection of the trough and the crossbeam of steel orthotropic bridge decks, *Proceedings of the Conference Eurosteel*, 1999: 411–414.
- [76] M.H. Kolstein, J. Wardenier, A new type of fatigue failures in steel orthotropic bridge decks, *Proceedings of Fifth Pacific Structural Steel Conference*, Techno Press, Korea, 1998: 483–488.
- [77] P. Mehue, Repair procedure for cracks in steel orthotropic decks, in: 1992.
- [78] N. McFadyen, R. Brady, I. Firth, Resurfacing of orthotropic bridge decks in the UK-Practical and design considerations, in: *Structural Engineering Institute*, Sacramento, California, USA, 2004: 489–512.
- [79] Technical Committee of Japan Bridge Construction Association, Current status of fatigue damages at weld lines between deck and closed ribs in orthotropic steel deck bridges oversea, Japan Bridge Construction Association, 2011. (in Japanese)
- [80] D.W. Hoepfner, V. Chandrasekaran, C. Elliott, *Fretting fatigue: Current technology and practices*, ASTM International, USA, 2000.
- [81] V.K. Jadon, S. Verma, *Analysis and design of machine elements*, IK International Pvt Ltd, 2010.
- [82] P.J. Haagenzen, IIW’s round robin and design recommendations for improvement methods, IIW Conference on Performance of Dynamically Loaded Welded Structures, San Francisco, 1997.

- 
- [83] A. Bhargava, Fatigue analysis of steel bridge details: hot spot stress approach, The George Washington University, 2010.
- [84] J.A. Collins, Failure of materials in mechanical design: Analysis, Prediction, Prevention, John Wiley & Sons, 1993.
- [85] Japanese Society of Steel Construction, Fatigue design recommendations for steel structures, Gihodo Shuppan, Tokyo, 2012. (in Japanese)
- [86] N. Pugno, M. Ciavarella, P. Cornetti, A. Carpinteri, A generalized Paris' law for fatigue crack growth, *Journal of the Mechanics and Physics of Solids*. 54 (2006) 1333–1349.
- [87] J.S. Leendertz, Fatigue behaviour of closed stiffener to crossbeam connections in orthotropic steel bridge decks, TU Delft Library, 2008.
- [88] S.J. Maddox, Review of fatigue assessment procedures for welded aluminium structures, *International Journal of Fatigue*. 25 (2003) 1359–1378.
- [89] H. Kihara, T. Kusuda, K. Iida, T. Maeda, T. Matsuoka, Effect of residual stresses on the behavior of brittle fracture propagation, *Journal of Zosen Kiokai*. 1960, 385–393. (in Japanese)
- [90] L. Gannon, Y. Liu, N. Pegg, M.J. Smith, Effect of welding-induced residual stress and distortion on ship hull girder ultimate strength, *Marine Structures*. 28 (2012) 25–49.
- [91] S.F. Estefen, T. Gurova, D. Werneck, A. Leontiev, Welding stress relaxation effect in butt-jointed steel plates, *Marine Structures*. 29 (2012) 211–225.
- [92] X. Cheng, J.W. Fisher, H.J. Prask, T. Gnäupel-Herold, B.T. Yen, S. Roy, Residual stress modification by post-weld treatment and its beneficial effect on fatigue strength of welded structures, *International Journal of Fatigue*. 25 (2003) 1259–1269.
- [93] M.S. Pfeil, R.C. Battista, A.J.R. Mergulhão, Stress concentration in steel bridge orthotropic decks, *Journal of Constructional Steel Research*. 61 (2005) 1172–1184.
- [94] J.Y. Liao, Fatigue damage in the orthotropic steel deck with respect to the trough-to-deck plate joint in between the crossbeams, Master, Department of Design and Construction, Delft University of Technology, 2011.
- [95] R. Wolchuk, A. Ostapenko, Secondary stresses in closed orthotropic deck ribs at floor beams, *Journal of Structural Engineering*. 118 (1992) 582–595.
- [96] A. Bruls, Assessment of fatigue life of orthotropic steel decks, Proceedings IABSE Workshop Remaining Fatigue Life of Steel Structures, Lausanne, Switzerland, 1990: 259–269.
- [97] M. Aygül, M. Al-Emrani, S. Urushadze, Modelling and fatigue life assessment of orthotropic bridge deck details using FEM, *International Journal of Fatigue*. 40 (2012) 129–142.
- [98] S. Kainuma, S. Onoue, K. Miura, S. Inokuchi, A. Kawabata, D. Uchida, Development of an experimental system for fatigue-cracking from weld roots between deck plate and u-rib in orthotropic steel decks, *Journal of Japan Society of Civil Engineers A*. 64 (2008) 297–302. (in Japanese)
- [99] Japanese Standards Association, Japanese Industrial Standard G3106, 2008. (in Japanese)
- [100] S. Inokuchi, Research on fatigue durability improvement and rationalization of orthotropic steel

- deck, Doctoral Thesis, Kyushu University, 2010. (in Japanese)
- [101] S.J. Maddox, *Fatigue strength of welded structures*, Woodhead Publishing, 1991.
- [102] C. Acevedo, A. Nussbaumer, J.M. Drezet, Evaluation of residual welding stresses and fatigue crack behavior in tubular K-joints in compression, *Stahlbau*. 80 (2011) 483–491.
- [103] G.S. Schajer, Measurement of non-uniform residual stresses using the hole-drilling method. Part II—Practical application of the integral method, *Journal of Engineering Materials and Technology*. 110 (1988) 344–349.
- [104] S. Inokuchi, S. Kainuma, D. Uchida, D. Shiro, Influence of press reforming in fabrication process on stress properties of welded joint between deck plate and U-shaped rib in orthotropic steel decks, *Steel Construction Engineering, JSSC*. 19 (2013) 1–8. (in Japanese)
- [105] M. Birkholz, X-ray diffraction study on residual stress and preferred orientation in thin titanium films subjected to a high ion flux during deposition, *Journal of Applied Physics*. 96 (2004) 7202–7211.
- [106] Japanese Standards Association, *Japanese Industrial Standard G3101*, 2008. (in Japanese)
- [107] Y. Luo, H. Murakawa, Y. Ueda, Prediction of welding deformation and residual stress by elastic FEM based on inherent strain (Report I) : Mechanism of inherent strain production (Mechanics, strength & structure design), *Transactions of JWRI*. 26 (1997) 49–57.
- [108] Y. Ueda, T. Yamakawa, Analysis of thermal elastic-plastic stress and strain during welding by finite element method, *Transactions of the Japan Welding Society*. 2 (1971) 186–196.
- [109] S. Kainuma, T. Mori, M. Ichimiya, Propagation behavior of fatigue crack originated from the weld root of fillet welded cruciform joints, *Steel Construction Engineering, JSSC*. 4 (1997) 1–8. (in Japanese)
- [110] S. Kainuma, D. Takamatsu, Fatigue behavior of fillet welded cruciform joint under compressive cyclic stress, *Journal of Constructional Steel, JSSC*. 8 (2000) 723–730. (in Japanese)
- [111] S. Kainuma, I.T. Kim, Fatigue strength evaluation of load-carrying cruciform fillet-welded joints made with mild steel plates of different thickness, *International Journal of Fatigue*. 27 (2005) 810–816.
- [112] F. Machida, C. Miki, Y. Hirabayashi, H. Tokida, T. Shimozato, Fatigue of weld connections to trough stiffeners in orthotropic steel bridge decks, *Proceeding of 2003 Annual Assembly of International Institute of Welding*, 2003.
- [113] R. Wolchuk, Lessons from weld cracks in orthotropic decks on three European bridges, *Journal of Structural Engineering*. 116 (1990) 75–84.
- [114] H. Yuan, *Optimization of rib-to-deck welds for steel orthotropic bridge decks*, Doctoral Thesis, Virginia Tech, 2011.
- [115] S. Inokuchi, D. Uchida, S. Hirayama, A. Kawabata, Evaluation method for fatigue life of welding joint between deck plate and U-shaped rib in orthotropic steel decks, *Journal of Japan Society of Civil Engineers, Ser. A1 (Structural Engineering & Earthquake Engineering)*. 67 (2011) 464–476. (in Japanese)

- [116] P.A. Deschênes, J. Lanteigne, Y. Verreman, D. Paquet, J.-B. Lévesque, M. Brochu, A new experimental method to study the influence of welding residual stresses on fatigue crack propagation, *International Journal of Fatigue*. 100, Part 1 (2017) 444–452.
- [117] E. Breitbarth, M. Besel, Energy based analysis of crack tip plastic zone of AA2024-T3 under cyclic loading, *International Journal of Fatigue*. 100, Part 1 (2017) 263–273.
- [118] P. Gallo, H. Remes, J. Romanoff, Influence of crack tip plasticity on the slope of fatigue curves for laser stake-welded T-joints loaded under tension and bending, *International Journal of Fatigue*. 99, Part 1 (2017) 125–136.
- [119] S. Kainuma, Y.S. Jeong, J.H. Ahn, T. Yamagami, S. Tsukamoto, Behavior and stress of orthotropic deck with bulb rib by surface corrosion, *Journal of Constructional Steel Research*. 113 (2015) 135–145.
- [120] M. Yang, B.H. Ji, Z.Q. Fu, H.J. Xu, Contrastive analysis of fatigue life prediction methods for welding roots in U-rib and orthotropic steel bridge deck, *Journal of Zhengzhou University: Engineering Science*. 36 (2016) 22–27. (in Chinese)
- [121] A.S. Noureldin, Development of temperature coefficients for the AASHTO flexible pavement design equation, *Proceedings of the Conference: Road Safety in Europe and Strategic Highway Research Program (SHRP)*, 1996.
- [122] S. Kainuma, K. Yamada, Y. Johsen, M. Iwasaki, T. Nishikawa, Test and analysis of influence of cracked ribs on orthotropic steel deck, *Journal of Structural Engineering, JSCE*. 42A (1996) 927–936. (in Japanese)
- [123] D.T. Ngoula, H.T. Beier, M. Vormwald, Fatigue crack growth in cruciform welded joints: Influence of residual stresses and of the weld toe geometry, *International Journal of Fatigue*. 101, Part 2 (2017) 253–262.
- [124] P.F.P. de Matos, D. Nowell, Numerical simulation of plasticity-induced fatigue crack closure with emphasis on the crack growth scheme: 2D and 3D analyses, *Engineering Fracture Mechanics*. 75 (2008) 2087–2114.
- [125] X. Hu, T.Q. Bui, J. Wang, W. Yao, L.H.T. Ton, I.V. Singh, S. Tanaka, A new cohesive crack tip symplectic analytical singular element involving plastic zone length for fatigue crack growth prediction under variable amplitude cyclic loading, *European Journal of Mechanics - A/Solids*. 65 (2017) 79–90.
- [126] K. Gotoh, T. Niwa, Y. Anai, Numerical simulation of fatigue crack propagation under biaxial tensile loadings with phase differences, *Marine Structures*. 42 (2015) 53–70.
- [127] A. Tabiei, W. Zhang, Cohesive element approach for dynamic crack propagation: Artificial compliance and mesh dependency, *Engineering Fracture Mechanics*. 180 (2017) 23–42.
- [128] B. Wang, P. Lu, Y. Shao, Fatigue test and simulation research of rib-to-diaphragm welded connection, *Journal of Convergence Information Technology*. 8 (2013) 770–777.
- [129] H.T. Nguyen, Q.T. Chu, S.E. Kim, Fatigue analysis of a pre-fabricated orthotropic steel deck for light-weight vehicles, *Journal of Constructional Steel Research*. 67 (2011) 647–655.